Poly(phenyl isocyanide)s with Controlled Structures and Functions

(ポリフェニルイソシアニドの構造制御による機能開拓)

Hiroki Hayashi

February 2019

Poly(phenyl isocyanide)s with Controlled Structures and Functions

(ポリフェニルイソシアニドの構造制御による機能開拓)

Hiroki Hayashi

Doctoral Program in Materials Science

Submitted to the Graduate School of
Pure and Applied Sciences
In Partial Fulfillment of the Requirements
for the Degree of Doctor of Philosophy in
Engineering

at the
University of Tsukuba

Acknowledgment

First of all, I would like to express my gratitude to my supervisor, Prof. Hiromasa Goto, for everything in lab life and research. I really appreciate the wonderful and exciting opportunity to work here in Goto laboratory. His guidance always motivated and stimulated me to further work on the research.

I sincerely would like to thank Prof. Masashi Kijima, Prof. Masami Kobayashi and Prof. Kohsuke Kawabata for kindly accepting to be referees in my doctoral defense.

I would like to thank from the bottom of my heart Dr. MBA. Rafaël H. L. Kiebooms. His continuous support for Goto-lab and Goto-lab members has been the driving force for every activity in the laboratory. His kind indications on research attitude, mindset, organization of the research environment, are my fundamental basis for my research.

I always thank coauthors, Dr. Reiji Kumai, Dr. Hajime Sagayama for synchrotron X-ray diffraction measurements, and Dr. Shigeki Nimori for high-intensity magnetic orientation using superconducting magnet.

I really appreciate the opportunity studying in Prof. David Weitz lab in Harvard University from October 2016 to January 2017. I would like to thank my mentor, Prof. Hyomin Lee, for providing me wonderful indications about doing research and living in Cambridge.

I am deeply grateful to Prof. Takanari Kashiwagi for SQUID measurements, Dr. Yoshitaka Matsushita for measuring temperature-variable XRD measurement, Prof. Nozomu Obana for using confocal fluorescence microscopy, and Prof. Hidehisa Kawashima and Fumihiro Aso for GPC measurements.

All the Goto lab members are always helping and motivating me to do the research. I would like to express my special thanks to Tomokazu Iseki for providing me right directions to continue the research, Ryosuke Kikuchi and Takuya Yonehara for working together on the polyisocyanide project.

A part of this work was supported by NIMS microstructural characterization platform as a program of "Nanotechnology Platform" of the Ministry of Education, Culture, Sports, Science and Technology (MEXT), Japan. For SEM observation, I would like to express my thank to Chie Ishii for her kind help with SEM observations.

I would like to thank the OPEN FACILITY, Research Facility Center for Science and Technology, University of Tsukuba for using NMR, PL, DLS, ESI, MALDI, AFM, and Glass Work Shop of University of Tsukuba.

Synchrotron X-ray diffraction measurement was performed under the approval of the Photon Factory Program Advisory Committee (Proposal No. 2017G003).

This work was supported by JSPS KAKENHI Grant Number JP17J05652.

Finally, my deepest gratitude to my family for kind and warm support for my student life.

Table of content

Chapter 1: General introduction

1.1	Brief history of synthetic helical polymers and polyisocyanides	·····	1
1.2	Representative helical polymers and helix inversion barrier	·····	2
1.3	Natural helical biopolymers in biological system	·····	2
1.4	Synthesis of isocyanide	·····	3
1.5	Common synthetic scheme for phenyl isocyanide	·····	3
1.6	Polyphenylisocyanide	·····	5
1.7	Living polymerization of isocyanides	·····	6
1.8	Block copolymerization of isocyanides with other type of polymers	·····	9
1.9	Helical structures of polyisocyanides	·····	14
1.10	Determination of helical sense of polyisocyanide	·····	14
1.11	Construction of preferred one-handed helical structure of polyisocyanide	·····	16
1.12	Stereoregularity of helical structure of polyisocyanide	·····	18
1.13	Long persistence length in polyisocyanide	·····	19
1.14	Lyotropic liquid crystalline phase formation in rod-shaped polyisocyanide	·····	20
1.15	Accumulation of functional group in helical scaffold	·····	20
1.16	Application of helical polyisocyanide as chiral materials	·····	22
1.17	Summary and future perspective	·····	22
	References	·····	23

Chapter 2: Lyotropic liquid crystalline chromic block copolymers with multi-stimuli responsiveness

2.1	Abstract	·····	28
2.2	Introduction	·····	28
2.3	Chromic property of semiconducting polymers	·····	29
2.4	Chiral polythiophene	·····	30
2.5	Lyotropic liquid crystalline semiconducting	·····	31
2.6	Molecular design	·····	32
2.7	Preparation of block copolymers	·····	32
2.8	Aggregation process in good/poor solvent mixture	·····	34
2.9	Solvent vapor-induced lyotropic liquid crystallinity	·····	35
2.10	PPI-length dependent lyotropic liquid crystallinity	·····	38
2.11	Magnetic orientation	·····	40

2.12 Self-recovering mechanochromism 43
2.13 Chiral communication between blocks in BCPs 44
2.14 Conclusion and perspective 46
References 47
Experimental 49

Chapter 3: Functional chromic block copolymers with mesogenic pendant: sheet-like micelle formation and polymerization-induced colloid formation

3.1 Abstract 53
3.2 Introduction 53
3.3 Preparation of mesogen-pendant containing block copolymers 54
3.4 Lyotropic liquid crystallinity and structural analysis 55
3.5 Shear- and magnetic field-assisted macroscopic orientation 58
3.6 Photo-isomerization 58
3.7 2D sheet-like micelle formation 59
3.8 Polymerization-induced colloid formation 61
3.9 Conclusion and perspectives 63
Experimental 63

Chapter 4: 1D Rod-shaped polymers for 0D small molecular crystallization

4.1 Abstract 67
4.2 Introduction 67
4.3 Preparation of rod-shaped PPI and C_{60}/PPI composite film 69
4.4 PPI-assisted unidirectional assembly of C_{60} crystals with highly anisotropic elongation 72
4.5 Molecular weight effects of PPI on C_{60} crystals anisotropic assembly 73
4.6 Ultralong fiber formation of C_{60} crystals and anisotropic assemblies of other organic building blocks 75
4.7 Side chain effects of PPI on C_{60} crystals anisotropic assembly 78
4.8 Plausible mechanism for C_{60} ultralong whisker and fiber formation 79
4.9 Photo-regulated control over C_{60} crystallization 81
4.10 Inorganic iron-oxide nanoparticle clusters into unidirectional assembly 82
4.11 Conclusion and perspective 84
References 84
Experimental 87

Chapter 5: Toward helix-sense-selective living polymerization in cholesteric liquid crystalline medium for highly stereoregular helical poly(phenyl isocyanide)s

5.1	Abstract	.....	95
5.2	Introduction	.....	95
5.3	Preparation of polymerization system in CLC	.....	96
5.4	Asymmetric living polymerization nature in CLC	.....	97
5.5	Conclusion and perspective	.....	98
	References	.....	98
	Experimental	.....	99

Chapter 6: Conclusion and prospects 102

List of publications 103

List of awards 103

List of grants 104

Chapter 1: General introduction

1.1 Brief history of synthetic helical polymers and polyisocyanides

Inspired by the beautiful and elaborated helical structure of biomolecules such as DNA and proteins, many researchers, especially chemists, have been attempting to create novel helical structures that are similar or superior to the helical biomolecules in an artificial way. First historical example is isotactic polypropylene, synthesized by G. Natta et al. in 1955[1]. They successfully confirmed that isotactic polypropylene form helical structure in crystalline state. However, this polymer cannot maintain helical form in solution resulting in the random-coil structure. At that time, no helical polymers can form stable helical structure in solution state.

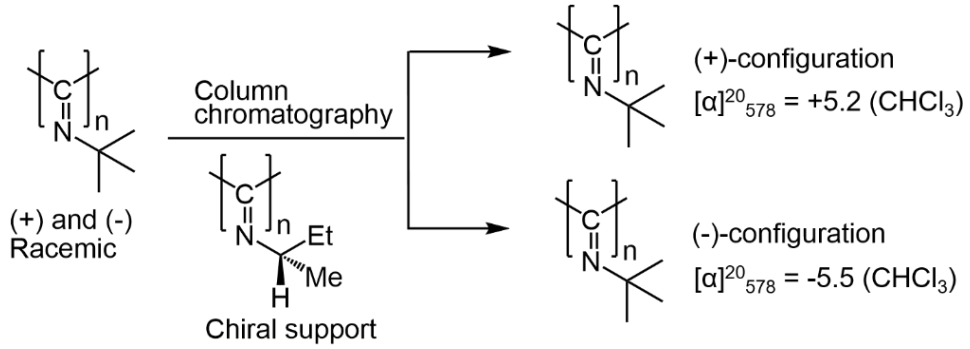

Figure 1.1. Optical resolution of poly(*tert*-butylisocyanide) into right- and left-handed helices.

Later in 1974, Drench and Nolte et al. reported on the optical resolution of helical poly(*tert*-butylisocyanide) into right- and left-handed counterparts[2] (**Figure 1.1)**. The hypothesis for the existence of a non-racemic helical conformation in poly(isocyanide)s was first suggested by Millich[3]. Drench and Nolte et al. demonstrated for the first time that the helical polymer with bulky substituents form stable helix not only in solid state but also in solution state in common organic solvents. Poly(*tert*-butylisocyanide) falls into static helical polymer since it maintains helical form even at high temperature, indicating it possesses high helix inversion barrier.

In 1979 and 1980, Okamoto et al. reported for the first time on the practical chiral application: chiral stationary phase for optical resolution[4,5]. They synthesized completely one-handed helical poly(methacrylic acid triphenylmethyl ester) by asymmetric anion polymerization in the presence of chiral ligands. The bulky triphenylmethyl substituent stabilizes the helical structure by steric repulsion between the repeating units. His developed chiral stationary phase for high performance liquid chromatography (HPLC) using poly(methacrylic acid triphenylmethyl ester) or naturally derived polysaccharides, like cellulose and amylose, is now commercially available and widely used in optical resolution of synthetic medicines as well as basic research.

M. M Green et al.[6-10] and Fujiki et al.[11] experimentally demonstrated the helical structures of polyisocyanate and polysilane. M. M. Green proposed basic concepts on the chiral-amplification mechanism: majority rule and sergeant-soldier effect. He revealed the non-linear chiral amplifications in helical polymers. Now these concepts are applicable to supramolecular chiralities.

1.2 Representative helical polymers and helix inversion barrier

Synthetic helical polymers are categorized into two class of helical polymers according to the criteria of helix inversion barriers: static and dynamic helical polymers[12]. The helical inversion occurs when the external stimuli such as heat and interaction with additives gives the energy enough to overcome the energy of the helical inversion barrier. The helix inversion is largely dependent on the bulkiness of the side chains and stiffness of polymer backbone. Examples (**Figure 1.2**) are poly(methacrylate)s, polyisocyanides, polychloral, poly(quinoxaline-2,3-diyl)s, polycarbodiimides, polyacetylenes, polyisocyanates, polysilanes. There have been substantial studies on control over helical senses, helical pitches, stiffness of the polymer backbone.

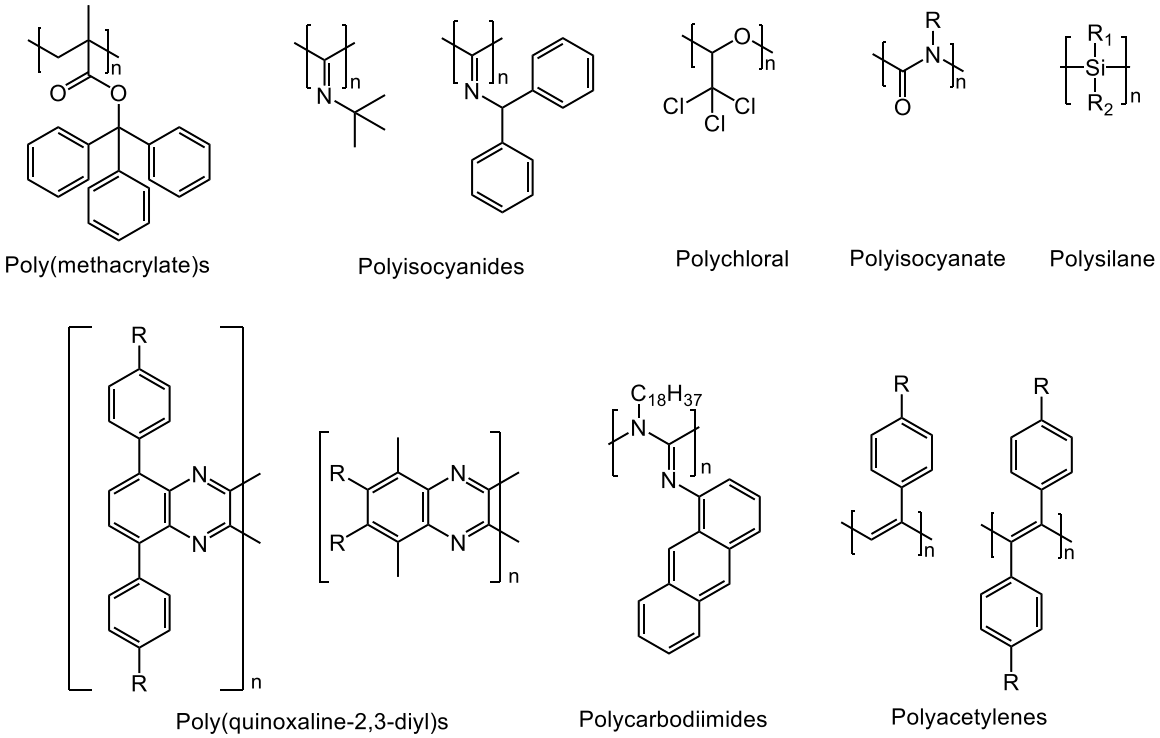

Figure 1.2. Representative examples of synthetic helical polymers.

1.3 Natural helical biopolymers in biological system

Helical structures are often seen in biological systems. In living cells of our body, there exist various kinds of helical biomolecules, such as proteins, nucleic acids and complex sugars in very condensed state (up to 400 grams per litre). Helical biopolymers such as double-stranded DNA[13], triple-stranded collagen[14], and bacteria phage virus[15] form rod-shaped structure arising from the stiff helical backbones. The efficiency of biochemical reactions and folding behavior of proteins confined in cells are much different from those in dilute solution conditions, which is called “macromolecular crowding” effect[16]. This condensed aqueous solution is confined by the cell wall composed of lipid bilayer with the liquid-crystalline like lamellae structure. In such condensed phase, enzymes and ribosome possess vital roles of production of chiral biopolymers with accurately-controlled molecular weight and helical senses utilizing an asymmetric environment.

1.4 Synthesis of isocyanide

The brief summary of synthesis of isocyanide, which is also called isonitrile, or iminomethylene, is described here. Historically Hoffmann reaction[17,18] was first developed for the convenient methods to synthesize isocyanides (**Figure 1.3**). In Hoffmann reaction, $CHCl_3$ was used. This reaction allows for the direct access to isocyanide from amines using chloroform and sodium hydrate. However, the yield is not so satisfactory and many by-products that should be eliminated are expected.

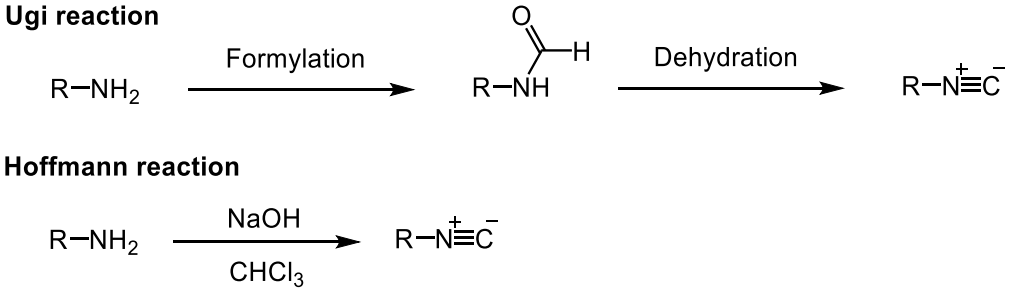

Figure 1.3. Ugi reaction and Hoffmann reaction.

For the synthesis of isocyanides, Ugi reaction[19-21] is standard protocol and has been frequently used for a long time because this reaction can be applied to the reaction of both *N*-aryl-formamide and *N*-alkyl counterparts with various substituents (**Figure 1.3**). On dehydration process, however, acyl halides of group IV–VI elements like triphosgene and phosphoryl chloride are required in the presence of base. These dehydration reagents are extremely harmful and toxic, and the use of them is restricted to some extent in some countries. Recently, Wang et al. found that the combination of PPh_3/I_2 has an effective dehydration ability for formyl amides to afford the corresponding isocyanides in the presence of tertiary amine like triethylamine[22] (**Figure 1.4**). This PPh_3 and I_2 combination is advantageous over phosgene reagents because of less toxicity and inexpensive. Furthermore, this reaction can be carried out at ambient in open flask condition. This reaction was adopted in *Chapter 5*.

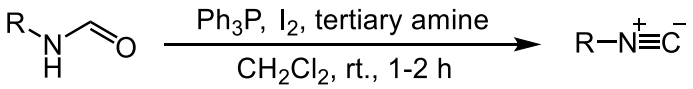

Figure 1.4. Ph_3P/I_2 dehydration reaction of formyl amide.

1.5 Common synthetic scheme for phenyl isocyanide

For the synthesis of aryl isocyanide monomers, the below reaction scheme (**Scheme 1.1**) is usually employed. First reaction is introduction of side chain group by Steglich esterification. In second step, reduction by H_2 gas in the presence of Pd/C catalyst proceeds almost quantitatively. In third and fourth reactions are Ugi reactions, that is, formylation and dehydration reactions. Nitrobenzene derivatives are often the starting materials because they are easily accessible and inexpensive.

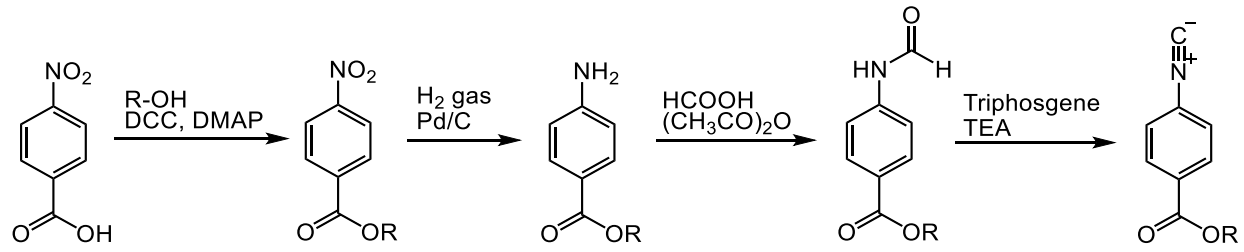

Scheme 1.1

In **Scheme 1.1**, use of hydrogen gas is required for reduction of nitrobenzene derivative in the presence of Pd/C catalyst, which has potential to explode in the dried state. In **Scheme 1.2**, to avoid the reduction reaction, aniline derivatives are employed as the starting materials as alternative scheme. The potential drawback of this scheme is the insolubility of formyl amide derivatives in common organic solvents, but soluble in high-temperature polar solvent like DMF. This reaction is adopted in *Chapter 2*.

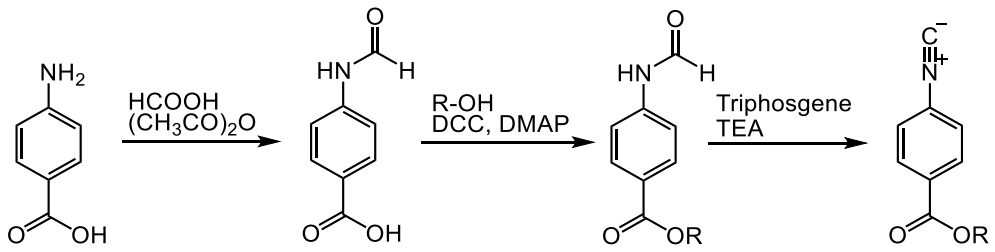

Scheme 1.2

For the synthesis of poly(aryl isocyanide)s, the preparation of various isocyanide monomers with different side chains is desired for the systematic investigation of side chain effect and self-assembly behavior. Traditionally, the introduction of side chains is usually carried out in the early stage in synthetic schemes. This would be troublesome because the synthesis of one isocyanide monomer with one side chain requires at least 2-step reactions. For example, if a chiral side alkyl alcohol is introduced to 4-nitro-benzoic acid, more 4 steps (esterification-reduction-formylation-dehydration) are required to isocyanide monomers. To resolve this time-consuming problem and huge synthetic manipulation, Su et al. reported the alternative approach for the synthesis of isocyanide monomers with various side chains using transesterification reaction from activated-ester isocyanides[23,24] (**Scheme 1.3**). This method is often utilized for the synthesis of synthetic oligopeptides. They first synthesized pentafluorophenyl-ester substituted isocyanide and then, introduced various alkyl alcohols and alkylamines vis transesterification. This transesterification reaction proceeds quantitively in the presence of DMAP and triethylamine. Furthermore, they demonstrated a facile synthetic route to stereoregular helical poly (phenyl isocyanide)s with various pendants through the transesterification reaction and living polymerization by Pd-ethynyl complex in one-pot. Usually, helical polymers bearing functional pendants can be synthesized through the directed polymerization monomers bearing desired functional group or post-modification after polymerization. Their method is advantageous for the preparation of various poly(aryl isocyanide)s with different pendants. This reaction is adopted in *Chapter 3.*

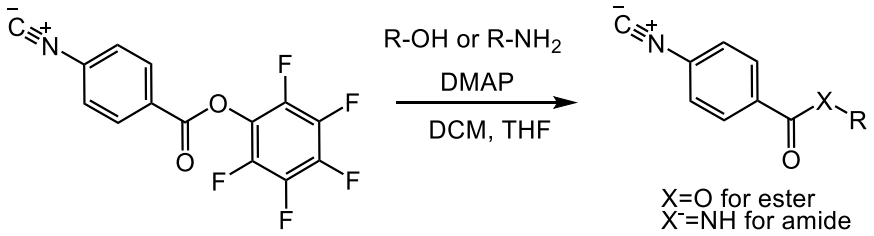

Scheme 1.3

1.6 Polyphenylisocyanide

Polyisocyanide, which used to be called poly(iminomethylene) or poly(isonitrile), is a class of synthetic helical polymers with main chain helicity. Precise synthesis of PPIs has been well-established, and the monomers can be polymerized in a living manner using Ni, Pd, and Rh catalysts. When PPIs possess sufficiently bulky substituents, the PPI main chain can twist in one direction by steric repulsion between repeating units, which results in the formation of helical structures. Such PPIs can form stable helices not only in the solid state but also in solution state. Furthermore, PPI is classified as a stiff rod-shaped helical polymer because of its very long persistence length (ca. 30 - 220 nm). Owing to the resultant 1D structural anisotropy, PPIs exhibit lyotropic liquid crystallinity in concentrated solution, leading to liquid crystal-like structural formation in the solid state through the solvent drying process. Achiral isocyanide monomers are considered polymerized into racemic helical polymers (equimolar of right (*P*) - and left (*M*) -handed helicity). Since PPIs has the unique chiral functionalities originating from one-handed helical motif of the PPI backbone by introducing chiral side chains, many application-oriented researches have been carried out such as chiral sensor, chiral stationary phase, and asymmetric catalysts. The synthesis and characterization of polyisocyanide are well documented the comprehensive reviews[25-28]. Followings are the brief descriptions of history of polyisocyanides and interesting optical properties and self-assembly structures.

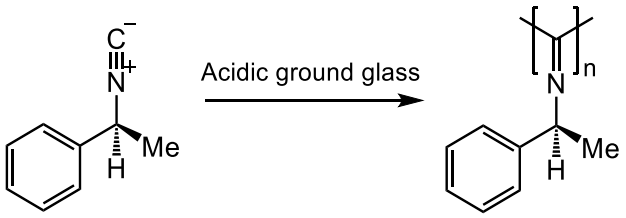

Figure 1.5. Acid-coated ground glass-initiated polymerization of optically active isocyanide by Millich.

In early stage, the polymerization of isocyanides was carried out by protonic acid or Lewis acid via cationic mechanism. In 1960s, Millich et al. carried out polymerization of optically pure (*D)*- and (*L)*-phenylethyl isocyanide in the presence of an acidic ground glass catalyst[3] (**Figure 1.5**). Stackman[29] and Yamamoto[30] also reported the polymerization of isocyanides by BF_3. Recently in 2005, Cornelissen[31] group reported the trifluoro acetic acid (TFA)-initiated polymerization of isocyanopeptides.

After the cationic mechanism was developed, the coordination-insertion mechanism using late transition metal (Ni, Pd, Rh, etc.) catalyst was proposed. Nolte et al. systematically investigated Ni(II) catalytic activities and found that Ni(II) salts, $NiCl{\cdot}6H_2O$, $Ni(acac)_2$, $Ni(ClO_4){\cdot}6H_2O$ are excellent catalysts for the polymerization of isocyanide. Ni(II)

salts have been the most common polymerization catalyst for isocyanides. For the polymerization mechanism by Ni catalyst, "merry-go-round" was proposed by Nolte[32] (**Figure 1.6**). First, Ni(II) forms tetra-coordination of four isocyanide ligands. Nucleophiles like amine or alcohol attack the Ni center to form three isocyanide ligands and a carbene-like ligand. The activated carbon attacks the neighboring carbon of isocyanide, where the direction of propagation is determined by steric repulsion of the substituents of the isocyanide when the substituents are suffiently bulky. This reaction continued after the successive insertion of isocyanides to Ni center.

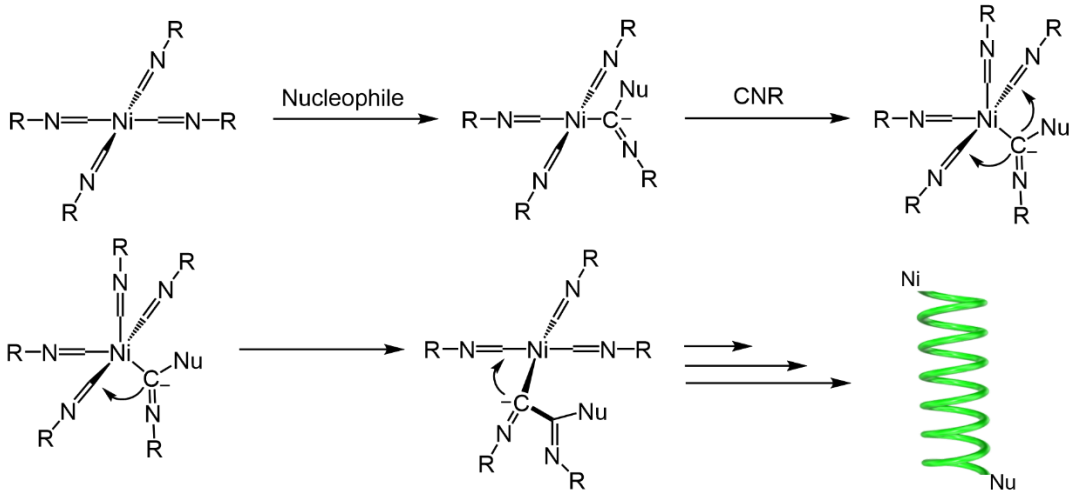

Figure 1.6. "Merry-go-round" mechanism for Ni catalyst-initiated polymerization of isocyanides.

Very recently, Yan et al. reported on novel polymerization method for isocyanide through carbocationic polymerization mechanism using $[Ph_3C][B(C_6F_5)_4]$ catalyst[33]. This metal free catalyst is alternative attractive method because the no metal residue is expected after polymerization. Generally, the metal residue often degrades the physical properties of polyisocyanides and prevents the potential use for biological applications. In this context, novel metal-free catalyst, which has comparable catalytic activity to metal catalysts, for the synthesis of polyisocyanide is desired for future advanced applications.

1.7 Living polymerization of isocyanides

Living polymerization is chain-growth polymerization, where the termini of the polymer propagating end is "living", meaning that chain termination and chain transfer reactions are eliminated in the system. In many cases for living polymerization system, the rate of initiation reaction is faster than that of chain propagation reaction. Compared to other polymerization methods, living polymerization affords polymers possessing very narrow polydispersity ($M_w/M_n \leq 1.1$). The recent advancement in synthetic protocol for living polymerization gives access to controlled molecular weight, narrowly dispersed polyisocyanide with defined pendants. The resulting polymers have well-defined physical and optical properties suitable for analysis, where the effects from the length distribution are quite small. Usually for achievement of living polymerization, the choice of catalyst is important factor to determine the polymer property. As for poly(phenyl isocyade)s, typically five kinds of isocyanide monomer structure have been reported (**Figure 1.7**). In many cases, electron-withdrawing ester *p*-substituted phenyl isocyanides are adopted as

first choice because of easy to synthesize and polymerize. This electron-poor phenyl isocyanide is relatively active for polymerization, where many catalysts can be adopted. Contrary, electron-rich phenyl isocyanides, such as alkyl, ether, amine substituted isocyanides, are usually challenging monomers because they are difficult to polymerize with controlled manner by common catalysts, especially phenyl isocyanide with high electro-donating ether pendant. More challengingly, sterically-hindered, especially ortho-substituted phenyl isocyanides are hard to polymerize with common Ni and Pd catalysts except for a few examples.

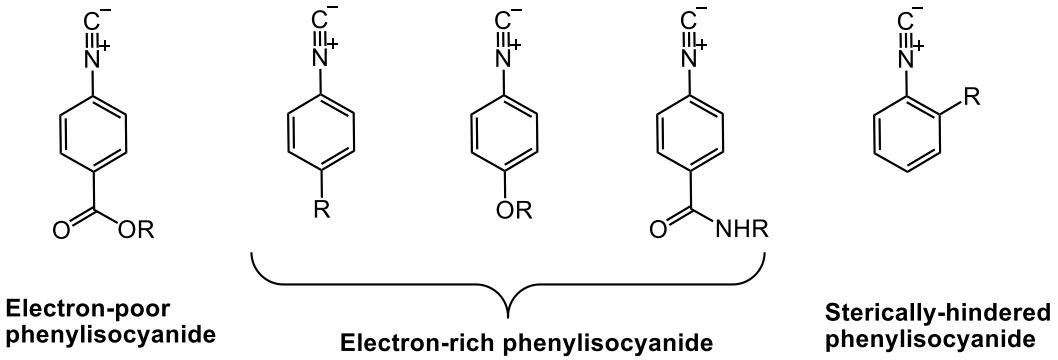

Figure 1.7. Different types of phenyl isocyanide monomers.

Here, representative living polymerization catalysts for polyisocyanides, mainly for poly(phenyl isocyanide)s, are presented. Key criteria for polymerization of isocyanides are followings: affordable high molecular weight and narrow polydispersity, polymerization speed/reactivity, stability in air, scope of monomer structure, chiral selectivity, stereoregularity. In general, polyisocyanides are mainly synthesized by the late-transition metals like Ni, Pd, Rh, and even Co. Followings are the representative living late-transition metal catalyst through the coordination-insertion mechanism. Characteristic properties of Ni, Pd, and Rh catalysts are summarized in **Table 1.1**.

Table 1.1. Typical catalytic properties for poly(phenyl isocyanide)s of Ni, Pd, and Rh living catalysts.

Catalyst	Condition	Stereoregularity	Affordable M_n	Notes
Ni	Usually at rt.	Medium	High	- weak for electron-rich, sterically-
	(for min to few hrs)	(moderate $\Delta\varepsilon$)	(up to ~500 kDa)	hindered phenyl isocyanides
Pd	at 55°C or THF reflux	High	Medium	- weak for electron-rich, sterically-
	(for ~6 -12 h)	(high $\Delta\varepsilon$)	(up to ~50 kDa)	hindered phenyl isocyanides
Rh/PPh_3*	at rt.	Medium	Medium	- tolerant for sterically-hindered
			(up to ~38 kDa**)	isocyanides

$\Delta\varepsilon$: mole *PPh_3 is needed as cocatalyst. ** for ortho-substituted phenyl isocyanide.

In 1990s, living polymerization for isocyanides was first developed using Ni complexes. Deming and Novak et al. reported for the first time that Ni allyl complexes showed living character in the polymerization of isocyanides[34,35] (**Figure 1.8 (1)**). Iyoda group demonstrated that aniline-adduct Ni tetra-coordinated catalyst initiate the living polymerization[36] (**Figure 1.8 (2)**). Suginome et al. reported that aryl Ni complex possess excellent ability to afford

poly(aryl isocyanide)s and poly(quinoxaline-2,3-diyl)s with controlled molecular weight and very narrow polydispersity[37] (**Figure 1.8 (3)**). Very recently, phosphine-chelated Ni aryl complex has exceptionally versatility for living polymerization of challenging isocyanide monomers such electron-rich and sterically-hindered isocyanide monomers[38] (**Figure 1.8 (4)**). Since Ni is abundant source from earth and quite air-stable, it is the first choice to polymerize isocyanide. However, stereoregularity and resulting chiroptical properties are often inferior to that prepared by Pd complexes. The as-prepared polyisocyanides form kinetically favored helical structure and not thermodynamically favored complete one-handed helical backbones. To induce the thermodynamically stable state, thermal annealing is required for a long time (e.g. toluene 100°C for 12 days for poly(aryl isocyanide) with amide pendant) because of high helical inversion barrier of polyisocyanide.

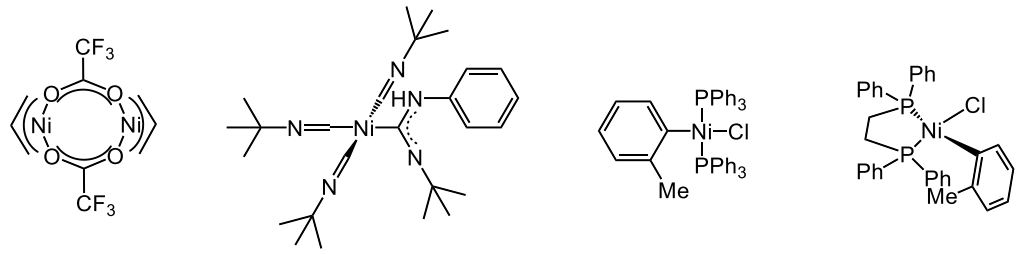

1 2 3 4

Figure 1.8. Ni catalysts reported for living polymerization of isocyanides.

Pd-Pt μ-ethynediyl dinuclear complexes have been developed for living polymerization of aryl isocyanides. Takahashi, Onitsuka et al. reported Pt-Pd dinuclear ethynyl complexes afford high stereoregular helical poly(aryl isocyanide)s in refluxed THF condition[39] (**Figure 1.9 (1)**). Although this catalyst is not active for polymerization of alkyl isocyanide, it affords high-helix-selective polymerization of aryl isocyanide. However, this excellent initiator has some drawbacks: very difficult to synthesize and unstable in air. Wu et al. have reported that a family of novel air-stable alkyne-Pd(II) mono-nuclear complexes that shows living character. The Pd-ethynyl complex[40] (**Figure 1.9 (2)**) is easy to synthesize by Sonogashira coupling and quite stable in air, which allows for the living polymerization of the electron-rich phenyl isocyanides but cannot initiate electron-rich and sterically-hindered aryl isocyanides. They further demonstrated that the Pd-diethynyl complex[41] (**Figure 1.9 (3)**) is tolerant to a wide range of isocyanide monomers including alkyl and phenyl isocyanides and even sterically hindered ortho-substituted aryl isocyanide, although 4 steps are required to synthesize it and the diacetylene precursor is very unstable in air. In general, polymerization in refluxing THF in the presence of Pd complex initiator yield polyisocyanide with higher stereoregularity and higher helix-selectivity during polymerization compared to that prepared by Ni catalyst.

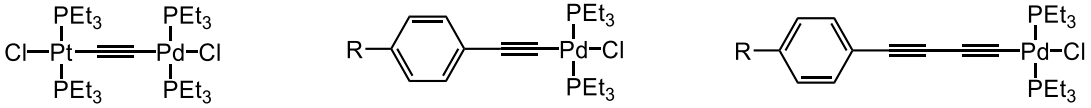

1 2 3

Figure 1.9. Pd catalysts reported for living polymerization of isocyanides.

Wu et al. reported that facile preparation of poly(aryl isocyanide)s with various side chains in one-pot reaction using ester-activated aryl isocyanide monomer and ethynyl-Pd mono-nuclear initiator[24] (**Figure 1.10**). They postulated that trans-esterification occurs before the living polymerization proceeds. This one-pot living polymerization accompanying simultaneous side chain modification gives access to wide variety of poly(phenyl isocyanide)s in the very convenient method.

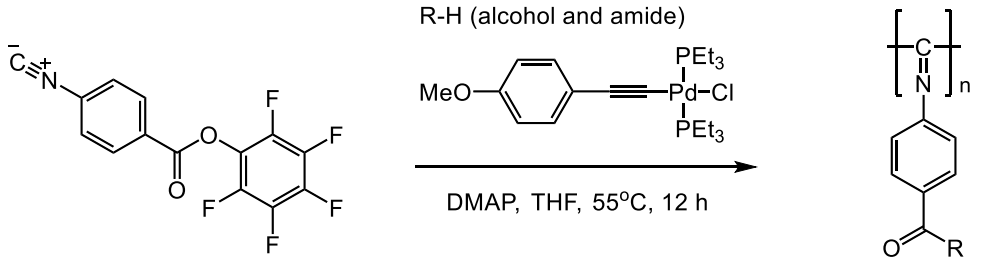

Figure 1.10. One-pot synthesis of poly(aryl isocyanide)s with various pendant from activated-ester aryl isocyanide.

Although the steric effect from substituent has significant on the formation of helical structure, there had been challenging issues on the synthesis of sterically hindered ortho-substituted poly(aryl isocyanide)s. Onitsuka and Takahashi et al. have developed Rh complex for living polymerization of sterically hindered aryl isocyanide[42] (**Figure 1.11**). This catalyst proceeds living polymerization in the presence of PPh_3, indicating high tolerance for steric hinderance at *ortho*-position of phenyl isocyanide monomers.

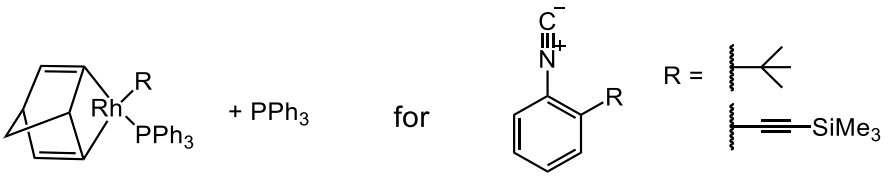

Figure 1.11. Rh catalyst reported for living polymerization of ortho-substituted phenyl isocyanides.

1.8 Block copolymerization of isocyanides with other type of polymers

There have been substantial interests in developing multi-functional polymers. Recent advancements in precise polymerization methods give access to block copolymer and multi-block copolymers, graft polymers, brush-polymers, and star-shaped polymers using living polymerization methods. Herein recent advancement in block copolymer containing polyisocyanide block is described.

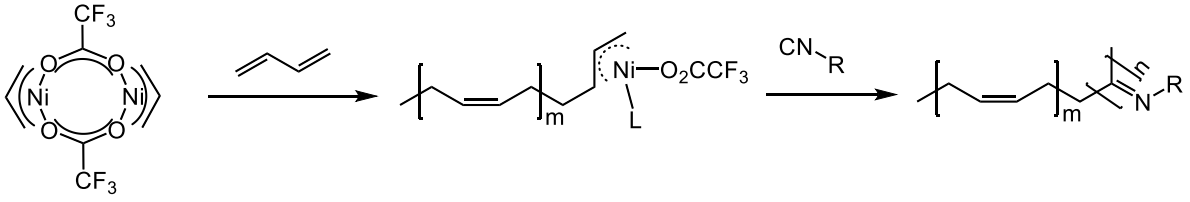

Figure 1.12. Block copolymerization using Ni single catalyst with two mechanistically distinct manner.

First report on synthesis of block copolymer containing polyisocyanide block is disclosed by Deming and Novak[43] (**Figure 1.12**). They demonstrated that the block copolymerization of polyisocyanide with other polymer (polybutadiene) using living Ni catalyst. The interesting point is that although the block copolymerization proceeds with single Ni catalyst, polymerization mechanism of butadiene and isocyanide is mechanistically distinct. The key point is probably the living chain end of poly(butadiene).

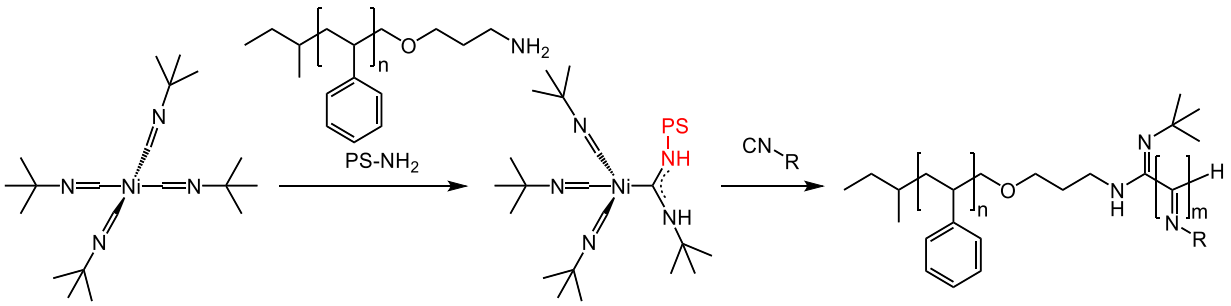

Figure 1.13. Block copolymerization via amine-adduct Ni complex formation.

Block copolymer containing polyisocyanide block in the block copolymer architecture for the construction of superstructures was developed by Cornelissen and Nolte group[44] (**Figure 1.13**). They first strategically prepared amine-terminated polystyrene segment. It attacks the Ni center to form carbene-like structure, which initiates the polymerization of isocyanides. They successfully prepared helical superstructures by utilizing amphiphilicity of the resulting block copolymers. The helical sense of the helical bundles can be controlled by the helical sense of the poly(isocyanopeptides) segment. Müllen[45] group also employed this methodology to prepare spherical nanoparticles with stimuli responsiveness from poly(ethylene glycol)-*b*-poly(isocyanopeptides) copolymers.

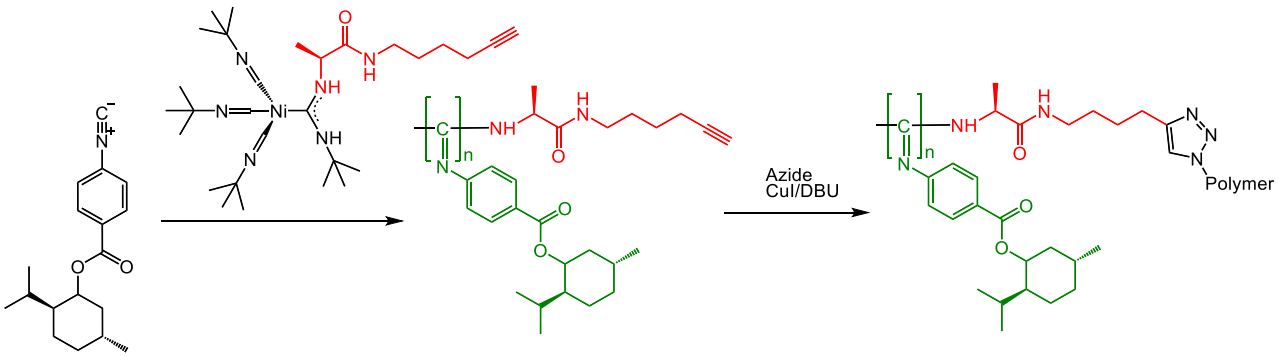

Figure 1.14. Block copolymerization by azide-alkyne reaction.

Recently click-chemistry has evolved in the last decade. Among them, azide-alkyne Cu click reaction and thiol/ene or /yne reaction are often utilized in polymer chemistry. Weck group designed and prepared alkyne segment-containing amine-adduct Ni initiator, which initiated the polymerization of enantiopure isocyanide[46] (**Figure 1.14**). The resulting polyisocyanide possesses the alkyne segment in the chain end. This alkyne chain end can subject to azide-alkyne reaction with azide-termini functionalized polymers to afford the corresponding block copolymers

quantitatively. This methodology is now widely used to synthesize various block copolymers.

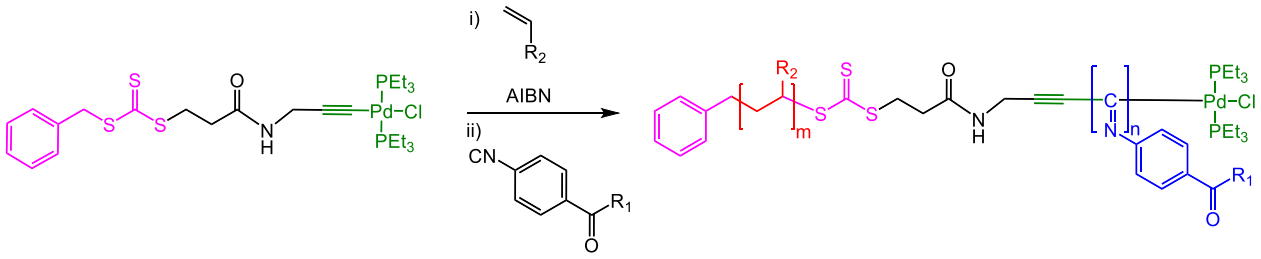

Figure 1.15. Block copolymerization using bi-functional polymerization initiator.

Bi-functional living polymerization catalysts for polyisocyanides and other polymers have been developed by Wu et al. For example, they prepared bi-functional catalyst that possess initiation ability of coordination-insertion polymerization of isocyanides and reversible addition fragmentation chain transfer (RAFT) polymerization of styrenes[47] (**Figure 1.15**). They successfully demonstrate the living block copolymerization of polystyrene block and polyisocyanide block from the same catalyst. They also prepared catalysts that possess ring-opening metathesis polymerization (ROMP) and living polymerization of isocyanides.

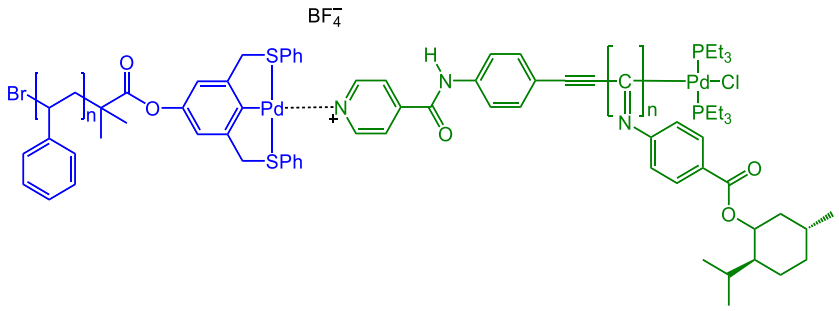

Figure 1.16. Supramolecular block copolymerization using coordination bonding.

Supramolecular concept for the construction of block copolymers using non-covalent bonding between polyisocyanide segment and other polymer block has been developed by Weck et al. They strategically designed living catalyst possessing functional group for Pd or pyridine-terminated polymer blocks. They employed coordination bonding between Pd and N atoms in pyridine moiety to form supramolecular block copolymers[48]. The secondary structure of the supramolecular block copolymers was also investigated (**Figure 1.16**).

In 2010, Wu and Bielawski et al. reported on one-pot synthesis of poly(3-alkylthiophene)-*block*-poly(aryl isocyanide) by two sequential, mechanistically distinct polymerizations using single Ni(dppp)Cl_2 catalyst[49] (**Figure 1.17**). First, Ni-terminated poly(3-alkylthiophene) is prepared by Kumada catalyst-transfer (or called Grignard metathesis reaction) from dibromo(3-alkylthiophene) in quisi-living manner. This macroinitiator initiate the living polymerization of aryl isocyanide in the same flask to afford the corresponding poly(3-alkylthiophene)-*block*-poly(aryl isocyanide) copolymers. They have reported on a variety of morphologies of polythiophene-*block*-

polyphenylisocyanide derivatives that form nanofibril, micelle and vesicle in a mixture of good and poor solvents and its pH-responsiveness. In addition to Ni-terminated polythiophene, Ni-terminated poly(2,5-dialcoxyphenylene) and poly(*N*-alkyl pyrrole) prepared by the same Kumada catalyst transfer reaction initiate the living polymerization of *N*-aryl isocyanide and *N*-alkyliscyanide in one-pot system[50]. Because of intrinsic semiconducting nature of conjugated polymers, the resulting block copolymers exhibit multi-responsive chromic properties in visible wavelength range. This synthetic scheme is adopted in *Chapter 2 and 3*.

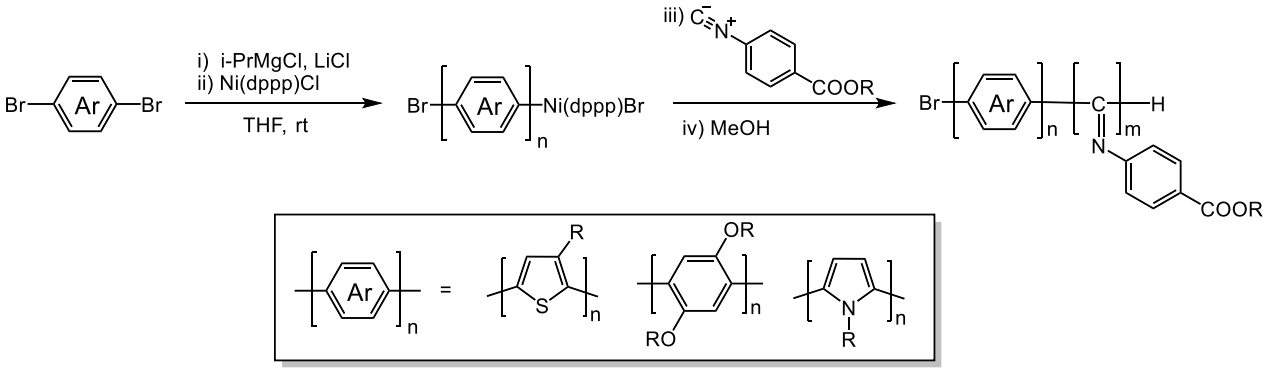

Figure 1.17. Ni-terminated macroinitiators for living polymerization of isocyanides.

They applied this methodology to the synthesis of poly (phenyleneethynylene)-*block*-polyisocyanide copolymer using ethynyl Pd complex initiator[51]. The ethynyl-Pd complex allows for the Sonogashira coupling for poly (phenyleneethynylene) in living manner, and then Pd-terminated poly (phenyleneethynylene) initiate the living polymerization of aryl isocyanide in refluxed THF (**Figure 1.18**). This methodology could be combined with other cross-coupling reactions using Pd catalyst such as Suzuki-Miyaura, Negishi, Heck coupling reactions.

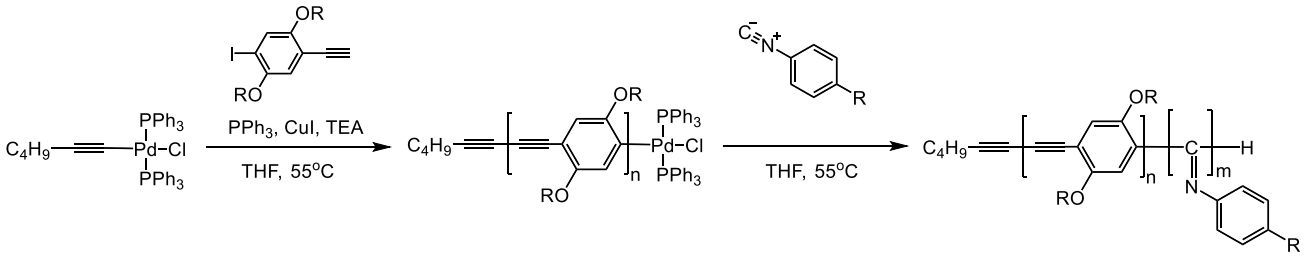

Figure 1.18. Pd-terminated macroinitiators for living polymerization of isocyanides.

To further obtain the insight into the helical formation, investigation on chiral-selective polymerization process is desired. In 2000, Takei et al. reported that screw-sense-selective polymerization of enantiomerically pure *m*- and *p*-menthoxycarbonylphenyl isocyanides from chiral oligomers (30mers) initiated by Pd-Pt μ-ethynediyl dinuclear complex[52]. They found out that pheynylisocyanide with bulky substituents are polymerized in screw-sense-selective living manner from chiral oligo-initiator, whereas hexylisocyanide with less bulky substituents are polymerized in non-chiral selective manner. Later in 2009, Wu and Yashima et. al. reported on helix-selective-polymerization of enantiomerically pure phenyl isocyanide bearing an *L*-alanine pendant with a long n-decyl chain[53] (**Figure 1.19**).

They demonstrated that Pd-Pt μ-ethynediyl dinuclear complex initiate the living polymerization of enantiomerically pure phenyl isocyanide bearing an *L*-alanine pendant with a long n-decyl chain to afford the diastereomeric mixture of major product, high molecular weight (*M*)-helix, and minor, low molecular weight (*P*)-helix. This diastereomeric mixture can be fractionated by acetone solvent. The purified complete one-handed helical polyisocyanides can promote subsequent polymerization of isocyanide (block copolymerization). (*M*)-Helical macroinitiator efficiently initiate the polymerization of isocyanide with *L*-alanine pendant compared to that with *D*-alanine pendant (vice versa). This chiral selective recognition in helix-sense-selective polymerization is probably enhanced to some extent by the intermolecular hydrogen bonding between enantiomerically pure isocyanide and helical sense of macroinitiator.

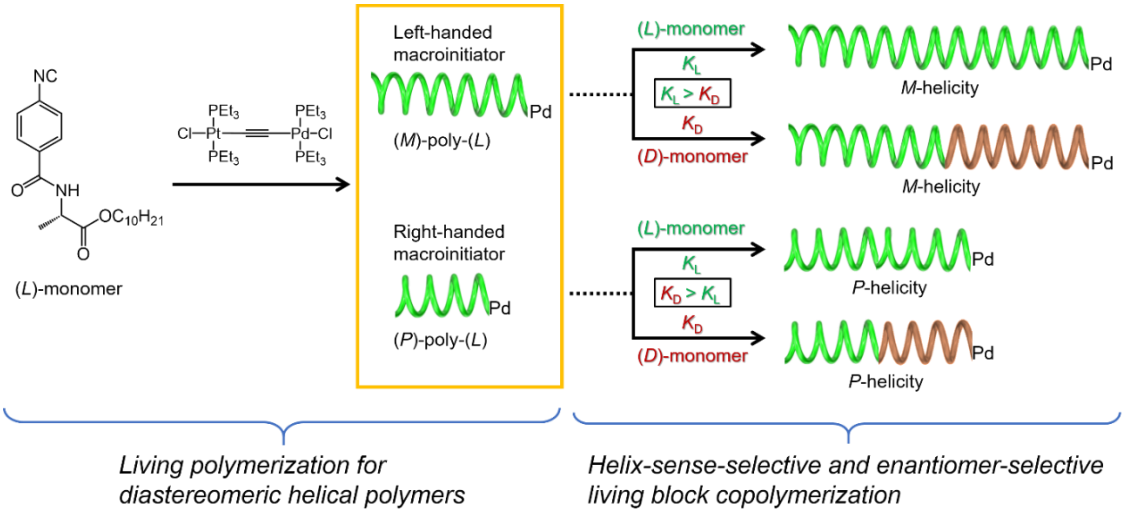

Figure 1.19. Helix-sense-selective and enantiomer-selective polymerization from single-handed macroinitiator.

Very recently, Lee et al. reported on very fast living polymerization in only 1 min for synthesis of pentablock polyisocyanide block copolymers using o-tol(dppe)NiCl[54] (**Figure 1.20**). This Ni catalyst has broad monomer scope including electron-poor, electron-rich, and sterically-hindered phenyl isocyanides. This fast polymerization methodology will offer the more and wide opportunities for facile preparation of multi-functional multi-block copolymers.

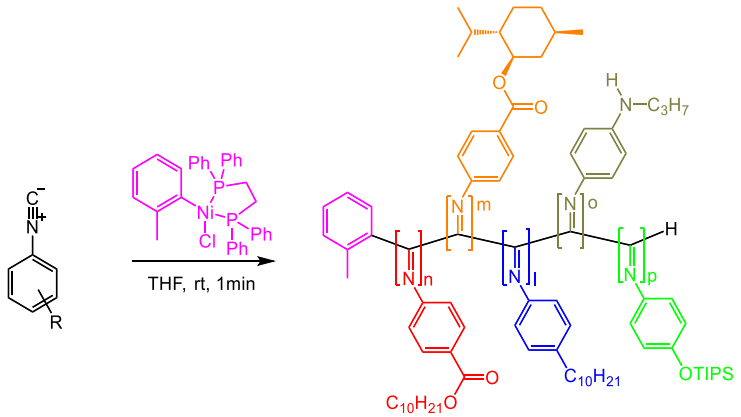

Figure 1.20. Penta-block copolymerization in only 1 min using o-tol(dppe)NiCl.

1.9 Helical structures of polyisocyanides

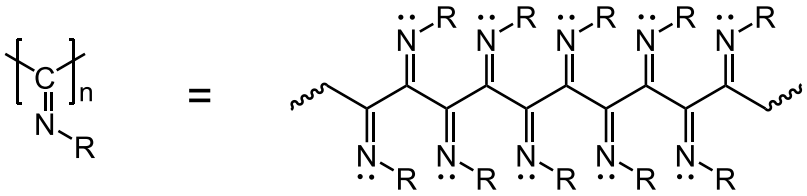

Figure 1.21. Electronic repulsion vs steric effects.

Millich first postulated that polyisocyanides with bulky side group form 4-unit/1-turn (4/1) helical structure[3]. Later Nolte and Hoffman confirmed it experimentally and theoretically. Hoffmann claimed that the electronic repulsion between the lone pairs on N atoms forces the polyisocyanide backbone to adopt non-planar conformation. On the other hand, the steric repulsion between substituents also lead to the non-planar conformation when the substituents are sufficient bulky (**Figure 1.21**).

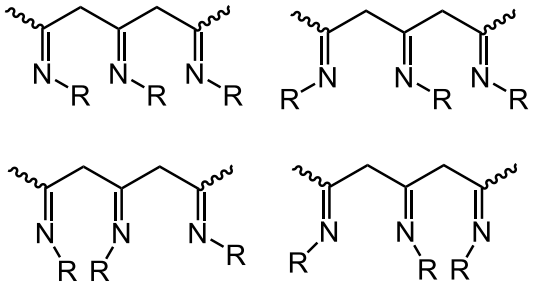

Figure 1.22. Syn-anti isomerization of imino (C=N) bond.

Green et. al. suggested that polyisocyanide can adopt irregular conformation, wherein the stereo-irregularity is arising from "syn-anti isomerization" of imino bonds[56] (**Figure 1.22**). This indicates that as-prepared polyisocyanide does not always form thermodynamically stable helical structure, instead, kinetically-trapped state with some irregular conformation in the helical backbone.

1.10 Determination of helical sense of polyisocyanide

Electronic circular dichroism (ECD) is a convenient and valid method to measure chiropticality of the intermolecular aggregates and interactions between molecules if the electronic transition is observable in typically UV-vis wavelength range[57]. Exciton chirality method is often utilized to determine the configuration and conformation of small molecules and supramolecular structures[58-60]. For chiral polyisocyanides, positive or negative peak at 365 nm arising from n-π* transition of imino (C=N) moiety in ECD is a key factor to determine the helical sense of poly(phenyl isocyanide)s helical backbones (**Figure 1.23**). As for chiral poly(phenyl isocyanide)s, the absorption and circular dichroism at 254 nm coming from phenyl moiety are also seen in UV-vis absorption and ECD spectroscopy.

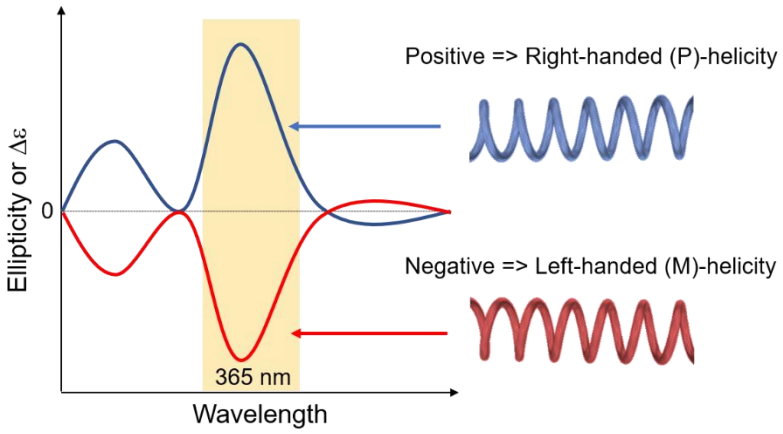

Figure 1.23. Typical CD spectra of predominantly single-handed poly(phenyl isocyanide)s.

Although the ECD method is robust method to determine the helical sense of polyisocyanide and polyphenylisocyanide, the absorption of imino moiety often overlaps with other absorption, which makes it difficult to quantitatively estimate the helicity. In this context, introduction of spectator chromophores into polyisocyanide helical backbone allows for the more pricese determination of helical senses of polyisocyanide backbone (**Figure 1.24**). Takahashi, Onitsuka et al[61] demonstrated that porphyrin moiety is very useful functional group to utilize the exciton chiral method because of very large extinction coefficient derived from the Soret band of porphyrin pendant. On the other hand, Nolte et al[62] synthesized poly(alkyl isocyanide) bearing diazo moiety as spectator chromophore with acid sensitiveness to determine the helical sense of poly (alkyl isocyanide).

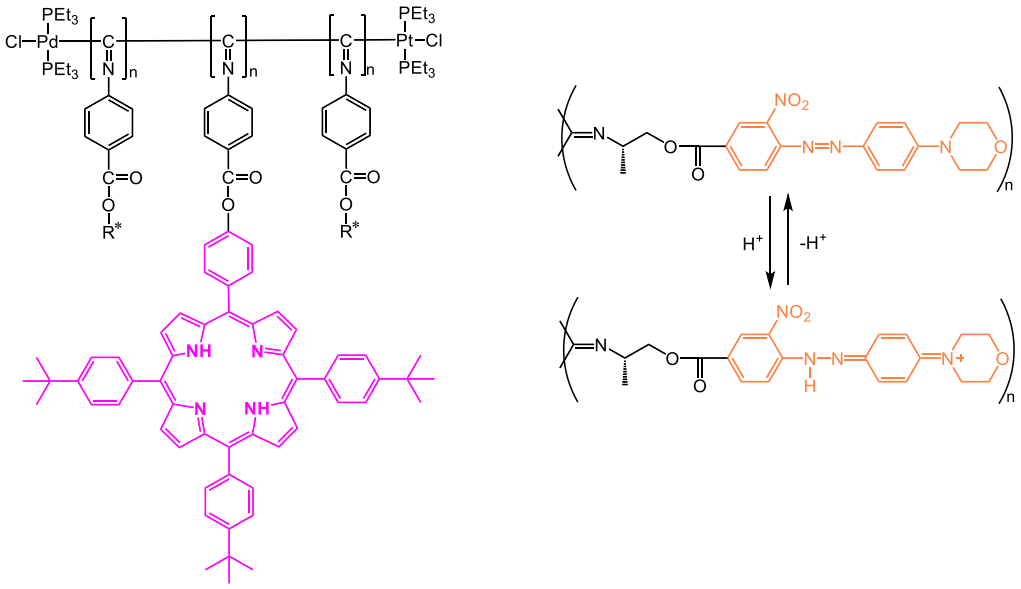

Figure 1.24. Spectator chromophore for determination of helical senses.

Helical pitch and helical sense of polyisocyanide can be determined by X-ray diffraction (XRD). Yashima et al precisely determined the helical structure of poly(phenyl isocyanide) bearing *n*-decyl alanine residue[63].

Recently, the direct observation of helical structure of each polymer using AFM made it possible to determine the helical senses[64]. Although the observation of helical structure of polyisocyanide molecules requires skilled experiences, the obtained AFM images are strong evidence in determination of helical pitches, helical angles and helical diameter and length.

Vibrational circular dichroism (VCD) is also valid way to help the understanding of the helical structures, which determine the helical configuration of molecular vibration modes[65-67].

1.11 Construction of preferred one-handed helical structure of polyisocyanide

Preferred single-handed helical polyisocyanides are usually prepared from chiral monomers or chiral initiators/catalysts. Followings are examples for chiral side chains of poly(phenyl isocyanide)s (**Figure 1.25**).

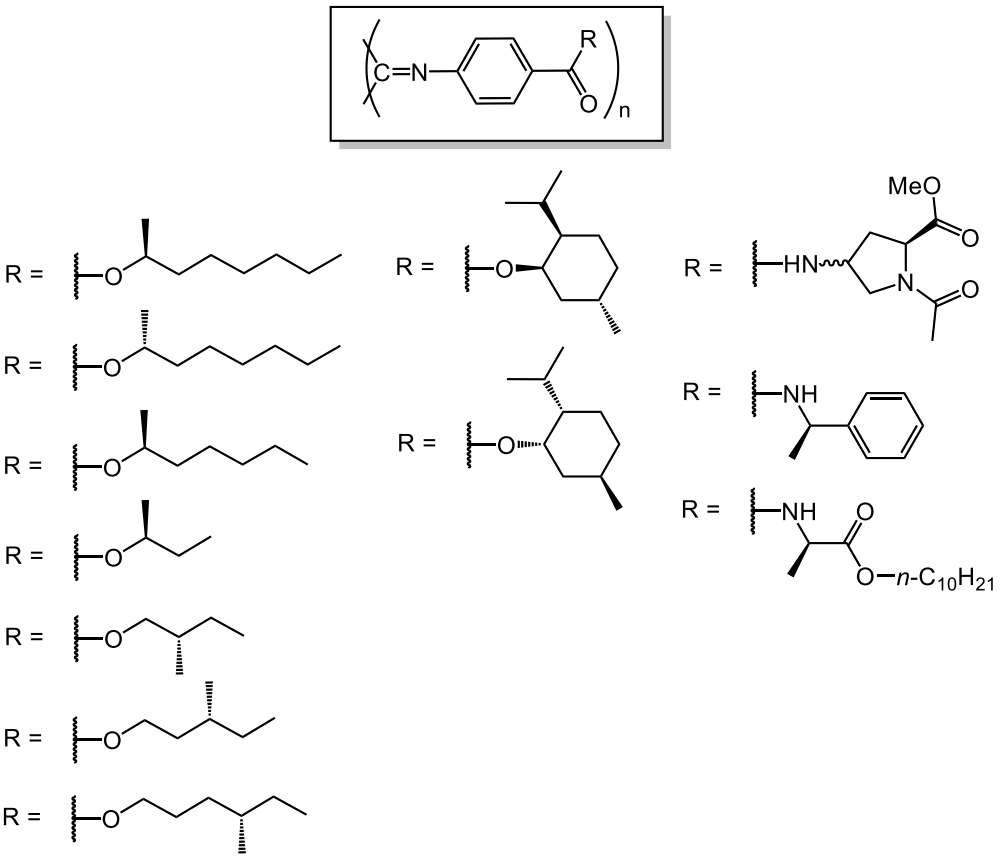

Figure 1.25. Representative examples of chiral substituents for poly(phenyl isocyanide).

Kajitani et al. reported on a series of optically active phenyl isocyanides bearing various amino acid residues such as L-alanine, L-alaninol, L- phenylalanine, and L-lactic acid with n-decyl alkyl chains[68]. Xu et al used proline as chiral source for construction of preferentially single-handed poly(phenyl isocyanide)[69].

Sergeant-soldier effect in polymerization process was investigated by Takahashi et al. They used chiral and achiral monomer with similar reactive level to randomly copolymerize[70]. They found out that the nonlinear positive effect was observed when the isocyanide with bulky substituent was used, which is consistent with the theory developed by M. M. Green et al (**Figure 1.26**).

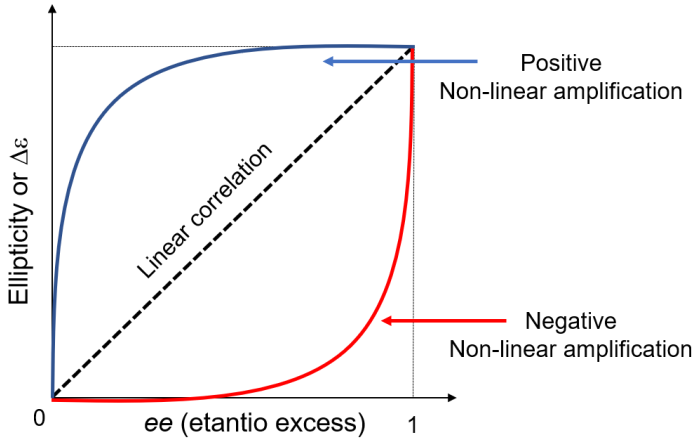

Figure 1.26. Typical chiral amplification correlation against enantio-excess (ee).

Nolte et al found that interesting chiral polymerization process when chiral and achiral monomers with different reactivity were used[71] (**Figure 1.27**). First, achiral monomers are polymerized into racemic mixture of (*M*) and (*P*)-helical polymers. However, once chiral monomers react with a polymerizing chain-end, the chiral unit-attached polymer become less reactive. As a result, chiral monomer unit suppress the polymerization of isocyanide whose helicity is not matched with chiral unit. This process can be called "chiral poisoning".

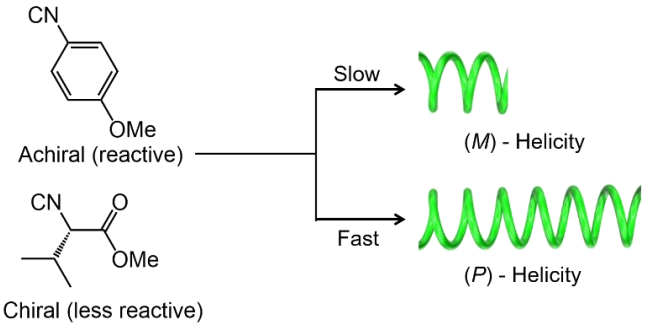

Figure 1.27. Helix-sense-selective polymerization in the presence of reactive achiral and less reactive chiral monomers.

Drench et al. demonstrated that the chiral selective polymerization in the presence of chiral amine using Ni catalyst[72]. Wu et al. demonstrated that helix-sense-selective polymerization of isocyanide using *L*- or *D*- lactide as additive in the presence of Pd complex initiator affords one-handed helical polyisocyanides[73]. The resulting polyisocyanide contain no chiral atoms, and the chirality is solely from the preferentially one-handed helical backbone of polyisocyanide. The additives can be recycled without significant loss in chiral induction ability at least 4 times.

Polyphenylisocyanide with bulky substituents was believed to be one of the static helical polymers without no helical inversions. In 2009, Yashima et al. reported that poly (4-carboxyphenyl isocyanide) exhibited the helical inversion according to the configuration of chiral amines in water[74].

Goto et al. have reported on asymmetric polymerization methods in cholesteric liquid crystal (CLC) to afford chiral polymers from achiral monomers using CLC as chiral reaction field: Ni-catalyzed polymerization for one-handed helical poly(aryl isocyanide)s[75,76]. For synthesis of poly(aryl isocyanide)s in CLC, ortho-substitution has significant effects on preparation of one-handed helical PPIs. During polymerization, they assume that CLC medium facilitate the one-side attack of nucleophile to Ni center, which results in the formation of single-handed helical polyisocyanide through inter-lock manner.

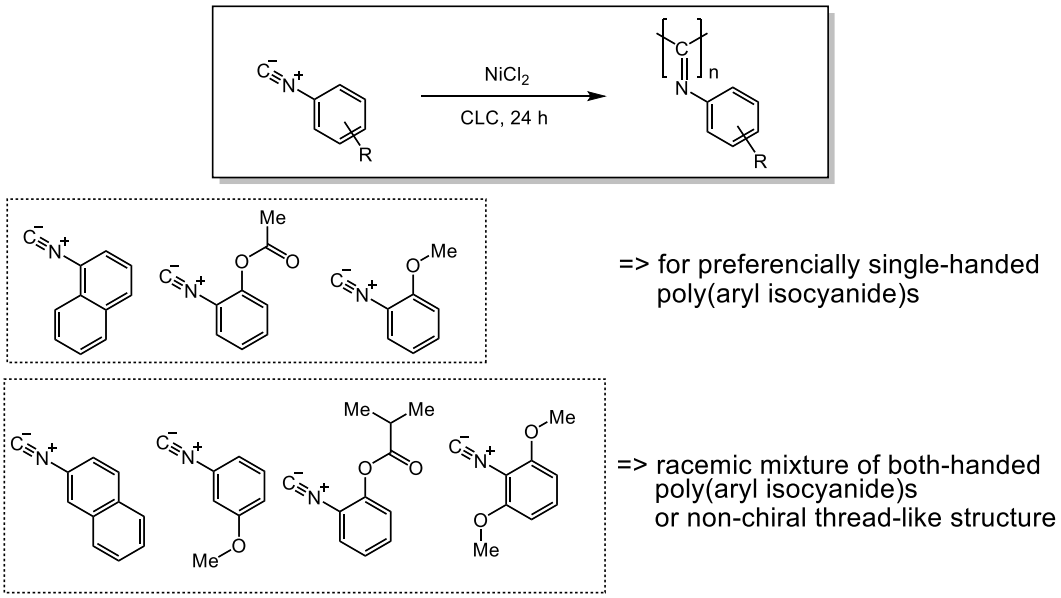

Figure 1.28. Catalytic selective polymerization of aryl isocyanides in cholesteric LC (CLC).

1.12 Stereoregularity of helical structure of polyisocyanide

As mentioned in *Chapter 1.9*, polyisocyanides can adopt "syn or anti" conformation in the helical backbone. Stereoregularity has relationship with chiropticality, which can be detected by CD spectroscopy arising from imino band absorption. Stereoregularity of PPI helical structure can also be estimated by ^{13}C NMR signal from C atoms in the polymer backbone.

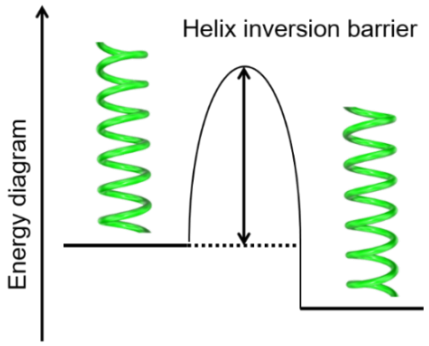

Figure 1.29. Simple schematic energy diagram for helix inversion barrier of diastereomeric helical polyisocyanide.

Helical senses of polyisocyanides are determined kinetically during polymerization process. Onitsuka and Takahashi et al. reported that using poly (aryl isocyanide) with optically active ester pendants thermal annealing in refluxing THF for 15 h enhanced the chiroptical properties[77]. Yashima et al. also reported poly(aryl isocyanide) with optically active amide pendants required the thermal annealing for 12 days to obtain maximum CD intensity[78]. The PPIs with amide pendant seem to have high helix-inversion barrier because of hydrogen bonding between the repeating amide group. Their study indicates that thermal annealing converts kinetically stable helix of polyisocyanides into thermally stable preferred helix of polyisocyanides.

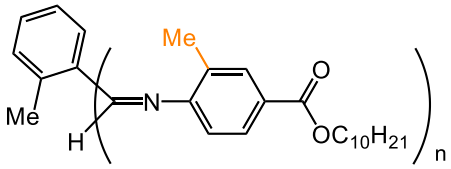

Figure 1.30. High stereoregular poly(phenyl isocyanide) with ortho-methyl substitution.

Very recently, Lee et al. reported that ortho-methyl substituted poly(aryl isocyanide) prepared by using o-tolylNi(dppe)Cl catalyst show significantly higher stereoregularity compared to the non-ortho-methyl substituted one[54]. In ^{13}C NMR spectroscopy, ortho-methyl substituted poly(aryl isocyanide) displayed very sharp signal of carbon at polymer backbone, indicating high stereoregularity of the helical backbone. Although the authors have not synthesized ortho-methyl substituted poly(aryl isocyanide) with chiral side chains, this finding would lead to the new molecular design for the high stereoregular helical poly(aryl isocyanide)s, which may provide the rigid, well-defined helical scaffold for functional side chains aimed for circular polarized luminescence, high chiral catalytic activity, helical spin arrays and so on.

1.13 Long persistence length in polyisocyanide

Persistence length q, a useful criterion to evaluate the stiffness of rod-shaped polymers, can be estimated by size exclusion chromatography (SEC) equipped with multiangle laser light scattering (MALS) and refractive index detectors on the assumption that rod-shaped helical polymers form helical worm-like model. Many biological helical polymers form stiff helical backbones, for examples the triple-stranded helical collagen (q : 160-180 nm), schizophyllan (q : 150-200nm), the double-stranded helical DNA (q : 60 nm), and xanthan (q : 120 nm).

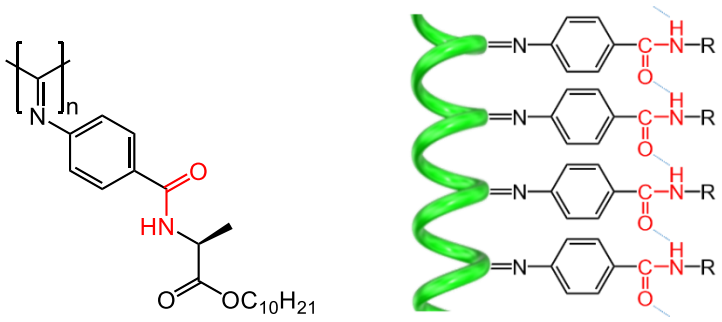

Figure 1.31. Polyphenylisocyanide with exceptionally long persistence length.

Okoshi et. al. reported that anomalous stiff helical backbone of poly(phenyl isocyanide) with amide alkyl pendant. They concluded that intramolecular hydrogen bonding between repeating units enhance the rigidity of helical backbones. The persistence length (q) is 220 nm, which is the best record in the synthetic helical polymers[79].

Rowan et al. used a single molecule wide-field fluorescence microscopy technique to analyze the dynamics of fluorescent-labeled polyisocyanide in entangled unlabeled polymer solutions[80,81]. They demonstrated that confining potentials of labeled polyisocyanide as a function of concentration and persistence length in the unlabeled, surrounding polymers.

1.14 Lyotropic liquid crystalline phase formation in rod-shaped polyisocyanide

Liquid crystalline phases were often seen in biomolecules line DNA, viruses, and colloidal suspension of crystal particles. According to Onsager theory[82] and Flory theory[83], liquid crystalline phase is induced from high-aspect-ratio rod-shape colloidal particles. It is suggested that the gain in packing entropy is the main driving force to express the liquid crystalline phase when the packing entropy exceeds the loss of the transitional entropy.

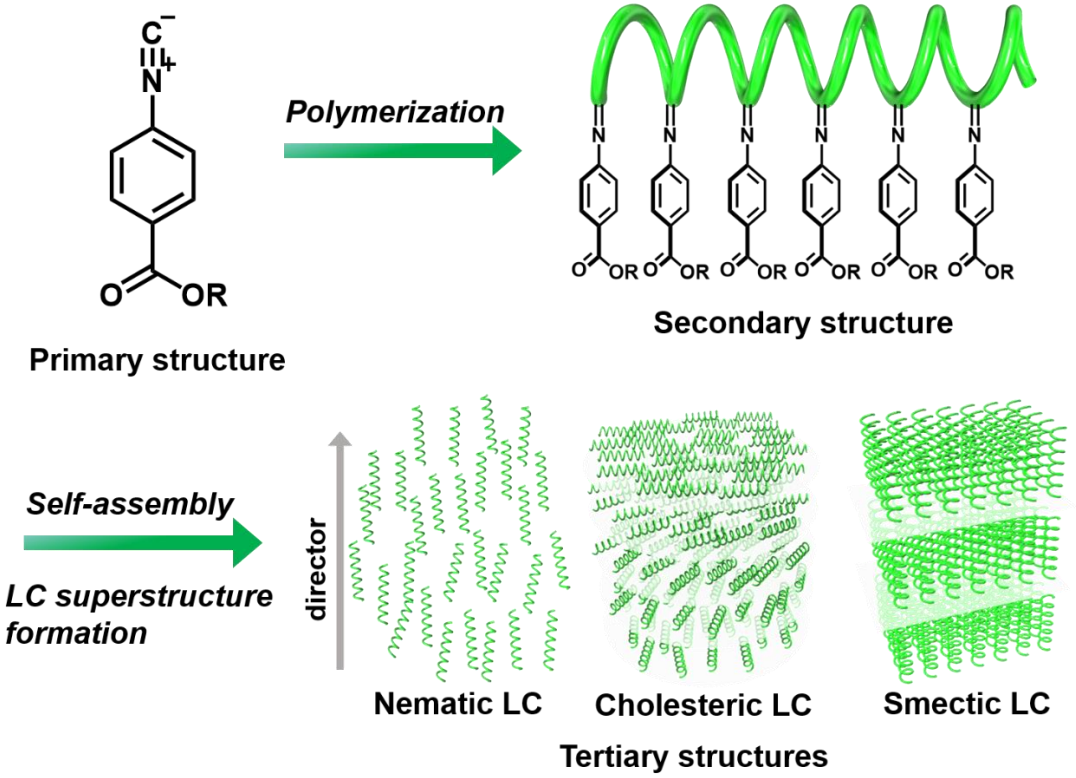

Figure 1.32. Schematic illustration of liquid crystalline superstructures composed of rod-shaped helical polymers.

High molecular weight, high-aspect-ratio poly(isocyanide) has potential to exhibit lyotropic liquid crystalline phase in concentrated solution, which is called "liquid crystalline superstructure". Poly(isocyanide)s with broad polydispersity (M_w/M_n) and narrow polydispersity are expected to show nematic LC phase[84] and smectic LC phase[91-

[95], respectively. If poly(isocyanide) with large polydispersity possess preferentially one-handed helical structure (non-racemic form), it can exhibit cholesteric LC superstructure[85-88].

Polyisocyanopeptides with alanine pendant shows lyotropic cholesteric liquid crystalline phase in tetrachloroethane. Concentration-dependent helical pitch of cholesteric helical structure[89], and helical inversion[90] of cholesteric superstructure have been reported in cholesteric LC superstructures. Okoshi et al demonstrated that polysilanes and polyisocyanides prepared by living polymerization with narrow distribution exhibits high-order smectic LC phase irrespective of chirality of helical backbone[91-95].

1.15 Accumulation of functional group in helical scaffold

Side chain pendant of polyisocyanide is accumulated around the polymer backbone. For example, Cornelissen et. al. reported that peptide chains of polyisocyanopeptide arrange in *β*-sheet like fashion[96]. Vibration propagation in polyisocyanopeptide through intramolecular hydrogen bonding was observed. Various functional groups can be introduced to the polyisocyanide backbone such as redox-active moiety[97-99], aggregation-induced emission (AIE)[100] moiety and so on. Energy transfer is observed in porphyrin- and tetrathiafulvalene-substituted polyisocyanides, which can be applied as one-dimensional conducting wires.

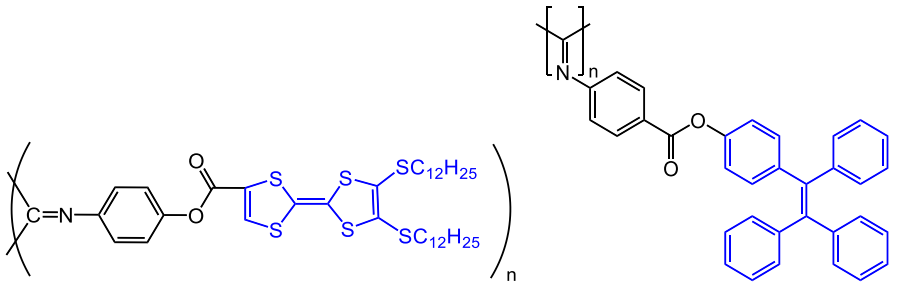

Figure 1.33. Multifunctional tetrathiafulvalene- and tetraphenylethylene-substituted polyisocyanide.

In 1990s, Meijer group[101,103] and Veciana group[102] reported independently on the synthesis of poly(isocyanide)s with radical pendants and their magnetic property. They intended to create ferromagnetic materials taking advantage of helical scaffold of polyisocyanide backbone to accumulate and arrange radical pendants in helical manner. However, they could not observe the ferro or anti-ferro magnetic behavior probably because of small interactions between radical species.

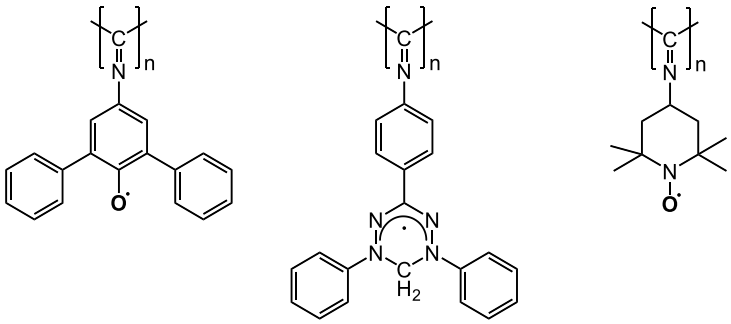

Figure 1.34. Examples of polyisocyanide with stable radical pendant.

1.16 Application of helical polyisocyanide as chiral materials

In 1995, Nolte et al reported that supramolecular second-order nonlinearity from chiral polyisocyanopeptide bearing chromophores as side chain[104]. Biomimetic applications have also been intended using polyisocyanopeptide hydrogel with tunable gelation temperature, strain-stiffening properties. Rowan and Nolte et al. demonstrated the responsive biomimetic networks from polyisocyanopeptide[105-107]. This synthetic hydrogel is readily modified for the specific application in bio-medical applications. Święszkowski, Nolte, Rowan demonstrated that potential application in bioink for 3D printing[108], programming artificial dendric cell[108], substrate for DNA-sliding clamp proteins[109], and affinity-based purification method[110].

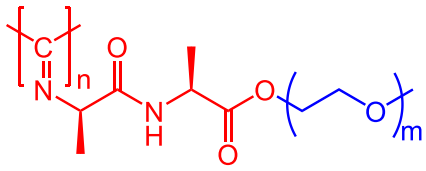

Figure 1.35. Bio-mimetic hydrogel-forming polyisocyanopeptide with oligo(ethylene glycol) substitution.

Poly(phenyl isocyanide) with chiral pendants have also been investigated as potential application for alignment medium in NMR spectroscopy[111,112], chiral stationary phase for optical resolution[114-116], chiral catalysts[117-119], chiral memory[120]. Chiral detection and amplification through induction of helical polymer formation has been sought using dynamic helical polymers such as polyacetylene, polyisocyanate and so on. Polyisocyanides with bulky substituents are usually classified as static helical polymers, indicating chiral detection and amplification through the helical conformation changes are not expected. Yashima et al. reported that exceptional poly(phenyl isocyanide) with carboxylic acid which has low helix inversion barrier showing chiral amine-induced helical inversions and chiral amplifications[120]. Recently, Wu et al. found that enantioselective crystallization ability of chiral poly(phenyl isocyanide) for amino-acid crystallization[121]. They also reported that rod-shaped helical polyisocyanide block has cell-penetrating property, where the block copolymer micelles effectively enter into the cell through endocytosis[122]. This block copolymer micelles can be used as capsules for drug delivery systems. Donor-acceptor type and non-volatile sensor-oriented researches have also been carried out[123,124].

1.17 Summary and future perspective

Since its helical structure was revealed by Millich, Nolte and Drench, the rigid helical backbone of polyisocyanide has been one of the wonderful scaffolds for specific designs to pioneer new functionalities. The recent well-established synthetic protocol for living polymerization gives access to controlled molecular weight, narrowly dispersed polyisocyanide with defined pendants. The polyisocyanide with sufficient bulky substituents form stiff helical backbone with long persistence length providing thermally stable, solvent-tolerant properties, which is suitable for applications such as chiral catalyst, chiral stationary phase. However, the performance of asymmetric synthesis and chiral column chromatography is still inadequate for practical applications. The much higher stereoregularity and the resulting ordered assembly of pendants will be desired. The lyotropic liquid crystalline properties originating from excluded volume effect and Van-derWaals interaction of high-aspect-ratio, rod-shaped

helical polyisocyanide molecules will allows for the spontaneous organization into higher order in solution-drying process, which is practical in the roll-to-roll process. For example, the solid films with liquid crystalline structure will provide selective reflections at certain wavelength from cholesteric liquid crystalline periodic structure, and circular polarized luminescence derived from luminophores of pendant attached to the helical backbones. In summary, poly(phenyl isocyanide)s are interesting hierarchical properties: monomer (primary structure), helical polymer (secondary structure), and lyotropic LC assembly (tertiary structure). As perspective, the study on the combination of different dimentionality is desired for the future material design.

References

[1] Natta, G., Pino, P., Corradini, P., Danusso, F., Mantica, E., Mazzanti, G., & Moraglio, G. (1955). Crystalline high polymers of α-olefins. Journal of the American Chemical Society, 77(6), 1708-1710.

[2] Nolte, R. V., Van Beijnen, A. J. M., & Drenth, W. (1974). Chirality in polyisocyanides. Journal of the American Chemical Society, 96(18), 5932-5933.

[3] Millich, F., & Baker, G. K. (1969). Polyisonitriles. Iii. Synthesis and Racemization of Optically Active Poly (A-Phenylethylisonitrile). Macromolecules, 2(2), 122-128.

[4] Okamoto, Y., Suzuki, K., Ohta, K., Hatada, K., & Yuki, H. (1979). Optically active poly (triphenylmethyl methacrylate) with one-handed helical conformation. Journal of the American Chemical Society, 101(16), 4763-4765.

[5] Yuki, H., Okamoto, Y., & Okamoto, I. (1980). Resolution of racemic compounds by optically active poly (triphenylmethyl methacrylate). Journal of the American Chemical Society, 102(20), 6356-6358.

[6] Green, M. M., Reidy, M. P., Johnson, R. D., Darling, G., O'Leary, D. J., & Willson, G. (1989). Macromolecular stereochemistry: the out-of-proportion influence of optically active comonomers on the conformational characteristics of polyisocyanates. The sergeants and soldiers experiment. Journal of the American Chemical Society, 111(16), 6452-6454.

[7] Green, M. M., Garetz, B. A., Munoz, B., Chang, H., Hoke, S., & Cooks, R. G. (1995). Majority rules in the copolymerization of mirror image isomers. Journal of the American Chemical Society, 117(14), 4181-4182.

[8] Green, M. M., Andreola, C., Munoz, B., Reidy, M. P., & Zero, K. (1988). Macromolecular stereochemistry: a cooperative deuterium isotope effect leading to a large optical rotation. Journal of the American Chemical Society, 110(12), 4063-4065.

[9] Green, M. M., Peterson, N. C., Sato, T., Teramoto, A., Cook, R., & Lifson, S. (1995). A helical polymer with a cooperative response to chiral information. Science, 268(5219), 1860-1866.

[10] Green, M. M., Park, J. W., Sato, T., Teramoto, A., Lifson, S., Selinger, R. L., & Selinger, J. V. (1999). The macromolecular route to chiral amplification. Angewandte Chemie International Edition, 38(21), 3138-3154.

[11] Fujiki, M. (1994). Ideal exciton spectra in single-and double-screw-sense helical polysilanes. Journal of the American Chemical Society, 116(13), 6017-6018.

[12] Yashima, E., Ousaka, N., Taura, D., Shimomura, K., Ikai, T., & Maeda, K. (2016). Supramolecular helical systems: helical assemblies of small molecules, foldamers, and polymers with chiral amplification and their functions. Chemical reviews, 116(22), 13752-13990.

[13] Strzelecka, T. E., Davidson, M. W., Rill, R. L. Multiple liquid crystal phases of DNA at high concentrations. Nature 1998, 331, 457.

[14] Giraud-Guille, M. M., Besseau, L., Chopin, C., Durand, P., Herbage, D. Structural aspects of fish skin collagen which forms ordered arrays via liquid crystalline states. Biomaterials 2000, 21, 899-906.

[15] Lee, B. Y., et al. Virus-based piezoelectric energy generation. Nat. Nanotech. 2012, 7, 351.

[16] Ellis, R. J., & Minton, A. P. (2003). Cell biology: join the crowd. Nature, 425(6953), 27.

[17] A.W. Hofmann, Ann. Chem., 144 114 (1867)

[18] Mocci, R., Murgia, S., De Luca, L., Colacino, E., Delogu, F., & Porcheddu, A. (2018). Ball-milling and cheap reagents breathe green life into the one hundred-year-old Hofmann reaction. Organic Chemistry Frontiers, 5(4), 531-538.

[19] Ugi, I., Fetzer, U., Eholzer, U., Knupfer, H., & Offermann, K. (1965). Isonitrile syntheses. Angewandte Chemie International Edition in English, 4(6), 472-484.

[20] Ugi, I. (1982). From isocyanides via four-component condensations to antibiotic syntheses. Angewandte Chemie International Edition in English, 21(11), 810-819.

[21] Obrecht, R., Herrmann, R., & Ugi, I. (1985). Isocyanide synthesis with phosphoryl chloride and diisopropylamine. Synthesis, 1985(04), 400-402.

[22] Wang, X., Wang, Q. G., & Luo, Q. L. (2015). Synthesis of isonitriles from N-substituted formamides using triphenylphosphine and iodine. Synthesis, 47(01), 49-54.

[23] Su, M., Liu, N., Wang, Q., Wang, H., Yin, J., & Wu, Z. Q. (2015). Facile synthesis of poly (phenyleneethynylene)-block-

polyisocyanide copolymers via two mechanistically distinct, sequential living polymerizations using a single catalyst. Macromolecules, 49(1), 110-119.
[24] Yin, J., Xu, L., Han, X., Zhou, L., Li, C., & Wu, Z. Q. (2017). A facile synthetic route to stereoregular helical poly (phenyl isocyanide) s with defined pendants and controlled helicity. Polymer Chemistry, 8(3), 545-556.
[25] Millich, F. (1972). Polymerization of isocyanides. Chemical Reviews, 72(2), 101-113.
[26] Nolte, R. J. (1994). Helical poly (isocyanides). Chemical Society Reviews, 23(1), 11-19.
[27] Suginome, M., & Ito, Y. (2004). Transition metal-mediated polymerization of isocyanides. In Polymer Synthesis (pp. 77-136). Springer, Berlin, Heidelberg.
[28] Schwartz, E., Koepf, M., Kitto, H. J., Nolte, R. J., & Rowan, A. E. (2011). Helical poly (isocyanides): past, present and future. Polymer Chemistry, 2(1), 33-47.
[29] Stackman, R. W. (1968). Addition Polymers of Cyclohexyl Isonitrile. Journal of Macromolecular Science—Chemistry, 2(2), 225-236.
[30] Yamamoto, Y., Takizawa, T., & Hagihara, N. (1967). Nippon Kagaku Zasshi, 87, 1355 (1966). CrossRef| CAS.
[31] Metselaar, G. A., Cornelissen, J. J., Rowan, A. E., & Nolte, R. J. (2005). Acid-initiated stereospecific polymerization of isocyanopeptides. Angewandte Chemie International Edition, 44(13), 1990-1993.
[32] Metselaar, G. A., Adams, P. H. M., Nolte, R. J., Cornelissen, J. J., & Rowan, A. E. (2007). Polyisocyanides derived from tripeptides of alanine. Chemistry–A European Journal, 13(3), 950-960.
[33] Yan, X., Zhang, S., Zhang, P., Wu, X., Liu, A., Guo, G., ... & Li, X. (2018). [Ph_3C][B (C_6F_5) $_4$]: Highly Efficient Metal-Free Single-Component Initiator for Helical-Sense-Selective cationic Copolymerization of Chiral Aryl Isocyanide and Achiral Aryl Isocyanide. Angewandte Chemie International Edition.
[34] Deming, T. J., & Novak, B. M. (1991). Organometallic catalysis in air and water: oxygen-enhanced, nickel-catalyzed polymerizations of isocyanides. Macromolecules, 24(1), 326-328.
[35] Deming, T. J., & Novak, B. M. (1991). Polyisocyanides using [(η_3-C_3H_5) Ni (OC (O) CF_3)] $_2$: rational design and implementation of a living polymerization catalyst. Macromolecules, 24(22), 6043-6045.
[36] Asaoka, S., Joza, A., Minagawa, S., Song, L., Suzuki, Y., & Iyoda, T. (2013). Fast controlled living polymerization of arylisocyanide initiated by aromatic nucleophile adduct of nickel isocyanide complex. ACS Macro Letters, 2(10), 906-911.
[37] Yamada, T., & Suginome, M. (2010). Synthesis of Helical Rod− Coil Multiblock Copolymers by Living Block Copolymerization of Isocyanide and 1, 2-Diisocyanobenzene Using Arylnickel Initiators. Macromolecules, 43(9), 3999-4002.
[38] Lee, J., Shin, S., & Choi, T. L. (2018). Fast Living Polymerization of Challenging Aryl Isocyanides Using an Air-Stable Bisphosphine-Chelated Nickel (II) Initiator. Macromolecules, 51(19), 7800-7806.
[39] Onitsuka, K., Joh, T., & Takahashi, S. (1992). Syntheses and properties of heterodinuclear μ-ethynediyl complexes containing palladium and platinum. Bulletin of the Chemical Society of Japan, 65(4), 1179-1181.
[40] Xue, Y. X., Chen, J. L., Jiang, Z. Q., Yu, Z., Liu, N., Yin, J., ... & Wu, Z. Q. (2014). Living polymerization of arylisocyanide initiated by the phenylethynyl palladium (II) complex. Polymer Chemistry, 5(22), 6435-6438.
[41] Xue, Y. X., Zhu, Y. Y., Gao, L. M., He, X. Y., Liu, N., Zhang, W. Y., ... & Wu, Z. Q. (2014). Air-stable (phenylbuta-1, 3-diynyl) palladium (II) complexes: highly active initiators for living polymerization of isocyanides. Journal of the American Chemical Society, 136(12), 4706-4713.
[42] Onitsuka, K., Yamamoto, M., Mori, T., Takei, F., & Takahashi, S. (2006). Living polymerization of bulky aryl isocyanide with arylrhodium complexes. Organometallics, 25(5), 1270-1278.
[43] Deming, T. J., & Novak, B. M. (1991). " Change of mechanism" block copolymerizations: formation of block copolymers containing helical polyisocyanide and elastomeric polybutadiene segments. Macromolecules, 24(19), 5478-5480.
[44] Cornelissen, J. J., Fischer, M., Sommerdijk, N. A., & Nolte, R. J. (1998). Helical superstructures from charged poly (styrene)-poly (isocyanodipeptide) block copolymers. Science, 280(5368), 1427-1430.
[45] Kumar, A., Hertel, B., & Müllen, K. (2018). Self-Assembly and Responsive Behavior of Poly (peptide)-Based Copolymers. Macromolecular Chemistry and Physics, 219(11), 1800101.
[46] Croom, A., Tarallo, R., & Weck, M. (2016). End-group functionalization and postpolymerization modification of helical poly (isocyanide) s. Journal of Polymer Science Part A: Polymer Chemistry, 54(17), 2766-2773.
[47] Jiang, Z. Q., Zhao, S. Q., Su, Y. X., Liu, N., & Wu, Z. Q. (2018). Combination of RAFT and Pd (II)-initiated isocyanide polymerizations: A versatile method for facile synthesis of helical poly (phenyl isocyanide) block and star copolymers. Macromolecules, 51(3), 737-745.
[48] Elacqua, E., Manning, K. B., Lye, D. S., Pomarico, S. K., Morgia, F., & Weck, M. (2017). Supramolecular Multiblock Copolymers Featuring Complex Secondary Structures. Journal of the American Chemical Society, 139(35), 12240-12250.
[49] Wu, Z. Q., Ono, R. J., Chen, Z., & Bielawski, C. W. (2010). Synthesis of poly (3-alkylthiophene)-block-poly (arylisocyanide): Two sequential, mechanistically distinct polymerizations using a single catalyst. Journal of the American Chemical Society, 132(40), 14000-14001.
[50] Wu, Z. Q., Radcliffe, J. D., Ono, R. J., Chen, Z., Li, Z., & Bielawski, C. W. (2012). Synthesis of conjugated diblock copolymers: two mechanistically distinct, sequential living polymerizations using a single catalyst. Polymer Chemistry, 3(4), 874-881.

[51] Su, M., Liu, N., Wang, Q., Wang, H., Yin, J., & Wu, Z. Q. (2015). Facile synthesis of poly (phenyleneethynylene)-block-polyisocyanide copolymers via two mechanistically distinct, sequential living polymerizations using a single catalyst. Macromolecules, 49(1), 110-119.
[52] Takei, F., Yanai, K., Onitsuka, K., & Takahashi, S. (2000). Screw-Sense-Selective Polymerization of Aryl Isocyanides Initiated by a Pd-Pt μ-Ethynediyl Dinuclear Complex: A Novel Method for the Synthesis of Single-Handed Helical Poly (isocyanide) s with the Block Copolymerization Technique. Chemistry–A European Journal, 6(6), 983-993.
[53] Wu, Z. Q., Nagai, K., Banno, M., Okoshi, K., Onitsuka, K., & Yashima, E. (2009). Enantiomer-selective and helix-sense-selective living block copolymerization of isocyanide enantiomers initiated by single-handed helical poly (phenyl isocyanide) s. Journal of the American Chemical Society, 131(19), 6708-6718.
[54] Lee, J., Shin, S., & Choi, T. L. (2018). Fast Living Polymerization of Challenging Aryl Isocyanides Using an Air-Stable Bisphosphine-Chelated Nickel (II) Initiator. Macromolecules, 51(19), 7800-7806.
[55] Kollmar, C., & Hoffmann, R. (1990). Polyisocyanides: electronic or steric reasons for their presumed helical structure? Journal of the American Chemical Society, 112(23), 8230-8238.
[56] Green, M. M., Gross, R. A., Schilling, F. C., Zero, K., & Crosby III, C. (1988). Macromolecular stereochemistry: effect of pendant group structure on the conformational properties of polyisocyanides. Macromolecules, 21(6), 1839-1846.
[57] Pescitelli, G., Di Bari, L., & Berova, N. (2014). Application of electronic circular dichroism in the study of supramolecular systems. Chemical Society Reviews, 43(15), 5211-5233.
[58] Berova, N., Di Bari, L., & Pescitelli, G. (2007). Application of electronic circular dichroism in configurational and conformational analysis of organic compounds. Chemical Society Reviews, 36(6), 914-931.
[59] Harada, N., & Nakanishi, K. (1972). Exciton chirality method and its application to configurational and conformational studies of natural products. Accounts of Chemical Research, 5(8), 257-263.
[60] Harada, N., Nakanishi, K., & Berova, N. (2012). Electronic CD exciton chirality method: principles and applications. Comprehensive chiroptical spectroscopy, 2, 115-166.
[61] Takei, F., Hayashi, H., Onitsuka, K., Kobayashi, N., & Takahashi, S. (2001). Helical chiral polyisocyanides possessing porphyrin pendants: determination of helicity by exciton-coupled circular dichroism. Angewandte Chemie International Edition, 40(21), 4092-4094.
[62] Cornelissen, J. J., Sommerdijk, N. A., & Nolte, R. J. (2002). Determination of the helical sense in alanine based polyisocyanides. Macromolecular Chemistry and Physics, 203(10-11), 1625-1630.
[63] Kajitani, T., Okoshi, K., Sakurai, S. I., Kumaki, J., & Yashima, E. (2006). Helix-sense controlled polymerization of a single phenyl isocyanide enantiomer leading to diastereomeric helical polyisocyanides with opposite helix-sense and cholesteric liquid crystals with opposite twist-sense. Journal of the American Chemical Society, 128(3), 708-709.
[64] Kumaki, J., Sakurai, S. I., & Yashima, E. (2009). Visualization of synthetic helical polymers by high-resolution atomic force microscopy. Chemical Society Reviews, 38(3), 737-746.
[65] Nafie, L. A., & Freedman, T. B. (1998). Vibrational circular dichroism: an incisive tool for stereochemical applications. Enantiomer, 3(4-5), 283-297.
[66] Schwartz, E., Domingos, S. R., Vdovin, A., Koepf, M., Buma, W. J., Cornelissen, J. J., ... & Woutersen, S. (2010). Direct access to polyisocyanide screw sense using vibrational circular dichroism. Macromolecules, 43(19), 7931-7935.
[67] Schwartz, E., Liegeois, V., Koepf, M., Bodis, P., Cornelissen, J. J., Brocorens, P., ... & Champagne, B. (2013). Beta sheets with a twist: the conformation of helical polyisocyanopeptides determined by using vibrational circular dichroism. Chemistry–A European Journal, 19(39), 13168-13174.
[68] Kajitani, T., Okoshi, K., & Yashima, E. (2008). Helix-sense-controlled polymerization of optically active phenyl isocyanides. Macromolecules, 41(5), 1601-1611.
[69] Xu, A., Hu, G., Hu, Y., Zhang, X., Liu, K., Kuang, G., & Zhang, A. (2013). Remarkable structure effects on chiroptical properties of polyisocyanides carrying proline pendants. Chemistry–An Asian Journal, 8(9), 2003-2014.
[70] Takei, F., Onitsuka, K., & Takahashi, S. (1999). Nonproportional effects of optical purity of chiral aryl isocyanide monomers possessing (d) or (l)-menthoxycarbonyl groups on induction of screw-sense in poly (aryl isocyanide) s. Polymer journal, 31(11_2), 1029.
[71] Kamer, P. C., Cleij, M. C., Nolte, R. J., Harada, T., Hezemans, A. M., & Drenth, W. (1988). Atropisomerism in polymers. Screw-sense selective polymerization of isocyanides by inhibiting the growth of one enantiomer of a racemic pair of helices. Journal of the American Chemical Society, 110(5), 1581-1587.
[72] Kamer, P. C., Nolte, R. J., & Drenth, W. (1988). Screw sense selective polymerization of achiral isocyanides catalyzed by optically active nickel (II) complexes. Journal of the American Chemical Society, 110(20), 6818-6825.
[73] Chen, J. L., Yang, L., Wang, Q., Jiang, Z. Q., Liu, N., Yin, J., ... & Wu, Z. Q. (2015). Helix-Sense-Selective and Enantiomer-Selective Living Polymerization of Phenyl Isocyanide Induced by Reusable Chiral Lactide Using Achiral Palladium Initiator. Macromolecules, 48(21), 7737-7746.
[74] Hase, Y., Nagai, K., Iida, H., Maeda, K., Ochi, N., Sawabe, K., ... & Yashima, E. (2009). Mechanism of helix induction in poly (4-carboxyphenyl isocyanide) with chiral amines and memory of the macromolecular helicity and its helical structures. Journal of the American Chemical Society, 131(30), 10719-10732.

[75] Goto, H., Ohkawa, S., & Ohta, R. (2011). Structural chirality of cholesteric liquid crystal produces atropisomerism: Chiroptical polyisocyanides from achiral monomer in cholesteric liquid crystal matrix. Polymer, 52(9), 1932-1937.
[76] Iseki, T., Kawabata, K., Kawashima, H., & Goto, H. (2014). Catalysis direction selective asymmetric polymerization in chiral liquid crystal medium. polymer, 55(1), 66-72.
[77] Takei, F., Onitsuka, K., & Takahashi, S. (2005). Thermally induced helical conformational change in poly (aryl isocyanide) s with optically active ester groups. Macromolecules, 38(4), 1513-1516.
[78] Kajitani, T., Okoshi, K., Sakurai, S. I., Kumaki, J., & Yashima, E. (2006). Helix-sense controlled polymerization of a single phenyl isocyanide enantiomer leading to diastereomeric helical polyisocyanides with opposite helix-sense and cholesteric liquid crystals with opposite twist-sense. Journal of the American Chemical Society, 128(3), 708-709.
[79] Okoshi, K., Nagai, K., Kajitani, T., Sakurai, S. I., & Yashima, E. (2008). Anomalous stiff backbones of helical poly (phenyl isocyanide) derivatives. Macromolecules, 41(20), 7752-7754.
[80] Keshavarz, M., Engelkamp, H., Xu, J., Braeken, E., Otten, M. B., Uji-i, H., ... & Nolte, R. J. (2015). Nanoscale study of polymer dynamics. ACS nano, 10(1), 1434-1441.
[81] Keshavarz, M., Engelkamp, H., Xu, J., van den Boomen, O. I., Maan, J. C., Christianen, P. C., & Rowan, A. E. (2017). Confining Potential as a Function of Polymer Stiffness and Concentration in Entangled Polymer Solutions. The Journal of Physical Chemistry B, 121(22), 5613-5620.
[82] Onsager, L. (1949). The effects of shape on the interaction of colloidal particles. Annals of the New York Academy of Sciences, 51(4), 627-659.
[83] Flory, P. J. (1956). Phase equilibria in solutions of rod-like particles. Proc. R. Soc. Lond. A, 234(1196), 73-89.
[84] Kumaki, J., Kajitani, T., Nagai, K., Okoshi, K., & Yashima, E. (2010). Visualization of Polymer Chain Conformations in Amorphous Polyisocyanide Langmuir− Blodgett Films by Atomic Force Microscopy. Journal of the American Chemical Society, 132(16), 5604-5606.
[85] Metselaar, G. A., Wezenberg, S. J., Cornelissen, J. J., Nolte, R. J., & Rowan, A. E. (2007). Lyotropic liquid-crystalline behavior of polyisocyanodipeptides. Journal of Polymer Science Part A: Polymer Chemistry, 45(6), 981-988.
[86] Wezenberg, S. J., Metselaar, G. A., Rowan, A. E., Cornelissen, J. J., Seebach, D., & Nolte, R. J. (2006). Synthesis, characterization, and folding behavior of β-amino acid derived polyisocyanides. Chemistry–A European Journal, 12(10), 2778-2786.
[87] Cornelissen, J. J., Graswinckel, W. S., Rowan, A. E., Sommerdijk, N. A., & Nolte, R. J. (2003). Conformational analysis of dipeptide-derived polyisocyanides. Journal of Polymer Science Part A: Polymer Chemistry, 41(11), 1725-1736.
[88] Kajitani, T., Okoshi, K., Sakurai, S. I., Kumaki, J., & Yashima, E. (2006). Helix-sense controlled polymerization of a single phenyl isocyanide enantiomer leading to diastereomeric helical polyisocyanides with opposite helix-sense and cholesteric liquid crystals with opposite twist-sense. Journal of the American Chemical Society, 128(3), 708-709.
[89] Kimura, H., Hosino, M., & Nakano, H. (1982). Statistical Theory of Cholesteric Ordering in Hard-Rod Fluids and Liquid Crystalline Properties of Polypeptide Solutions. Journal of the Physical Society of Japan, 51(5), 1584-1590.
[90] Watson, M. J., Horsburgh, M. K., Goodby, J. W., Takatoh, K., Slaney, A. J., Patel, J. S., & Styring, P. (1998). A phenomenological approach to the inversion of the helical twist sense in the chiral nematic phase. Journal of Materials Chemistry, 8(9), 1963-1969.
[91] Okoshi, K. (2016). Smectic Phases of Liquid Crystalline Rod-Like Helical Polymers. In Liquid Crystalline Polymers (pp. 501-515). Springer, Cham.
[92] Hase, Y., Mitsutsuji, Y., Ishikawa, M., Maeda, K., Okoshi, K., & Yashima, E. (2007). Unexpected thermally stable, cholesteric liquid-crystalline helical polyisocyanides with memory of macromolecular helicity. Chemistry–An Asian Journal, 2(6), 755-763.
[93] Kajitani, T., Onouchi, H., Sakurai, S. I., Nagai, K., Okoshi, K., Onitsuka, K., & Yashima, E. (2011). Latticelike smectic liquid crystal phase in a rigid-rod helical polyisocyanide with mesogenic pendants. Journal of the American Chemical Society, 133(24), 9156-9159.
[94] Banno, M., Wu, Z. Q., Nagai, K., Sakurai, S. I., Okoshi, K., & Yashima, E. (2010). Two-Dimensional Bilayer Smectic Ordering of Rigid Rod− Rod Helical Diblock Polyisocyanides. Macromolecules, 43(16), 6553-6561.
[95] Okoshi K. (2016) Smectic Phases of Liquid Crystalline Rod-Like Helical Polymers. In: Thakur V., Kessler M. (eds) Liquid Crystalline Polymers. Springer, Cham
[96] Cornelissen, J. J., Donners, J. J., de Gelder, R., Graswinckel, W. S., Metselaar, G. A., Rowan, A. E., ... & Nolte, R. J. (2001). β-Helical polymers from isocyanopeptides. Science, 293(5530), 676-680.
[97] Hida, N., Takei, F., Onitsuka, K., Shiga, K., Asaoka, S., Iyoda, T., & Takahashi, S. (2003). Helical, chiral polyisocyanides bearing ferrocenyl groups as pendants: synthesis and properties. Angewandte Chemie, 115(36), 4485-4488.
[98] Gomar-Nadal, E., Mugica, L., Vidal-Gancedo, J., Casado, J., Navarrete, J. T. L., Veciana, J., ... & Amabilino, D. B. (2007). Synthesis and doping of a multifunctional tetrathiafulvalene-substituted poly (isocyanide). Macromolecules, 40(21), 7521-7531.
[99] Schraff, S., Sun, Y., & Pammer, F. (2018). Fulvenyl-Functionalized Polyisocyanides: Cross-Conjugated Electrochromic Polymers with Variable Optical and Electrochemical Properties. Macromolecules, 51(14), 5323-5335.
[100] He, Y. G., Shi, S. Y., Liu, N., Ding, Y. S., Yin, J., & Wu, Z. Q. (2015). Tetraphenylethene-functionalized conjugated helical poly (phenyl isocyanide) with tunable light emission, assembly morphology, and specific applications. Macromolecules, 49(1), 48-58.
[101] Abdelkader, M., Drenth, W., & Meijer, E. W. (1991). Synthesis and characterization of a stable poly (iminomethylene) with pendant phenoxyl radicals. Chemistry of Materials, 3(4), 598-602.

[102] Bosch, J., Rovira, C., Veciana, J., Castro, C., & Palacio, F. (1993). Synthesis and study of a stable polyradical macromolecule with a helical structure. A poly (iminomethylene) with verdazyl radicals as side groups. Synthetic metals, 55(2-3), 1141-1146.
[103] Vlietstra, E. J., Nolte, R. J. M., Zwikker, J. W., Drenth, W., & Meijer, E. W. (1990). Synthesis and magnetic properties of a rigid high spin-density polymer with piperidine-N-oxyl pending groups. Macromolecules, 23(4), 946-948.
[104] Kauranen, M., Verbiest, T., Boutton, C., Teerenstra, M. N., Clays, K., Schouten, A. J., ... & Persoons, A. (1995). Supramolecular second-order nonlinearity of polymers with orientationally correlated chromophores. Science, 270(5238), 966-969.
[105] Kouwer, P. H., Koepf, M., Le Sage, V. A., Jaspers, M., van Buul, A. M., Eksteen-Akeroyd, Z. H., ... & Picken, S. J. (2013). Responsive biomimetic networks from polyisocyanopeptide hydrogels. Nature, 493(7434), 651.
[106] Kouwer, P. H., de Almeida, P., ven den Boomen, O., Eksteen-Akeroyd, Z. H., Hammink, R., Jaspers, M., ... & Rutten, M. G. (2018). Controlling the gelation temperature of biomimetic polyisocyanides. Chinese Chemical Letters, 29(2), 281-284.
[107] Schoenmakers, D. C., Rowan, A. E., & Kouwer, P. H. (2018). Crosslinking of fibrous hydrogels. Nature communications, 9.
[108] Celikkin, N., Simó Padial, J., Costantini, M., Hendrikse, H., Cohn, R., Wilson, C. J., ... & Święszkowski, W. (2018). 3D Printing of Thermoresponsive Polyisocyanide (PIC) Hydrogels as Bioink and Fugitive Material for Tissue Engineering. Polymers, 10(5), 555.
[109] Nam, E. V., Hammink, R., Kijas, A. W., Figdor, C. G., & Rowan, A. E. Synthetic Dendritic Cells.
[110] van Dongen, S. F. M., Clerx, J., van den Boomen, O. I., Pervaiz, M., Trakselis, M. A., Ritschel, T., ... & Nolte, R. J. M. (2018). Synthetic polymers as substrates for a DNA-sliding clamp protein. Biopolymers, 109(5), e23119.
[111] Hammink, R., Eggermont, L. J., Zisis, T., Tel, J., Figdor, C. G., Rowan, A. E., & Blank, K. G. (2017). Affinity-based purification of polyisocyanopeptide bioconjugates. Bioconjugate chemistry, 28(10), 2560-2568.
[112] Dama, M., & Berger, S. (2011). Polyisocyanides as a new alignment medium to measure residual dipolar couplings for small organic molecules. Organic letters, 14(1), 241-243.
[113] Reller, M., Wesp, S., Koos, M. R., Reggelin, M., & Luy, B. (2017). Biphasic Liquid Crystal and the Simultaneous Measurement of Isotropic and Anisotropic Parameters by Spatially Resolved NMR Spectroscopy. Chemistry–A European Journal, 23(54), 13351-13359.
[114] Tamura, K., Miyabe, T., Iida, H., & Yashima, E. (2011). Separation of enantiomers on diastereomeric right-and left-handed helical poly (phenyl isocyanide) s bearing L-alanine pendants immobilized on silica gel by HPLC. Polymer Chemistry, 2(1), 91-98.
[115] Chu, B. F., Chu, J. H., Zhao, S. Q., Liu, N., & Wu, Z. Q. (2018). Facile synthesis of optically active helical poly (phenyl isocyanide) brushes on a silicon surface and their chiral resolution ability. Polymer Chemistry, 9(12), 1379-1384.
[116] Wang, Q., Chu, B. F., Chu, J. H., Liu, N., & Wu, Z. Q. (2018). Facile synthesis of optically active and thermoresponsive star block copolymers carrying helical polyisocyanide arms and their thermo-triggered chiral resolution ability. ACS Macro Letters, 7(2), 127-131.
[117] Miyabe, T., Hase, Y., Iida, H., Maeda, K., & Yashima, E. (2009). Synthesis of functional poly (phenyl isocyanide) s with macromolecular helicity memory and their use as asymmetric organocatalysts. Chirality: The Pharmacological, Biological, and Chemical Consequences of Molecular Asymmetry, 21(1), 44-50.
[118] Zhou, L., Chu, B. F., Xu, X. Y., Xu, L., Liu, N., & Wu, Z. Q. (2017). Significant improvement on enantioselectivity and diastereoselectivity of organocatalyzed asymmetric aldol reaction using helical polyisocyanides bearing proline pendants. ACS Macro Letters, 6(8), 824-829.
[119] Shen, L., Xu, L., Hou, X. H., Liu, N., & Wu, Z. Q. (2018). Polymerization Amplified Stereoselectivity (PASS) of Asymmetric Michael Addition Reaction and Aldol Reaction Catalyzed by Helical Poly (phenyl isocyanide) Bearing Secondary Amine Pendants. Macromolecules. 2018, 51, 23, 9547-9554.
[120] Ishikawa, M., Maeda, K., Mitsutsuji, Y., & Yashima, E. (2004). An unprecedented memory of macromolecular helicity induced in an achiral polyisocyanide in water. Journal of the American Chemical Society, 126(3), 732-733
[121] Yang, L., Tang, Y., Liu, N., Liu, C. H., Ding, Y., & Wu, Z. Q. (2016). Facile synthesis of hybrid silica nanoparticles grafted with helical poly (phenyl isocyanide) s and their enantioselective crystallization ability. Macromolecules, 49(20), 7692-7702.
[122] Han, X., Zhang, J., Qiao, C. Y., Zhang, W. M., Yin, J., & Wu, Z. Q. (2017). High-efficiency cell-penetrating helical poly (phenyl isocyanide) chains modified cellular tracer and nanovectors with thiol ratiometric fluorescence imaging performance. Macromolecules, 50(11), 4114-4125.
[123] Ono, R. J., Todd, A. D., Hu, Z., Vanden Bout, D. A., & Bielawski, C. W. (2014). Synthesis of a donor–acceptor diblock copolymer via two mechanistically distinct, sequential polymerizations using a single catalyst. Macromolecular rapid communications, 35(2), 204-209.
[124] Tian, X., Cao, Y., Zhang, B., Huang, S., & Chen, Y. (2018). Donor-acceptor type helical polyisocyanide bearing carbazole as the pendant groups for nonvolatile memory effect. European Polymer Journal, 106, 196-201.

Chapter 2: Lyotropic liquid crystalline chromic block copolymers with multi-stimuli responsiveness

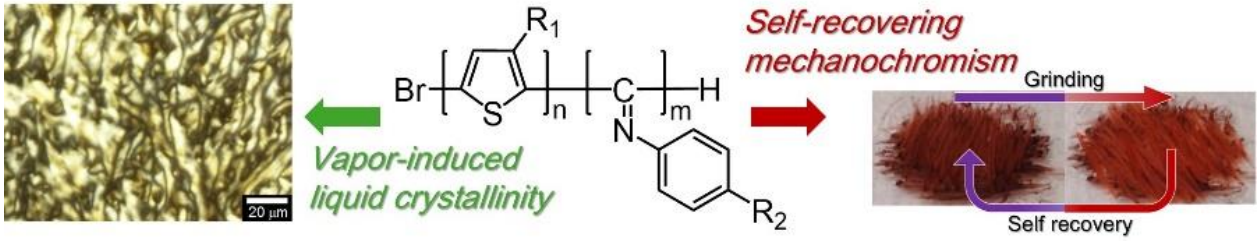

2.1 Abstract

New molecular design of conjugated polymer that possess high sensitivity to vapor and self-recovering property against pressure is proposed. We synthesized a rod-rod diblock copolymer, polythiophene-*block*-poly(phenyl isocyanide) (PTh-*b*-PPI), composed of a π-conjugated polymer and a rod-type helical coiled polymer. Introduction of PPI block in the block copolymer architecture enabled PTh-*b*-PPI film to exhibit solid-to-liquid crystal phase transition by exposure to chloroform vapor, accompanied with color change, which is the first report on a new phenomenon of "vapor-induced liquid crystallinity". In addition, PTh-*b*-PPI film showed color change during mechanical shearing, and spontaneously recovered under ambient conditions. We concluded that rod-type helical coiled polymer PPI block performs crucial roles as intrinsically vapor-induced liquid crystallinity and self-reassembling property in the architecture of PTh-*b*-PPI.

2.2 Introduction

Stimuli-responsive materials have attracted substantial attention for a wide variety of potential applications such as sensors[1], drug delivery systems[2] and actuators[3]. Responsiveness to external stimuli, for example heat, light, electrical and magnetic field, vapor and pressure, involves changes of molecular conformation and packing structure of molecules that converts physical signals into optical, electrical, mechanical and thermal signals[4]. One of the strategies to create stimuli-responsive materials is the incorporation of liquid crystal (LC) component in the molecular structure. LC material is one of the self-organized soft materials originating from weak interactions of van der Waals force and the excluded volume effect[5]. LC materials spontaneously form organized structures and possess dynamic properties against external stimuli such as shear-stress, electrical and magnetic field. With these advantages, the materials incorporated with well-designed LC moiety into the molecular structure show mechanical-induced phase transition[6,7], and form spontaneous ordered structures with anisotropic functionalities[8,9] and photo- and magnetic field-assisted macroscopic orientations[10-11] and so on.

Herein, new molecular design of conjugated polymers that possess high sensitivity to vapor and self-recovering property against pressure is proposed. We synthesized a rod-rod diblock copolymer, polythiophene-block-poly(phenyl isocyanide) (PTh-*b*-PPI), composed of a π-conjugated polymer and a rod-type helical coiled polymer using the reported methodology. Introduction of PPI block in the block copolymer architecture enabled PTh-*b*-PPI

film to exhibit solid-to-liquid crystal phase transition by exposure to chloroform vapor, accompanied with color change, which is the first report on a new phenomenon of "vapor-induced liquid crystallinity". Macroscopic orientation of polymer film was achieved using high-intensity magnetic field. In addition, PTh-*b*-PPI film showed color change during mechanical shearing, and spontaneously recovered under ambient conditions. We have published this phenomenon in *Scientific Reports* (7, Article number: 3948 (2017))[12].

Based on the above finding, we systematically prepared a series of polythiophene derivatives (1-5) and investigated the properties of the corresponding block copolymers. Each block copolymer exhibits lyotropic liquid crystallinity and solvent-induced color changes. From gazing-incident X-ray diffraction (GIXRD) measurements for the films, incorporation of rod-shaped PPI block induces the liquid crystalline-like structure in solid state. Polarizing optical microscopy (POM) observations for drop-cast poly1-*b*-PPI copolymer films also showed that lyotropic LC formation was dependent on the molecular weight of PPI (rod-shaped polymer) block. We found that grain size (LC domain) of poly1-*b*-PPI LC assembly increased as the molecular weight of PPI block increased. These results suggest that the aspect-ratio of PPI block is a key factor for the block copolymer to show LC phase. Introduction of PPI block to the semiconducting polymer block allow the corresponding block copolymer to show moderate magnetic anisotropy and grain size enough for magnetic orientation.

2.3 Chromic property of semiconducting polymers

In this study, based on the recent advancement of supramolecular chemistry, we first strategically designed block copolymer, poly(3-((3S)-3,7-dimethyl-octyl)-thiophene)-*block*-poly(4-octyl phenyl isocyanide) (PTh*-*b*-PPIC$_8$), composed of a conjugated polymer (CP) and a rod-type helical coiled polymer as shown in Figure 1. Polythiophene is one of CPs and exhibits color changes in visible range originating from the conformational changes in the polymer backbone between the planar state (purple) and the twisted state (yellow). The dihedral angle (**Figure 2.1**) between repeating units is key factor to determine the conjugation length along the backbone because the delocalization of π-conjugation of p-orbitals is dependent on the coplanarity of the conjugated polymer backbone[13]. The conformation of polythiophene that has chiral side chain has also been investigated, and it is considered to form helical packing of predominantly planar chains in the aggregation state driven by strong π–π interaction. Electrochemical oxidation/reduction can also tune the absorption spectra by redox-property of semiconducting nature of conjugated polymers. Introducing chiral side chain into polythiophene block also allows us to investigate the aggregation process in detail since we can track its process using circular dichroism (CD) spectroscopy. Therefore, we expect that the poly(3-((3S)-3,7-dimethyl-octyl)-thiophene (PTh) block can act as a color-changing chiral chromophore in visible range by external stimuli.

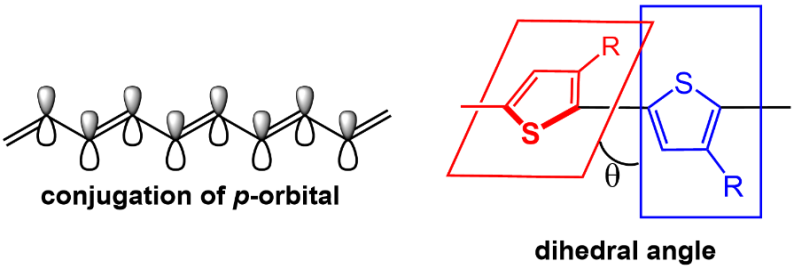

Figure 2.1. π-conjugation and dihedral angle of conjugated polymer backbone.

2.4 Chiral polythiophene

A series of poly(3-alkylthiophene)s with chiral side chain has been reported by Meijer group in 1990s[14-16]. First chiral aggregation of polythiophene was reported in 1995[15] (**Figure 2.3 (1)**).

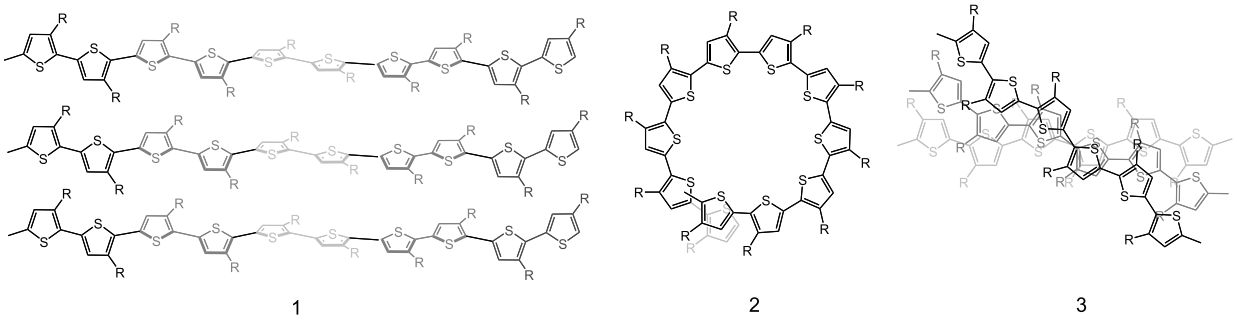

Figure 2.2. Chiral conformation of polythiophenes: helical transoid (1), helical cisoid (2), helical packing (3).

Chiral polythiophene derivatives have been intensively studied for interesting non-linear chiroptical properties. In 2000, Langeveld-Voss et. al. proposed three possible chiral conformation of polythiophenes: helical transoid, helical cisoid, and helical packing of predominantly planar backbone[14]. There have been long debates on the conformation of chiral polythiophenes.

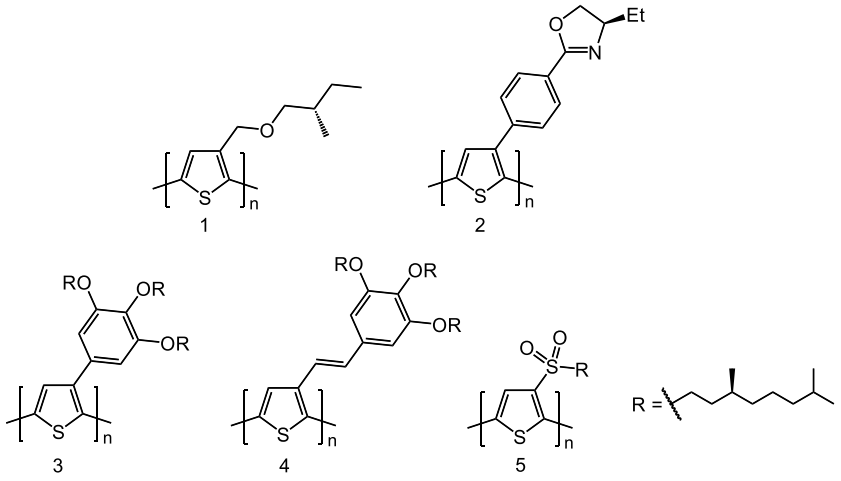

Figure 2.3. Representative examples of polythiophene with chiral pendants.

To investigate the detail conformation and the aggregation process, chiral polythiophenes with various chiral pendant have been synthesized and investigated their chiroptical property by CD spectroscopy. The chiral conformation and chital assembly are largely dependent on the substituents. Yashima et al that chiral polythiophene[17] (**Figure 2.3 (2)**) form helical stacking aggregation with predominantly planar backbone. Guy Koeckelberghs et al[18] experimentally demonstrated that poly(3-phenylthiophene) (**Figure 2.3 (3)**) and poly(3-ethylenephenylthiophene) (**Figure 2.3 (4)**) form helical stacking and helical cisoid, respectively. Recently, Swager et al postulated that poly-3-(alkyl sulfone)thiophene[19] (**Figure 2.3 (5)**) with chiral center form helical transoid which is supported by CD, DFT calculation and MD simulation. Additionally, direct observation by using scanning tunneling microscopy (STM) for chiral thiophene at liquid/solid interfaces was attempted[20].

2.5 Lyotropic liquid crystalline semiconducting

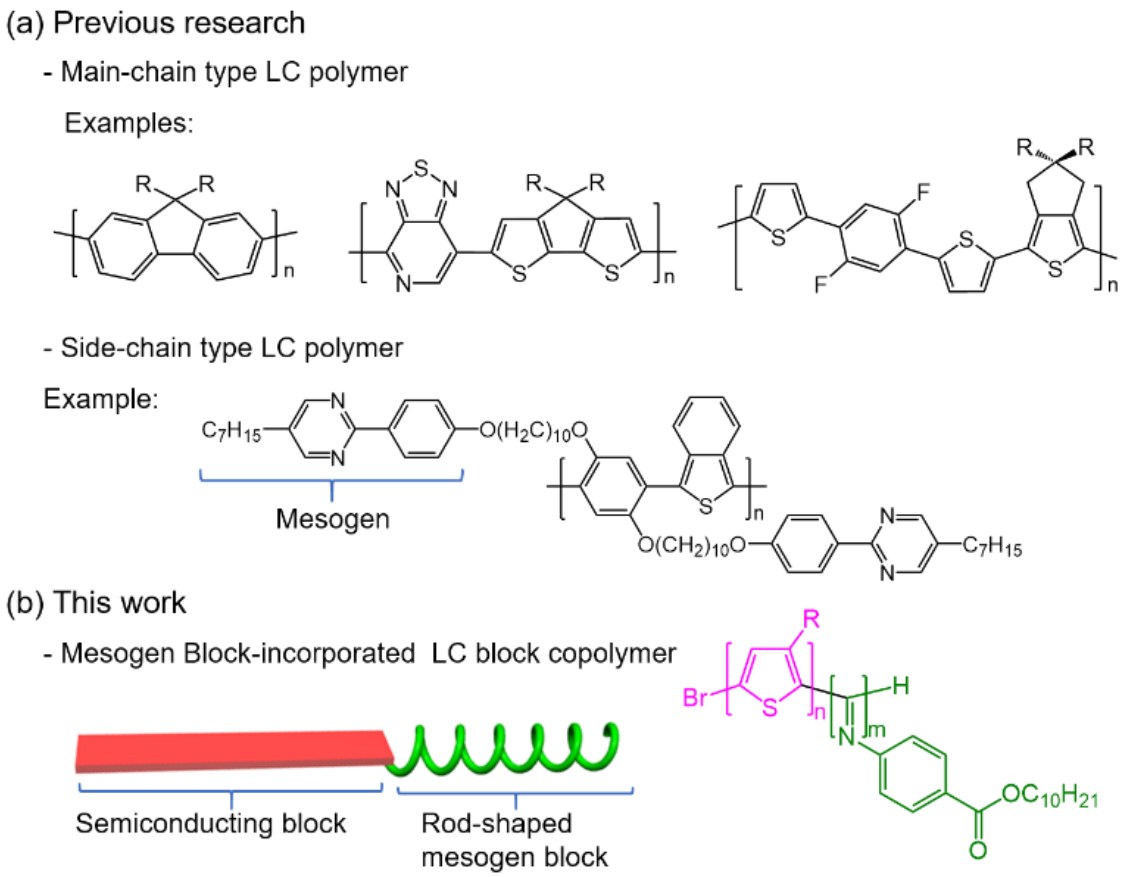

Figure 2.4. Representative examples of lyotropic liquid crystalline semiconducting polymers.

Semiconducting polymers possessing lyotropic liquid crystallinity are very rare[21-26]. Intrinsic stiff polymer backbone may not induce the mesophase. In many papers on developing LC semiconducting polymers, they incorporated small molecular LC component as side chain ("side-chain type LC polymers"[23]). However, this approach often deteriorates the intrinsic semiconducting nature of the semiconducting polymer. Furthermore, introduction of small LC moiety does not always guarantee the liquid crystallinity of the polymers because of the difficult control over the balance between stiffness of polymer backbone and softness of the LC side chains. Very recently, Segalman group[24-26] reported on donor-acceptor, main-chain type lyotropic liquid crystalline semiconducting polymers with appropriate side chain design. However, it requires elaborated design for side chain modifications to achieve moderate amphiphilicity. To push the conjugated polymers into the more practical applications, conjugated polymers possessing lyotropic liquid crystallinity are desired for next generation electronic materials.

2.6 Molecular design

Molecular design of conjugated polymers with high stimuli-responsiveness is challenging task. Because conjugated polymers possess strong π–π interaction between polymer chains in aggregation state, the film hardly

shows responsiveness to external stimuli. To control the conformation of the conjugated polymer backbones, various side chain modifications have developed, which provides the improvement in solubility, promotion of self-organization into higher order, and even suppression of the interaction between conjugated polymer backbones[27,28]. However, it is still challenging to create conjugated polymer films with high sensitivities to weak external stimuli, such as vapor and low pressure. conjugated polymer are attractive systems since they have π-electrons delocalized over the polymer backbone that are origins of electronic, optical and magnetic properties. In this context, "soft conjugated polymers" with high sensitivity to the above stimuli is greatly desired for future smart polymers. If such small stimuli are converted to the dynamic conformation change of the conjugated polymers, the signals are amplified, resulting in the drastic changes in color, conductivity and other electronic property.

Recently, Wu and Bielawski first reported the one-pot synthesis of polythiophene-block-polyphenylisocyanide, consisting of poly(3-hexylthiophene) and poly(decyl 4-phenylisocyanide)[29]. They have reported on a variety of morphologies of polythiophene-block-polyphenylisocyanide derivatives that form nanofibril, micelle and vesicle in a mixture of good and poor solvents and its pH-responsiveness[30-33].

We coincidentally found potentially important phenomena of PTh-*b*-PPI film: vapor-induced liquid crystallinity and self-recovering mechanochromism. We found out PPI block performs crucial roles in the block copolymer, which are intrinsically vapor-induced liquid crystallinity and self-reassembling property. PTh-*b*-PPI film possesses the softness and flexibility enough to show high sensitivity to solvent vapors and shear stresses.

2.7 Preparation of block copolymers

PTh-*b*-PPIs was synthesized according to the previously reported literature using the Grignard metathesis (GRIM) reaction[29,34,35] (**Figure 2.5, 2.6**). First, we prepared Ni-terminated poly(3-alkylthiophene) macro-initiator from 2,5-dibromothiophene in a flask, then PPI monomer was added. When the polymerization ceased, the resultant polymer was washed with a large volume of methanol and collected by filtration. The high value of PDI is probably caused by the broad polydispersity nature of Ni-terminated PTh macroinitiator as reported in the literature[36]. PTh-*b*-PPI was thoroughly characterized by NMR, IR, UV, CD, and PL and all the basic properties were well in accordance with those previously reported for polythiophene-block-polyphenylisocyanide derivatives[29-33].

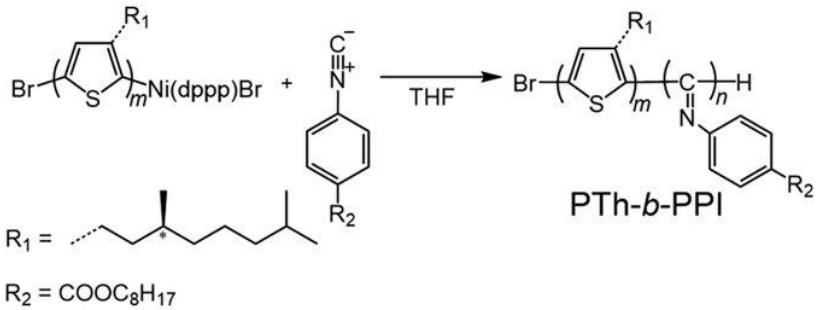

Figure 2.5. Synthetic route for PTh*-*b*-PPIC$_8$ through Grignard metathesis (GRIM) reaction in one-pot. dppp = 1,3-Bis(diphenylphosphino)propane. THF = Tetrahydrofuran. The GPC result for PTh*-*b*-PPIC$_8$: M_n = 16000, PDI = 4.47.

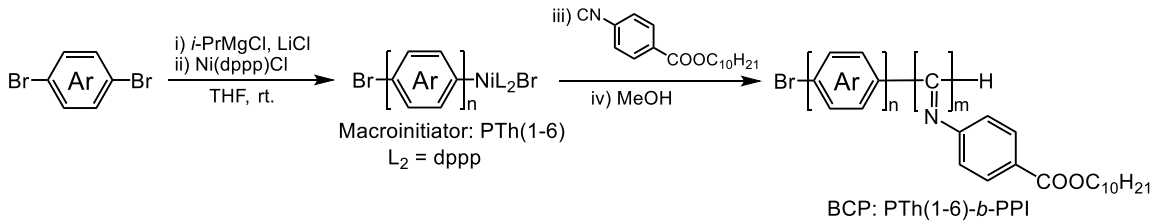

Figure 2.6. Block copolymerization initiated by Ni-terminated macroinitiator prepared by catalyst-transfer Kumada coupling.

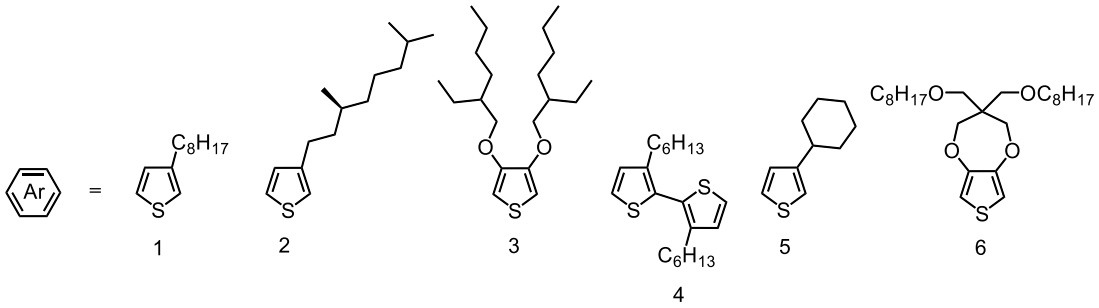

Figure 2.7. PTh blocks: 3-octylthiophene (1), 3-((*3S*)-3,7-dimethyl)thiophene (2), 3,4-di(2-ethylhexyloxy)thiophene (3), 3,3'-dihexyl-2,2'-bithiophene (4), 3-cyclohexylthiophene (5), ProDOT-COC_8 (6).

Table 2.1. Block copolymer and macroinitiator properties.

Entry	Polymer	Macroinitiator (PTh)		Block copolymer (PTh-*b*-PPI)	
		M_n (kDa) [b]	M_w/M_n [b]	M_n (kDa)[b]	M_w/M_n [b]
1	$PTh(1)_{23}$-*b*-PPI_6	4.8	1.27	6.6	1.10
2	$PTh(1)_{23}$-*b*-PPI_{12}	4.8	1.27	8.3	1.07
3	$PTh(1)_{25}$-*b*-PPI_{30}	5.2	1.27	14.0	1.06
4	$PTh(1)_{25}$-*b*-PPI_{90}	5.2	1.27	31.0	1.04
5	$PTh(1)_{25}$-*b*-PPI_{136}	5.2	1.27	44.2	1.78
6	$PTh(1)_{36}$-*b*-PPI_{14}	7.3	1.26	11.5	1.11
7	$PTh(1)_{36}$-*b*-PPI_{20}	7.3	1.26	13.2	1.10
8	$PTh(1)_{36}$-*b*-PPI_{44}	7.3	1.26	19.9	1.08
9	$PTh(1)_{94}$-*b*-PPI_{295}	18.3	1.41	102.9	1.14
10	$PTh(1)_{99}$-*b*-PPI_{27}	19.5	1.29	27.1	1.68
11	$PTh(2)_{33}$-*b*-PPI_{51}	7.5	1.32	22.1	1.17
12	$PTh(3)_{12}$-*b*-PPI_{73}	4.0	1.11	25.0	1.08
13	$PTh(3)_{12}$-*b*-PPI_{194}	4.0	1.11	59.8	1.12
14	$PTh(3)_{14}$-*b*-PPI_{72}	5.3	1.13	26.1	1.09
15	$PTh(3)_{14}$-*b*-PPI_{316}	5.3	1.13	96.2	1.20
16	$PTh(4)_{28}$-*b*-PPI_{678}	4.8	1.48	199.6	1.13
17	$PTh(5)_{32}$-*b*-PPI_{102}	4.9	1.30	34.1	1.09
18	PTh(6)*	7.1	1.44	-	-

b. Molecular weight and molecular distribution estimated by GPC analysis calibrated by polystyrene standard (eluent: THF, rt.). c. isolated yield in two steps. *No block copolymerization occurred from PTh(6).

2.8 Aggregation process in good/poor solvent mixture

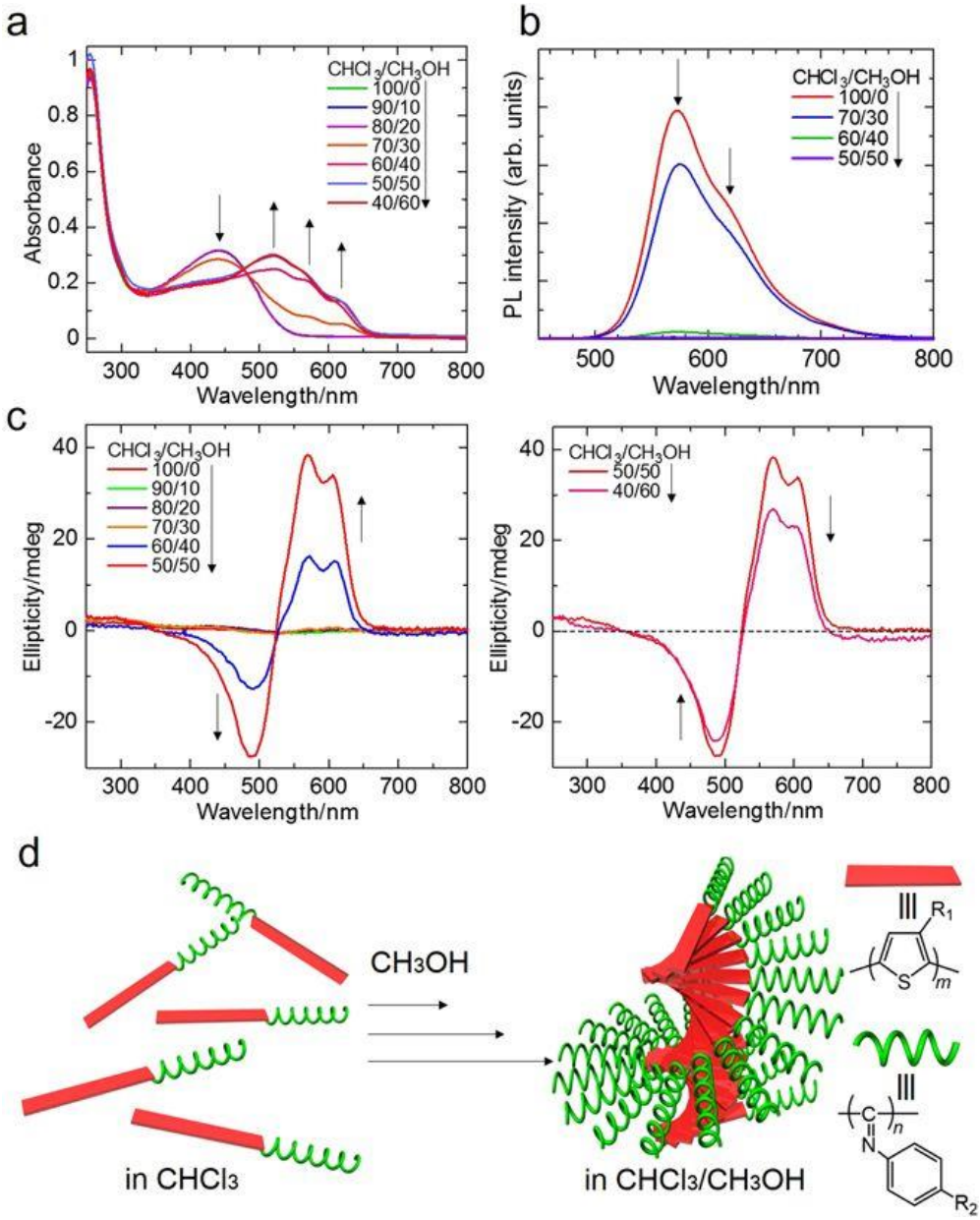

Figure 2.8. Chiral aggregation process of PTh*-*b*-PPIC$_8$ in solution driven by interaction of PTh blocks. (a) UV-vis absorption spectra, (b) Photoluminescence (PL) spectra (λex = 420 nm) and (c) Circular dichroism (CD) spectra of PTh-*b*-PPI in CHCl3/CH3OH solution (0.02 mg/ml) in various ratios. In high ratios of methanol, the spectra show film-like aggregation state. (d) Schematic illustration of PTh-*b*-PPI chiral aggregation in good/poor solvent mixture.

We first investigated the aggregation formation of PTh*-*b*-PPIC$_8$ in good/poor solvent-mixture. This characterization gives us the insights of film formation process and the interactions of PTh*-*b*-PPIC$_8$. In UV-vis spectra (**Figure 2.8a**), PTh*-*b*-PPIC$_8$ in chloroform shows absorption maxima at 255 nm (mainly from the PPI block) and 441 nm (derived from twisted state of the PTh block). Addition of methanol to the polymer solution decreases the absorption peak at 411 nm, and new signals appear near 520, 570, and 620 nm. This large red-shift indicates conformational change of the PTh block into *J*-aggregation states with planar main-chain conformation. The spectra

strongly support formation of PTh*-*b*-PPIC$_8$ aggregation driven by π–π interaction between the PTh blocks[36]. PL spectra (**Figure 2.8b**) also reveals that the chloroform solution state PTh*-*b*-PPIC$_8$ shows luminescence at 572 nm with a shoulder peak at ~ 630 nm. The PL signal is derived from twisted PTh blocks. As methanol is increased in the solution the PL intensity decreases, indicating formation of aggregation of PTh blocks. Furthermore, the chiroptical properties of PTh*-*b*-PPIC$_8$ were investigated by CD spectroscopy (**Figure 2.8c**). The PTh*-*b*-PPIC$_8$ in chloroform shows no CD signal, indicating random conformation of PTh*-*b*-PPIC$_8$. In the chloroform/methanol (40/60 v/v), the CD signals appeared at 605, 570 nm (positive) and 490 nm (negative). Additionally, the wavelength at the cross section from positive to negative (at 523 nm) corresponds to the maximum absorption wavelength of PTh*-*b*-PPIC$_8$ (at ~ 520 nm), indicating right-handed helical aggregation of PTh chromophores[37]. In high ratios of methanol, the CD intensity decreases because of the precipitation. These optical measurements suggest that *J*-aggregation of PTh*-*b*-PPIC$_8$ is driven by π–π interaction of PTh blocks.

2.9 Solvent vapor-induced lyotropic liquid crystallinity

We prepared PTh*-*b*-PPIC$_8$ film by a drop-casting method from chloroform solution (2.0 mg/mL) onto a quartz substrate. Subsequently, PTh*-*b*-PPIC$_8$I film was exposed to chloroform vapor annealing at room temperature. Very interestingly, the film color changed from purple to transparent yellow in ~ 1 min in chloroform vapor (**Figure 3.8a**). More surprisingly, polarizing optical microscopy (POM) observation evaluated the texture to be Schlieren structure of nematic liquid crystal phase **(Figure 3.8b, 3.8f)**. Other solvent vapors, such as tetrahydrofuran and dichloromethane, also induced the vapor-induced liquid crystal for the sample. After the removal of the vapor, the PTh*-*b*-PPIC$_8$ film recovered their color (yellow to purple) in ~ 1 sec. This reversible color change is repeatable.

To examine the vapor-induced conformation change of PTh*-*b*-PPIC$_8$ films, we performed optical measurements on the solid state (without vapor) and the LC state (with chloroform vapor). As shown in UV-vis spectra (**Figure 3.8c**), PTh*-*b*-PPIC$_8$ in solid state showed absorption peaks ~ 250 nm (π-π* transition of PPI block), 400 nm (n-π* transition of imine unit), and 527, 569, and 615 nm (PTh block). On the other hand, the LC-state PTh*-*b*-PPIC$_8$ showed blue shift with the characteristic absorption peaks at ~ 250 nm (π-π* transition of PPI block) and ~ 427 nm (the sum of n-π* transition of imine unit and PTh block). The large blue shift was due to the reduced effective π-conjugated length, which is probably caused by permeation of the solvent vapor molecules intruded between main chains. In contrast, the absorption maximum of the PPI block at 250 nm did not change even exposed to the solvent vapor, implying that the PPI rigid helical coil was not subjected to intrusion by the vapor, and maintained a stable helical conformation. CD spectroscopy (**Figure 3.8d**) shows PTh*-*b*-PPIC$_8$ in solid state exhibited first-positive and second-negative Cotton effect, while the LC state of PTh*-*b*-PPIC$_8$ showed no CD signals. The disappearance of CD spectra suggests the interruption of chiral interactions between PTh block by chloroform vapor. Additionally, PL spectroscopy (**Figure 3.8e**) shows PTh*-*b*-PPIC$_8$ in solid-state exhibited no signal in the visible region, while PTh*-*b*-PPIC$_8$ in LC state showed photoluminescence at ~ 610 nm, which is ascribed to PTh block (excitation wavelength: 420 nm). The optical measurements suggest that the molecules in the vapor phase intrude between main chains of PTh*-*b*-PPIC$_8$, and they depress the π-π interaction of PTh and expand the distance between the polymers, resulting in the blue-shift in UV-vis, the disappearance of the CD signal and the relaxation of the aggregation-induced quenching. It should be noted that PTh*-*b*-PPIC$_8$ in LC state has blue-shifted absorption and red-shifted luminescence

peaks compared to PTh*-*b*-PPIC$_8$ in solution state (**Figure 2.8a,b**). It implies that PTh chain in LC state is more twisted than in solution state, and the excited energy transfer between PTh chain may occur in the LC state

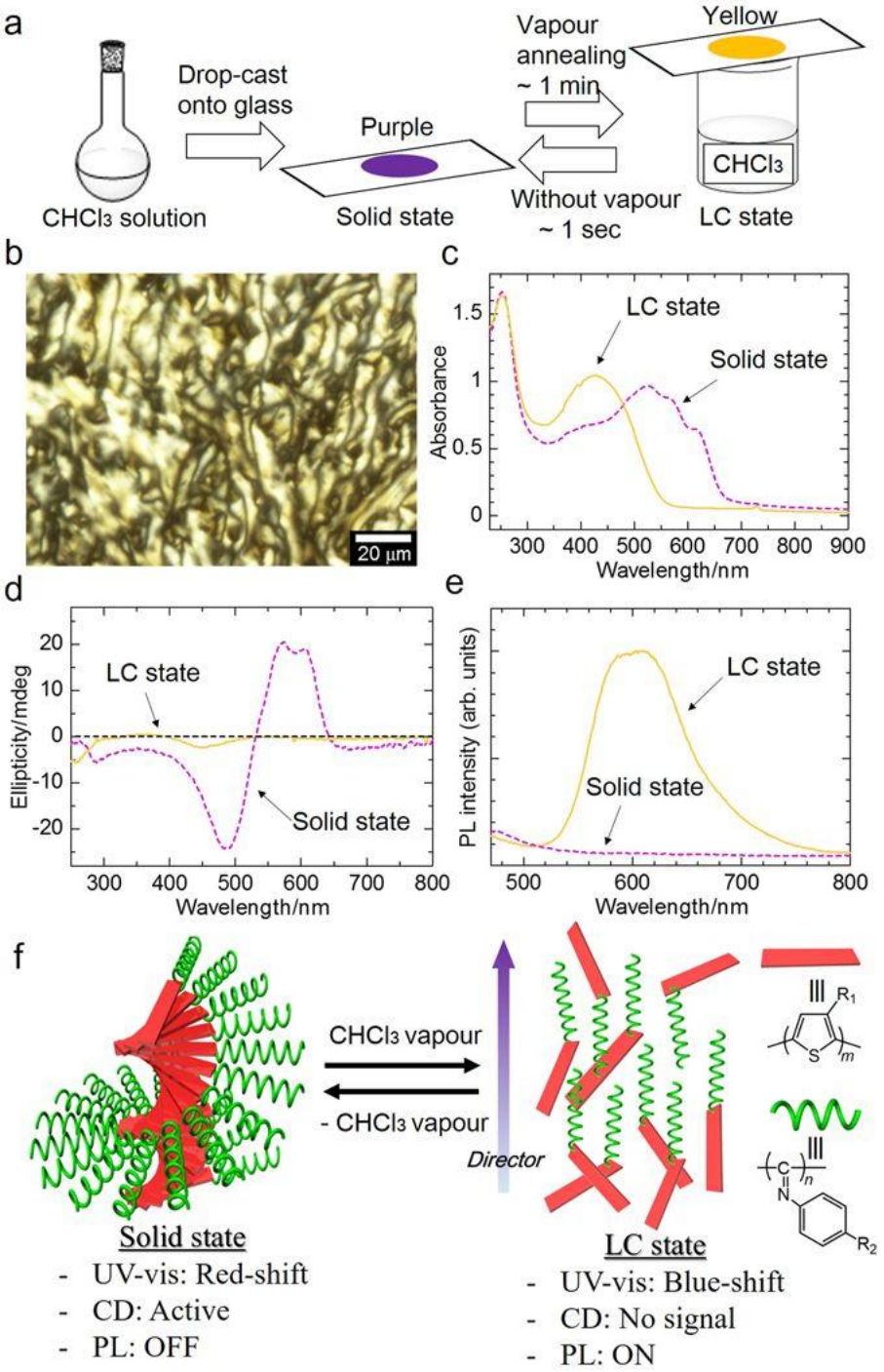

Figure 2.9. Vapor-induced liquid crystallinity of PTh*-*b*-PPIC$_8$. (a) Schematic representation of PTh*-*b*-PPIC$_8$ film preparation and vapor exposure. The film shows purple in solid state and yellow in liquid crystal (LC) state (under chloroform vapor). (b) Polarizing optical microscopy (POM) image of PTh*-*b*-PPIC$_8$ film in LC state (when exposed to chloroform vapor). (c) Absorption, (d) CD and (e) PL spectra (λex = 420 nm) of PTh*-*b*-PPIC$_8$ film in solid state and LC state. (f) Schematic illustration of reversible phase-transition behavior between solid state and nematic-like LC state of PTh*-*b*-PPIC$_8$ PPI blocks serve as mesogens and have orientation along the director.

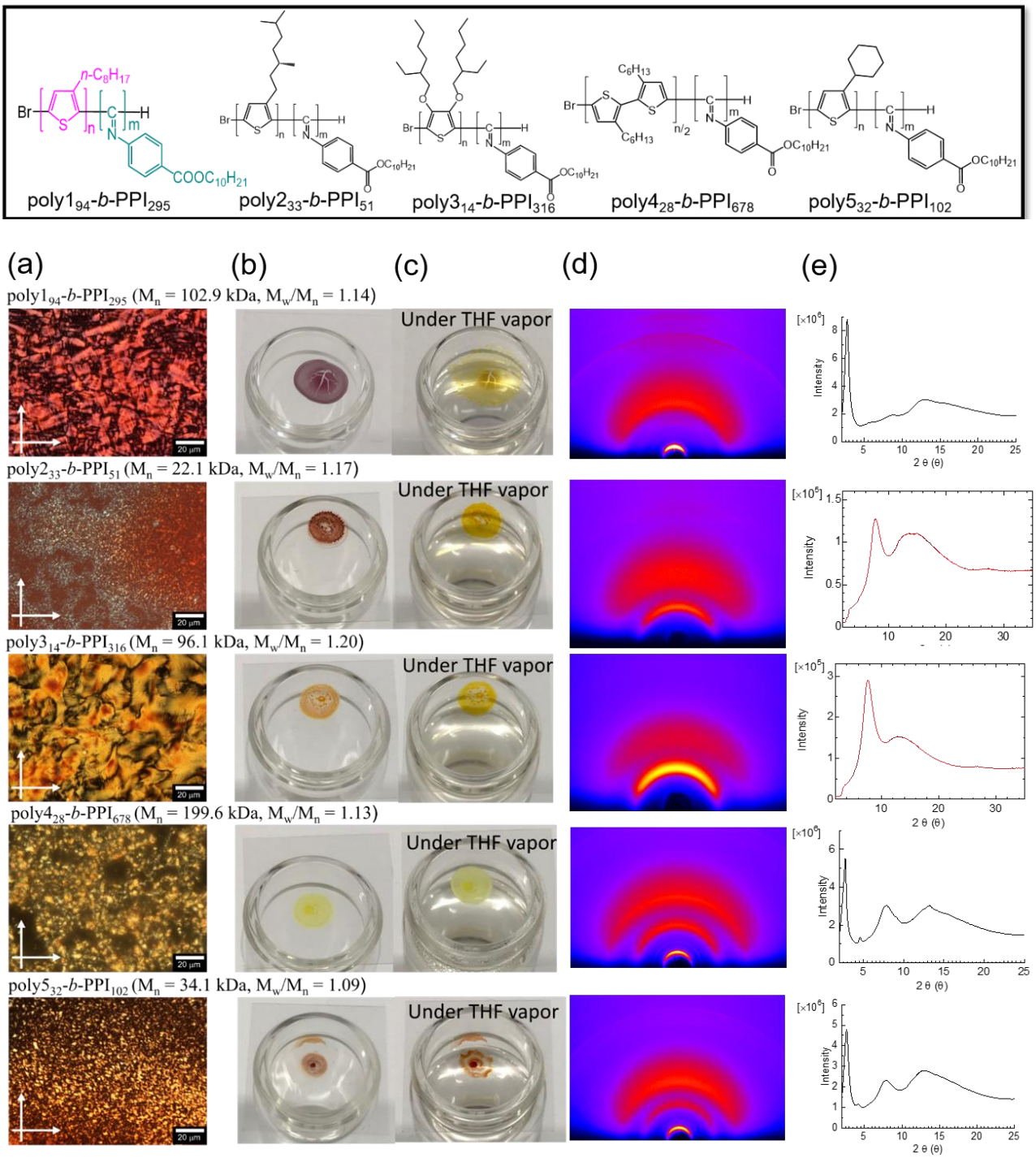

Figure 2.10. Lyotropic liquid crystallinity and GIXRD measurements for **PTh-*b*-PPI** films. (a) POM images, (b) photographs of films without vapor and (c) films under THF vapor, (d) GIXRD diffraction profiles of **PTh-*b*-PPI** films.

We envisioned that incorporation of PPI block to other polythiophene derivatives also allows the expression of lyotropic liquid crystallinity. To explore the monomer scope of this block copolymerization methodology, five kinds of **PTh-*b*-PPI**s, poly1$_{94}$-*b*-PPI$_{295}$, poly2$_{33}$-*b*-PPI$_{51}$, poly3$_{14}$-*b*-PPI$_{316}$, poly4$_{28}$-*b*-PPI$_{678}$, poly5$_{32}$-*b*-PPI$_{102}$ with different polythiophene derivatives were synthesized (**Figure 2.10**). The GPC results are summarized in **Table 2.1**. High-molecular-weight PTh-containing poly1$_{94}$-*b*-PPI$_{295}$ also exhibits vapor-induced phase transition under THF vapor.

This supports that incorporation of PPI gives the moderate softness to the intrinsic stiff semiconducting polythiophene. GIXRD measurements for poly1$_{94}$-*b*-PPI$_{295}$ film indicates that poly1$_{94}$-*b*-PPI$_{295}$ form liquid crystalline structure originating from the liquid crystalline nature of PPIs. Other PPI-incorporated polythiophene derivatives, poly2$_{33}$-*b*-PPI$_{51}$, poly3$_{14}$-*b*-PPI$_{316}$, poly4$_{28}$-*b*-PPI$_{678}$, poly5$_{32}$-*b*-PPI$_{102}$ exhibit similar manner. Chiral side chain-modified poly2$_{33}$-*b*-PPI$_{51}$, exhibits chiral structural change as discussed in **Figure 2.9d**. Ether-alkyl modified poly3$_{14}$-*b*-PPI$_{316}$ showed the different color appearance because electron-donating nature of ether-alkyl pendant induce the electron-rich polythiophene. Compared to poly1 and poly2, poly3 has regio-synmetric structure, where the neighboring side chain faces one another resulting in the distortion of repeating units. We assume that this symmetric structure of poly3$_{14}$-*b*-PPI$_{316}$ hinders the planarization of polythiophene backbone even in the solid state, showing the blue-shifted electronic absorption. No color change is observed in poly3$_{14}$-*b*-PPI$_{316}$ film under THF vapor, probably because of no planar-twist conformation change between solid state and liquid or liquid crystalline state. Similar phenomenon was observed in bulky cyclohexyl-modified poly5$_{32}$-*b*-PPI$_{102}$ film. Although poly5 has regio-regular structure in the main chain, the steric effect bulky substituent probably promotes non-planar polythiophene backbone both in solid state and THF vapor-exposed state (no conformation change). These experiments gave the insight into the color change arising from conformation change of polythiophene block under THF vapor. Furthermore, "PPI-incorporated liquid crystallinity" concept is applicable to wide range of polythiophene derivatives.

2.10 PPI-length dependent lyotropic liquid crystallinity

To precisely investigate the effects of the length of PPI block on the liquid crystallinity, five kinds of PTh-*b*-PPIs, **poly1$_{23}$-*b*-PPI$_{6}$**, **poly1$_{23}$-*b*-PPI$_{12}$**, **poly1$_{25}$-*b*-PPI$_{30}$**, **poly1$_{25}$-*b*-PPI$_{90}$**, **poly1$_{25}$-*b*-PPI$_{136}$** were synthesized with different PPI length while the length of polythiophene blocks were almost constant. Since PPIs form stiff rod-shaped helical structures, we assumed that the aspect ratio of the 1D shape of PPI would be proportional to the molecular weight. PTh-*b*-PPI films were prepared by drop-cast from the corresponding THF solutions. The resulting films were observed by POM without any annealing (heat or solvent vapor) process. As expected, high-molecular-weight PPI-incorporated PTh-*b*-PPI, **poly1$_{25}$-*b*-PPI$_{90}$**, **poly1$_{25}$-*b*-PPI$_{136}$**, showed nematic liquid crystalline structure in solid state, whereas low-molecular-weight PPI-incorporated PTh-b-PPI, **poly1$_{23}$-*b*-PPI$_{6}$**, **poly1$_{23}$-*b*-PPI$_{12}$**, **poly1$_{25}$-*b*-PPI$_{30}$** showed almost no birefringence indication no LC periodic structure (**Figure 2.11**). This indicates that high-molecular-PPI incorporated **poly1$_{25}$-*b*-PPI$_{90}$**, **poly1$_{25}$-*b*-PPI$_{136}$** form films through lyotropic liquid crystalline state on solvent drying process. GIXRD measurements for PTh-b-PPI films indicate that all the block copolymer PTh-*b*-PPIs shows the distinct peak corresponding to interchain packing (23.7 Å), which is clearly different from that of PTh homopolymers, **PTh$_{23}$** and **PTh$_{25}$**. In semi-crystalline poly1$_{23}$ and poly1$_{25}$, the (100) reflection asignable to the poly(3-octylthiophe) interlayer distance was observed along with higher order reflection (200) and (300). Poly1$_{23}$ and poly1$_{25}$ also showed a diffraction at 3.6 Å, which corresponds to the poly(3-octylthiophe) π-stacking (010) distance. It is noteworthy that even incorporation of small fraction of PPI (e.g. PPI$_6$) to PTh block significantly change the XRD patterns. The peaks derived from interchain packing became sharper as the molecular weight of PPI block increased. This results clearly demonstrated that rod-shaped PPI block is crucial important factor to induce the lyotropic liquid crystalline phase in the PTh-*b*-PPI copolymer architecture.

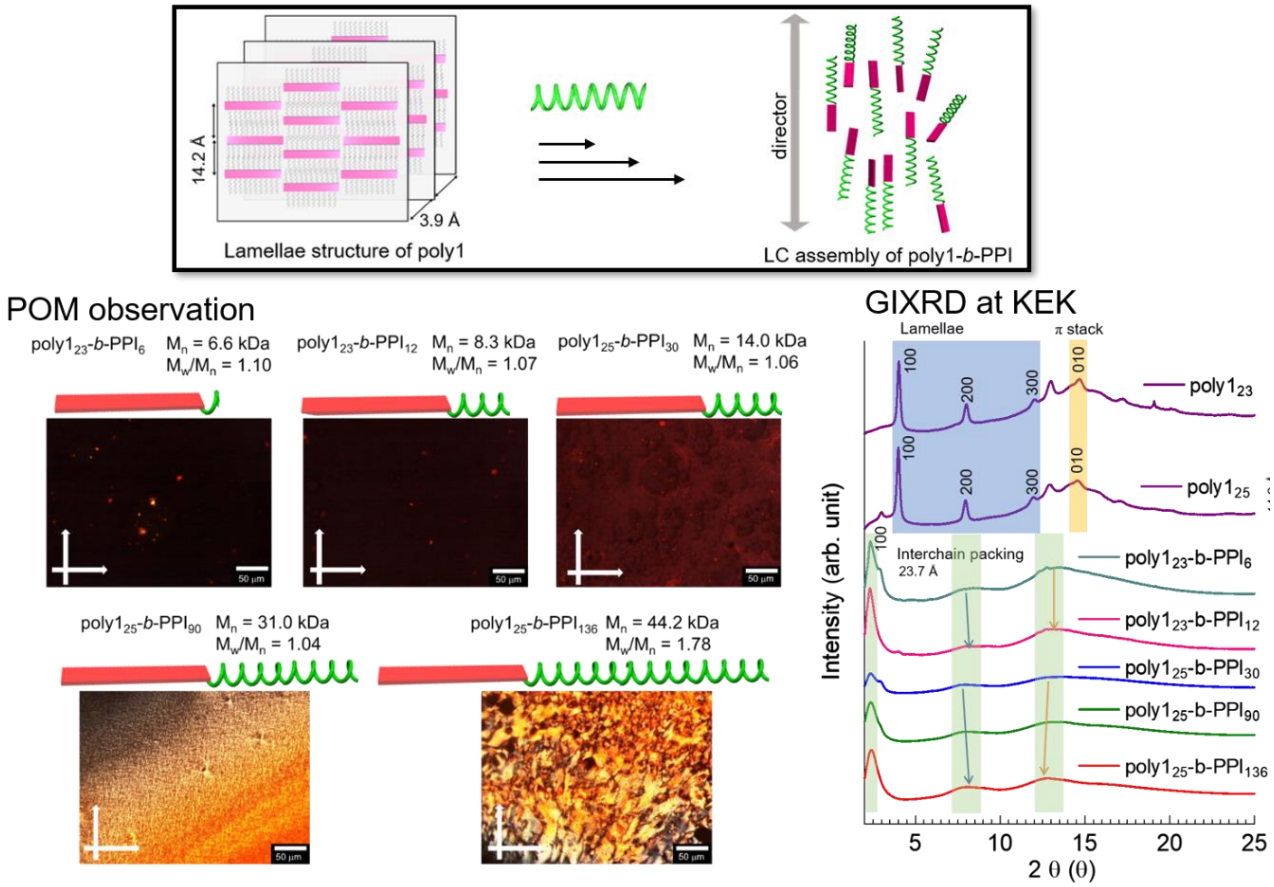

Figure 2.11. PPI-length dependent liquid crystallinity. POM observations and GIXRD measurements for poly1$_{23}$-*b*-PPI$_6$, poly1$_{23}$-*b*-PPI$_{12}$, poly1$_{25}$-*b*-PPI$_{30}$, poly1$_{25}$-*b*-PPI$_{90}$, poly1$_{25}$-*b*-PPI$_{136}$ films.

2.11 Magnetic orientation

Magnetic orientation with high-magnetic flux is one of the robust methods to orient the sample macroscopically because of non-destructive, non-contact, and highly space-penetrating nature of magnetic field. Magnetic alignment occurs when

$$|\Delta E_m| = |\Delta \epsilon_m| V_g \gg kBT$$

Where $\Delta\epsilon_m = -\Delta\chi B^2/2\mu_0$ is difference in magneto static energy density between orthogonal grain orientations (V_g : volume of a grain with characteristic dimension k_BT: thermal energy). For practical orientation time scale τ,

$$\tau \sim \frac{\eta}{\Delta\chi B^2} \quad (\eta\text{: generalized system viscosity})$$

To demonstrate the merit of vapor-induced LC properties of PTh*-*b*-PPIC$_8$ film, magnetic orientation of the film exposed to chloroform vapor was carried out (**Figure 2.12a**). Liquid crystalline nature of PPI block will provide geometrical anisotropic magnetic susceptibility, sufficient grain size, and moderate viscosity. As shown in **Figure**

2.12b, an intense magnetic field of 12 Tesla for 4 hours during the vapor-annealing successfully formed unidirectional orientation of PTh*-*b*-PPIC$_8$ films (**Figure 2.12b**). To investigate the unidirectionally oriented polymer structure, we employed linear dichroism (LD) spectroscopy. From the LD spectroscopy, we can determine the orientation of the sample,

$$LD = OD_{//} - OD_{\perp} = \log 10\ (I_{\perp}/I_{//})$$

where, OD is optical density, I is intensity of transmitted light in parallel ($_{//}$) and perpendicular ($_{\perp}$) direction relative to the magnetic field. **Figure 2.12c** shows the negative signal (550 - 750 nm) derived from the PTh block, and positive peak (300-500 nm) coming from the PPI block (**Figure 2.12 LD spectra (right)**). Generally, PTh (conjugated polymer) possesses π-π* electron transition moment along its backbone. That is, the positive signal indicates the PTh main chain is oriented perpendicular to the magnetic field. On the other hand, because the phenyl rings of the PPI helical block extend at the peripheral position of the helix core, the transition moment is perpendicular to the helical cylinder[38]. Therefore, the negative signal means that the phenyl group in the side chain aligns parallel, and the helical axis perpendicular relative to the magnetic field (**Figure 2.12d**). This alignment was realized by vapor-induced LC of PTh*-*b*-PPIC$_8$ and the magnetically anisotropic susceptibility, grain size, and moderate viscosity of PPI block.

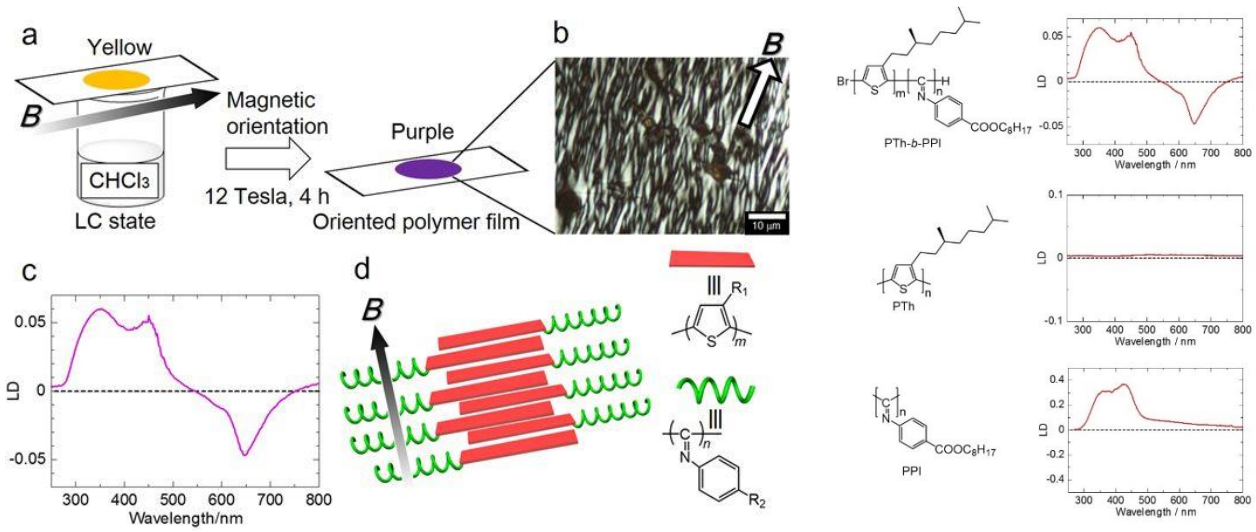

Figure 2.12. Magnetic orientation of PTh*-*b*-PPIC$_8$ film. (a) Schematic representation of magnetic orientation of PTh- b -PPI film with exposure to chloroform vapor. (b) POM image of magnetically oriented PTh*-*b*-PPIC$_8$ film. (c) Linear dichroism (LD) spectrum of magnetically oriented PTh- b -PPI film. (d) Schematic illustration of magnetically oriented PTh*-*b*-PPIC$_8$. Here, the parallel direction is along the direction of the magnetic field.

To further investigate the PPI-length dependent magnetic orientation of **PTh-*b*-PPI**s, precisely-synthesized **poly1$_{25}$-*b*-PPI$_{30}$**, **poly1$_{25}$-*b*-PPI$_{90}$**, **poly1$_{25}$-*b*-PPI$_{136}$**, **PPI$_{199}$** were used for magnetic orientation in 12 Tesla under THF vapors for 1 h. The orientational order of magnetically-treated **PTh-*b*-PPI** films was characterized by polarizing optical microscopy with the sample rotation of 45°. As expected, high molecular weight PPI-incorporated **PTh-*b*-PPI**, **poly1$_{25}$-*b*-PPI$_{136}$** film was unidirectionally aligned by magnetic field, whereas low molecular weight PPI-incorporated **PTh-*b*-PPI**, **poly1$_{25}$-*b*-PPI$_{30}$**, **poly1$_{25}$-*b*-PPI$_{90}$** films did not show any distinct orientation. **Poly1$_{25}$-*b*-**

PPI_{136} possesses sufficient anisotropic magnetic susceptibility from molecules and enough grain size from molecular assembly for magnetic orientation.

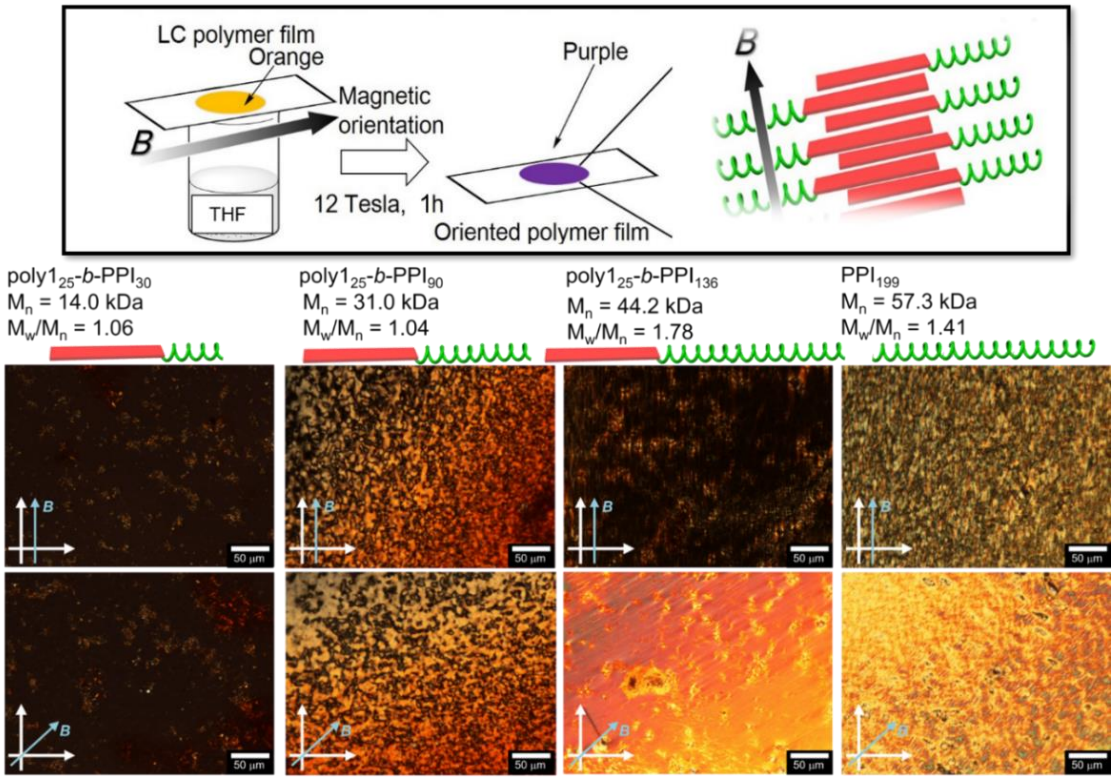

Figure 2.13. PPI-length dependent magnetic orientation. High-intensity magnetic field of 12 Tesla for 1 hour was applied for PPI-*b*-PPI films under THF vapor. The resulting films were observed by POM under cross-Nicols with angle of 0° and 45° against the direction of applied magnetic field

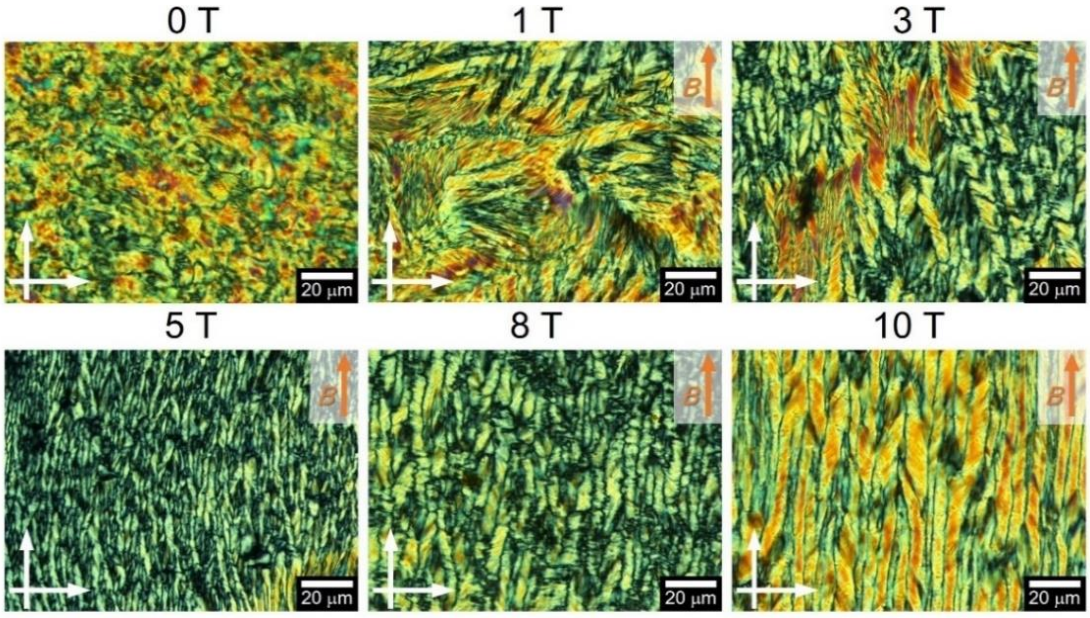

Figure 2.14. POM images for magnetically oriented $PPIC_{12}$ films under chloroform vapor in 0-10 Tesla.

To pursue the origin of magnetic field-assisted orientation, magnetic orientation of homopolymer PPI was also carried out. PPI bearing dodecyl side chain ($PPIC_{12}$) homopolymer films were employed in this experiment. As show in **Figure 2.14**, POM observation for $PPIC_{12}$ films demonstrated higher intensity magnetic field induced more unidirectionally ordered structures. Interestingly, the increase of grain size was observed as the magnetic field intensity increase in POM observation. To estimate the degree of unidirectional orientation, LD spectra was measured for the films, and the peak intensity was plotted against magnetic field intensity (**Figure 2.15**). The threshold for magnetic alignment is around 5-8 Tesla. This experiment demonstrated that $PPIC_{12}$ homopolymer possesses intrinsic vapor-induced liquid crystallinity and the resultant liquid crystalline grain formation sufficient for magnetic alignment.

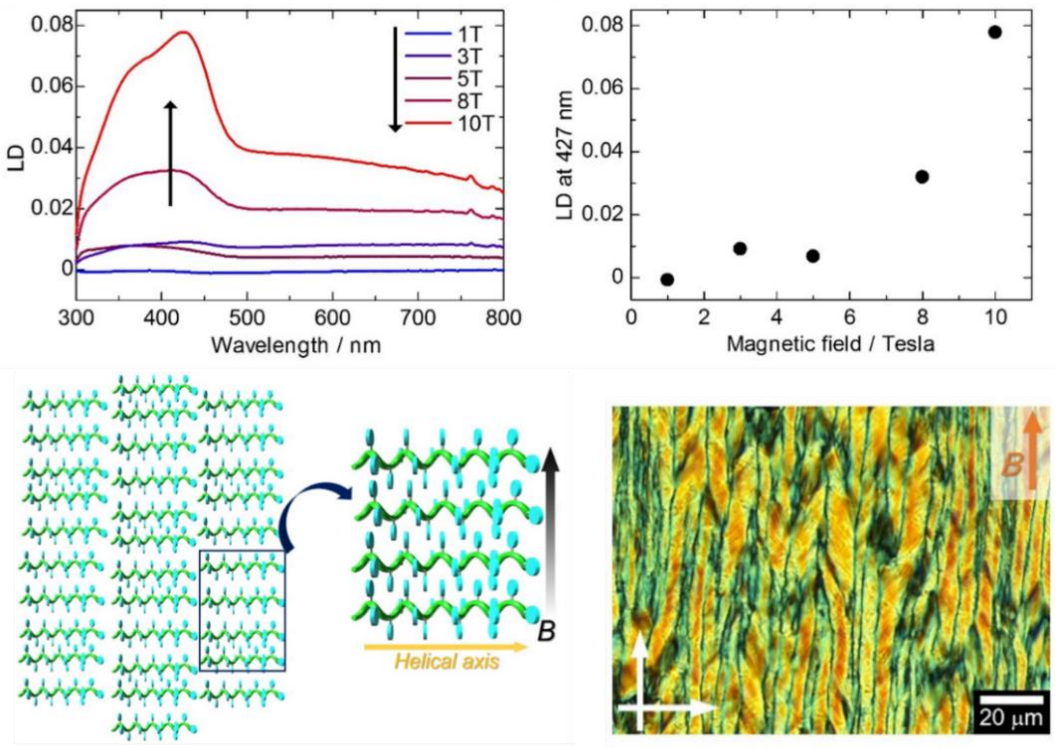

Figure 2.15. LD spectra for PPIC12 films and the corresponding plots (LD vs Tesla). Schematic illustration for oriented polymer assembly under magnetic field.

2.12 Self-recovering mechanochromism

Additionally, we performed a grinding test for the PTh*-*b*-$PPIC_8$ solid film (**Figure 2.16a**). Interestingly, we found that the film gradually turned to vermillion from purple during mechanical shearing. After the removal of the force, the color recovered to purple under ambient conditions without any treatment in ~ 30 sec (**Figure 2.16b**). In addition, the shear-stressed film showed anisotropic absorption between the parallel and perpendicular shear directions, which was confirmed by visible inspection through polarizers. As shown in the LD spectroscopy (**Figure 2.16c**), the broad positive peak at 450 - 800 nm is ascribed to the PTh block. Thus, the LD spectra indicates parallel orientation of the PTh chains to the shear direction. This implies that the rod shaped PTh block also can function as mesogen in shear-induced orientation. This shear-induced anisotropic orientation could be repeated, indicating a capability for

overwriting/rewriting. This self-recovery mechanochromism is a unique phenomenon because many mechanochromism materials require aging treatment such as annealing, fuming and recrystallization to regain original color[39]. The color change during the shear process probably comes from conformation and aggregation change of the PTh block. Although the detailed mechanism of the phenomenon is unclear, we assume that friction heat of shear stress causes conformation change of PTh block (**Figure 2.17**). After removal of the shear stress, the liquid crystalline PPI moiety probably facilitates the rearrangement to the original packing structure.

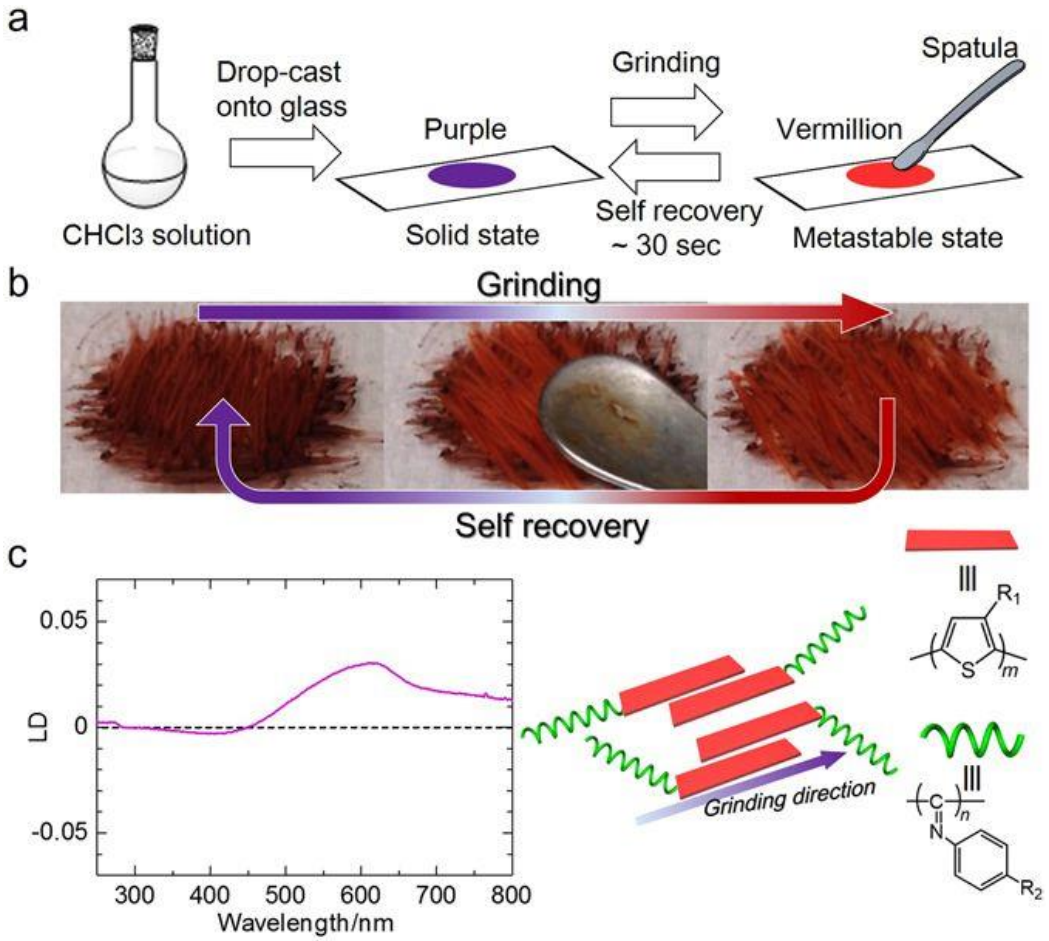

Figure 2.16. Self-recover mechanochromism of PTh*-*b*-PPIC$_8$. (a) Schematic representation of mechanical treatment of PTh*-*b*-PPIC$_8$ films. (b) Photographs of PTh*-*b*-PPIC$_8$ before and after mechanical stress. (c) LD spectrum of mechanically oriented PTh-b-PPI film and schematic illustration of mechanically oriented PTh*-*b*-PPIC$_8$. Here, the parallel direction is along the grinding direction

To investigate the thermo-properties of PTh*-*b*-PPIC$_8$, the PTh*-*b*-PPIC$_8$ film was monitored using polarizing optical microscopy (POM) on the temperature variable stage. The temperature range was 25 – 350°C and heating rate was 10°C/min. In the range of 25 – 120°C, the color of the film turned to yellow from purple. This state was liquid crystal phase. On the heating process in 120 - 150°C, phase transition occurred, and the film formed network structure. This partial melting was originated from the glass transition of PTh block. In the range of 150 – 350°C, the film showed no changes. Finally, at 350°C, the PTh*-*b*-PPIC$_8$ was completely melt, indicating the phase transition to isotropic phase.

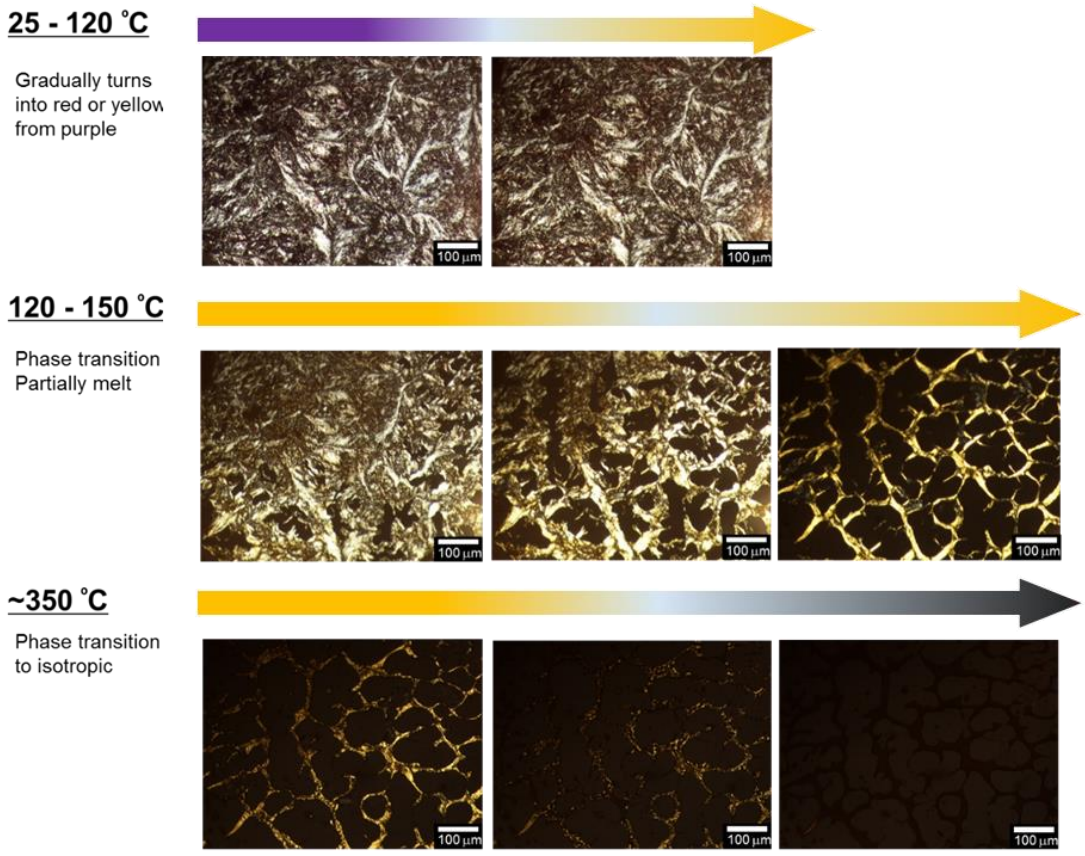

Figure 2.17. POM images of thermochromism behavior of PTh*-*b*-PPIC$_8$ film on glass substrate.

2.13 Chiral communication between blocks in BCPs

Chiral communication between blocks in **PTh-*b*-PPI** architecture is another intriguing topic. To address this issue, we synthesized three chiral block copolymers **PTh-*b*-PPI*** comprising regio-regular, achiral poly(3-octylthiophene) and poly(phenyl isocyanide) bearing chiral pendant with L-alanine residue. The GPC results are summarized in Table 2.2. All the **PTh-*b*-PPI***s exhibited positive Cotton effect at around 365 nm derived from n-π* transition of C=N imino moiety, indicating that **PPI*** block forms right-handed helical structure ((*P*)-helicity). It should be noted that the CD intensity of **PTh-*b*-PPI*** increased as the molecular weight of **PPI*** increased. On the other hand, (*L*)-PPI synthesized by $NiCl_2 \cdot 6H_2O$ catalyst in THF at room temperature showed negative Cotton effect at around 365 nm, indicating that **PPI*** homopolymer forms left-handed helical structure ((*M*)-helicity). It is reported that the polyisocyanide analogue bearing the similar *n*-decyl-(*L*)-alanine residue forms left-handed helical structure in thermodynamically stable state. This means that $NiCl_2 \cdot 6H_2O$ catalyzed polymerization affords preferentially left-handed helical polymer, while Ni-terminated P3OT macroinitiator initiates the preferentially right-handed helical "Merry-go-round" polymerization of phenyl isocyanide, which is kinetically-determined state. The resultant diastereomeric products from the same chiral monomer would give the further insight into the block copolymerization between catalyst-transfer Kumada coupling and Ni-catalyzed "Merry-go-round" polymerization.

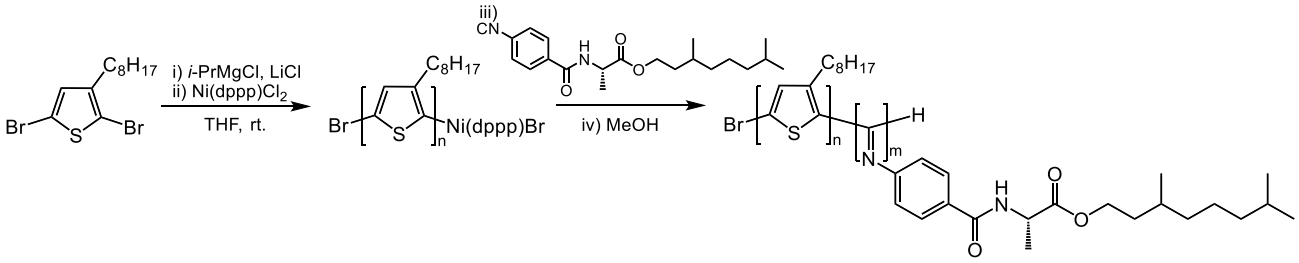

Figure 2.18.

Table 2.2. Block copolymer and macroinitiator properties.

Entry	Polymer	Macroinitiator (PTh)		Block copolymer (PTh-*b*-PPI)	
		M_n (kDa) [b]	M_w/M_n [b]	M_n (kDa)[b]	M_w/M_n [b]
1	PTh-*b*-(*L*)PPI*	5.8	1.36	147.4	1.13
2	PTh-*b*-(*L*)PPI*	5.8	1.36	250.9	1.28
3	PTh-*b*-(*L*)PPI*	5.8	1.36	290.1	1.25
4*	(*L*)PPI*	418.9	1.70	-	-

b. Molecular weight and molecular distribution estimated by GPC analysis calibrated by polystyrene standard (eluent: THF containing 0.1% tetrabutylammonium bromide (TBAB), rt.). c. isolated yield in two steps. d. Block ratio of block copolymers (mol ratio of PTh to PPI) calculated by ^{1}H NMR integration. *Entry 4 was prepared by Ni(II) salt.

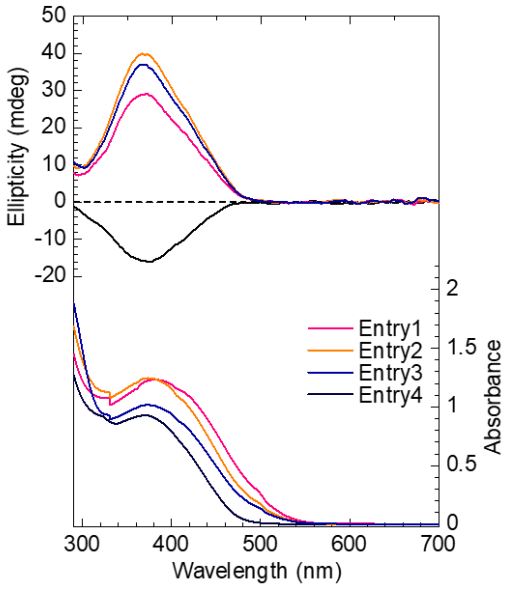

Figure 2.19. CD and UV-vis absorption specta for PPI and P3OT-*b*-PPIs (0.2 mg/mL in THF or chroloform at rt).

2.14 Conclusion and perspective

We demonstrated vapor-induced liquid crystallinity and self-recovering mechanochromism of PTh-*b*-PPI. We found out new promising properties of rod-type helical coiled polymer PPI block: intrinsically vapor-induced liquid crystallinity and self-reassembling property. Introduction of PPI block offers anisotropic magnetic susceptibility, large grain size, and moderate viscosity enough for PTh-*b*-PPI film to possess high sensitiveness to solvent vapor

and self-recovery property against shear stress at ambient condition. In addition, PPI block in PTh-*b*-PPI produces the anisotropic magnetic susceptibility for magnetic alignment. As far as we know, PTh-*b*-PPI is the first material that exhibits vapor-induced liquid crystallinity. PPI helical structural motif has been employed mainly as chiral catalyst[40], chiral separation[41], chiral recognition[42] because PPI can form one-handed helical conformation. Our study will pioneer new functionalities of rod-shaped helical polymers. Furthermore, magnetic orientation for vapor-exposed films provides a simple and convenient method to examine the films, offering a new orientation approach for block copolymers that possess anisotropic magnetic susceptibility units. We believe this block copolymer can be applied in phase-transition-type vapor sensors, pressure sensors, and as a memory medium for shear directions.

References

[1] Holtz, J. H., & Asher, S. A. Polymerized colloidal crystal hydrogel films as intelligent chemical sensing materials. Nature 389, 829-832 (1997).
[2] Mura, S., Nicolas, J., & Couvreur, P. Stimuli-responsive nanocarriers for drug delivery. Nat. Mater. 12, 991-1003 (2013).
[3] Ahn, S. K., Kasi, R. M., Kim, S. C., Sharma, N., & Zhou, Y. Stimuli-responsive polymer gels. Soft Matter 4, 1151-1157 (2008).
[4] Stuart, Martien A. Cohen, et al. Emerging applications of stimuli-responsive polymer materials. Nat. Mater. 9, 101-113 (2010).
[5] Handbook of Liquid Crystals (Eds.: D. Demus, J.W. Goodby, G.W. Gray, H.-W. Spiess, V. Vill),Wiley-VCH,Weinheim, 1998.
[6] Schmitt, V., Lequeux, F., Pousse, A., & Roux, D. Flow behavior and shear induced transition near an isotropic/nematic transition in equilibrium polymers. Langmuir 10, 955-961 (1994).
[7] Pujolle-Robic, C., & Noirez, L. Observation of shear-induced nematic–isotropic transition in side-chain liquid crystal polymers. Nature 409, 167-171(2001).
[8] Yoshio, M., Mukai, T., Ohno, H., & Kato, T. One-dimensional ion transport in self-organized columnar ionic liquids. J. Am. Chem. Soc. 126, 994-995 (2004).
[9] Ohtake, T., Ogasawara, M., Ito-Akita, K., Nishina, N., Ujiie, S., Ohno, H., & Kato, T. Liquid-crystalline complexes of mesogenic dimers containing oxyethylene moieties with LiCF3SO3: Self-organized ion conductive materials. Chem. Mater. 12, 782-789 (2000).
[10] Ichimura, K. Photoalignment of liquid-crystal systems. Chem. Rev. 100, 1847-1874 (2000).
[11] Tao, Y., Zohar, H., Olsen, B. D., & Segalman, R. A. Hierarchical nanostructure control in rod-coil block copolymers with magnetic fields. Nano Lett. 7, 2742–2746 (2007).
[12] Hayashi, H., Iseki, T., Nimori, S., & Goto, H. (2017). Vapour-Induced Liquid Crystallinity and Self-Recovery Mechanochromism of Helical Block Copolymer. Scientific Reports, 7(1), 3948.
[13] Beaujuge, P. M., & Reynolds, J. R. (2010). Color control in π-conjugated organic polymers for use in electrochromic devices. Chemical reviews, 110(1), 268-320.
For chiral conjugated polymers,
[14] Langeveld-Voss, B. M. W., Janssen, R. A. J., & Meijer, E. W. (2000). On the origin of optical activity in polythiophenes*. Journal of Molecular Structure, 521(1-3), 285-301.
[15 Bouman, M. M., & Meijer, E. W. (1995). Stereomutation in optically active regioregular polythiophenes. Advanced Materials, 7(4), 385-387.
[16] Langeveld-Voss, B. M. W., Christiaans, M. P. T., Janssen, R. A. J., & Meijer, E. W. (1998). Inversion of optical activity of chiral polythiophene aggregates by a change of solvent. Macromolecules, 31(19), 6702-6704.
[17] Goto, H., & Yashima, E. (2002). Electron-induced switching of the supramolecular chirality of optically active polythiophene aggregates. Journal of the American Chemical Society, 124(27), 7943-7949.
Helical cisoid, helical packing
[18] Leysen, P., Teyssandier, J., De Feyter, S., & Koeckelberghs, G. (2018). Controlled Synthesis of a Helical Conjugated Polythiophene. Macromolecules, 51(9), 3504-3514.
Helical transoid
[19] Wang, P., Jeon, I., Lin, Z., Peeks, M. D., Savagatrup, S., Kooi, S. E., ... & Swager, T. M. (2018). Insights into Magneto-Optics of Helical Conjugated Polymers. Journal of the American Chemical Society.
Direct observation
[20] Cao, H., Van Den Eede, M. P., Koeckelberghs, G., Mali, K. S., & De Feyter, S. (2017). Direct observation of the influence of chirality on the microstructure of regioregular poly (3-alkylthiophene) s at the liquid/solid interface. Chemical Communications, 53(1), 153-156.
[21] Kim, B. G., Jeong, E. J., Chung, J. W., Seo, S., Koo, B., & Kim, J. (2013). A molecular design principle of lyotropic liquid-crystalline conjugated polymers with directed alignment capability for plastic electronics. Nature materials, 12(7), 659.

[22] Luzio, A., Criante, L., D'innocenzo, V., & Caironi, M. (2013). Control of charge transport in a semiconducting copolymer by solvent-induced long-range order. Scientific reports, 3, 3425.
[23] Goto, H., Wang, A., Nimori, S., & Kawabata, K. (2013). Mechanical orientation in thermotropic liquid crystal state and magnetic orientation in solvent evaporation process via lyotropic liquid crystal state of an amphotropic low-bandgap liquid-crystalline π-conjugated polymer. Liquid Crystals, 40(9), 1159-1166.
[24] Bridges, C. R., Ford, M. J., Popere, B. C., Bazan, G. C., & Segalman, R. A. (2016). Formation and structure of lyotropic liquid crystalline mesophases in donor–acceptor semiconducting polymers. Macromolecules, 49(19), 7220-7229.
[25] Bridges, C. R., Ford, M. J., Bazan, G. C., & Segalman, R. A. (2017). Molecular Considerations for Mesophase Interaction and Alignment of Lyotropic Liquid Crystalline Semiconducting Polymers. ACS Macro Letters, 6(6), 619-624.
[26] Bridges, C. R., Ford, M. J., Thomas, E. M., Gomez, C., Bazan, G. C., & Segalman, R. A. (2018). Effects of Side Chain Branch Point on Self Assembly, Structure, and Electronic Properties of High Mobility Semiconducting Polymers. Macromolecules, 51(21), 8597-8604.
[27] Mei, J. and Bao, Z. Side chain engineering in solution-processable conjugated polymers. Chem. Mater. 26, 604-615 (2013).
[28] Kawabata, K., Saito, M., Takemura, T., Osaka, I., & Takimiya, K. Effects of branching position of alkyl side chains on ordering structure and charge transport property in thienothiophenedione-and quinacridone-based semiconducting polymers. Polymer Journal 49, 169-176 (2017).
[29] Wu, Z. Q., Ono, R. J., Chen, Z., & Bielawski, C. W. Synthesis of poly (3-alkylthiophene)-block-poly (arylisocyanide): Two sequential, mechanistically distinct polymerizations using a single catalyst. J. Am. Chem. Soc. 132, 14000–14001 (2010).
[30] Wu, Z.-Q., et al. One-pot synthesis of conjugated poly (3-hexylthiophene)-b-poly (phenyl isocyanide) hybrid rod–rod block copolymers and its self-assembling properties. Polym. Sci. A. Polym. Chem. 51, 2939–2947 (2013).
[31] Wu, Z. Q., Radcliffe, J. D., Ono, R. J., Chen, Z., Li, Z., & Bielawski, C. W. Synthesis of conjugated diblock copolymers: two mechanistically distinct, sequential living polymerizations using a single catalyst. Polym. Chem. 3, 874-881 (2012).
[32] Liu, N., Qi, C. G., Wang, Y., Liu, D. F., Yin, J., Zhu, Y. Y., & Wu, Z. Q. Solvent-Induced White-Light Emission of Amphiphilic Rod–Rod Poly (3-triethylene glycol thiophene)-block-poly (phenyl isocyanide) Copolymer. Macromolecules 46, 7753−7758 (2013).
[33] Zhu, Y.-Y., et al. Poly (3-hexylthiophene)-block-poly (5, 8-di-p-tolylquinoxaline-2, 3-diyl) conjugated rod–rod copolymers: one pot synthesis, self-assembly and highly selective sensing of cobalt. RSC Adv. 4, 40241-40250 (2014).
[34] Loewe, R. S., Ewbank, P. C., Liu, J., Zhai, L., & McCullough, R. D. Regioregular, head-to-tail coupled poly (3-alkylthiophenes) made easy by the GRIM method: investigation of the reaction and the origin of regioselectivity. Macromolecules 34, 4324–4333 (2001).
[35] Miyakoshi, R., Yokoyama, A., & Yokozawa, T. Catalyst-transfer polycondensation. Mechanism of Ni-catalyzed chain-growth polymerization leading to well-defined poly (3-hexylthiophene). J. Am. Chem. Soc. 127, 17542–17547 (2005).
[36] Vandeleene, S., Jivanescu, M., Stesmans, A., Cuppens, J., Van Bael, M. J., Verbiest, T., & Koeckelberghs, G. Influence of the Supramolecular Organization on the Magnetic Properties of Poly (3-alkylthiophene) s in Their Neutral State. Macromolecules 44, 4911-4919 (2011).
[37] Bidan, G., Guillerez, S., & Sorokin, V. Chirality in regioregular and soluble polythiophene: an internal probe of conformational changes induced by minute solvation variation. Adv. Mater. 8, 157-160 (1996).
[38] Feng, F., Miyashita, T., Takei, F., Onitsuka, K., & Takahashi, S. Formation of an Optically Active Helical Polyisocyanide Langmuir-Blodgett Film. Chem. Lett. 30, 764–765 (2001).
[39] Sagara, Y., & Kato, T. Mechanically induced luminescence changes in molecular assemblies. Nat. Chem. 1, 605–610 (2009).
[40] Miyabe, T., Hase, Y., Iida, H., Maeda, K., & Yashima, E. Synthesis of functional poly (phenyl isocyanide) s with macromolecular helicity memory and their use as asymmetric organocatalysts. Chirality 21, 44–50 (2009).
[41] Miyabe, T., Iida, H., Ohnishi, A., & Yashima, E. Enantioseparation on poly (phenyl isocyanide) s with macromolecular helicity memory as chiral stationary phases for HPLC. Chem. Sci. 3, 863–867 (2012).
[42] Ishikawa, M., Maeda, K., Mitsutsuji, Y., & Yashima, E. An unprecedented memory of macromolecular helicity induced in an achiral polyisocyanide in water. J. Am. Chem. Soc. 126, 732–733 (2004).

Experimental

Synthesis of Br-terminated chiral alkyl chain

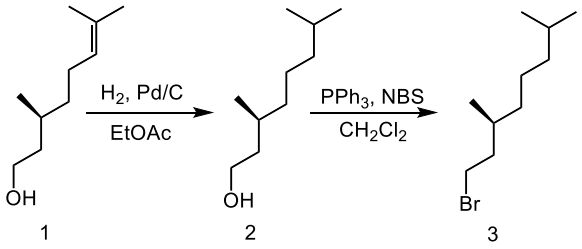

(*S*)-3,7-Dimethyl-1-octanol (2) A mixture of compound 2 (3 g, 19.2 mmol) and Pd/C (0.152 g, 5% by weight) in ethyl acetate was stirred at room temperature under H_2 atmosphere. After 2 days stirring, the crude product was filtered with Celite to yield colorless liquid (2.85 g, 17.98 mmol, 93.6%). ^{1}H NMR (400 MHz, $CDCl_3$): δ 3.71-3.65 (m, 2H), 1.61-1.50 (m, 3H), 1.40-1.26 (m, 5H), 1.17-1.11 (m, 2H), 0.90-0.85 (m, 9H). ^{13}C NMR (100 MHz, $CDCl_3$): δ 61.27, 39.99, 39.26, 37.37, 29.50, 27.97, 24.68, 22.70, 22.60, 19.65.

(3*S*)-1-Bromo-3,7-dimethyloctan (3) To a solution of compound 3 (2.8 g, 17.7 mmol) and triphenylphosphine (5.13 g, 19.5 mmol) in dichloromethane (30 mL) was added NBS (3.32 g, 18.6 mmol) in portions. After stirring for 4 h at room temperature, the reaction mixture was evaporated and extracted with *n*-hexane/H_2O followed by $MgSO_4$ drying. The crude product was purified by column chromatography (eluent: *n*-hexane) to yield colorless oil (2.49 g, 11.2 mmol, 63%). ^{1}H NMR (400 MHz, $CDCl_3$): δ 3.50-3.37 (m, 2H), 1.92-1.84 (m, 1H), 1.71-1.64 (m, 2H), 1.15-1.47 (m, 1H), 1.30-1.26 (m, 3H), 1.19-1.09 (m, 3H), 0.89-0.86 (m, 9H). ^{13}C NMR (100 MHz, $CDCl_3$): δ 77.32, 77.00, 76.68, 40.06, 39.15, 36.25, 32.25, 31.65, 27.93, 24.53, 22.68, 22.57, 18.94.

Synthesis of Thiophene monomer.

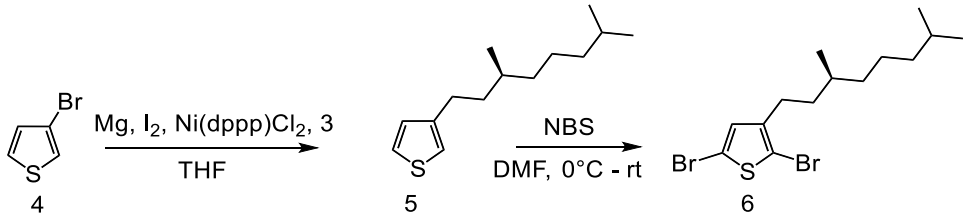

4 5 6

3-((3*S*)-3,7-Dimethyl-octyl)-thiophene (5) To a suspension of magnesium turnings (0.380 g, 15.6 mmol) in THF (10 mL) was added iodine (0.15 g). The suspension was refluxed for 2 h to activate magnesium resulting in yellow solution. **5** (3.18 g, 14.4 mmol) was added to the yellow mixture at 0°C and then refluxed for another 1h. The resulting gray solution was cooled to room temperature. To a another flask were added **6** (1.01 mL, 10. 66 mmol) and Ni(dppp)Cl_2 (0.07 g, 0.13 mmol) and dissolved in THF (10 mL). To this solution was added the gray solution dropwise at 0°C and then refluxed for 21h. The reaction was quenched by 2N hydrochloric acid at room temperature. The reaction mixture was evaporated and extracted with diethyl ether/H_2O followed by $MgSO_4$ drying. The crude product was purified by column chromatography (eluent: *n*-hexane) to yield the target product (1.76 g, 7.85 mmol, 74%). ^{1}H NMR (400 MHz, $CDCl_3$): δ 7.25-7.22 (m, 1H), 6.95-6.91 (m, 2H), 2.65-2.58 (m, 2H), 1.67-1.62 (m, 1H), 1.53-1.42 (m, 4H), 1.32-1.10 (m, 6H), 0.91-0.87 (m, 10H). ^{13}C NMR (100 MHz, $CDCl_3$): δ 143.44, 128.27, 125.04, 119.60, 39.30, 37.80, 37.12, 32.46, 27.96, 27.84, 24.69, 22.70, 22.61, 19.56.

2,5-Dibromo-3-((3*S*)-3,7-dimethyl-octyl)-thiophene (6) To a solution of **7** (1.76 g, 7.9 mmol) in DMF (55 mL) was added NBS (3.07 g, 17.3 mmol) in portions at 0°C. After stirring for 2 days at room temperature under N_2 atmosphere, the reaction was quenched by saturated $NaHCO_3$ aq. The reaction mixture was extracted with EtOAc/H2O followed by $MgSO_4$ drying. The crude product was purified by column chromatography (eluent: *n*-hexane) to yield **1b** (2.75 g, 7.2 mmol, 92%). ^{1}H NMR (400 MHz, $CDCl_3$): δ 6.78 (s, 1H), 2.54-2.47 (m, 2H), 1.56-1.10 (m, 11H), 0.92-0.90 (d, 3H), 0.87-0.86 (d, 6H). ^{13}C NMR (100 MHz, $CDCl_3$): δ 143.15, 130.89, 110.31, 107.74, 39.29, 36.95, 36.71, 32.87, 27.98, 27.17, 24.65, 22.72, 22.64, 19.55.

Into oven-dried three-neck flask were added 3-*n*-octyl thiophene (3.19 g, 16.2 mmol) and DMF (30 mL) under argon atmosphere. The solution was cooled to 0°C in ice bath and stirred for 10 min. *N*-bromo succinimide (6.36 g, 35.7 mmol) was added to the solution in portions. After stirring for 10 min at 0°C and then warm up to rt. and stirred for additional 3 days. The obtained yellow solution was quenched with $NaHCO_3$ aq. The mixture was extracted with

ethylacetate, washed with water three times. The combined organic phase was dried over magnesium sulfate. The crude product was purified by column chromatography (eluent: hexane) to afford clear colorless oil (4.11 g, 71%). ^{1}H NMR (400 MHz, $CDCl_3$, δ from TMS): δ 6.77 (s, 1H), 2.50 (t, 2H, J = 8.0 Hz), 1.54 (broad, 2H), 1.52-1.12 (m, 10H), 0.88 (t, 3H, J = 6.4 Hz).

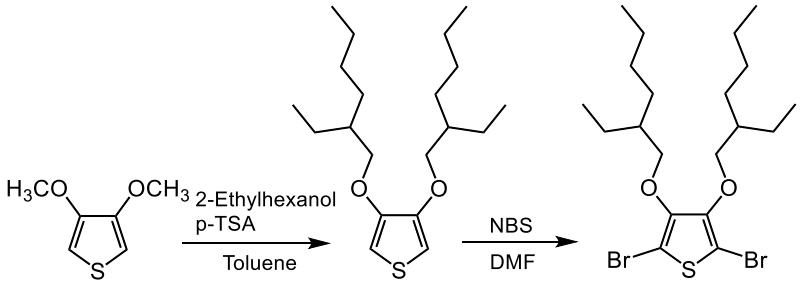

To a solution of 3,4-dimethoxythiophene (3.84 g, 26.6 mmol) and 2-ethylhexanol (16.8 mL, 106.6 mmol) in toluene (100 mL) was added *p*-toluene sulfonic acid (*p*-TSA, 0.46 g, 2.7 mmol) in Soxhlet extraction apparatus filled with molecular sieve. The mixture was heated up to 140°C and refluxed for 18 h. After cooling to rt., the solvent was evaporated under vacuum. The crude product was purified by column chromatography (eluent: hexane) twice to afford clear colorless oil (6.28 g, 69%). ^{1}H NMR (400 MHz, $CDCl_3$, δ from TMS): δ 6.16 (s, 2H), 3.85 (d, 4H, J = 5.6 Hz), 1.76 (septet,. 2H, J = 6.4 Hz), 1.55-1.26 (m, 16H), 0.90 (m, 12H). ^{13}C NMR (100 MHz, $CDCl_3$, δ from TMS): δ 148.00, 96.82, 73.12, 39.22, 30.57, 29.05, 23.92, 23.03, 14.05, 11.14.

Into oven-dried three-neck 200 mL flask were added 3,4-di(2-ethylhexyloxy)thiophene (4.01 g, 11.75 mmol) and DMF (100 mL) under argon atmosphere. The solution was cooled to 0°C in ice bath and stirred for 5 min. *N*-bromo succinimide (4.60 g, 25.84 mmol) was added to the solution in one portion. After stirring for 5 min at 0°C and then warm up to rt. and stirred for additional 2 days. The obtained solution was quenched with $NaHCO_3$ aq and stirred for 20 min. The mixture was extracted with ethylacetate, washed with brine three times. The combined organic phase was dried over magnesium sulfate. The crude product was purified by column chromatography (eluent: hexane) to afford clear colorless oil (3.94 g, 67%). ^{1}H NMR (400 MHz, $CDCl_3$, δ from TMS): δ 3.94 (4H), 1.65 (septet, 2H, J = 6.0 Hz), 1.60-1.26 (m, 16H), 0.91 (m, 12H). ^{13}C NMR (100 MHz, $CDCl_3$, δ from TMS): δ 147.89, 94.83, 76.41, 40.15, 30.16, 29.05, 23.52, 23.06, 14.10, 11.10.

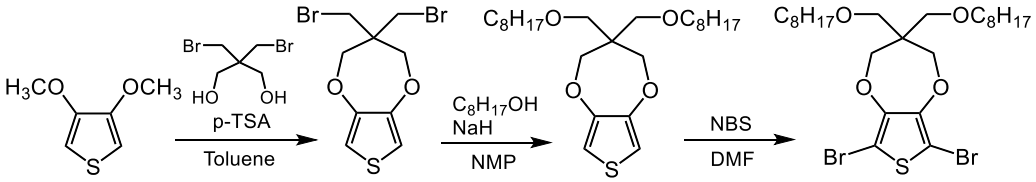

To a solution of 3,4-dimethoxythiophene (3.00 g, 20 mmol) and 2,2-bis(bromomethyl)-1,3-propanediol (10.48 g, 40 mmol) in toluene (100 mL) was added *p*-toluene sulfonic acid (*p*-TSA, 0.35 g, 2 mmol) in Soxhlet extraction apparatus filled with molecular sieve. The mixture was heated up and refluxed for 19 h. After cooling to rt., the obtained dark purple solution was washed with water, saturated $NaHCO_3$ and brine. The organic phase was dried over magnesium sulfate and evaporated under vacuum. The crude product was purified by column chromatography (eluent: hexane/dichloromethane = 3/2 (v/v)) and recrystallized from hexane to afford white crystalline solid (5.35 g, 78%). ^{1}H NMR (400 MHz, $CDCl_3$, δ from TMS): δ 6.50 (s, 2H), 4.10 (s, 4H), 3.61 (s, 4H). ^{13}C NMR (100 MHz, $CDCl_3$, δ from TMS): δ 148.61, 105.73, 74.11, 46.17, 34.39.

A solution of ProDOT_Br2 (4.86 g, 15 mmol), 1-octanol (7.2 mL, 45 mmol) and sodium hydride (2.17 g, 90 mmol) in *N*-methylpyrrolidone (100 mL) was stirred at rt., and H_2 gas bubbles were observed. After disappearance of gas bubbles, the reaction mixture was heated up to 70°C and refluxed for 25 h. The obtained black solution was extracted with ethylacetate and washed with brine three times. The combined organic phase was dried over magnesium sulfate and the solvent was evaporated. The crude product was purified by column chromatography (eluent:

hexane/dichloromethane = 3/2 (v/v)) to afford clear colorless oil (5.64 g, 85%). ^{1}H NMR (400 MHz, $CDCl_3$, δ from TMS): δ 6.44 (s, 2H), 4.01 (s, 4H), 3.48 (s, 4H), 3.40 (t, 4H, J = 6.8 Hz), 1.52 (broad, 4H), 1.27 (broad, 20H), 0.88 (t, 6H, J = 6.4 Hz). ^{13}C NMR (100 MHz, $CDCl_3$, δ from TMS): δ 149.711, 105.03, 73.75, 71.74, 69.58, 47.70, 31.84, 29.53, 29.42, 29.29, 26.14, 22.66, 14.10.

Into oven-dried three-neck 200 mL flask were added ProDOT_OC8H17 (4.42 g, 10 mmol) and DMF (75 mL) under argon atmosphere. The solution was cooled to 0°C in ice bath and stirred for 15 min. *N*-bromo succinimide (5.40 g, 30 mmol) was added to the solution in one portion. After stirring for 15 min at 0°C and then warm up to rt. and stirred for additional 28 h. The obtained red-brown solution was quenched with $NaHCO_3$ aq. The mixture was extracted with ethylacetate, washed with water three times. The combined organic phase was dried over magnesium sulfate. The crude product was purified by column chromatography (eluent: hexane/dichloromethane = 4/1 (v/v)) to afford clear pale-yellow oil at rt., and white solid in fridge (4.09 g, 68%). ^{1}H NMR (400 MHz, $CDCl_3$, δ from TMS): δ 4.08 (s, 4H), 3.49 (s, 4H), 3.39 (t, 4H, J = 7.2 Hz), 1.53 (broad, 4H), 1.28 (broad, 20H), 0.88 (t, 6H, J = 6.8 Hz). ^{13}C NMR (100 MHz, $CDCl_3$, δ from TMS): δ 147.04, 90.98, 74.25, 71.69, 69.34, 47.81, 31.84, 29.49, 29.40, 29.28, 26.11, 22.66, 14.10. MS m/z (MALDI-TOF) $[M+Na]^+$ Calculated: 621.1048, Found: 621.0093.

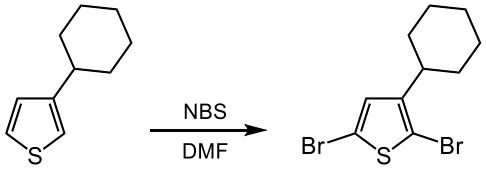

Into oven-dried three-neck flask were added 3-cyclohexylthiophene (1.00 g, 6.0 mmol) and DMF (20 mL) under nitrogen atmosphere. The solution was cooled to 0°C in ice bath and stirred for 5 min. N-bromo succinimide (2.69 g, 15 mmol) was added to the solution in one portion. After stirring for 15 min at 0°C and then warm up to rt. and stirred for additional 25 h. The reaction was quenched with $NaHCO_3$ aq. The mixture was extracted with ethylacetate, washed with brine three times. The combined organic phase was dried over magnesium sulfate. The crude product was purified by column chromatography (eluent: hexane) to afford colorless liquid (1.66 g, 86%). ^{1}H NMR (400 MHz, $CDCl_3$, δ from TMS): δ 6.81 (s, 1H), 2.65 (tt, 1H, J = 12.0 Hz), 1.82-1.72 (m, 6H), 1.43-1.17 (m, 6H). ^{13}C NMR (100 MHz, $CDCl_3$, δ from TMS): δ 147.73, 128.96, 110.46, 106.75, 39.13, 33.06, 26.46, 25.91.

Synthesis of Phenylisocyanide monomer

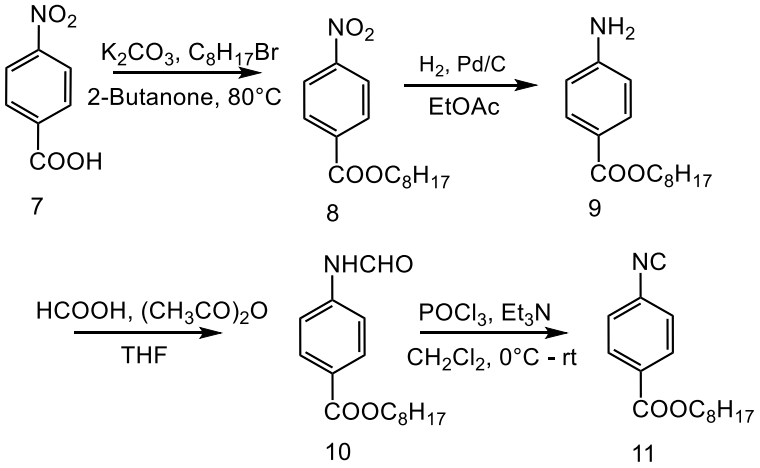

Octyl 4-nitrobenzoate (8). To a solution of nitrobenzoic acid **7** (2.99 g, 17.9 mmol) and 1-bromooctane (4.67 mL, 26.84 mmol) in 2-butanone (100 mL) was added potassium carbonate (3.96 g, 28.6 mmol) and then refluxed for 16 h. After reaction, the reaction solution was evaporated and extracted with chloroform/H_2O followed by $MgSO_4$ drying. The residue was purified by column chromatography (eluent: *n*-hexane, chloroform) to yield **9** (3.62 g, 12.9 mmol, 72.5%). ^{1}H NMR (400 MHz, $CDCl_3$): δ 8.29 (d, 2H, J = 8.8 Hz), 8.21 (d, 2H, J = 8.7 Hz), 4.37 (t, 2H, J = 6.6 Hz),

1.81-1.76 (m, 2H), 1.46-1.29 (m, 10H), 0.89 (t, 3H, J = 5.3 Hz). ^{13}C NMR (100 MHz, $CDCl_3$): δ 164.75, 150.55, 135.90, 130.64, 123.51, 66.12, 31.76, 29.19, 29.16, 28.58, 25.96, 22.61, 14.07.

Octyl 4-aminobenzoate (9) Compound 5 was synthesized as the same procedure as compound 3. Yield: **10** (2.59 g, 80.6%). ^{1}H NMR (400 MHz, $CDCl_3$): δ 7.87-7.83 (m, 2H), 6.65-6.62 (m, 2H), 4.25 (t, 2H, J = 6.6 Hz), 4.04 (s, 2H), 2.88-1.27 (m, 12H), 0.88 (t, 3H, J = 6.9 Hz). ^{13}C NMR (100 MHz, $CDCl_3$): δ 166.74, 150.66, 131.53, 120.15, 113.75, 64.52, 31.79, 29.26, 29.19, 28.80, 26.05, 22.62, 20.39, 14.08.

Octyl 4-formamidobenzoate (10). A solution of formic acid (0.90 mL, 23.8 mmol) and acetic anhydride (2.25 mL, 23.8 mmol) was stirred at 54°C and then another solution of 9 (2.7 g, 10.8 mmol) in diethylether (50 mL) was added dropwise at 0°C. The mixture was stirred for 28 h at room temperature and then quenched by 10% aq $NaHCO_3$ solution. The crude product was extracted with EtOAc/H_2O and purified by column chromatography (eluent: chloroform/ethylacetate = 4/1) to yield white solid (2.50 g, 83.1%). **^{1}H** NMR (400 MHz, $CDCl_3$): δ 8.83 (d, 0.44H, NH in trans, J = 11 Hz), 8.44 (d, 0.56H, NH in cis, J = 1.4 Hz), 8.27 (d, 0.44H, HCO in trans, J = 11 Hz), 8.06-8.02 (m, 2H, Hm to NH in cis and Hm to NH in trans), 7.64 (d, 1.2H, Ho to NH in cis, J = 9.2 Hz), 7.26 (s, 0.56H, HCO in cis), 7.14 (d, 0.88H, Ho to NH in trans, J = 8.2 Hz), 4.33-4.28 (m, 4H), 1.79-1.28 (m, 12H), 0.88 (t, 3H, J = 6.9 Hz). ^{13}C NMR (100 MHz, $CDCl_3$): δ 166.03, 165.82, 161.73, 158.89, 140.79, 131.48, 130.83, 127.03, 126.54, 119.01, 117.15, 65.30, 65.17, 31.77, 29.23, 29.18, 28.69, 26.03, 22.63, 14.09.

Octyl 4-isocyanobenzoate (11). To an oven-dried Schlenk flask were added compound 10 (277 mg, 1.0 mmol), dichloromethane (8 mL) and triethylamine (0.38 mL, 2.7 mmol) under Ar atmosphere. $POCl_3$ (0.10 mL, 1.1 mmol) was added dropwise slowly at 0°C and then stirred at 0°C for 10 min. The reaction mixture was warmed up to room temperature and stirred for another 1 h. Then Na_2CO_3aq (10%) 20 mL was added and extracted with chloroform followed by $MgSO_4$ drying. The residue was purified by column chromatography (eluent: hexane/ CH_2Cl_2 = 7/3) to yield phenylisocyanide monomer (244 mg, 94%). IR (KBr, cm^{-1}): 2122 ($\nu_{C\equiv N}$), 1724 ($\nu_{C=O}$ ester). **^{1}H** NMR (400 MHz, $CDCl_3$): δ 8.08 (d, 2H, J = 8.8 Hz), 7.45 (d, 2H, J = 8.0 Hz), 4.33 (t, 2H, J = 6.8 Hz), 1.77 (quin, 2H, J = 6.8 Hz), 1.47 – 1.28 (m, 10H). 0.89 (t, 3H, J = 6.8 Hz). ^{13}C NMR (100 MHz, $CDCl_3$): δ 165.04, 131.31, 130.78, 126.40, 65.75, 37.74, 29.18, 29.14, 28.59, 25.96, 22.60, 14.05.

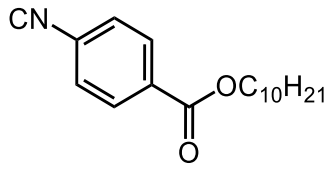

Decyl-4-isocyanobenzoate; Pale-yellow solid (Yield: 17% in 2 steps). The structure was confirmed by matching its spectroscopic data with corresponding reported data. ^{1}H NMR (400 MHz, $CDCl_3$, δ from TMS): δ 8.08 (dt, 2H), 7.45 (dt, 2H), 4.33 (t, 2H, J = 6.4 Hz), 1.77 (quint., 2H, J = 7.2 Hz), 1.45-1.28 (m, 14H), 0.88 (t, 3H, J = 6.8 Hz).

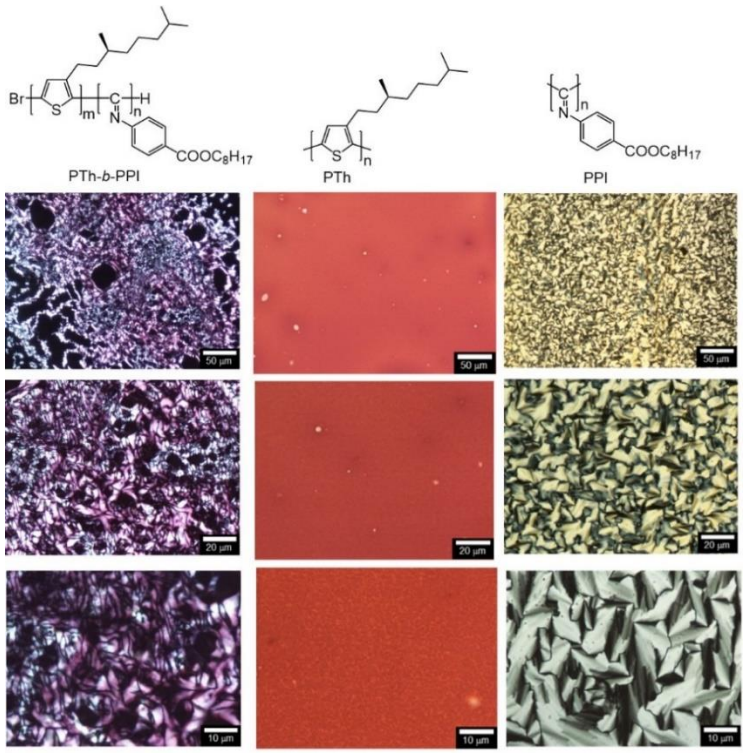

Figure 2-S1. Polarizing optical microscopy (POM) images of PTh-*b*-PPI, PTh and PPI films in solid state at different magnification.

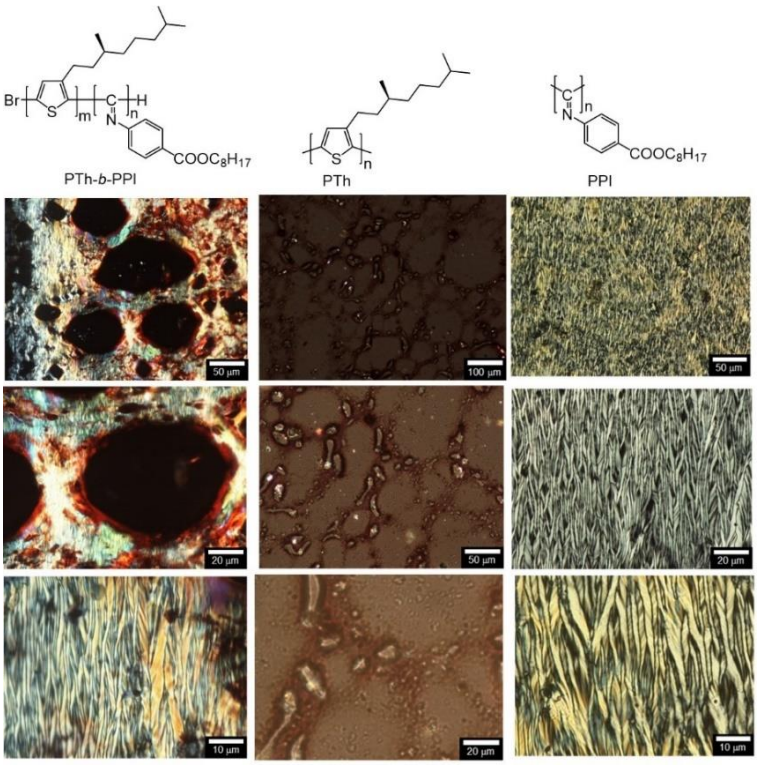

Figure 2-S2. POM images of PTh-*b*-PPI, PTh and PPI films in solid state after magnetic orientation with exposed chloroform vapor at different magnification.

Chapter 3: Functional chromic block copolymers with mesogenic pendants: sheet-like micelle formation and polymerization-induced colloid formation

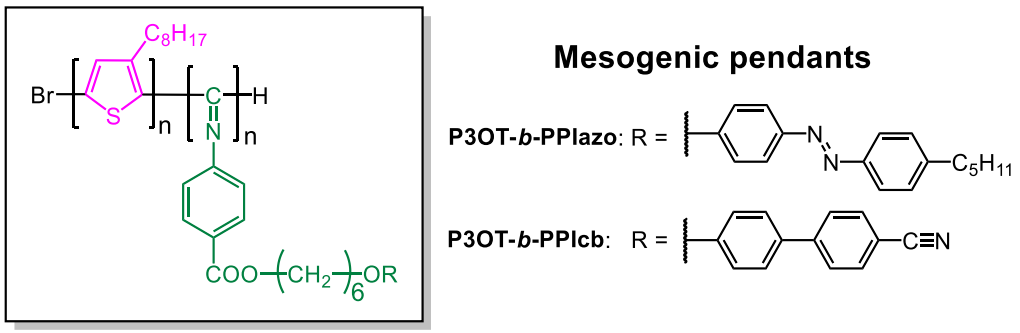

3.1 Abstract

Multi-functional liquid crystalline materials should play key roles toward the next generation of the materials. Here, functional block polymers were prepared by introduction of mesogenic moiety in the side chain of PPIs using living polymerization from poly(3-ocylthiphene) (P3OT) macroinitiator. These pendants are expected to accumulate around the PPI backbone and to arrange in helical manner. As azobenzene (Azo) moiety possess photo-isomerization property, P3OT-*b*-PPIazo exhibits UV-induced *trans-cis* isomerization and visible light-induced *cis-trans* isomerization in THF solution. P3OT-*b*-PPIazo with long PPI block (M_n = 74.1 kDa, M_w/M_n = 1.09, P3OT:PPIazo = 8:92) exhibits lyotropic liquid crystalline phase in THF concentrated solution. Utilizing vapor-induced liquid crystalline nature of P3OT-*b*-PPIazo, several orientation methods are applicable like gentle-shear stress and magnetic field-assisted unidirectional orientations. Interestingly, P3OT-*b*-PPIazo is dissolved in hot cyclohexane, which is selective solvent for PPIazo block, and subsequent cooling to room temperature leads to micro-sized sheet formation. This phenomenon is probably related to crystallization-driven self-assembly (CDSA) of "core-forming" semi-crystalline P3OT block and "corona-forming" PPIazo block in cyclohexane. Cyanobiphenyl (CB) moiety incorporated P3OT-*b*-PPIcb (M_n = 16.6 kDa, M_w/M_n = 1.50) shows colloid-forming property in THF (0.04 mg/mL) because of poor solubility of CB moiety. As P3OT block possess semiconducting nature, P3OT-*b*-PPIcb colloid would exhibit redox-activity. GIXRD measurement for the solid film shows high order of P3OT-*b*-PPIcb film, which is probably derived from CB moiety-incorporated PPIcb block.

3.2 Introduction

Liquid crystalline property gives the materials fluidity and order, which allows for the spontaneous organization and stimuli-responsiveness such electric-field and magnetic-field assisted orientaions. Traditionally, liquid crystalline semiconducting polymers have been developed because they are advantageous over pure semiconducting polymers

in terms of feasible processability, macroscopic orientation, and spontaneous organization (**Figure 3.1**).

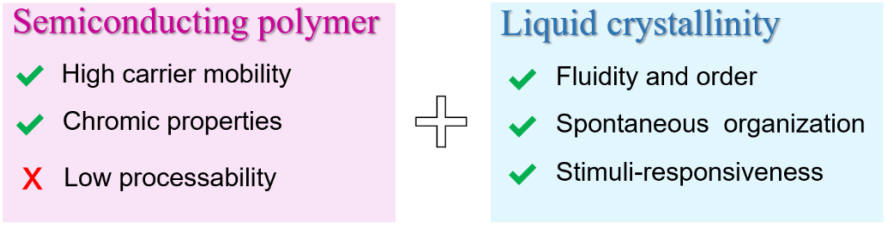

Figure 3.1. Conceptional illustration of liquid crystalline semiconducting polymers.

3.3 Preparation of mesogen-pendant containing block copolymers

P3OT-*b*-PPIs used in this paper compose a semiconducting, regioregular poly(3-octylthiophene) (P3OT) block and helix forming, rod-shaped poly(phenylisocyanide) bearing mesogenic pendants. P3OT-*b*-PPIs were prepared via sequential Grignard methathesis (GRIM) polymerization and Ni-catalyzed "Merry-go-round" polymerization with two mechanistically distinct manner with single Ni catalyst (**Scheme 3.1**). The synthetic procedure of a series of poly(3-alkylthiophene)-*block*-poly(arylisocyanide) has been developed by Wu et. al. We newly prepared azobenzene- and cyanobiphenyl-contaning phenylisocyanide monomers. Then we synthesized P3OT$_{30}$-*b*-PPIazo$_{39}$, P3OT$_{50}$-*b*-PPIazo$_{129}$, and P3OT$_{69}$-*b*-PPIcb$_{8}$ (the subscripts represent the degree of polymerization of each block which was estimated GPC results), and their characteristics were summarized in **Table 3.1**. Ni-terminated P3OT macroinitiator initiated the polymerization of phenylisocyanide to afford P3OT-*b*-PPIs, which is supported by clear unimodal elution peak shifts while maintaining narrow dispersity in gel permeation chromatography (GPC). Nuclear magnetic resonance (NMR) and Fourier transform infrared (FT-IR) spectroscopies also demonstrates well-defined structure of P3OT-*b*-PPIazo and P3OT-*b*-PPIcb. P3OT-*b*-PPIazo possess good solubility in common organic solvents such as tetrahydrofuran (THF), chloroform, dichloromethane, toluene, anisole at room temperature, and partially dissolved in hot ethyl acetate, hot cyclohexane, and cannot be dissolved in hexane and methanol. Contraty, P3OT-*b*-PPIcb is not dissolved in common organic solvents such as THF, chloroform, leading to the formation of suspension. Homopolymer, PPIazo, was also prepared by Ni-catalyzed polymerization and PPIcb by Pd-catalyzed living polymerization.

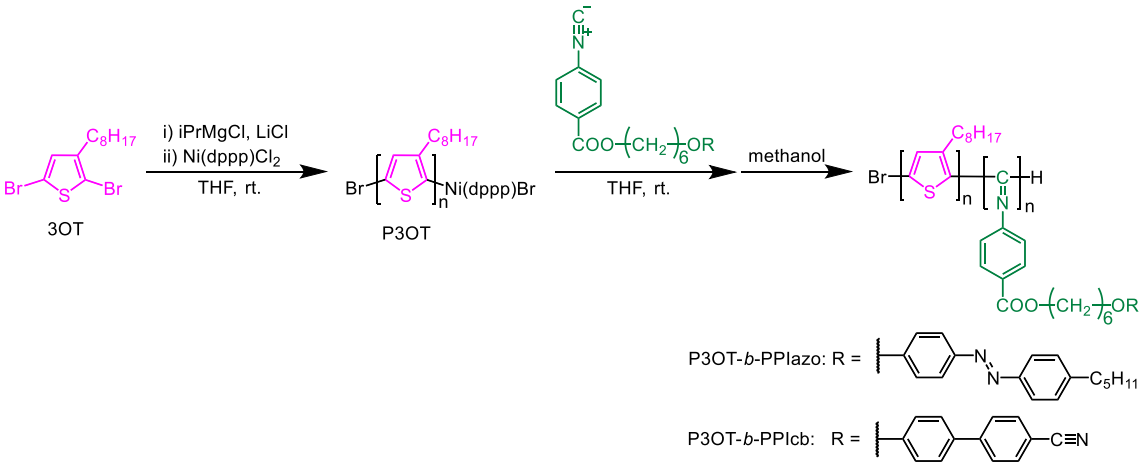

Scheme 3.1. Block copolymerization with poly(3-octylthiophene).

Table 3.1. Block copolymer and macroinitiator properties.

Entry	Macroinitiator (P3OT)		Block copolymer (P3OT-*b*-PPI)				
	M_n (kDa) [a]	M_w/M_n [a]	M_n (kDa)[a]	M_w/M_n [a]	Yield[b]	Ratio[c]	LC[d]
$P3OT_{30}$-*b*-$PPIazo_{39}$	6.0	1.34	25.4	1.07	61%	13:87	No
$P3OT_{50}$-*b*-$PPIazo_{129}$	9.7	1.35	74.1	1.09	89%	8:92	Yes
$P3OT_{69}$-*b*-$PPIcb_8$	13.4	1.31	16.6*	1.50*	52%	N.A.**	No

a. Molecular weight and molecular distribution estimated by GPC analysis calibrated by polystyrene standard (eluent: THF, rt.). b. isolated yield in two steps. c. Ratio determined by the integration in ^{1}H NMR. d. liquid crystallinity (LC) was evaluated by polarizing optical microscopy for corresponding solid films. *For THF soluble fraction. ** Not assigned owing to poor solubility.

3.4 Lyotropic liquid crystallinity and structural analysis

We first investigated P3OT-*b*-PPIazo for possible formation of liquid crystalline phase and micelle formations (**Figure 3.2**).

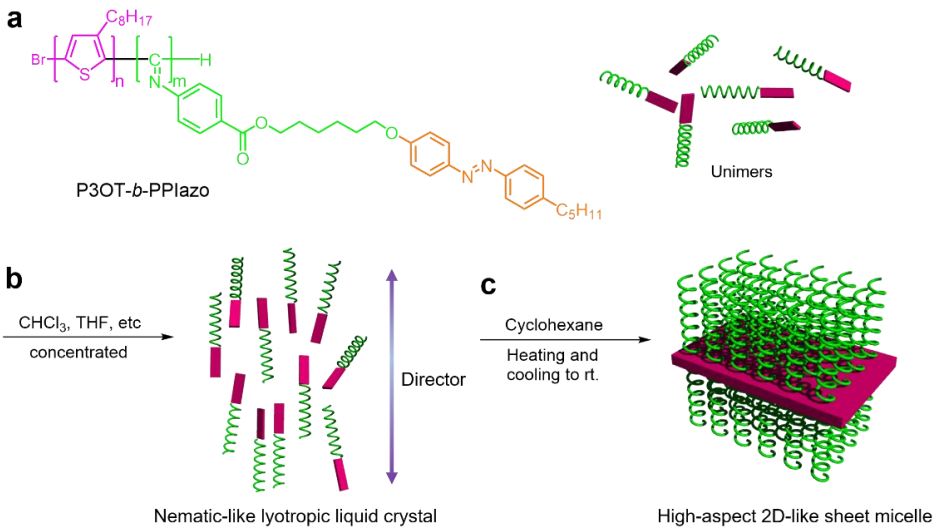

Figure 3.2. (a) Chemical structure and schematic illustration of (b) liquid crystal and (c) micelle formation of P3OT-*b*-PPIazo.

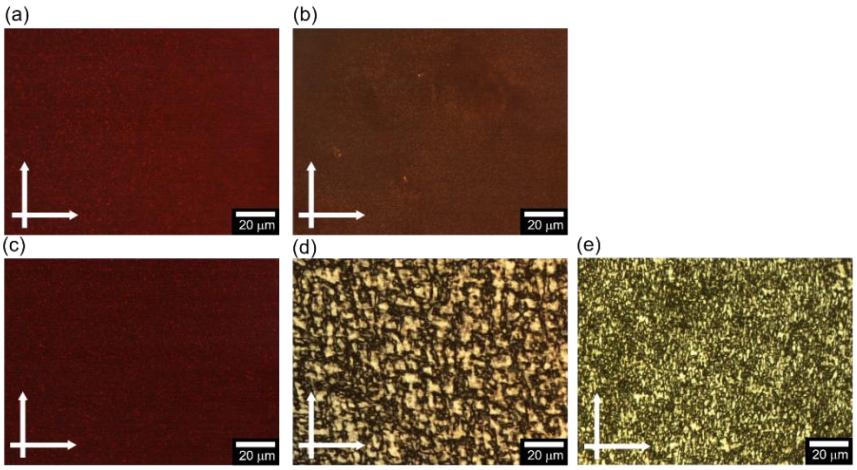

Figure 3.3. POM images of polymer films in solid state prepared by drop-casting from the corresponding chloroform solutions. (a) $P3OT_{30}$, (b) $P3OT_{30}$-*b*-$PPIazo_{39}$, (c)$P3OTh_{50}$, (d) $P3OT_{50}$-*b*-$PPIazo_{129}$, (e) PPIazo.

Lyotropic liquid crystalline mesophases of rod-shaped helical polymers are formed in concetrated solution. Such polymers spontaneously form ordered structure on solvent drying process, leading to the liquid crystalline structure in solid state. Accoding to Onsagar's theory, the expression of liquid crystalline mesophase is dependent on the aniotropic shape of molecules. In this context, we initially investigated the rod-shaped PPIazo-length dependent lyotropic liquid crystallinity by polarizing optical microscopy (POM) for the drop-cast films (**Figure 3.3**). P3OT$_{50}$-*b*-PPIazo$_{129}$ film exhibits clear birefrigence, showing nematic liquid crystal-like structure with Shlieren textures. Homopolymer, PPIazo, also displays nematic liquid crystal-like structure, indicating solidifying through the lyotropic liquid crystalline mesophase on solvent drying process probably because of anisotropy of rod-shaped PPIazo block. Contrary, P3OT$_{30}$-*b*-PPIazo$_{39}$, P3OT$_{30}$ and P3OT$_{50}$ films show neligible birefrigence (**Figure 3.3**). This result indicates that to express the lyotropic liquid crystallinity of P3OT-*b*-PPIazo, rod-shaped PPIazo block is necessary factor, and the long PPIazo part (high aspect ratio) in the block copolymer architecture is needed.

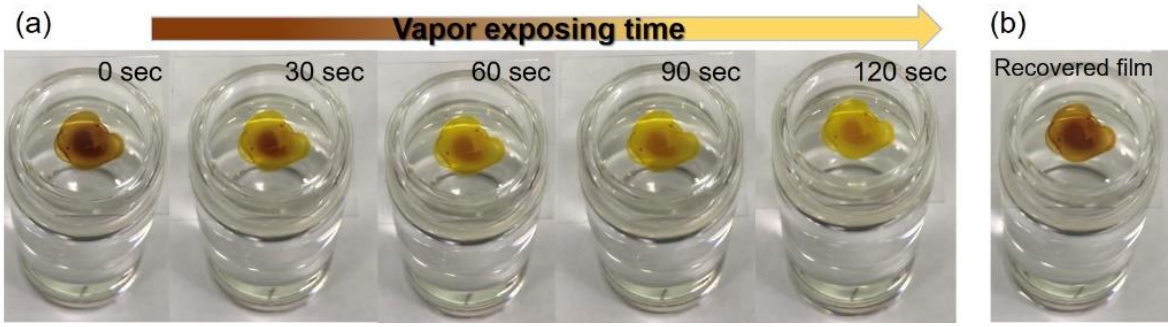

Figure 3.4. Vapor-induced chromism under THF vapor. (a) time laspe photos from brown to yellow. (b) the recovered film after removal of THF vapor.

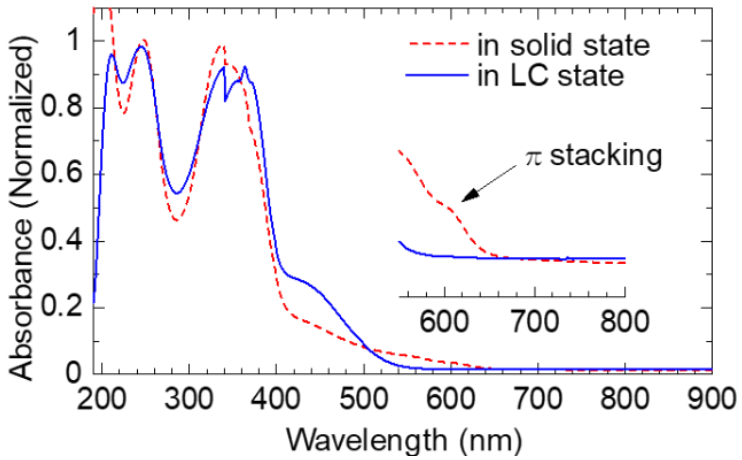

Figure 3.5. Electronic absorption spectra for PTh$_{50}$-*b*-PPIazo$_{129}$ film in solid state and in LC state (chlorodorm vapor-exposed state). The noise at around 350 nm is derived from the apparatus.

Figure 3.4 and **3.5** show chloroform vapor induced electronic absorption change of P3OT$_{50}$-*b*-PPIazo$_{129}$ film. In solid state, P3OT$_{50}$-*b*-PPIazo$_{129}$ film shows two characteristic peaks at 350 nm (π–π^* transition of *trans*-azobenzene

moiety) and shoulder peak at 610 nm (π-stacking of P3OT block, inset). In THF vapor-exposed phase, on the other hand, the peak at 610 nm disappeared and new absorption band at around 440 nm appeared. This demonstrates that the THF vapor molecules prevent π-stacking of P3OT block, and twisted conformation with less conjugation length of P3OT block is formed. The THF vapor-exposed film still shows birefringence in POM observation, and that film exbibits softness enough to be subject to shear stress orientation. These phenomena are well consistent with our previous report. We conclude that THF vapor-exposed phase is lyotropic liquid crystalline phase with very concentrated state, in which P3OT chains are solvated to some extent and rod-shaped PPIazo block acts as mesogen for lyotropic liquid crystallinity.

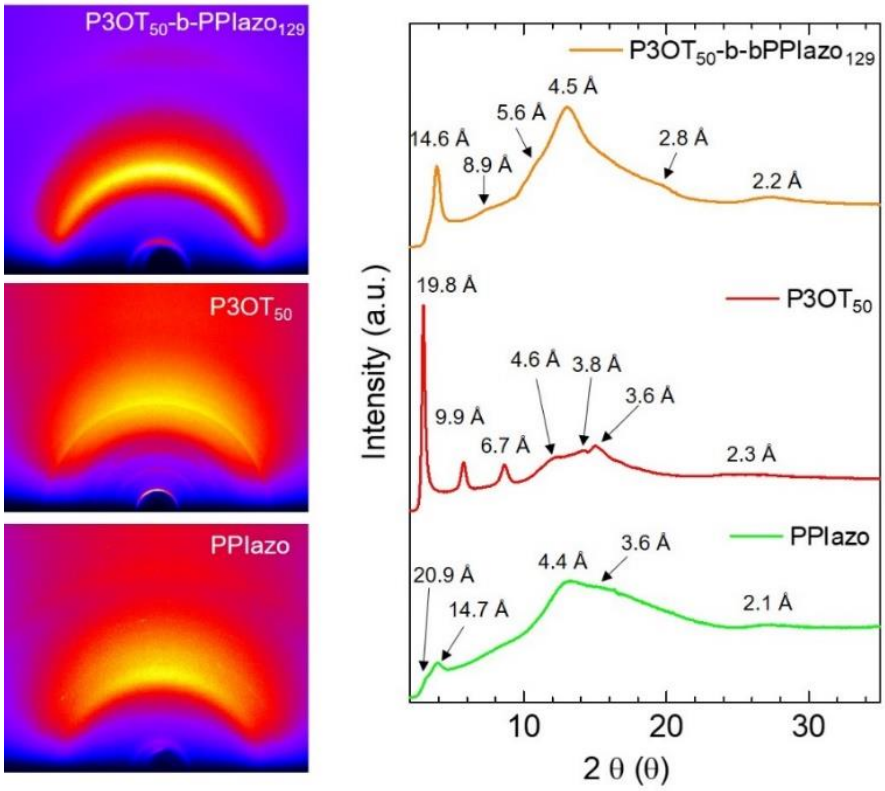

Figure 3.6. GIXRD measurements for P3OT-*b*-PPI, P3OT, and PPIazo films.

Synchrotron grazing-incidence X-ray diffraction (GIXRD) measurements were performed for $P3OT_{50}$-*b*-$PPIazo_{129}$, and homopolymers, $P3OT_{50}$ and PPIazo (M_n = 477.9 kDa, M_w/M_n = 2.15) films to investigate the self-assembled structures (**Figure 3.6**). Prior to the measurement, the film on glass substrate was annealed in THF vapor atmosphere at room temperature for an hour. In $P3OT_{50}$-*b*-$PPIazo_{129}$, the two major peaks were observed at 14.6 and 4.5 Å. In semi-crystalline $P3OT_{50}$, the (100) reflection asignable to the P3OT interlayer distance was observed at 19.8 Å along with higher order reflection at 9.9 Å (200) and 6.7 Å (300). Homopolymer $P3OT_{50}$ is considered to form lamellae structure. $P3OT_{50}$ also showed a diffraction at 3.6 Å, which corresponds to the P3OT π-stacking (010) distance. In liquid-crystalline PPIazo, the two major peaks were observed at 14.7 (interchain packing) and 4.4 Å (phenyl stacking), which is very similar profile to that of $P3OT_{50}$-*b*-$PPIazo_{129}$. This indicates that $P3OT_{50}$-*b*-$PPIazo_{129}$ possesses self-

assemble nature mainly derived from liquid crystalline PPIazo block. Although peaks from lamellae structured P3OT block was invisible in P3OT$_{50}$-*b*-PPIazo$_{129}$ profile, UV-vis absorption spectrum shows that P3OT block in the block copolymer form π-stacking between the backbones in solid state (~610 nm shoulder peak) (**Figure 3.5**), indicating that P3OT block cannnot form layered structure but π-stacking assembly in the block copolymer assembly.

3.5 Shear- and magnetic field-assisted macroscopic orientation

Utilizing vapor-induced liquid crystalline nature, several orientation methods are applicable to P3OT$_{50}$-*b*-PPIazo$_{129}$ film. Gentle shear against the film exposed to THF vapor afforded the uniform alignment of P3OT$_{50}$-*b*-PPIazo$_{129}$ backbones (**Figure 3.7a**). Application of horizontal 12 Tesla magnetic flux for an hour to the film exposed to THF vapor also resulted in macroscopically unidirectional alignment of P3OT$_{50}$-*b*-PPIazo$_{129}$ liquid crystalline assembly (**Figure 3.7b**). Two kinds of POM images show changes from bright to dark on each rotation of the sample by 45° between crossed polarizers, indicating macroscopically unidirectional alignment of block copolymer molecules. This result suggests that THF vapor exposed film possess appropriate viscosity susceptible for shear orientation and magnetic orientation with moderate time scale. Both of magnetic anisotropy and large grain size sufficient for magnetic orientation are probably attained from anisotropic rod-shaped liquid crystalline PPIazo block. Achievement of the above orientations also supports that THF vapor-exposed P3OT$_{50}$-*b*-PPIazo$_{129}$ film form vapor-induced lyotropic liquid crystalline phase.

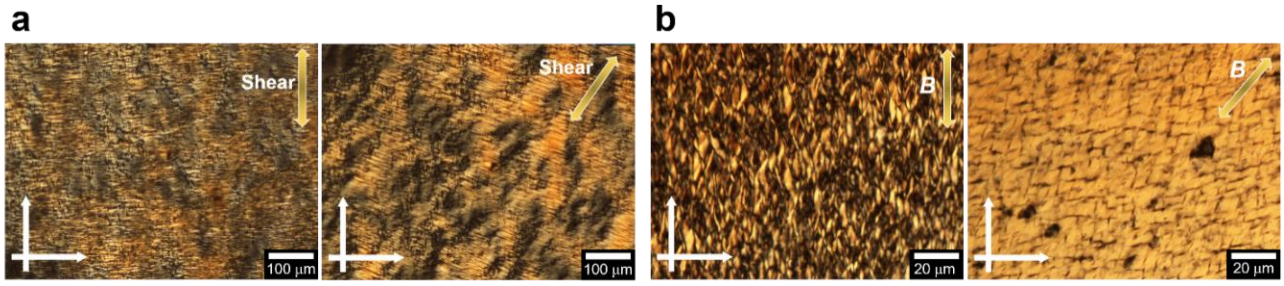

Figure 3.7. (a) Shear-induced and (b) magnetic-field assisted macroscopic orientation of P3OT$_{50}$-*b*-PPIazo$_{129}$ film.

3.6 Photo-isomerization of azobenzene moiety

To probe the photoisomerization of azobenzene unit in solution, we tracked absorption spectra changes by UV irradiation and visible light irradiation for P3OT$_{50}$-*b*-PPIazo$_{129}$ in solution state (0.02 mg/mL in THF). Under UV irradiation, the absorption peak at 350 nm decreased while the absorption peak at 440 nm increased, indicating that *trans*-form of azobenzene isomerized into *cis*-form (**Figure 3.8a**). Under visible-light (blue LED) irradiation, the opposite phenomenon was observed (**Figure 3.8b**). This photoisomerization was reversible for many times. Contrary, P3OT$_{50}$-*b*-PPIazo$_{129}$ in film state showed almost no photoisomerization behavior (**Figure 3.9**), although slight absorption changes were observed at around 350 nm and 450 nm. It is noteworthy that the absorption shoulder peak at 610 nm derived from π-stacking nature of P3OT block was not changed under UV light irradiation.

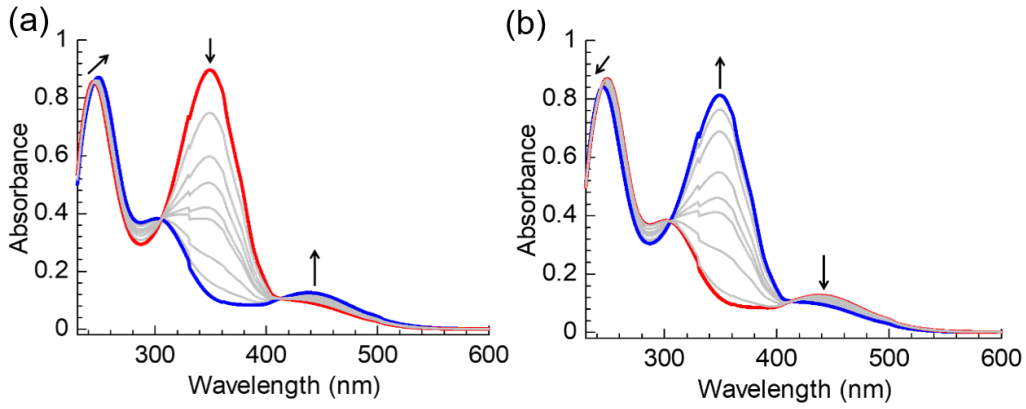

Figure 3.8. Absorption spectral change of (a) *trans*- to *cis*-isomeriztion of PTh_{50}-*b*-$PPIazo_{129}$ by UV irradiation and (b) *cis*- to *trans*-isomeriztion of PTh_{50}-*b*-$PPIazo_{129}$ by visible light irradiation in THF solution state (0.02 mg/mL).

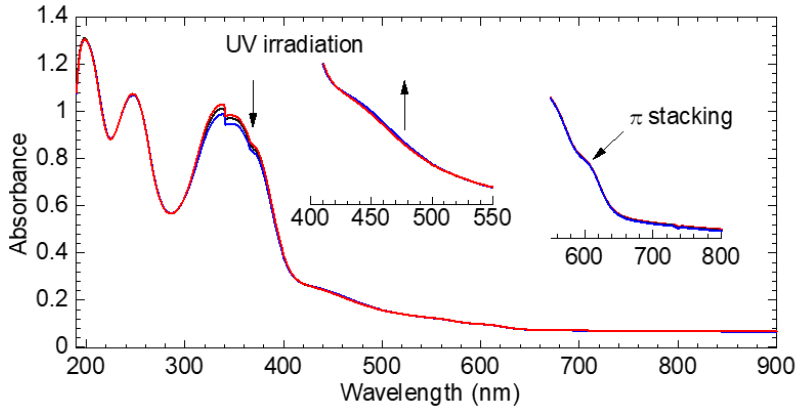

Figure 3.9. Photo-isomerization of PTh_{50}-*b*-$PPIazo_{129}$ in films state on quartz substrate. The noise at around 350 nm is derived from the apparatus.

3.7 2D sheet-like micelle formation

Manners et al. have reported a series of diblock copolymer micelles containing crystalline "core" forming block and solubilizing "corona" forming block that dissolves in selective solvent, in which the process of self-assembly is called crystallization driven self-assembly (CDSA). We envisioned that CDSA protocol might be applicable to $P3OT_{50}$-*b*-$PPIazo_{129}$ assembly by dissolving it to selective solvent for PPIazo block. **$P3OT_{50}$-*b*-$PPIazo_{129}$** was first suspended in cyclohexane then heated, and subsequently cooled to room temperature to facilitate the micelle formation. The resulting suspension of supernatant was taken out, and the aliquot was casted on glass plate. The microscopy images showed, to our surprise, the extraordinary large sheet-like micelle formation. Moreover, the POM images show changes from bright to dark on each rotation of the sample by 90° between crossed polarizers (**Figure 3.10a**). Moreover, this micelle exhibited photoluminescence under 450-490 nm wavelength excitation (**Figure 3.10b**). It should be noted that other sheet-like micelles also showed changes from bright to dark on each rotation by 90° , implying not uniaxial crystalline structure but in-plane multi-axial crystalline structure (**Figure 3.11**).We postulated that this extremely large micelle might be related to rod-rod diblock copolymer architecture, which stabilize the micelle formation. Possible micelle formation is depicted in **Figure 3.12**.

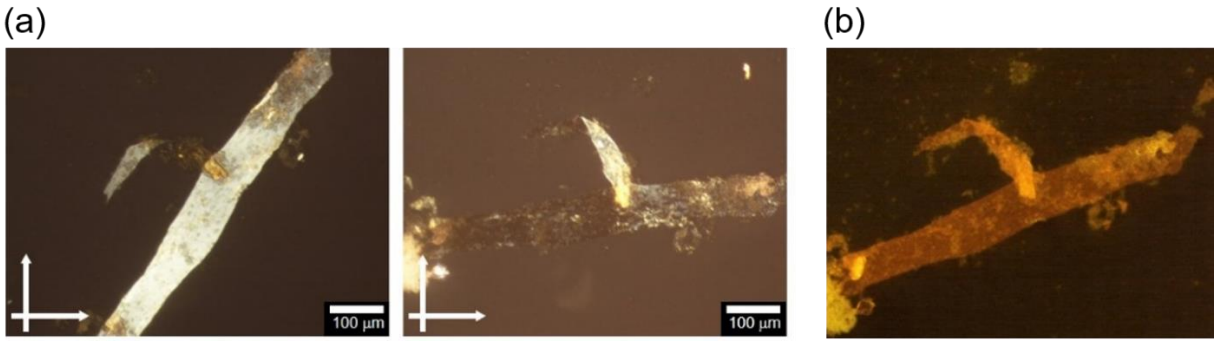

Figure 3.10. (a) Polarized microscopy images and (b) fluorescense microscopy image for P3OT$_{50}$-*b*-PPIazo$_{129}$ micelle. Excitation wavelength: 450-490 nm.

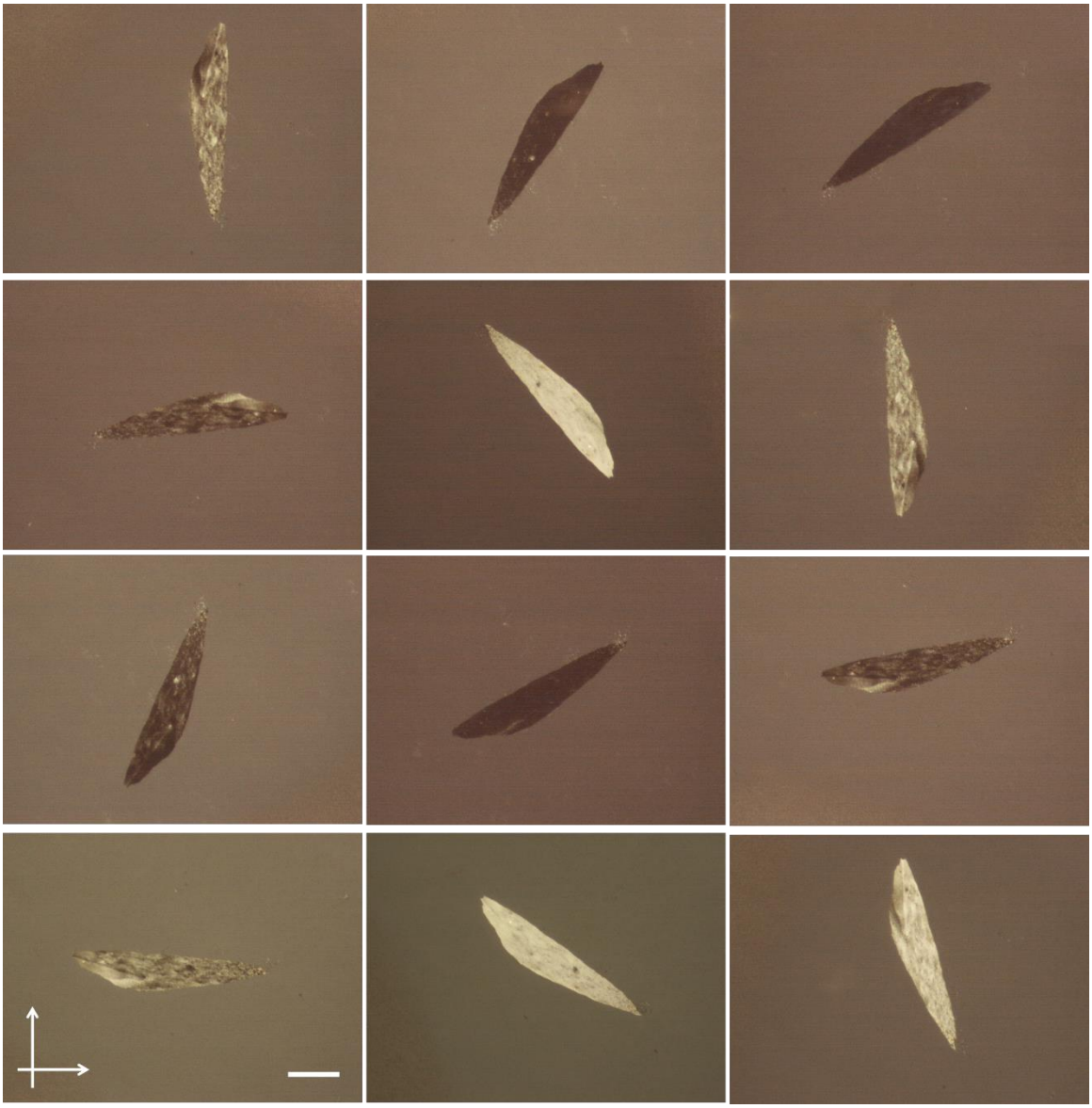

Figure 3.11. POM images of 2D sheet-like P3OT$_{50}$-*b*-PPIazo$_{129}$ micelle on glass substrate. Rotation of the stage cause the light intensity change between crossed Nicols. Scale bar: 100 μm.

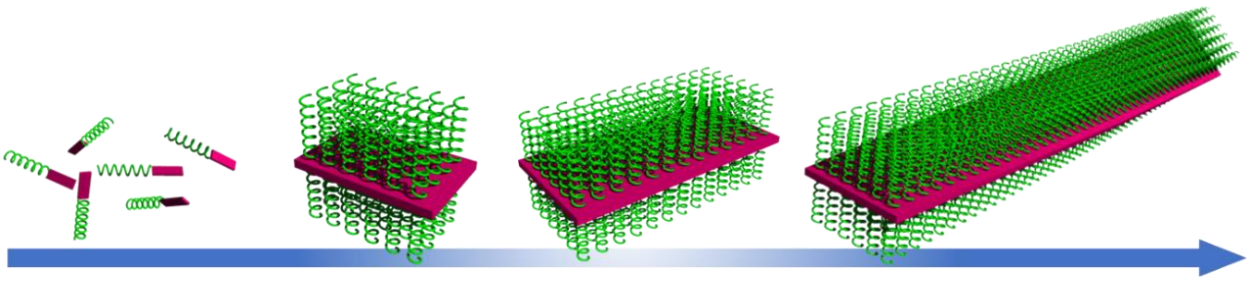

Figure 3.12. Schematic illustration for possible 2D sheet-like micelle formation of P3OT-*b*-PPIazo.

Synchrotron XRD measurements were carried out for the micelle of $P3OT_{50}$-*b*-$PPIazo_{129}$ prepared from suspension of supernatant in cyclohexane. New periodic structure in 2D sheet-like micelle of PTh-*b*-PPIazo (**Figure 3.13**) was seen, which was not observable in PTh-*b*-PPIazo prepared from THF solution (**Figure 3.6**). We speculated that CDSA mechanism allows for the crystalline micelle formation in cyclohexane.

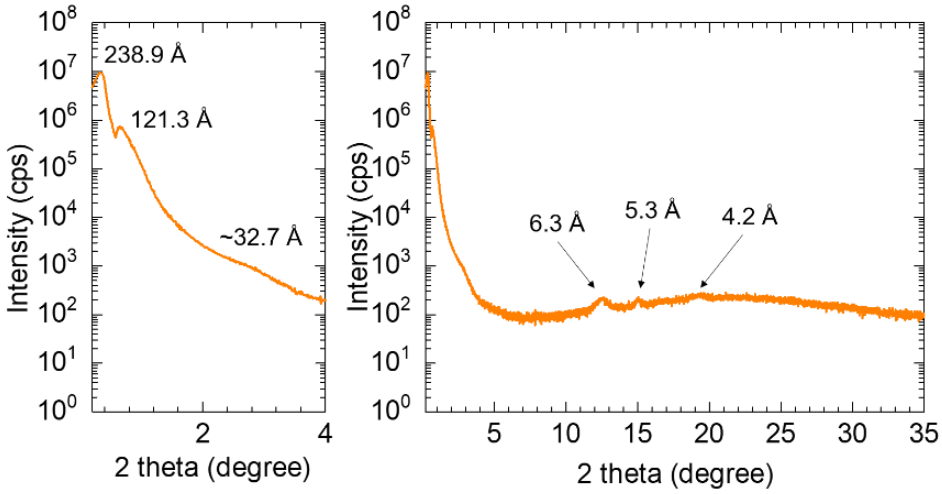

Figure 3.13. Synchrotron XRD measurement for 2D sheet-like micelle of $P3OT_{50}$-*b*-$PPIazo_{129}$.

3.8 Polymerization-induced colloid formation

During the polymerization of phenyl isocyanide bearing cyano-biphenyl side chain initiated by Ni-terminated poly(3-octylthiophene), we surprisingly found that the reaction solution turned into "aurora"-like orange from deep red of color of polythiophene in the first 5 min (**Figure 3.14a**). From the weight of Ni-terminated polythiophene macroinitiator and phenyl isocyanide monomers, the concertation was estimated to be 7.7 mg/mL in THF. After polymerization was carried out for another 30 min, the block copolymer, P3OT-*b*-PPIcb, was purified by precipitation in methanol. No liquid crystalline structure was observed in POM observation. Tyndall effects originating from Brownian motion of colloidal particles also were observed in diluted THF solution (0.04 mg/mL) (**Figure 3.14b**). From this phenomenon, we postulated that the block copolymerization with phenyl isocyanide bearing cyanobiphenyl moiety induces the *in-situ* colloidal formation.

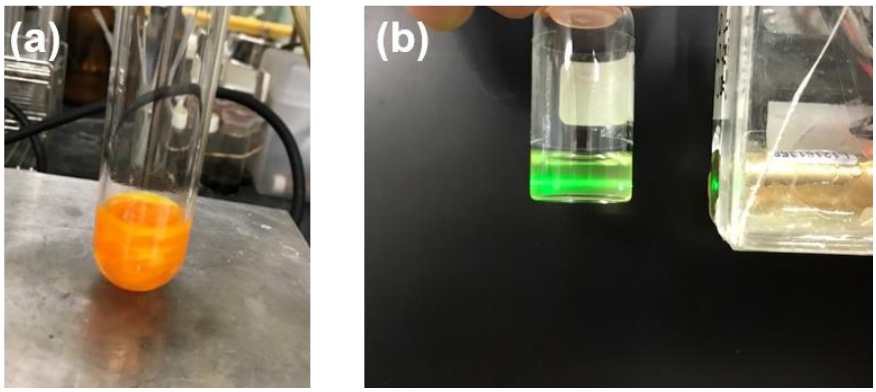

Figure 3.14. (a) Aurora-like appearance of polymerization-induced colloidal formation of P3OT-*b*-PPIcb in THF (7.7 mg/mL). (b) Tyndall effect of the polymer suspension, where handy green laser is irradiated from right side. (concentration = 0.04 mg/mL in THF).

To investigate the colloid forming property of P3OT-*b*-PPIcb, dynamic light scattering (DLS) measurement was used to measure the hydrodynamic diameter of P3OT-*b*-PPIcb colloid. DLS measurement for P3OT-*b*-PPIcb in THF (0.2 mg/mL) immediately after super sonication showed bimodal peaks which is corresponded to the diameters of 185.9±24.0 and 719.9±126.9 nm with narrow dispersity. Interestingly the hydrodynamic diameter of P3OT-*b*-PPIcb colloid increased in 70 min to the diameters of 390.9±164.9 and 2665.9±1094 nm with wide dispersity (**Figure 3.15**). Based on that poly(3-alkylthiophene)s are well dissolved in THF, it suggests that cyanobiphenyl-modified PPI promotes the aggregation of the corresponding P3OT-*b*-PPIcb copolymer molecules. Homopolymer PPIcb (M_n = 13.9 kDa, M_w/M_n = 1.27) showed unimodal peak with a diameter of 2191.9 nm (0.2 mg/mL in THF), which suggests that PPIcb possesses the intrinsic colloid-forming property in THF.

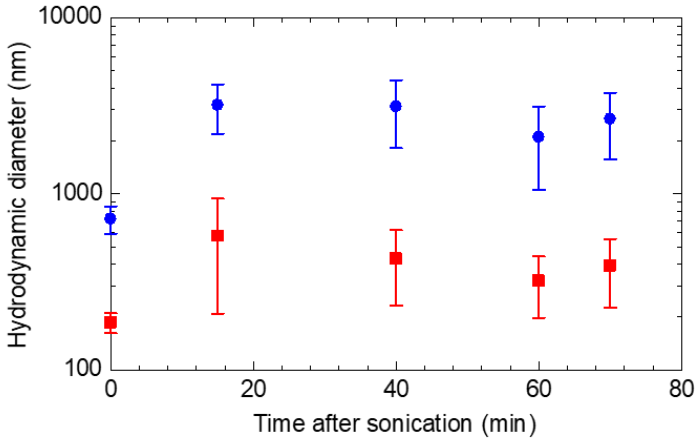

Figure 3.15. Time-dependent hydrodynamic diameter change monitored by DLS measurement (0.2 mg/mL in THF at 25 °C). The wavelength of the laser is 532.8 nm. The average diameters of bimodal peaks were plotted against time after sonication.

To further characterize the assembly of $P3OT_{69}$-*b*-$PPIcb_8$, GIXRD measurement was carried out for P3OT-*b*-PPIcb and homopolymer PPIcb (M_n = 13.9 kDa, M_w/M_n = 1.27) films prepared from THF suspension (**Figure 3.16**). Homopolymer PPIcb exhibited highly crystalline structure, which can be assigned to hexagonally packed columnar

structure. P3OT$_{69}$-*b*-PPIcb$_8$ showed both characteristics of P3OT lamellae structure (20.0 Å) and highly crystallinity of PPIcb. This result suggests that incorporation of PPIcb allows for the high order colloid formation in the P3OT-*b*-PPIcb block copolymer architecture.

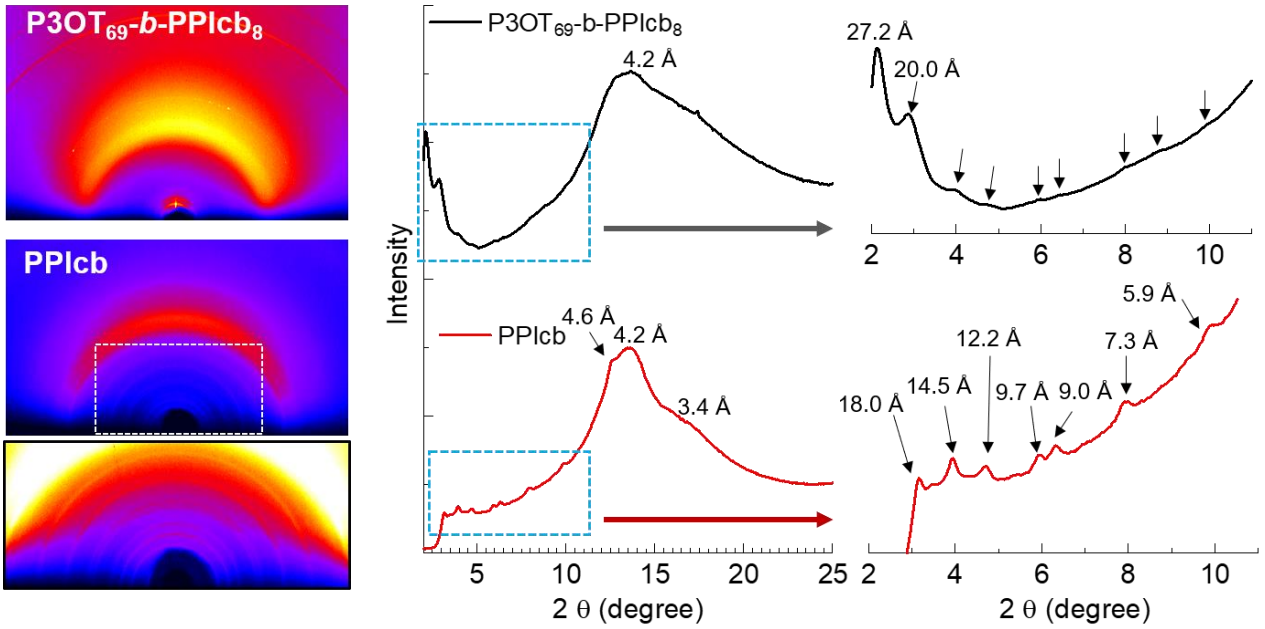

Figure 3.16. GIXRD measurements for P3OT$_{69}$-*b*-PPIcb$_8$ and PPIcb films (wavelength: 0.996 Å).

3.9 Conclusion and perspectives

We disclosed the interesting sheet-like micelle formation of P3OT-*b*-PPIazo and colloid forming property of P3OT-*b*-PPIcb. Especially, P3OT-*b*-PPIazo possess multi-functional properties such as vapor-induced lyotropic liquid crystallinity, shear- and magnetic field-assisted orientations in addition to the micelle formation. The photo-responsiveness can be combined with other functionalities like photo-controlled micelle formation or polarized light-assisted orientation. Intrinsic semiconducting nature also offer the possibility for redox-active, chromic materials. Since the architecture of P3OT-*b*-PPI block copolymer is readily modified, more functional block copolymers are expected to pioneer new functionalities.

Experimental

Synthesis

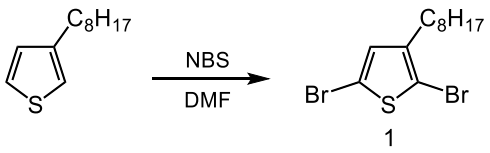

Synthesis of compound 1. Into oven-dried three-neck flask were added 3-*n*-octyl thiophene (3.19 g, 16.2 mmol) and DMF (30 mL) under argon atmosphere. The solution was cooled to 0°C in ice bath and stirred for 10 min. *N*-bromo

succinimide (6.36 g, 35.7 mmol) was added to the solution in portions. After stirring for 10 min at 0°C and then warm up to rt. and stirred for additional 3 days. The obtained yellow solution was quenched with $NaHCO_3$ aq. The mixture was extracted with ethyl acetate, washed with water three times. The combined organic phase was dried over magnesium sulfate. The crude product was purified by column chromatography (eluent: hexane) to afford clear colorless oil (4.11 g, 71%). ^{1}H NMR (400 MHz, $CDCl_3$, δ from TMS): δ 6.77 (s, 1H), 2.50 (t, 2H, J = 8.0 Hz), 1.54 (broad, 2H), 1.52-1.12 (m, 10H), 0.88 (t, 3H, J = 6.4 Hz).

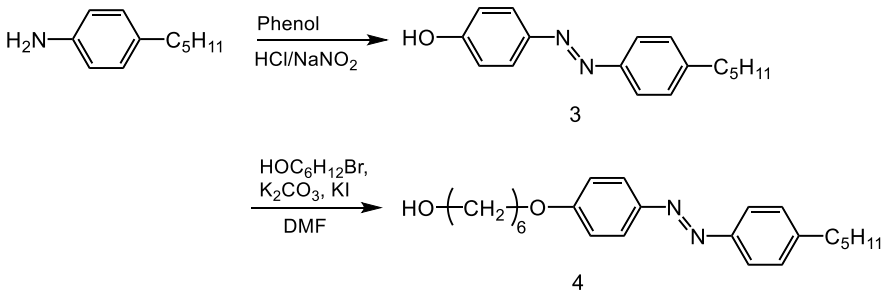

Synthesis of compound 3. Into 2 L beaker with stirring bar were added 4-pentylaniline (23.25 g, 142 mmol), HCl (11.33 M, 25 mL) and distilled water (100 mL) and the beaker was immersed into ice bath. The solution was stirred for 15 min until 4-pentylaniline was completely dissolved. To the solution was added dropwise $NaNO_3$ (12.28 g, 178 mmol) in water (80 mL) over 10 min, and the solution turned into orange. After stirring the solution for 5 min, a solution of phenol (16.3 g, 173 mmol), NaOH (8.75 g, 218 mmol) in distilled water (800 mL) was added dropwise over 30 min. The reaction mixture was stirred at 0°C for another 1 h and at rt. overnight (the color turned into ocher). The reaction mixture was neutralized with dilute HCl aq checked by pH indicator paper. The precipitates were filtered off and dissolved in ethylacetate, washed with water, Na_2CO_3 aq and brine. The organic phase was dried over magnesium sulfate and the solvent was evaporated. The crude product was purified by recrystallization from hexane at rt. to afford orange platelet crystal (16.34 g, 43%). The product was used in next steps without further purification. ^{1}H NMR (400 MHz, $CDCl_3$, δ from TMS): δ 7.85 (dt, 2H, J = 9.6 Hz), 7.89 (dt, 2H, J = 8.8 Hz), 7.30 (dd, 2H, J = 8.8 Hz), 6.93 (dt, 2H, J = 9.6 Hz), 5.38 (s, 1H), 2.67 (t, 2H, J = 7.6 Hz), 1.64 (quint., 2H, J = 7.6 Hz), 1.33 (m, 4H), 0.89 (t, 3H, J = 3.2 Hz).

Synthesis of compound 4. A suspension of compound 3 (2.19 g, 8.16 mmol), K_2CO_3 (5.64 g, 40.8 mmol) and catalytic amount of KI in DMF (30 mL) was heated up to 60°C. To the solution was added dropwise 6-bromo-1-hexanol (2.66 g, 14.7 mmmol) in DMF (10 mL) and then the solution was stirred at 70°C for 3 h. The mixture was extracted with ethylacetate, washed with water, $NaHCO_3$ aq, brine three times, respectively. The combined organic phase was dried over magnesium sulfate. The crude product was purified by column chromatography (eluent: hexane/ethyl acetate = 1/1 (v/v)), followed by recrystallization from methanol to afford orange solid (1.98 g, 69%). ^{1}H NMR (400 MHz, $CDCl_3$, δ from TMS): δ 7.89 (dd, 2H, J = 6.8 Hz), 7.89 (d, 2H, J = 6.0 Hz), 7.30 (d, 2H, J = 8.0 Hz), 6.99 (dd, 2H, J = 6.8 Hz), 4.04 (t, 2H, J = 6.4 Hz), 3.68 (t, 2H, J = 6.4 Hz), 2.67 (t, 2H, J = 7.2 Hz), 1.84 (quint., 2H, J = 6.4 Hz), 1.68-1.57 (m, 4H), 1.55-1.45 (m, 4H), 1.36-1.32 (m, 4H), 1.26 (m, 1H), 0.90 (t, 3H, J = 6.8 Hz).

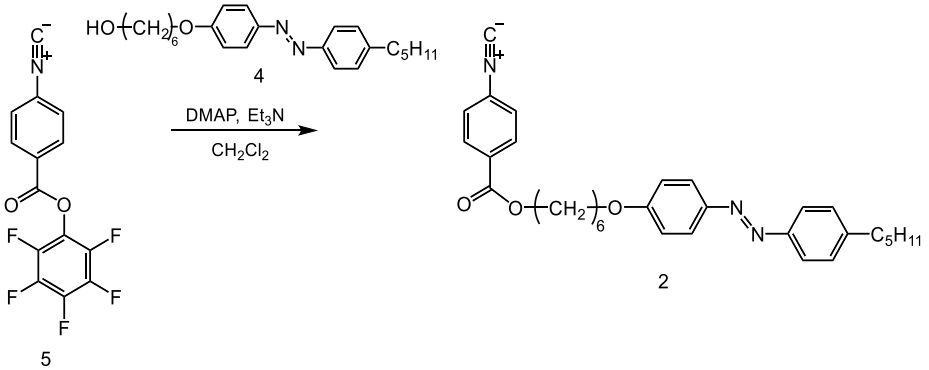

Synthesis of compound 2. To a solution of pentafluorophenyl-4-isocyanobenzoate (compound 5) (602 mg, 2.0 mmol), compound 4 (846 mg, 2.4 mmol) and triethylamine (1.12 mL, 8.0 mmol) in freshly distilled dichloromethane (15 mL) was added 4-dimethylaminopyridine (121 mg, 1.0 mmol) under argon atmosphere. The solution was stirred at room temperature for 46 h. The reaction was quenched with Na_2CO_3 aq (20 mL) and stirred for 30 min. The red-brown mixture was extracted with dichloromethane, washed with Na_2CO_3 aq, $NaHCO_3$ aq and brine. The combined organic phase was dried over magnesium sulfate. The crude product was purified by column chromatography (eluent: dichloromethane) and recrystallization from hexane/ethyl acetate to afford orange crystalline solid (556 mg, 56%). ^{1}H NMR (400 MHz, $CDCl_3$, δ from TMS): δ 8.08 (dt, 2H, *J* = 8.8 Hz), 7.88 (dt, 1.8H (*trans*), *J* = 8.8 Hz), 7.80 (d, 1.8H, *J* = 8.4 Hz), 7.45 (d, 2H, *J* = 8.0 Hz), 7.30 (d, 1.8H (*trans*), *J* = 8.8 Hz), 7.07 (d, 0.2H(*cis*), *J* = 8.8 Hz), 6.99 (dt, 1.8H (*trans*), *J* = 7.2 Hz), 6.89 (d, 0.2H(*cis*), *J* = 9.2 Hz), 6.79 (d, 0.2H(*cis*), *J* = 8.0 Hz), 6.73 (d, 0.2H(*cis*), *J* = 9.2 Hz), 4.36 (t, 2H, *J* = 6.8 Hz), 4.05 (t, 1.8H (*trans*), *J* = 6.4 Hz), 3.93 (t, 0.2H(*cis*), *J* = 6.4 Hz), 2.67 (t, 1.8H (*trans*), *J* = 7.6 Hz), 2.55 (t, 0.2H(*cis*), *J* = 7.6 Hz), 1.88-1.82 (m, 4H), 1.68-1.62 (m, 2H), 1.56-1.52 (m, 4H), 1.36-1.32 (m, 4H), 0.90 (t, 3H, *J* = 6.8 Hz). ^{13}C NMR (100 MHz, $CDCl_3$, δ from TMS): δ 216.42, 130.79, 129.04, 126.44, 124.54, 122.50, 68.02, 65.53, 35.81, 31.45, 31.01, 25.75, 25.07, 22.53, 14.02.

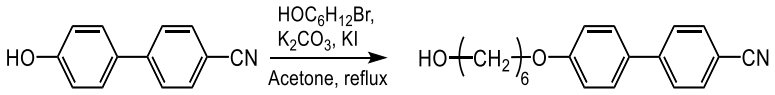

A suspension of 4-cyano-4'-hydroxybiphenyl (5.0 g, 25.6 mmol), K_2CO_3 (10.6 g, 76.8 mmol) and KI (3.3 g, 12.8 mmol) in acetone (200 mL) was stirred at room temperature. To the solution was added dropwise 6-bromo-1-hexanol (5.0 g, 25.6 mmol) in acetone (50 mL) and then the solution was stirred at 60°C for 23 h. The obtained pale-yellow solution was evaporated under vacuum, extracted with dichloromethane, washed three times. The combined organic phase was dried over magnesium sulfate. The crude product was first purified by recrystallization from hexane/ethyl acetate, and then purified by column chromatography (eluent: hexane/ethyl acetate = 2/1 (v/v)) to afford white solid (2.38 g, 31%). ^{1}H NMR (400 MHz, $CDCl_3$, δ from TMS): δ 7.67 (dd, 2H, *J* = 21.6 Hz), 7.52 (d, 2H, *J* = 8.0 Hz), 6.99 (d, 2H, *J* = 8.4 Hz), 4.02 (t, 2H, *J* = 6.4 Hz), 3.67 (quart., 2H, *J* = 5.6 Hz), 1.84 (quint., 2H, *J* = 6.8 Hz), 1.66-1.53 (m, 2H), 1.51-1.42 (m, 4H), 1.28-1.24 (m, 1H).

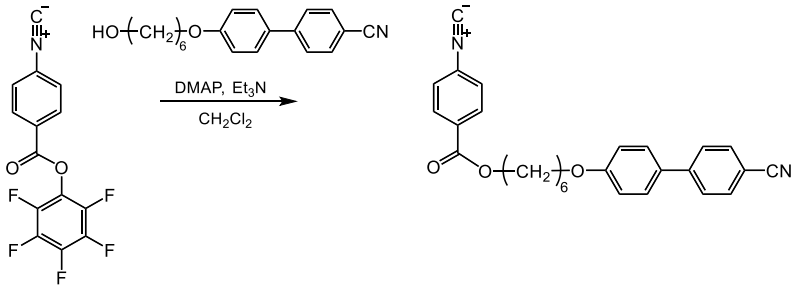

To a solution of pentafluorophenyl-4-isocyanobenzoate (602 mg, 2.0 mmol), 6-cyanobiphenylether-1-hexanol (709 mg, 2.4 mmol) and triethylamine (1.12 mL, 8.0 mmol) in freshly distilled dichloromethane (15 mL) was added 4-dimethylaminopyridine (122 mg, 1.0 mmol) under argon atmosphere. The solution was stirred at room temperature for 46 h. The reaction was quenched with Na_2CO_3 aq (20 mL) and stirred for 30 min. The mixture was extracted with dichloromethane, washed with Na_2CO_3 aq, $NaHCO_3$ aq and brine. The combined organic phase was dried over magnesium sulfate. The crude product was purified by column chromatography (eluent: dichloromethane) and recrystallization from hexane to afford pale-yellow solid (380 mg, 45%). ^{1}H NMR (400 MHz, $CDCl_3$, δ from TMS): δ 8.08 (dt, 2H, *J* = 8.0 Hz), 7.70 (dd, 2H, *J* = 6.4 Hz), 7.64 (dd, 2H, *J* = 6.8 Hz), 7.53 (dt, 2H, *J* = 8.4 Hz), 7.44 (dd, 2H, *J* = 6.8 Hz), 6.97 (dt, 2H, *J* = 9.6 Hz), 4.36 (t, 2H, *J* = 6.8 Hz), 4.02 (t, 2H, *J* = 6.4 Hz), 1.84 (sextet, 4H, *J* = 6.0 Hz), 1.55 (broad, 4H). ^{13}C NMR (100 MHz, $CDCl_3$, δ from TMS): δ 184.19, 166.49, 165.17, 132.58, 130.79, 128.33, 127.07, 126.44, 117.50, 115.02, 67.87, 65.53, 29.10, 25.78.

Block copolymerization for P3OT-b-PPIazo.

Typical polymerization is described as follows: 2,5-dibromo-3-octylthiophene (0.5 mmol) was placed in oven-dried

three-neck flask under argon atmosphere. After adding super dehydrated THF (10 ml) into the flask via a syringe, ~1.0 mol/L solution of i-PrMgCl·LiCl in THF (0.50 ml, 0.5 mmol) was added via a syringe, and the mixture was stirred at room temperature for 2 h. To initiate the polymerization, Ni(dppp)Cl_2 was added. The dark red solution was stirred at room temperature for another 2 h. During the polymerization, the aliquots were taken out via syringe to monitor the progress of polymerization. The methanol-quenched aliquot of poly(3-octylthiophene) shows M_n = 6.0-9.7 kDa, PDI = 1.34–1.35. Then, to the solution of phenyl isocyanide monomer in THF was added Ni-terminated polythiophene macroinitiator to allow the block copolymerization. The solution was stirred at room temperature for 1.5 – 2 h. The reaction was quenched with methanol to produce precipitation. The precipitated polymers were collected by centrifugation (3000 rpm, 15 min) and washed with methanol many times. The collected copolymers were dried under vacuum to afford the solids.

Ni catalyzed polymerization of isocyanide for PPIazo

Into a vial, compound 2 was dissolved in dichloromethane. To the solution was added catalytic amount of $NiCl_2$ at ambient condition, and the solution was stirred at room temperature overnight. Them the viscous orange solution was poured into large amount of methanol to precipitate and subsequent filtration. The obtained solid was dried under vacuum to afford yellow fiber-like solid (GPC result: M_n = 477.9 kDa, M_w/M_n = 2.15).

Chapter 4: 1D Rod-shaped polymers for 0D small molecular crystallization

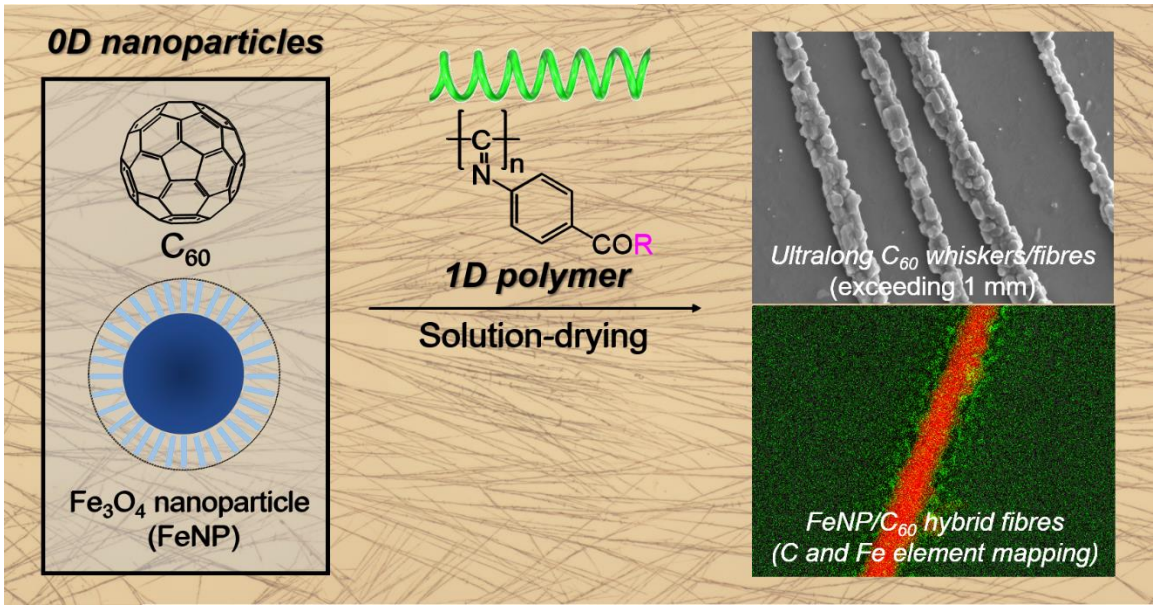

4.1 Abstract

Unidirectional assembly of 0D nanoparticles with controlled manner is still challenging because of the intrinsic geometrically isotropic structure of 0D particles. Herein we demonstrate that 1D rod-shaped polymers facilitate the unidirectional assembly of clusters of 0D nanoparticles. Systematic investigations were performed using poly(phenyl isocyanide) (PPI) as a well-defined 1D anisotropic rod-shaped polymer and fullerene C_{60} as a model crystalline 0D small organic molecule. We show that high-aspect-ratio PPIs with non-branched alkyl side chains facilitated 1D assemblies of C_{60} crystals into ultralong whiskers and fibers exceeding 1 mm length with diameter ca. 1 μm, where the C_{60} crystals were phase separated from PPI and solvent molecules on solution-drying process. Our methodology was also applicable to other small organic building blocks like fullerene C_{70}, 5,6,11,12-tetraphenylnaphthacene, tetraphenylethylene, and tetraphenylporphyrin to afford 1D molecular assemblies such as elongated whiskers, fibers, and dendritic structures. Furthermore, the addition of inorganic superparamagnetic iron-oxide nanoparticles (FeNP) resulted in the formation of unidirectional FeNP cluster assemblies along the ultralong C_{60} fibers. We propose the anisotropic depletion effect and the interfacial capillary force on solution-drying process are key factors for the unidirectional anisotropic assemblies of nanoparticle clusters. Since PPIs are readily modified, we believe that this study will pave the new way in the field of more functional rod-shaped polymers with long persistence length.

4.2 Introduction

Polymer-controlled crystallization of small inorganic/organic molecules has been an increasingly important approach to afford functional hierarchical materials with controlled dimensionality, where the crystals are phase-

separated (precipitated) from the solution phase. For example, using the above mechanism, biomacromolecules such as nucleic acids and proteins, exert specific functionality to produce precise and sized-controlled materials in biological systems. In this context, bio-inspired mineralization[1-3] using polymer additives such as proteins[4-6] has been employed by many researchers, where polymers exhibit impact on crystal growth and the self-assembly of superstructures but are excluded from the crystal. Polymer-controlled crystallization is not limited to inorganic crystals such as $CaCO_3$[7-10], $BaSO_4$[11], ZnO[12] and other inorganic species[13,14], but has been extended to small organic molecules such as perylene derivatives[15,16], indomethacin[17], acetaminophen[18], fullerene C_{60}[19-27] and other organic species. Wonderful sophisticated self-assembled structures have been constructed through the interaction between the polymer additives and small molecules/crystals using non-covalent interactions such as hydrophobic/hydrophilic interactions, hydrogen bonding, π-π interactions and van der Waals forces. However, the geometric effect of the polymer additives on the crystallization of small molecules has been virtually unexplored. Even more, versatile polymer additives or templates that are applicable to wide range of substances have been hardly reported so far. Especially, unidirectional alignment or assembly of 0D nanoparticles with controlled manner is still challenging task because of the geometrically isotropic structure of 0D particles.

Herein, we will apply the bio-inspired polymer-assisted organization methodology to the self-assembly of small 0D nanoparticles into superstructures by adding a precisely synthesized rod-shaped helical polymer (poly(phenyl isocyanide) (PPI)) to control the molecular crystallization. Rod-shaped helical polymer PPIs are reminiscent of helical biomacromolecules such as double-stranded DNA, triple-stranded collagen, and hard rod-shaped M13 bacteria phage virus. In contrast to the biomacromolecules, PPIs are readily modified, allowing for the controlled syntheses of well-defined PPIs with various side chains and molecular weight. A very simple small organic molecule, fullerene C_{60}, was employed as a model system. Self-organization of C_{60} (0D sphere: diameter is ca. 0.7 nm) into highly ordered structures has been one of the most intriguing topics to researchers in wide-spread areas since its discovery (1985) because its molecular assembly at the nano/macro level has a substantial effect on opto-electronic devices[29-33], sensor applications[34,35] and scaffolds for oriented cell growth[36]. Numerous studies on the self-assembly of C_{60}[37,38] were performed on the fabrication of C_{60} rods, wires, whiskers, tubes, sheets and spheres using the direct evaporation of C_{60} solutions[39,40], liquid–liquid interfacial precipitation[41-43] and reprecipitation. However, these methods require very long times (usually 1 - 4 days, even half a year), and therefore they are industrially unfavorable except for ultra-rapid liquid–liquid interfacial precipitation[44]. We consider that the solvent drying method is the most convenient and fastest process among the conventional methods from an industrial viewpoint, and we envisioned that appropriate polymer additives might assist the crystallization of C_{60} through a different out-of-equilibrium pathway in the fast solvent drying and resolve the time-consuming problem.

PPI used in this study is a class of synthetic helical polymers with main chain helicity (ca. 4_1 helix)[45]. Precise synthesis of PPIs has been well-established, and the monomers can be polymerized in a living manner using Ni, Rh catalysts or Pd complex initiators. When PPIs possess sufficiently bulky substituents, the PPI main chain can twist in one direction by steric repulsion between repeating units, which results in the formation of helical structures. Such PPIs can form stable helices not only in the solid state but also in solution state. The substituents or side chains attached to the phenyl ring are accumulated in a helical manner around PPI backbone since PPI main chain serves as scaffold for helical arrangement of the side chains. Furthermore, one very characteristic point is that PPI is classified

as a stiff rod-shaped helical polymer because of its very long persistence length (ca. 30 - 220 nm)[46]. Owing to the resultant 1D structural anisotropy, PPIs exhibit lyotropic liquid crystallinity in concentrated solution[47], which is also the case with double-stranded DNA[48], triple-stranded collagen[49], stiff rod-shaped M13 bacteria phage virus[50] and other helical biomacromolecules, leading to liquid crystal-like structural formation in the solid state through the solvent drying process. Although substantial studies have been carried out on the unique chiral functionalities originating from the one-handed helical motif of the PPI backbone by introducing chiral side chains, in this paper we focus on the effects of the anisotropic 1D rod-shaped structure of PPI on the C_{60} molecular crystallization. Achiral isocyanide monomers are considered to be polymerized into racemic helical polymers (equimolar of right (*P*) - and left (*M*) -handed helicity).

In this chapter, we demonstrate an approach for facile preparation of fullerene C_{60} whiskers and fibers in a highly anisotropic manner. We found that the addition of rod-shaped 1D PPI to 0D C_{60} in toluene solution highly facilitates the whisker and fiber formation of C_{60} in the evaporation process at ambient condition through anisotropic interactions between C_{60} and PPI. The resultant C_{60} whiskers and fibers are much longer in length than the conventional ones. Furthermore, we demonstrate the anisotropic assembly of inorganic iron-oxide nanoparticle clusters along C_{60} fibers. This study presents that the anisotropic shape of PPI has an exceptional ability to facilitate the anisotropic crystal assembly process of 0D nanoparticles. We propose that the attractive depletion effect in the lyotropic liquid crystal-like state formed by the high-aspect-ratio rod-shaped PPIs and meniscus-guided capillary flow during solution-drying are the key factors for the formation of the ultralong 1D assembly of C_{60} crystals and iron-oxide nanoparticles.

4.3 Preparation of rod-shaped PPI and C_{60}/PPI composite film

A series of PPIs was synthesized using Pd(II) complex as an initiator (4-methoxyphenylethynyl Pd complex) or Ni(II) catalyst ($NiCl_2 \cdot 6H_2O$, $NiCl_2$), according to the reported literature[51-54]. PPIs with 14 kinds of side chains (**Figure 4.1**), poly(methyl-4-isocyanobenzoate) (**poly1**), poly(*tert*-butyl-4-isocyanobenzoate) (**poly2**), poly((triethylene glycol monomethyl)-4-isocyanobenzoate) (**poly3**), poly((3,7-dimethyloctyl)-4-isocyanobenzoate) (**poly4**), poly(((3*S*)-3,7-dimethyloctyl)-4-isocyanobenzoate) (**poly5**), poly((*L*-alanine-based-3,7-dimethyloctylester)-4-isocyanobenzamine) (**poly6**), poly(pentafluorophenyl-4-isocyanobenzoate) (**poly7**), poly(decyl-4-isocyanobenzoate) (**poly8**), poly(octyl-4-isocyanobenzoate) (**poly9**), poly(*N*-decyl-4-isocyanobenzamine) (**poly10**), poly(*N*-octyl-4-isocyanobenzamine) (**poly11**), poly(4-isocyanobenzoic acid decyl thioester) (**poly12**), poly(4-isocyanobenzoic acid octyl thioester) (**poly13**), and light-responsive poly(phenyl isocyanide) bearing azobenzene moiety (**poly14**) were prepared to investigate the interfacial effects between polymer side chains and the C_{60} molecules/crystals. To precisely analyze the effects of the 1D anisotropy of PPI on the crystallization of C_{60}, a series of well-defined, controlled molecular weight, narrowly dispersed **poly8** (**entry 15-27**) (M_n = 3.6 - 30.4 (kDa), M_w/M_n < 1.13) was prepared through living polymerization initiated by 4-methoxyphenylethynyl Pd complex. PPIs were thoroughly characterized by gel permeation chromatography (GPC), and nuclear magnetic resonance (NMR) and Fourier transform infrared (FT-IR) spectroscopies (**Figure 4-S1**). The GPC results are summarized in **Table 4.1**. Grazing-incidence X-ray diffraction (GIXRD) measurements for PPI films were also carried out (**Figure 4-S4**) to examine the lyotropic liquid crystal-like structures in solid state.

C_{60}/PPI composite films were prepared by the drop-cast solvent drying method on a glass substrate. Stock solutions of C_{60} (1.0 mg/mL) and PPI (1.0 mg/mL) in toluene were prepared by sonication at room temperature, and then the two solutions were mixed at different ratios. The mixed solution was sonicated again and used immediately. The evaporation proceeded in ca. 1 h at room temperature in a closed petri dish to form the C_{60}/PPI composite films. To measure the length of the C_{60} whiskers and rods, we performed image analysis using software ImageJ (obtained from the U.S. National Institutes of Health) on the images obtained from optical microscopy.

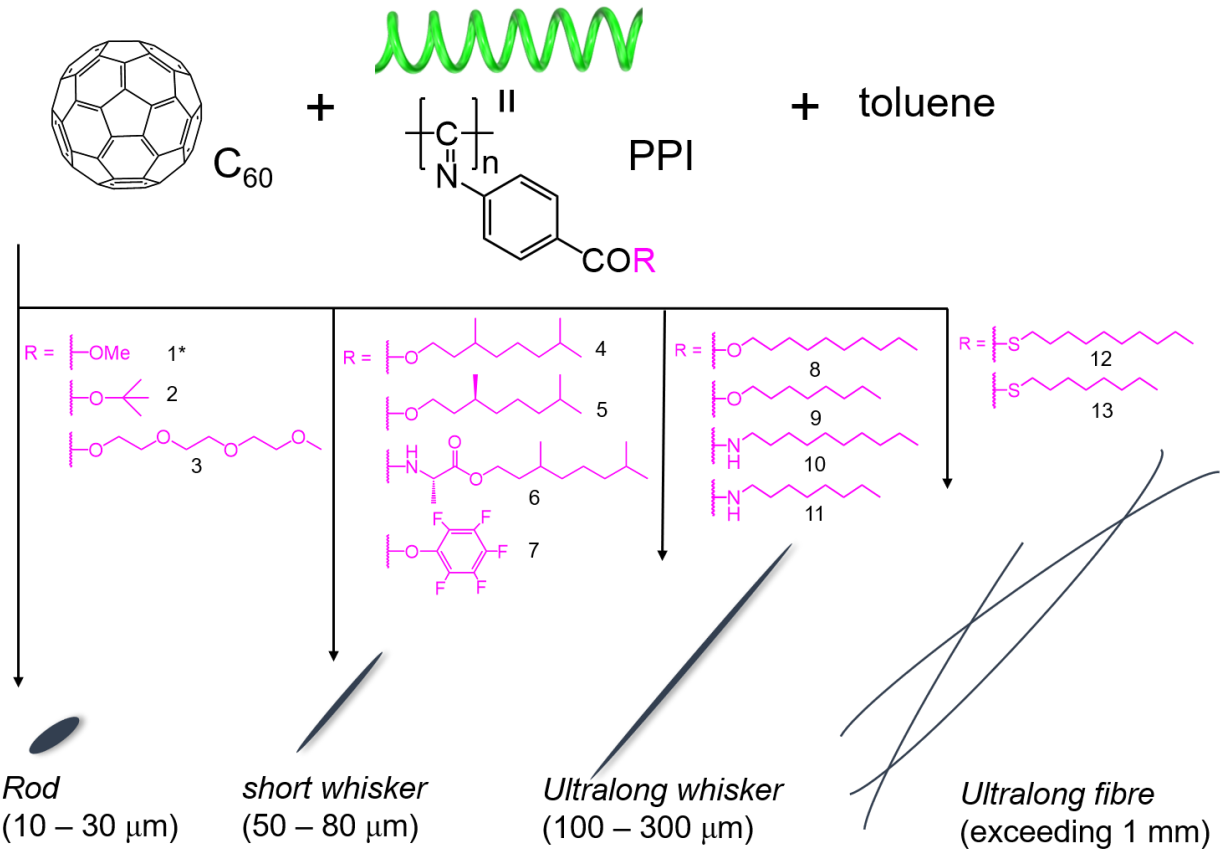

Figure 4.1. Rod-shaped 1D polymer, poly(phenyl isocyanide) (PPI), with various side chains and the corresponding fullerene C_{60} 1D self-assemblies. *Only **poly1** was an additive for C_{60} solution in 1,1,2,2-tetrachloroethane solution.

Table 4.1. GPC results and lyotropic liquid crystallinity for PPIs

Entry	Polymer	Initiator	Solvent	M_n[a] (kDa)	M_w/M_n[a]	Yield[c]	LC[e]
1	Poly1	$NiCl_2·6H_2O$	THF	176.8[b]	2.96[b]	>99%	++
2	Poly2	$NiCl_2·6H_2O$	THF	86.6	2.25	39%	+
3	Poly3	$NiCl_2·6H_2O$	THF	422.3	2.19	84%	++
4	Poly4	$NiCl_2·6H_2O$	THF	293.4	1.76	78%	++
5	Poly5	$NiCl_2·6H_2O$	THF	191.9	2.21	91%	++
6	Poly6	$NiCl_2·6H_2O$	THF	418.9	1.70	>99%	++
7	Poly7	$NiCl_2$	DCM	471.0	2.28	94%	N/A[f]
8	Poly8	$NiCl_2·6H_2O$	DCM	57.3	1.41	>99%	++
9	Poly8	$NiCl_2$	DCM	239.6	2.73	>99%	++
10	Poly9	$NiCl_2$	DCM	55.2	3.08	88%	++
11	Poly10	$NiCl_2·6H_2O$	THF	258.4	1.75	85%	++
12	Poly11	$NiCl_2·6H_2O$	THF	178.9	1.93	89%	++
13	Poly12	$NiCl_2·6H_2O$	THF	69.3	2.92	92%	++
14	Poly13	$NiCl_2·6H_2O$	THF	93.3	1.71	81%	++
15	Poly8	Pd complex	THF	3.6	1.02	-[d]	–
16	Poly8	Pd complex	THF	4.7	1.07	-[d]	–
17	Poly8	Pd complex	THF	6.2	1.08	-[d]	–
18	Poly8	Pd complex	THF	8.0	1.10	-[d]	+
19	Poly8	Pd complex	THF	9.7	1.12	-[d]	+
20	Poly8	Pd complex	THF	11.3	1.12	-[d]	+
21	Poly8	Pd complex	THF	17.5	1.13	-[d]	+
22	Poly8	Pd complex	THF	23.4	1.12	-[d]	++
23	Poly8	Pd complex	THF	26.2	1.12	-[d]	++
24	Poly8	Pd complex	THF	28.1	1.11	-[d]	++
25	Poly8	Pd complex	THF	29.4	1.10	-[d]	++
26	Poly8	Pd complex	THF	29.9	1.10	-[d]	++
27	Poly8	Pd complex	THF	30.4	1.10	-[d]	++

a. Molecular weight and molecular distribution were estimated by GPC analysis calibrated by PS standard (eluent: THF at rt for **poly1, 4, 5, 7, 8, 9, 12, 13** or THF with 0.1wt% TBAB at rt for **poly2, 3, 6, 10, 11**). b. M_n and M_w/M_n of **poly1** was estimated from GPC with $CHCl_3$ eluent due to the poor solubility to THF. c. isolated yield. d. the yields could not be determined precisely because they were aliquots (taken at different time periods) from the same reaction mixture. e. lyotropic liquid crystallinity (LC) was evaluated by polarizing optical microscopy for drop-cast **PPI** films (see Figure S4, S5). LC was evaluated at three levels: "- (No)", "+ (a little)", and "++ (Yes)". f. not applicable due to the poor film formation ability of **poly7**. THF: tetrahydrofuran, DCM: dichloromethane, Pd complex: 4-methoxy-phenylethynyl Pd complex.

4.4 PPI-assisted unidirectional assembly of C_{60} crystals with highly anisotropic elongation

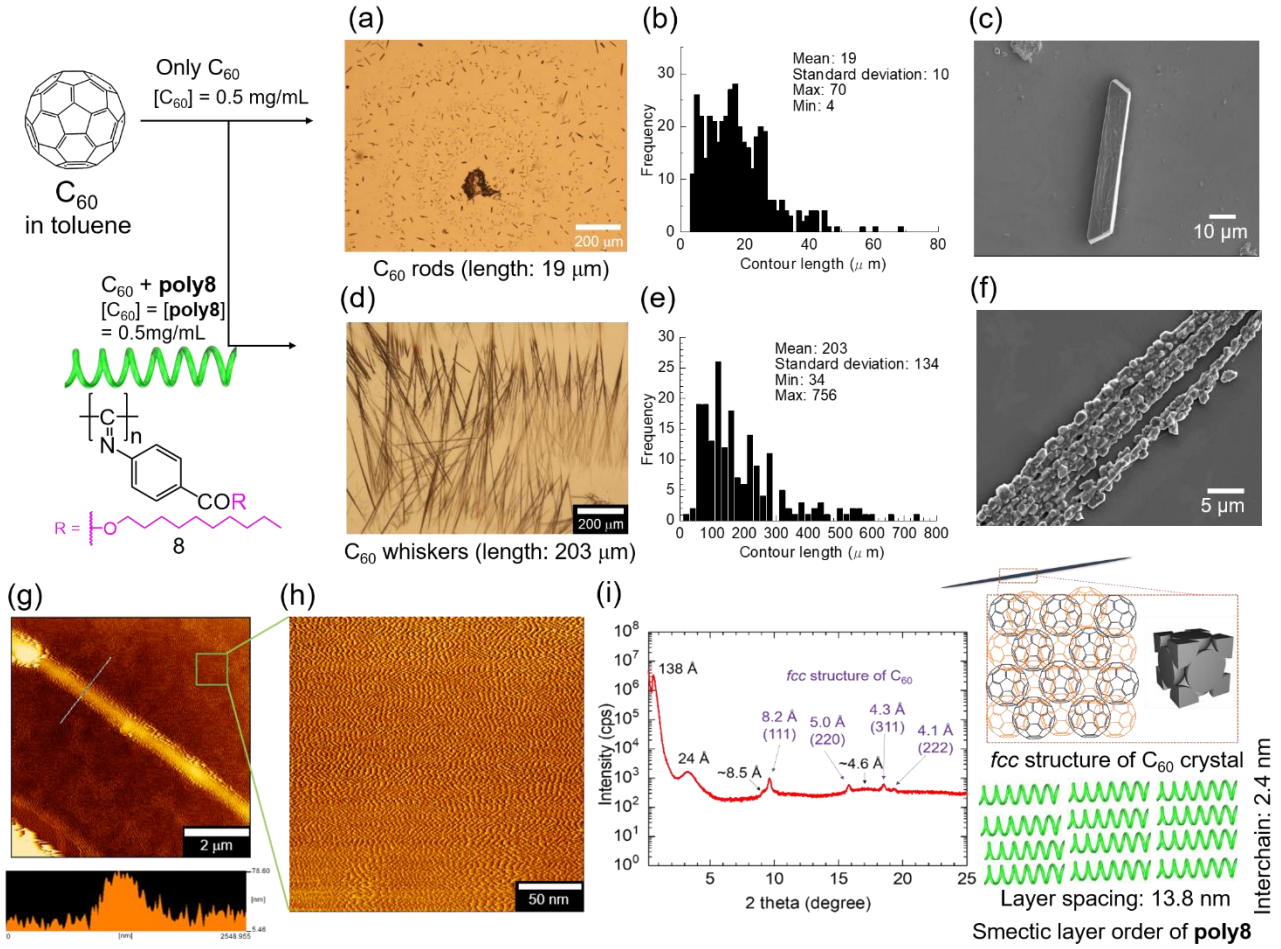

Figure 4.2. PPI-assisted C_{60} crystallization into highly anisotropic whiskers. C_{60} rod formation prepared from pure C_{60} toluene solution; (a) optical microscopy, (b) histogram for the length distribution of C_{60} rods, and (c) SEM image. C_{60} whisker formation prepared from C_{60}/**poly8 (entry 8)** toluene solution; (e) optical microscopy, (f) histogram for the length distribution of C_{60} whiskers, and (g) SEM image. (g) AFM measurement for C_{60} whisker/**poly8** film showing the height of a selected C_{60} whisker and (h) the smectic layers of **poly8**. (i) Synchrotron X-ray diffraction measurement for C_{60} whisker/**poly8** film on the glass substrate (wavelength of X-ray: 1.3761Å, 2θ/θ scan) with schematic illustration of C_{60} crystal and **poly8** smectic layer structure.

We first studied the weight ratio effect of PPI to C_{60} using relatively narrow dispersed **poly8 (entry8)** (M_n = 57.3 (kDa), M_w/M_n = 1.41), which was prepared by $NiCl_2 \cdot 6H_2O$. Mixed toluene solutions with different ratios ([C_{60}]/[**poly8**] = 1/30, 1/20, 1/15, 1/10, 1/5, 1/2.5, 1/1, 1/0.5, 1/0.25, 1/0.1, 1/0.02 (wt/wt)) were prepared to fabricate C_{60}/PPI composite films. We found that C_{60} in **poly8** formed two characteristic structures, 3D spherical aggregates and 1D whisker formation, whereas pure C_{60} toluene solution only yielded 1D rod-shaped structures (mean length: 19 μm) (**Figure 4.2a, b)**. Very interestingly, at certain weight ratios ([C_{60}]/[**poly8**] = 1/2.5 - 1/0.5), ultralong high-aspect-ratio C_{60} whisker structures (up to 760 μm) were observed (**Figure 4.2d, e**). Scanning electron microscopy (SEM) analysis of the C_{60} whiskers indicated that the majority of whiskers were composed of a cluster-attached beaded-like surface (**Figure 4.2f**), and the diameter of the whiskers is ca. 1 μm, whereas C_{60} rod prepared from pure toluene solution form relatively flat surface (**Figure 4.2c**). Atomic force microscopy (AFM) measurement (**Figure**

4.2h, i) on the C_{60} whisker/**poly8** film revealed that the height of a selected C_{60} whisker was ca. 70 nm, and it supported that **poly8** formed smectic layer ordering through a lyotropic liquid crystalline state in the solvent evaporation process. Synchrotron X-ray diffraction measurements (**Figure 4.2j**) for the C_{60} whisker/**poly8** films showed four typical peaks at 8.2 Å (111), 5.0 Å (220), 4.3 Å (311), and 4.1 Å (222) from the C_{60} face-centered cubic (*fcc*) lattices and broad peaks (at 138 Å (smectic layer spacing), 24 Å (chain-to-chain distance), 8.5 Å, and 4.6 Å) from **poly8** smectic liquid crystalline structures. No change of chain-to-chain distance compared to **poly8** film supports that almost no C_{60} molecular intrusion between **poly8** molecules in lateral direction (**Figure 4-S4**). This result indicates that the whiskers consisted of non-solvated pure C_{60} *fcc* crystal structures, and that **poly8** and toluene solvent molecules were predominantly excluded from the C_{60} whiskers crystal structures.

4.5 Molecular weight effects of PPI on C_{60} crystals anisotropic assembly

A series of well-defined, controlled molecular weight narrowly dispersed **poly8 (entry 15-27)** (M_n = 3.6 - 30.4 (kDa), M_w/M_n < 1.13) was used to precisely investigate the effects of the 1D anisotropy of PPI on the crystallization of C_{60}. These polymers (**poly8**) were prepared by taking the aliquots from the same reaction mixture at different polymerization periods using 4-methoxyphenylethynyl Pd complex as initiator (**Figure 4.3a**). The living nature was confirmed by clear shifts of elution peaks while maintaining narrow dispersity in GPC profiles (**Figure 4.3b**). Since PPIs form stiff rod-shaped helical structures, we assumed that the aspect ratio of the 1D shape would be proportional to the molecular weight (**Figure 4.3c**). Indeed, controlled molecular weight, narrowly dispersed **poly8** exhibited liquid crystallinity as the molecular weight increased and the other PPIs, high molecular weight **poly1-13**, also displayed liquid crystalline-like structures in the solid state, probably owing to the high-aspect-ratio 1D rod-shaped **PPI** molecular assemblies (**Figure 4-S2,3**). In all cases using controlled molecular weight narrowly dispersed **poly8**, C_{60} whiskers were observed in each C_{60}/**poly8** composited film (**Figure 4.3d**). We carefully examined and calculated the mean lengths and length distributions of the C_{60} whiskers, and we found that the mean length of C_{60} whiskers increased (from ca. 100 to 330 μm) as the molecular weight (M_n) of **poly8** increased (**Figure 4.3e**), while the weight ratios of C_{60} to **poly8** were constant. This result strongly suggests that the higher anisotropic 1D shape and the resultant LC formation of **poly8** enhances the unidirectional assemblies of C_{60} crystals in the solvent drying process.

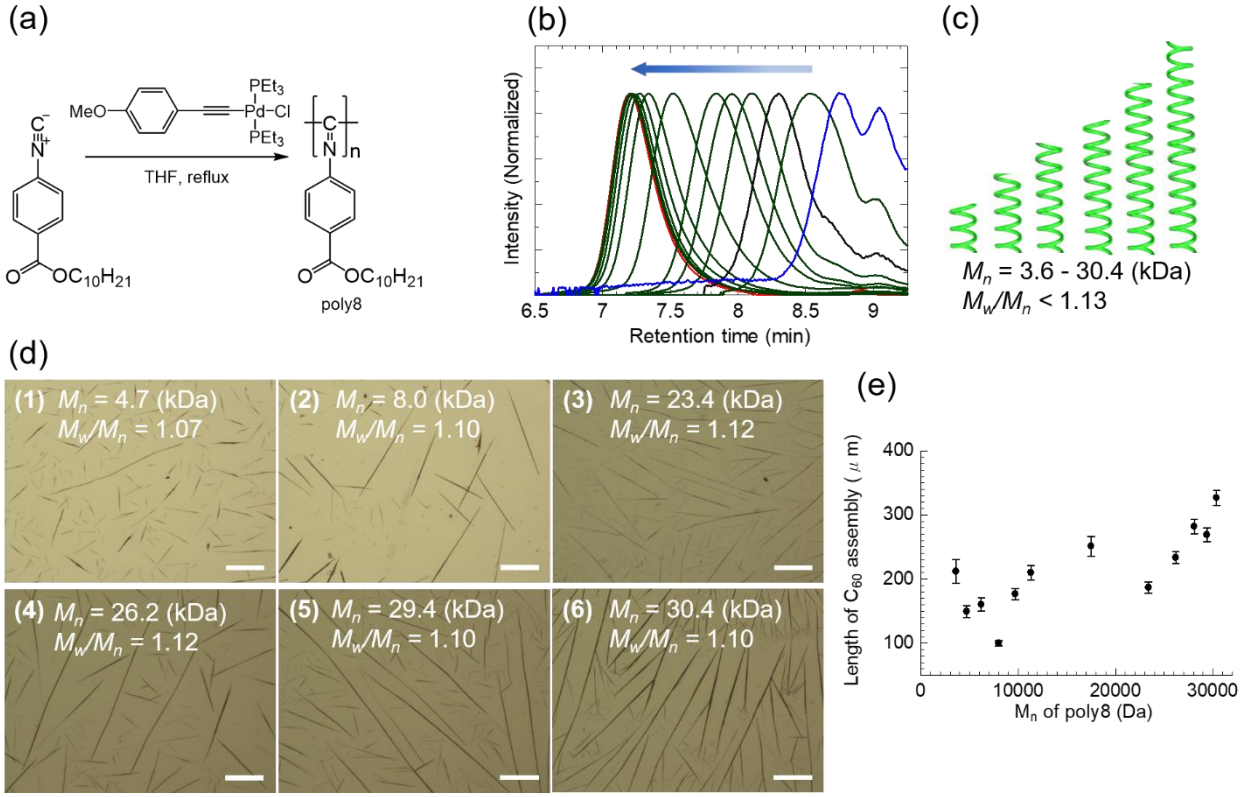

Figure 4.3. Molecular weight effects on the C_{60} crystallization. (a) Scheme for living polymerization for controlled molecular weight, narrowly dispersed **poly8 (entry 15-27)**. (b) GPC results and (c) schematic illustration of different molecular weight (different aspect-ratio) **poly8**. (d) Optical microscopy images of C_{60}/**poly8 (entry 15-27)** with different molecular weights. Scale bars, 200 μm. (e) Correlation between molecular weight of poly8 (entry 15-27) and the length of C_{60} assemblies (the solid dots are the mean values of contour lengths of C whiskers, and the error bars are the standard errors (N = 203 - 569)).

The C_{60} whiskers obtained using **poly8** were much longer with higher aspect-ratio than other C_{60} 1D structures prepared using other polymers such as poly(*p*-phenylene)[23] (whiskers; diameter: 30 - 40 nm; length: 30 - 50 μm), anthracene-ended hyperbranched poly(ether amine) [26] (nanorods; diameter: 50 - 90 nm; length: 2 - 12 μm), and poly(3-hexylthiophene)[27] (nanorods; diameter: 10 - 20 nm; aspect ratio: ca. 10). Other polymer or LC additives to C_{60} toluene solution such as polystyrene (PS: M_n = 190 (kDa), M_w/M_n = 1.04), 4-cyano-4'-pentylbiphenyl (5CB: M_n = 249.36 (Da)), and regioregular poly(3-octylthiophene) (P3OT: M_n = 17.6 (kDa), M_w/M_n = 1.39) also only yielded C_{60} short rods or spheres (**Figure 4.4**).

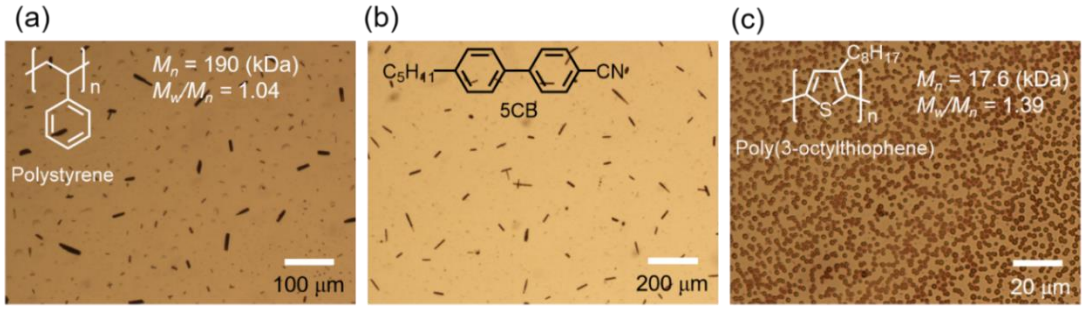

Figure 4.4. Optical microscopy images of C_{60} assemblies prepared from C_{60} in toluene solution (0.5 mg/mL) with the additives such as (a) polystyrene (PS), (b) 4-cyano-4'-pentylbiphenyl (5CB), and (c) poly(3-octylthiophene) (P3OT).

4.6 Ultralong fiber formation of C_{60} crystals and anisotropic assemblies of other organic building blocks

More surprisingly, ultralong high-aspect-ratio C_{60} fibers exceeding 1 mm were observed uniformly in the C_{60}/**poly12** composite film (**Figure 4.5a**). The fibers were also composed of small crystallites in SEM observation (**Figure 4.5b**). No typical structures were observed for pure **poly12** film in SEM observation. GIXRD measurement for C_{60}/**poly12** film suggested that the fibers were consist of C_{60} *fcc* structures (**Figure 4.6**). As far as we know, this C_{60} fiber is the longest that has been reported for C_{60} self-assembled structures prepared by the solvent drying method in the presence of polymer additives. The C_{60} fibers were so long and formed several bundles that we could not calculate the lengths quantitatively. A rough estimation was ca. 600 μm to 3 mm length, and the diameter of the fibers was ca. 1 μm. C_{60} fibers were lying down to the glass substrate, and the axis of fibers were preferentially oriented along the evaporation direction. On the various substrates, like bare glass, indium-tin-oxide (ITO) glass, hydrophobic glass, the ultralong C_{60} fibers were formed in the presence of **poly12**. Since **poly12** is relatively soluble in hexane, gentle immersion in hexane allows for the removal of **poly12** from C_{60}/**poly12** film without any destructive effect on C_{60} fibers. Element mapping utilizing energy dispersive X-ray spectroscopy equipped in SEM apparatus (SEM-EDX) for hexane-washed C_{60}/poly12 film indicated that the ratio of S atoms of **poly12** in the C_{60} fibers were low (the C/S atomic ratio is 57:1, corresponding ca. [C_{60}] : [**poly12**] unit = 2.4:1), probably supporting that C_{60} crystals and **poly12** were phase-separated in the process of solution-drying (**Figure 4.7**).

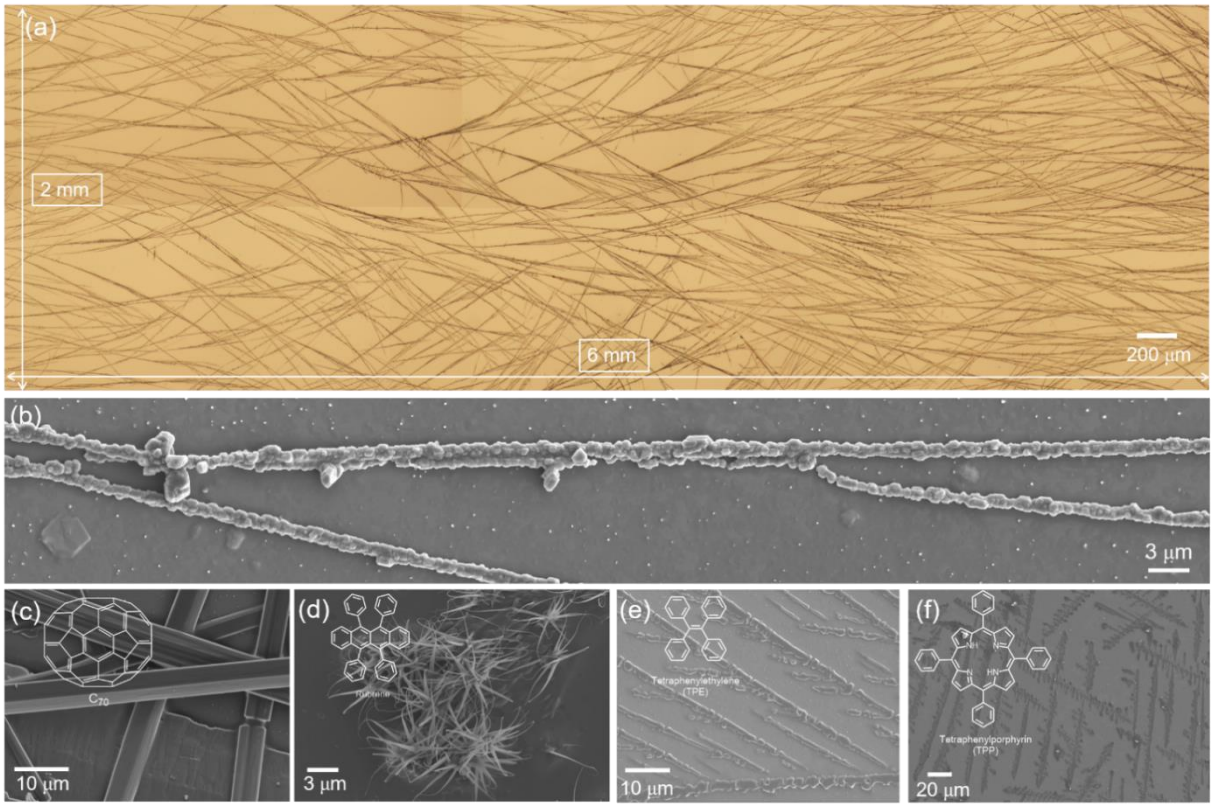

Figure 4.5. Ultralong C_{60} fiber formation and other organic small molecular crystallization assisted by **poly12** (**entry 13**). (a) Optical microscopy image of ultralong C_{60} fibers prepared from C_{60}/**poly12** toluene solution. This image was created by connecting the photos from the same sample. SEM image of (b) ultralong C_{60} fibers, (c) C_{70} whiskers, (d) fiber-like rubrene crystals, (e) dendric TPE crystals, and (f) dendric TPP crystals prepared from toluene solution with **poly12** as additive by drop-cast method.

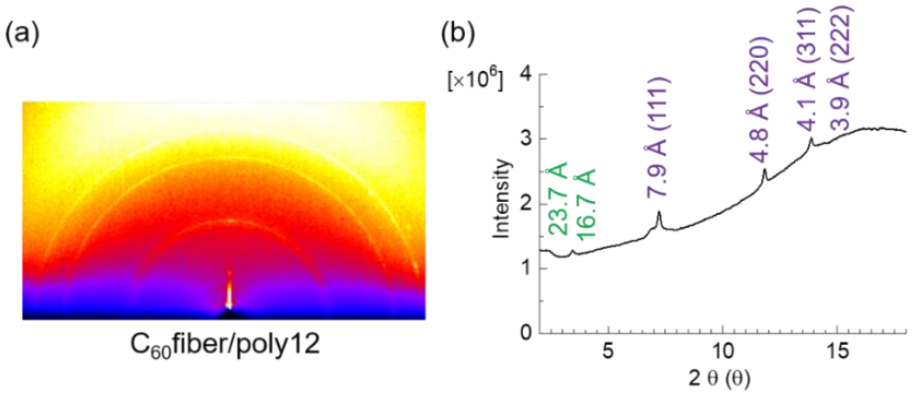

Figure 4.6. GIXRD for C_{60}fiber prepared from C_{60}/**poly12** solution: (a) diffraction pattern and (b) the corresponding 2θ/θ profile.

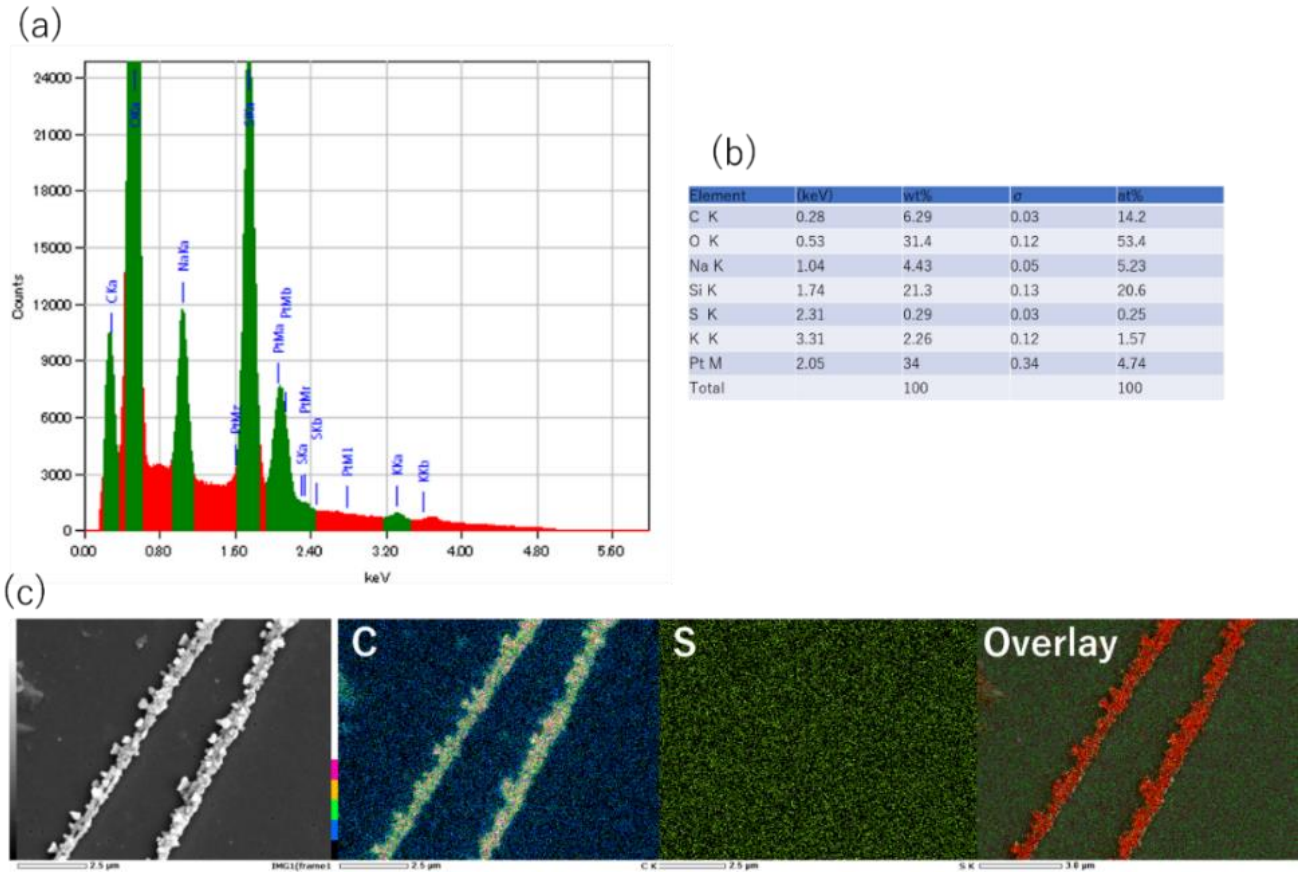

Element	(keV)	wt%	σ	at%
C K	0.28	6.29	0.03	14.2
O K	0.53	31.4	0.12	53.4
Na K	1.04	4.43	0.05	5.23
Si K	1.74	21.3	0.13	20.6
S K	2.31	0.29	0.03	0.25
K K	3.31	2.26	0.12	1.57
Pt M	2.05	34	0.34	4.74
Total		100		100

Figure 4.7. SEM-EDX measurement for hexane-washed C_{60}/**poly12** film. (a) EDX spectra, (b) element composition, and (c) element mapping.

Our interests extended to the application of this methodology to other small organic molecules. Four kinds of small organic molecules, fullerene C_{70}, 5,6,11,12-tetraphenylnaphthacene (rubrene), tetraphenylethylene (TPE) and tetaraphenylporphyrin (TPP), which are potential candidates for organic electronics[56-59], were employed to investigate the effect of PPI on the small organic molecular crystallization. The composite films were prepared by the solution drying method using **poly12** from the corresponding toluene solutions. C_{70}/**poly12** composite film

afforded long whiskers at the film edge (**Figure 4.8**) along with cross-shaped crystals around the center of the film, while pure C_{70} toluene solution only yielded small rod-shaped and cube structures. GIXRD measurements for C_{70}/**poly12** composite film indicates that C_{70} in the **poly12** matrix possesses hexagonal close-packed structure (**Figure 4.8**)[60]. For the preparation of rubrene crystals, thermal annealing at 120 °C for 30 min was required after toluene evaporation because the as-prepared film showed no birefringence (no crystals). After annealing, rubrene/**poly12** composite film yielded high-aspect-ratio thread-like crystals (**Figure 4.8**), whereas the pure rubrene film formed rectangular crystals (**Figure 4.8**). GIXRD measurements for rubrene/**poly12** composite film supports the rubrene form orthorhombic structure[61] in the presence of **poly12** (**Figure 4.8**). Dendritic structures were predominantly obtained for both TPE/**poly12** and TPP/**poly12** composite films (**Figure 4.8**) compared to the pure TPE and pure TPP films. TPE and TPP molecules in the corresponding composite films probably form monoclinic structure[62] and triclinic structure[63] respectively, from the GIXRD measurements (**Figure 4.8**). This result suggested that rod-shaped polymers, PPIs, have the potential to facilitate the 1D crystallization of various small organic molecules in the solution drying process to form whisker, thread, and dendritic structures which were not obtained with the conventional solution drying method, while maintaining the crystal nature of the molecules.

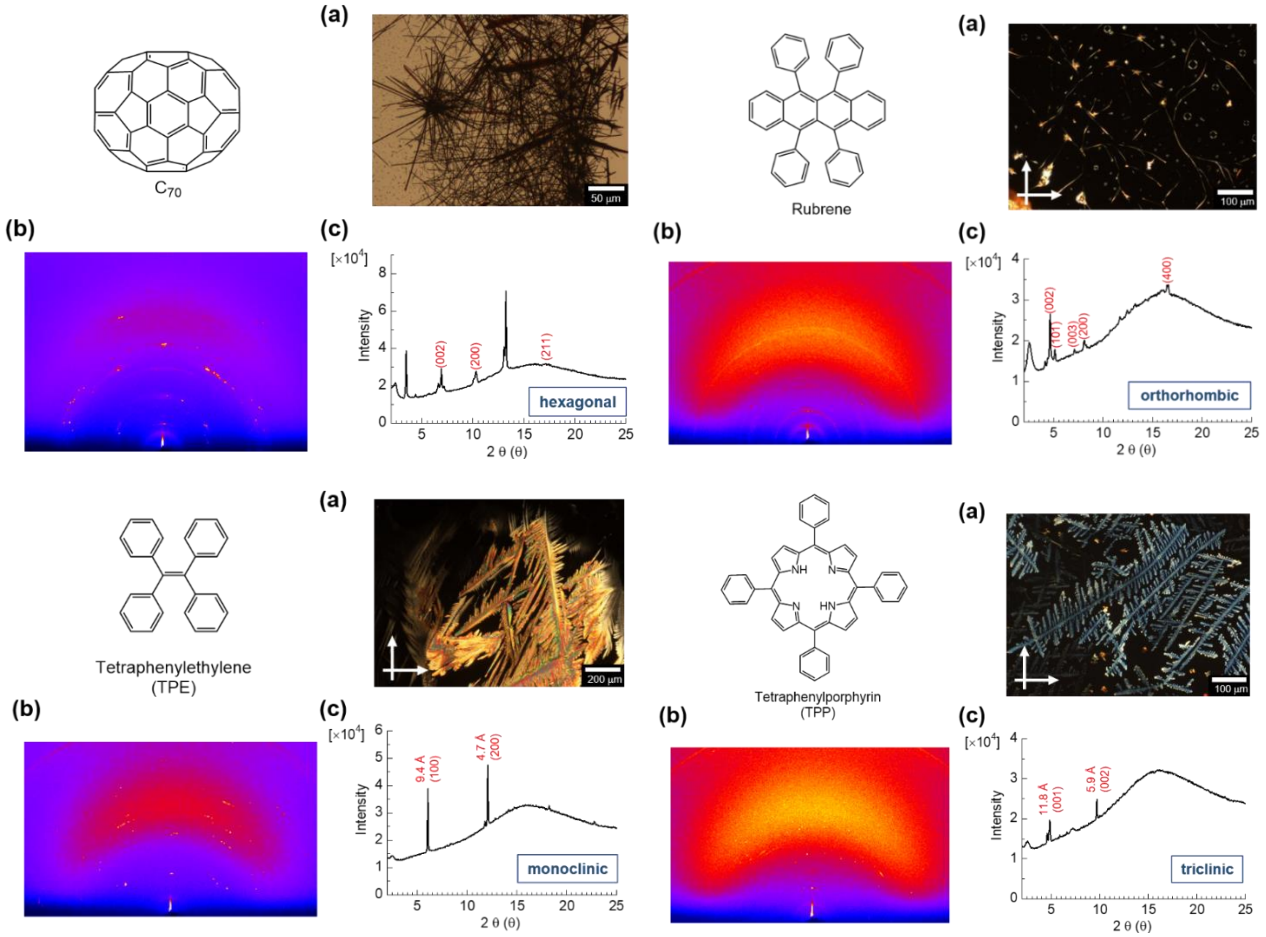

Figure 4.8. (a) Polarizing optical microscopy image and (b,c) GIXRD measurements for C_{70}/poly12, rubrene/poly12, TPE/**poly12, TPP/poly12** films (wavelength of X-ray: 0.9965Å). The broad halo at 2θ~16° is due to the amorphous diffraction of the glass substrate.

4.7 Side chain effects of PPI on C_{60} crystals anisotropic assembly

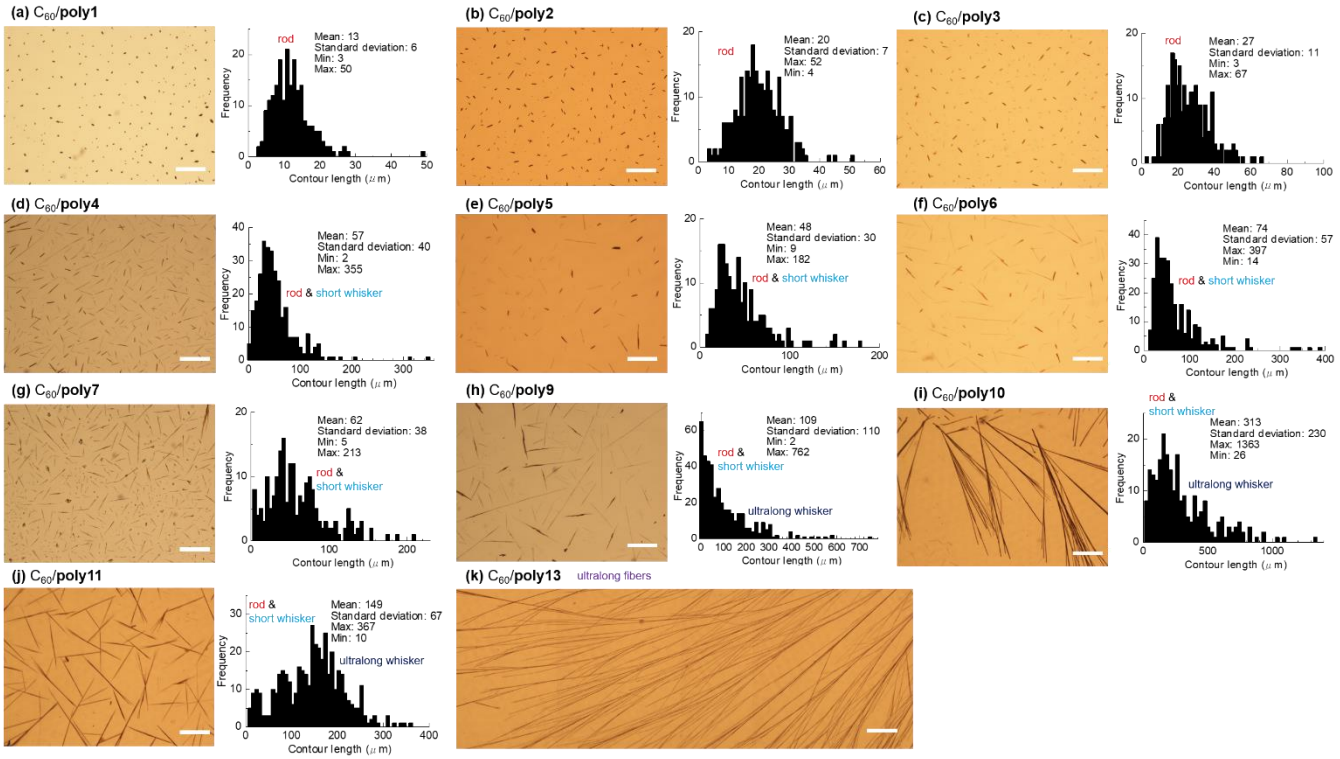

Figure 4.9. Side chain effects on the C_{60} crystallization. Optical microscopy images of C_{60}/**PPI** films and the corresponding histograms for the length of C_{60} assemblies; C_{60} rod formation in (a) C_{60}/**poly1**, (b) C_{60}/**poly2**, (c) C_{60}/**poly3** films, C_{60} short whisker formation in (d) C_{60}/**poly4**, (e) C_{60}/**poly5**, (f) C_{60}/**poly6**, (g) C_{60}/**poly7** films, C_{60} ultralong whisker formation in (h) C_{60}/**poly9**, (i) C_{60}/**poly10**, (j) C_{60}/**poly11** films, C_{60} ultralong fiber formation in (k) C_{60}/**poly13** film. The films were prepared from toluene solution, except (a) C_{60}/**poly1** film was prepared from 1,1,2,2-tetrachloroethane solution. The weight ratios of C_{60} to PPI were constant ([C_{60}] = [**PPI**] = 0.5 mg/mL) in each solution.

PPIs with 11 other kinds of side chains, **poly1-7, 9-11, 13** were used to investigate the PPIs effects of LC formation, solubility in toluene, chirality from one-handed helical backbone, and stiffness of the polymer backbone on the anisotropic assembly of C_{60} molecules/crystals. As mentioned, the side chains attached to the phenyl ring are accumulated around PPI backbone. We successfully categorized C_{60} 1D assemblies into 4 groups: rod, short whisker, ultralong whisker, and ultralong fiber (**Figure 4.1**). C_{60} rod formation was observed in the presence of short alkyl-chain modified **poly1, 2** (mean length: 13 and 20 μm, respectively) and hydrophilic side-chain modified **poly3** (mean length: 27 μm). Only in the preparation of C_{60}/**poly1** composite film, 1,1,2,2-tetrachloroethane was used as the solvent because **poly1** was well dissolved in chlorinated alkyl solvents such as chloroform, dichloromethane, 1,1,2,2-tetrachloroethane but not in common aromatic solvents such as toluene, chlorobenzene and *ortho*-dichlorobenzene. The pure 1,1,2,2-tetrachloroethane solution of C_{60} also yielded short rods. The short rod formation of C_{60} molecules can be ascribed to the poor LC formation or very small grain size of **poly1-3** (**Figure 4-S3**). C_{60} short whisker formation was observed in the presence of branched alkyl-chain modified **poly4, 5, 6** (mean length: 57, 48 and 74 μm, respectively) and pentafluorophenyl side-chain modified **poly7** (mean length: 62 μm). Modification of branched alkyl chains enhances the solubility of its polymer in organic solvent. Although the obtained C_{60} short whiskers in this study are relatively longer than those reported so far, the short elongation of C_{60} 1D assemblies can derive from largely different solubility of C_{60} and **poly4, 5, 6**. C_{60} molecules or clusters may not be subject to the effects of LC

formation of **poly4, 5, 6** in solution-drying process as a result of higher solubility and the high threshold for LC phase of **poly4, 5, 6**. It should be noted that chiral side-chain modified **poly5, 6**, that possess one-handed helical imine backbone, did not produce any chiral C_{60} objects, supporting that the anisotropic rod-shape of PPIs is a predominant factor in this study. Poor LC and film formation of **poly7** also resulted in the short whisker formation of C_{60}. C_{60} ultralong whisker formation was observed in the presence of non-branched, relatively long alkyl-chain modified **poly8, 9, 10, 11** (mean length: 203, 109, 313 and 149 μm, respectively). All **poly8, 9, 10, 11** form clear LC in solid state with relatively large grain size (**Figure 4-S3**). It should be mentioned that amide alkyl-chain modified **poly10, 11** yielded longer C_{60} whiskers than ester alkyl-chain modified **poly8, 9** within the same carbon number (C_8H_{17} or $C_{10}H_{21}$). It is reported that intramolecular hydrogen bonding between amide group in the repeating unit significantly reinforce the rigidity of PPI backbone, resulting in the very long persistence length[46]. This report supports that PPIs with stiffer backbone (**poly10, 11**) facilitates the longer C_{60} 1D assemblies in solution-drying process. C_{60} ultralong fiber formation was observed in the presence of non-branched, relatively long, thioester alkyl-chain modified **poly12, 13** (exceeding 1mm). Although extraordinary long elongation of anisotropic assembly of C_{60} crystals in the presence of **poly12,13** is still puzzling, intramolecular S-O interactions between thioester bonds of repeating units of **poly12,13** might have an impact on the conformation of the **poly12,13** helical backbone, which might assist the C_{60} crystallization. Indeed, **poly12,13** exhibited a slightly different electronic state in absorption spectroscopy, and sharper, and different vibrational modes in IR spectroscopy (**Figure 4-S1**), and relatively larger LC grain sizes in solid state (**Figure 4-S3**), and enhanced polymer packing (**Figure 4-4S**) compared to those of other **PPIs**. This comparative experiment demonstrated that non-branched, relatively long alkyl side chains (e.g., octyl (C_8H_{17}) or decyl ($C_{10}H_{21}$)) and stiffer backbone of PPIs should be suitable to facilitate the C_{60} 1D crystal assemblies thorough simple van der Waals force interactions and LC field derived from PPIs self-assembly.

4.8 Plausible mechanism for C_{60} ultralong whisker and fiber formation

The unidirectional crystal assemblies of C_{60} molecules into ultralong 1D structures observed in this study can be rationally understood to some extent by the microscopic depletion effect in the rod-sphere binary mixture and macroscopic meniscus-guided capillary flow in the solution-drying process. The binary system of rods and spheres, where high-aspect-ratio PPIs and low-solubility C_{60} can be regarded as high-aspect-ratio rods and spheres, respectively, has been extensively studied for colloidal materials exhibiting various and complex phase behaviors[64] originating from entropically-driven microphase separation by different steric repulsions due to the anisotropy of rods and the diameter of spheres, which is referred to as the depletion effect. Especially in the lyotropic nematic liquid crystalline state[65], small spherical colloids dispersed in the high-aspect-ratio rods should experience a highly directional attractive depletion interaction along the liquid crystal director. At the same time, meniscus and the resulting capillary flow and Marangoni flow are generated in solution-drying process[66] (**Figure 4.10a**).

Based on the aforementioned theory and discussions, we propose a model for the unidirectional assembly process of C_{60} crystals. From microscopic viewpoint, the C_{60}/PPI mixed solution is expected to experience four phases (I to IV) as evaporation proceeds in the concentration gradient. In phase I (immediately after the drop cast), PPIs and C_{60} molecules are diluted in toluene solvent. As evaporation proceeds, the poor solubility of C_{60} molecules results in C_{60} cluster formation (ca. 100 nm) in phase II, which is facilitated in the presence of miscibility-reducing agents like poor

solvent or polymers[67,68]. Further evaporation introduces phase III, where the depletion effect and resulting phase separations occur. Rod-shaped PPI molecules become parallel to each other to induce a lyotropic liquid crystalline order. On the other hand, C_{60} molecules and clusters should experience a highly directional attractive depletion interaction along the PPI liquid crystal director. Finally, in phase IV, nucleation and subsequent elongation of C_{60} occur along the liquid crystal director (**Figure 4.10b**). Indeed, POM observation (**Figure 4.10d, e**) shows that black lines (smectic layers) are preferentially perpendicular to the C_{60} whiskers, indicating **poly8** long axes are predominantly aligned parallel to the whisker long axis. AFM measurements (**Figure 4.2g**) also indicate that the whiskers are essentially along the director. We speculate that C_{60} colloidal assembly should experience a higher directional attractive depletion in higher aspect-ratio PPIs along the director (PPI long axis), resulting in crystallization into longer C_{60} 1D assemblies. However, this cannot completely explain the ultralong whisker and fiber formation over LC grain sizes. We postulate from macroscopic viewpoint that meniscus-guided capillary flow might continuously supply the C_{60} clusters to elongate the 1D assemblies and might align the axis of the high-aspect-ratio PPI molecules (capillary flow//PPI long axis) to assist the unidirectional assembly of C_{60} clusters over LC grain sizes together with anisotropic attractive depletion effect (**Figure 4.10b**).

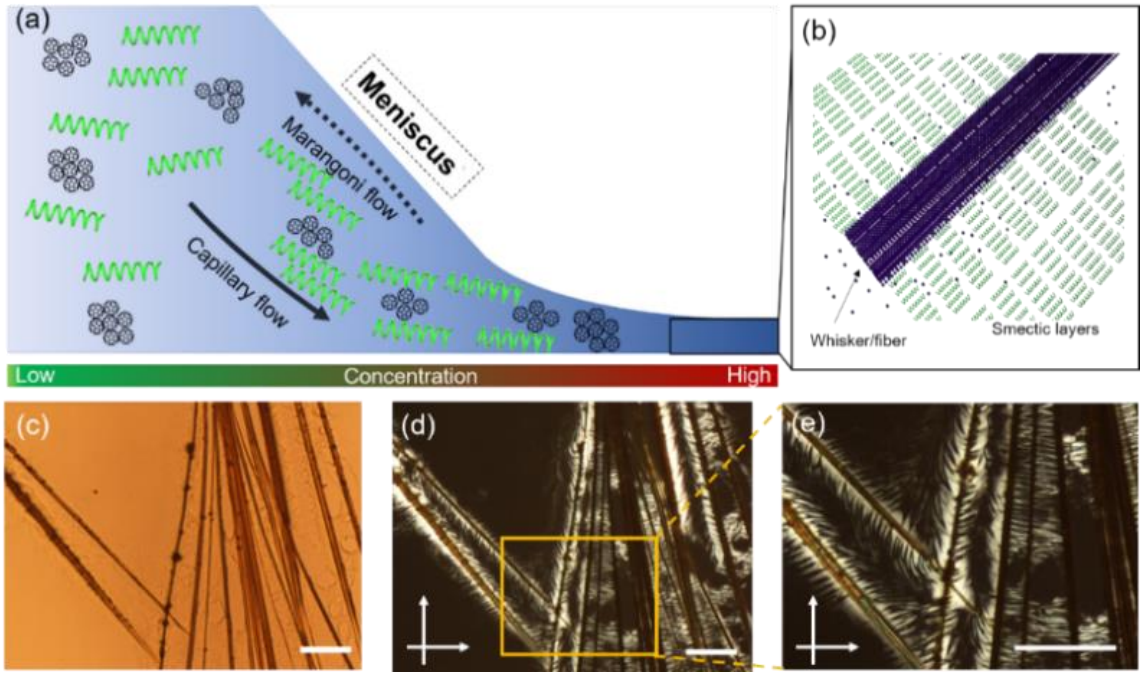

Figure 4.10. (a, b) Schematic illustration for plausible C_{60} crystallization and anisotropic assembly process into ultralong 1D assemblies. Unidirectional assembly of C_{60} crystals along the liquid crystal director in a locally high concentration region of C_{60} in virtue of interfacial capillary force. Toluene solvent molecules are omitted for clarity. (c) Optical microscopy image and (d,c) polarizing optical microscopy images of C_{60} whisker/PPI film in the same area with different magnification. Scale bar: 20 μm.

It should be mentioned that entropically-driven microphase segregation, where spherical particles preferentially segregate between the smectic layers formed by rod-like particles, has been theoretically predicted[69] using Monte Carlo simulations and experimentally reproduced[70] using rod-like poly(silane) and spherical branched alkyl squalene.

Note that the layer spacing of **poly8** near the C_{60} whiskers in the C_{60}/**poly8** composite film (**Figure 4.2g**) is larger than that at other areas, suggesting a locally high concentration of C_{60} and C_{60} segregation into **poly8** smectic layers. It has been suggested that the growth mechanism of C_{60} in a polymer matrix is based on a concentration profile growth[55]. The resulting shapes of crystalline materials depend on the local concentration profile where the depletion happens during crystal growth of C_{60} crystal seeds[55]. The AFM measurements (**Figure 4.2g**) support that the C_{60} ultralong whisker and fiber formation probably occurs locally in the relatively high concentration region of C_{60} molecules and colloidal assemblies, which is assisted by the meniscus-guided capillary flow and concentration increase in the solvent evaporation process.

4.9 Photo-regulated control over C_{60} crystallization

Based on the above experiment, we conceived "photo-regulated" control over C_{60} crystallization in the presence of photo-responsive poly(phenyl isocyanide). To this end, we synthesized PPI bearing azobenzene moiety (poly14) as additive for C_{60} toluene solution. The GPC result is shown in **Table 4.3**. The light-irradiation *cis-trans* isomerization property was discussed in **Figure 4.12**. Under visible light, C_{60} long whiskers (130 m) were prepared from C_{60}/poly14 toluene solution, whereas under UV-light irradiation C_{60} rods & short whiskers (76 m) were observed in C_{60}/poly14 films (**Figure 4.11, 4.13**). We speculate that relative straight azo-*trans* form enhances the C_{60} crystallization, while bent azo-*cis* form has no enhancement effect in the crystallization of C_{60}. Indeed, C_{60} pure solution only yielded rods under UV-light, which was the almost identical result from C_{60}/**poly14** toluene under UV light.

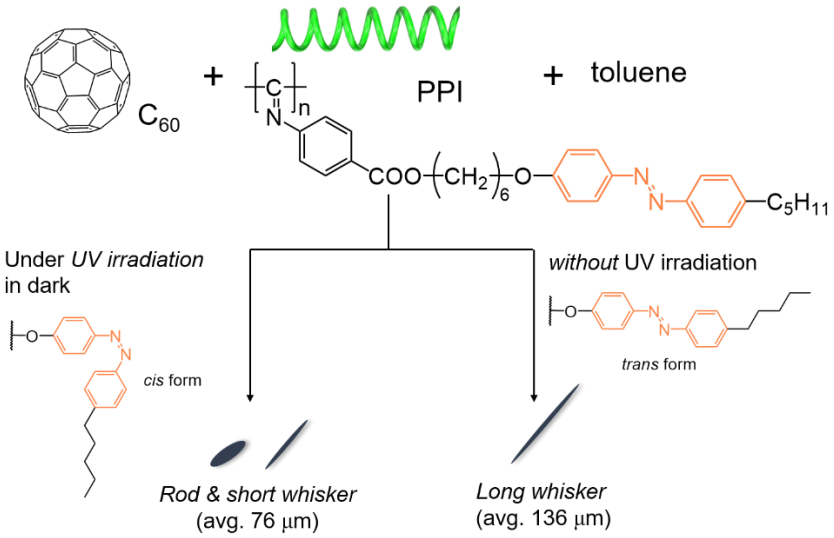

Figure 4.11. Azobenzene side chain effects for fullerene C_{60} 1D crystal assemblies. Under UV-irradiation, azobenzene unit isomerize into cis-form (photo stationary state).

Table 4.2. GPC results for PPI with azobenzene side chain (**poly14**).

Entry	Catalyst	Solvent	M_n[a](kDa)	M_w/M_n[a]	Yield[b]
Poly14	$NiCl_2 \cdot 6H_2O$	THF	216.1	2.31	>99%

a. Molecular weight and molecular distribution were estimated by GPC analysis calibrated by PS standard (eluent: THF, rt.). b. isolated yield. THF: tetrahydrofuran.

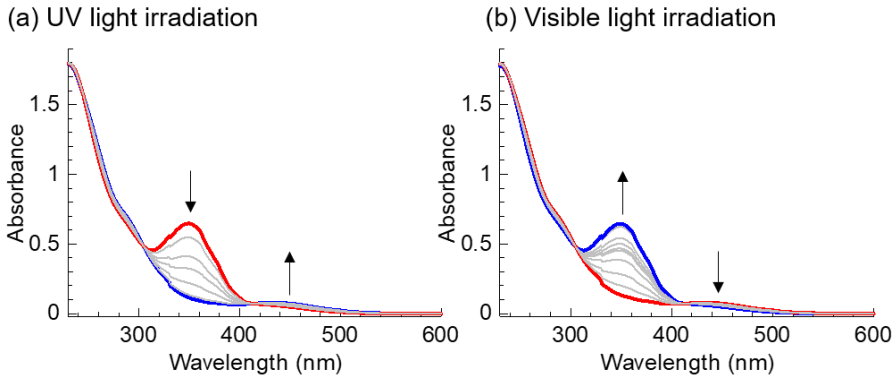

Figure 4.12. Absorption spectral change of *trans*- to *cis*-isomeriztion of **poly14** by UV irradiation in THF solution state (0.02 mg/mL).

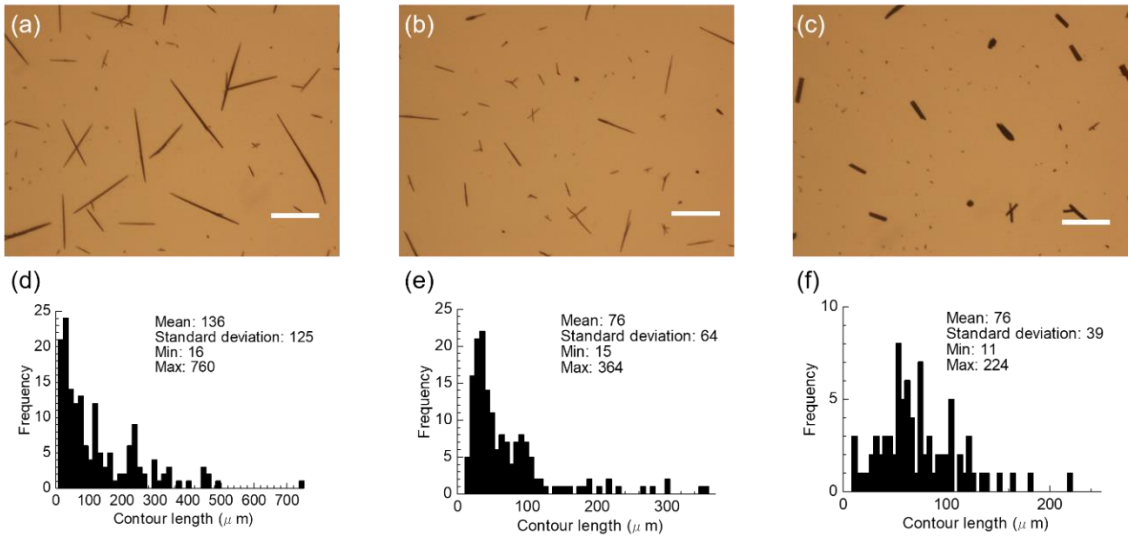

Figure 4.13. Optical microscopy images of C_{60}/**poly14** composite films. (a) under visible light and (b) under UV light conditions, and (c) pure C_{60} crystal from toluene solution under UV light.

4.10 Inorganic iron-oxide nanoparticle clusters into unidirectional assembly

We applied this methodology to inorganic nanoparticles anisotropic assembly. Superparamagnetic iron-oxide (Fe_3O_4) nanoparticle[71] (FeNP) (diameter ~10 nm in toluene containing oleic acid as stabilizer) was chosen in this system. Initially, we attempted to prepare the anisotropic assembly of FeNPs from FeNP/**poly12** binary system in toluene by drop-cast, however FeNPs did not form any crystallites as the FeNPs were well dispersed in **poly12** matrix. Fortunately, we found that FeNP/C_{60}/**poly12** ([FeNP] = [C_{60}] = [**poly12**] = 0.33 mg/mL) ternary system in toluene resulted in the formation of unidirectional FeNP cluster assemblies along the C_{60} fibers (**Figure 4.14a**), whereas pure FeNP toluene solution yielded island structures. Element mapping using SEM-EDX confirmed that ultralong C_{60} fibers are essentially composed of carbon atoms, and Fe atoms are preferentially distributed along the C_{60} fibers (**Figure 4.14b**). The magnified element mapping indicates that FeNPs form clusters or small crystallites near the C_{60} fibers, or FeNPs are embedded in the C_{60} fibers (**Figure 4.14c**). Interestingly in GIXRD measurement (**Figure 4.14d**), in addition to the peaks derived from Fe_3O_4[72], new peaks appeared in FeNP/C_{60}/**poly12** film at 26, 30, 43, 51, 53 degree, which were not seen in solution-dried FeNP film. These new peaks can not be indexed as other iron compound

such as Fe_2O_3, α-Fe, Fe_xC, or FeO, implying new FeNP·xC_{60} complex structures are formed in the fiber. The inset also demonstrates that C_{60} fibers form mixed phases of *fcc* and hexagonal[73] packing structure, which are not observed in the C_{60} fibers prepared from binary C_{60}/**poly12** toluene solution (*fcc* structure). To further investigate the magnetic and spin properties of unidirectionally assembly or embedded FeNP clusters, superconducting quantum interference device (SQUID) (**Figure 4.14g**) and electron spin resonance (ESR) (**Figure 4.14h**) measurements for FeNP/C_{60}/**poly12** film and solution-dried FeNP film were performed. The χ-value at 290 K, g-value, spin concentration, and peak-to-peak width (ΔH_{pp}) are summarized in **Table 4.3**. The χ-T curves for FeNP@C_{60}fiber/**poly12** film and FeNP film indicated the ferromagnetic behavior, where FeNP@C_{60}fiber/**poly12** showed enhanced magnetic susceptibility by 2.8 times compared to FeNP powder. The effects from diamagnetic species of C_{60} and **poly12** were negligible (10^{-7} – 10^{-6} emu/g). The ESR measurement for the spin property of Fe^{3+} *d*-orbital in the both samples clearly revealed the difference in g-value and ΔH_{pp}, suggesting different spin species and spin-spin interactions. As far as we know, this is the first report on the hybrid ultralong C_{60} fiber embedded with FeNPs. This methodology using the ternary system (FeNP/C_{60}/**poly12** in toluene) would be promising approach for production of organic/inorganic hybrid fibers with sub-micrometer diameters.

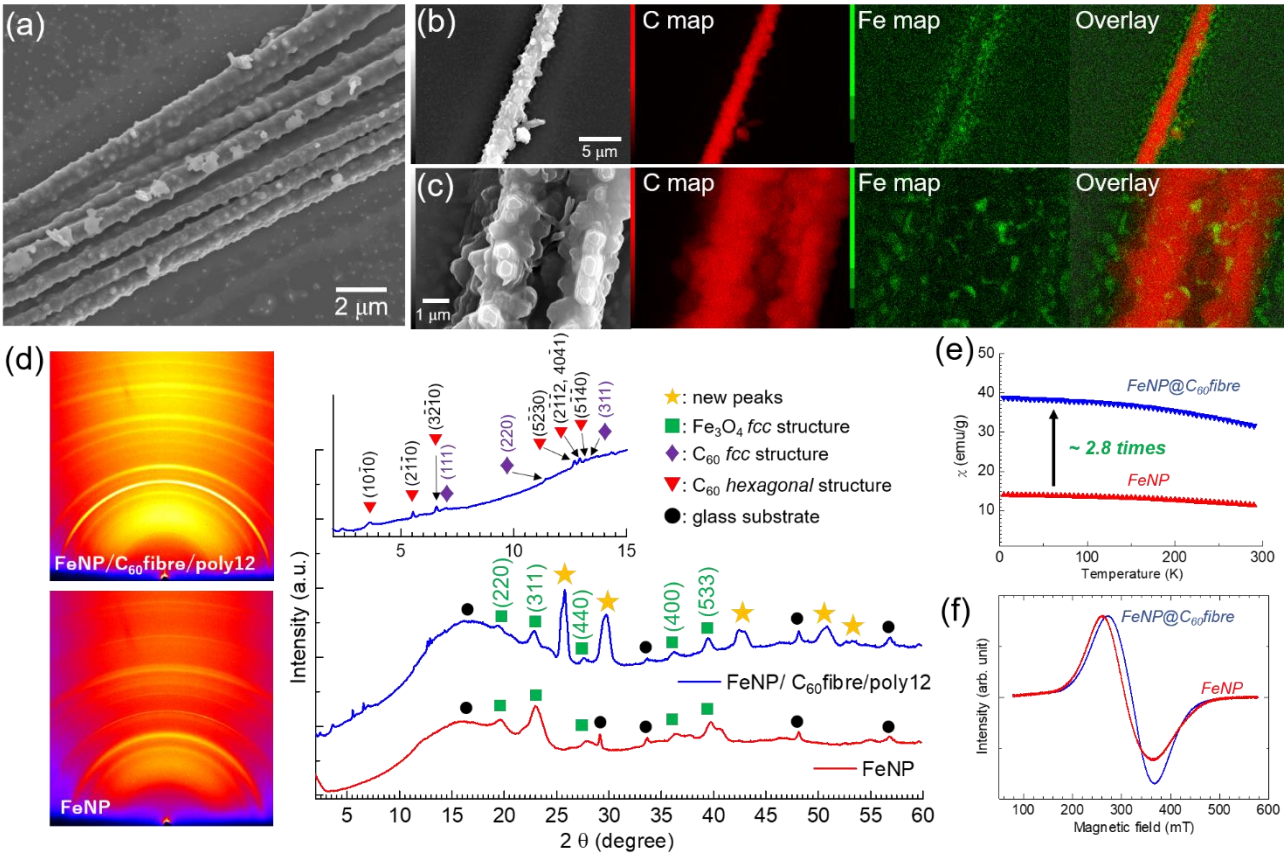

Figure 4.14. Anisotropic assembly of FeNP clusters along C_{60} fibers. (a) Schematic illustration of FeNP-coated C_{60} fibers prepared from FeNP/C_{60}/**poly12** ternary system in toluene. (b) SEM image of FeNP-coated C_{60} fiber. (c) SEM-EDX element mapping for FeNP-coated C_{60} fibers. (d) GIXRD measurements for FeNP/C_{60}/**poly12** film and solution-dried FeNP film (wavelength: λ 0.9965 Å). (e) SQUID measurements of FeNP magnetic behavior in 0.1 Tesla. χ-T curves for FeNP@C_{60}fiber/**poly12** (blue line) and for solution-dried FeNP (red line). (f) ESR measurements.

Table 4.3. SQUID and ESR measurements for magnetic properties of FeNP/C_{60}/**poly12** film and dried iron-oxide nanoparticles (FeNP) powders.

Entry	Constituents	χ (emu/g)[a]	g-value	Spin (/g)[b]	ΔH_{pp} (mT)
1	FeNP/C_{60}/poly12	31.6	2.05390	4.5×10^{24}	84
2	FeNP	11.3	2.14402	3.7×10^{24}	105

a. at 290 K. b. calibrated against $CuSO_4\cdot5H_2O$ powder.

4.11 Conclusion and perspective

In summary, we demonstrated versatile polymer additives, **PPIs**, are applicable to wide range of substances using C_{60}, organic building blocks, and Fe_3O_4 nanoparticles as model compounds. Using precisely synthesized **poly8**, we demonstrated the molecular weight of rod-shaped PPIs has a significant impact on the length of C_{60} 1D assemblies, suggesting the higher aspect-ratio of the 1D shape of PPI facilitates C_{60} crystal into 1D whiskers and fibers exceeding 1 mm with controlled mean length. Modification of side chains of PPIs allows for production of different 1D anisotropic assemblies of fullerene C_{60} such as rods, whiskers, and fibers. For efficient unidirectional crystallization through anisotropic geometric interactions, PPIs with non-branched relatively long alkyl side chains (**poly8-13**) and stiff PPIs with longer persistent length (**poly10,11**) are appropriate for extraordinary long whiskers and fibers. The resulting composite films can be applied to electronic textiles, sheet-type sensors, and electronic wiring with a controlled manner from bottom-up approach. This methodology was also applicable not only to small organic building blocks into 1D crystallization but also to anisotropic assembly of inorganic Fe_3O_4 nanoparticle clusters using the ternary system. The Fe_3O_4/C_{60} hybrid fibers has potential to be applied to magneto-optic ferromagnetic materials that exhibit large Faraday effects, and electrocatalytic materials that possess water-oxidation ability. We propose that the cooperative effect of highly anisotropic attractive depletion effect and interfacial capillary force, which are provided by the high-aspect-ratio rod-shaped PPI assemblies and meniscus-guided convections, is the key factor for the unidirectional assemblies of C_{60} crystals into ultralong whiskers, Fe_3O_4 nanoparticle into and organic/inorganic hybrid fibers consist of C_{60} crystals and Fe_3O_4 nanoparticle. The cluster formations might be facilitated by the addition of **PPIs**. We believe that this methodology can be combined with edge-casting method for a large-scale production, and that this concept also can be extended to other liquid crystalline rod-shaped polymers and biomacromolecules with long persistent length.

References

[1] Mann, S. et al. Crystallization at inorganic-organic interfaces: biominerals and biomimetic synthesis. *Science* **1993**, *261*, 1286-1292.
[2] Xu, A. W., Ma, Y., Cölfen, H. Biomimetic mineralization. *J. Mater. Chem.* **2007**, *17*, 415-449.
[3] Aizenberg, J. Crystallization in patterns: a bio‐inspired approach. *Adv. Mater.* **2004**, *16*, 1295-1302.
[4] Chang, Eric P., et al. Synergistic biomineralization phenomena created by a combinatorial nacre protein model system. *Biochemistry* **2016**, *55*, 2401-2410.
[5] Ge, J., Lei, J., Zare, R. N. Protein–inorganic hybrid nanoflowers. *Nat. Nanotech.* **2012**, *7*, 428.
[6] Natalio, Filipe, et al. Flexible minerals: self-assembled calcite spicules with extreme bending strength. *Science* **2013**, *339*, 1298-1302.
[7] Xu, A. W., Dong, W. F., Antonietti, M., Cölfen, H. Polymorph switching of calcium carbonate crystals by polymer‐controlled crystallization. *Adv. Funct. Mater.* **2008**, *18*, 1307-1313.
[8] Kato, T. et al. Effects of macromolecules on the crystallization of $CaCO_3$ the formation of organic/inorganic composites. *Supramol. Sci.* **1998**, *5*, 411-415.
[9] Neira-Carrillo, A., Vásquez-Quitral, P., Yazdani-Pedram, M., Arias, J. L. Crystal growth of $CaCO_3$ induced by monomethylitaconate

grafted polymethylsiloxane. *Eur. Polym. J.* **2010**, *46*, 1184-1193.
[10] Xu, A. W., Dong, W. F., Antonietti, M., Cölfen, H. Polymorph switching of calcium carbonate crystals by polymer‐controlled crystallization. *Adv. Funct. Mater.* **2008**, *18*, 1307-1313.
[11] Wang, T., Xu, A. W., Cölfen, H. Formation of Self‐Organized Dynamic Structure Patterns of Barium Carbonate Crystals in Polymer‐Controlled Crystallization. *Angew. Chem. Int. Ed*. **2006**, *45*, 4451-4455.
[12] Peng, Y., Xu, A. W., Deng, B., Antonietti, M., Cölfen, H. Polymer-controlled crystallization of zinc oxide hexagonal nanorings and disks. *J. Phys. Chem. B* **2006**, *110*, 2988-2993.
[13] Yu, S. H., Cölfen, H., Antonietti, M. Polymer-controlled morphosynthesis and mineralization of metal carbonate superstructures. *J. Phys. Chem. B* **2003**, *107*, 7396-7405.
[14] Ma, Y., et al. PY181 Pigment Microspheres of Nanoplates Synthesized via Polymer‐Induced Liquid Precursors. *Adv. Funct. Mater.* **2009**, *19*, 2095-2101.
[15] Huang, M., Schilde, U., Kumke, M., Antonietti, M., Cölfen, H. Polymer-induced self-assembly of small organic molecules into ultralong microbelts with electronic conductivity. *J. Am. Chem. Soc.* **2010**, *132*, 3700-3707.
[16] Huang, M., Antonietti, M., Cölfen, H. Morphology-controlled growth of perylene derivative induced by double-hydrophilic block copolymers. *APL Mater* **2016**, *4*, 015705.
[17] Huang, Y., et al. Direct Growth of Microspheres on Amorphous Precursor Domains in Polymer-Controlled Crystallization of Indomethacin. *Cryst. Growth Des.* **2016**, *16*, 1428-1434.
[18] Lang, M., Grzesiak, A. L., Matzger, A. J. The use of polymer heteronuclei for crystalline polymorph selection. *J. Am. Chem. Soc.* **2002**, *124*, 14834-14835.
[19] Zhang, C., et al. Supramolecular Gel‐Assisted Formation of Fullerene Nanorods. *Chem.- A Eur. J.* **2012**, *18*, 14954-14956.
[20] Lomas, C. R., Hodgkiss, J. M. Templated growth of fullerene C_{60} crystals by triptycene in polymer blend films. *Supramol. Chem.* **2012**, *24*, 526-531.
[21] Jenekhe, S. A., Chen, X. L. Self-assembled aggregates of rod-coil block copolymers and their solubilization and encapsulation of fullerenes. *Science* **1998**, *279*, 1903-1907.
[22] Zhang, X., Takeuchi, M. Controlled Fabrication of Fullerene C_{60} into Microspheres of Nanoplates through Porphyrin‐Polymer‐Assisted Self‐Assembly. *Angew. Chem. Int. Ed*. **2009**, *48*, 9646-9651.
[23] Nurmawati, M. H., Ajikumar, P. K., Renu, R., Sow, C. H., Valiyaveettil, S. Amphiphilic poly (p-phenylene)-driven multiscale assembly of fullerenes to nanowhiskers. *ACS nano* **2008**, *2*, 1429-1436.
[24] Nurmawati, M. H., Ajikumar, P. K., Heng, L. A., Li, H., Valiyaveettil, S. Cross-conjugated poly (p-phenylene) aided supramolecular self-organization of fullerene nanocrystallites. *Chem. Commun* **2008**, *0*, 4945-4947.
[25] Nawaz, M. H., Liu, J., Liu, F., Wang, X., Zhang, W. Synthesis of porphyrinic polystyrenes and their self-assembly with pristine fullerene (C_{60}). *Mater. Lett*. **2013**, *91*, 71-74.
[26] Su, Z., Yu, B., Jiang, X., Yin, J. Responsive Fluorescent Nanorods from Coassembly of Fullerene (C_{60}) and Anthracene-Ended Hyperbranched Poly (ether amine)(AN-hPEA). *Macromolecules* **2013**, *46*, 3699-3707.
[27] Lu, G., Li, L., Yang, X. Creating a uniform distribution of fullerene C_{60} nanorods in a polymer matrix and its photovoltaic applications. *Small* **2008**, *4*, 601-606.
[28] Li, H., et al. High-mobility field-effect transistors from large-area solution-grown aligned C_{60} single crystals. *J. Am. Chem. Soc.* **2012**, *134*, 2760-2765.
[29] Maeyoshi, Y., et al. Fullerene nanowires as a versatile platform for organic electronics. *Sci. Rep*. **2012**, *2*, 600.
[30] Wu, K. Y., Wu, T. Y., Chang, S. T., Hsu, C. S., Wang, C. L. A Facile PDMS‐Assisted Crystallization for the Crystal‐Engineering of C_{60} Single‐Crystal Organic Field‐Effect Transistors. *Adv. Mater.* **2015**, *27*, 4371-4376.
[31] Saran, R., Stolojan, V., Curry, R. J. Ultrahigh performance C_{60} nanorod large area flexible photoconductor devices via ultralow organic and inorganic photodoping. *Sci. Rep.* **2014**, *4*, 5041.
[32] Penterman, S. J., Singh, A., Zipfel, W. R., Liddell Watson, C. M. Anisometric colloidal fullerene rod and platelet solvates with enhanced photoluminescence. *Adv. Opt. Mater.* **2014**, *2*, 1024-1030.
[33] Nair, V. S., Mukhopadhyay, R. D., Saeki, A., Seki, S., Ajayaghosh, A. A π-gel scaffold for assembling fullerene to photoconducting supramolecular rods. *Science Advances* **2016**, *2*, e1600142.
[34] Wei, L., Lei, Y., Fu, H., Yao, J. Fullerene hollow microspheres prepared by bubble-templates as sensitive and selective electrocatalytic sensor for biomolecules. *ACS Appl. Mater. Interfaces* **2012**, *4*, 1594-1600.
[35] Wei, L., Yao, J., Fu, H. Solvent-assisted self-assembly of fullerene into single-crystal ultrathin microribbons as highly sensitive UV–visible photodetectors. *ACS nano* **2013**, *7*, 7573-7582.
[36] Krishnan, V., et al. Vortex-aligned fullerene nanowhiskers as a scaffold for orienting cell growth. *ACS Appl. Mater. Interfaces* **2015**, *7*, 15667-15673.
[37] Babu, S. S., Möhwald, H., Nakanishi, T. Recent progress in morphology control of supramolecular fullerene assemblies and its applications. *Chem. Soc. Rev*. **2010**, *39*, 4021-4035.
[38] Shrestha, L. K., et al. Fullerene nanoarchitectonics: from zero to higher dimensions. *Chem.–An Asian J.* **2013**, *8*, 1662-167.
[39] Geng, J., et al. Crystal structure and growth mechanism of unusually long fullerene (C_{60}) nanowires. *J. Am. Chem. Soc.* **2008**, *130*,

2527-2534.
[40] Park, C., Song, H. J., Choi, H. C. The critical effect of solvent geometry on the determination of fullerene (C_{60}) self-assembly into dot, wire and disk structures. *Chem. Commun.* **2009**, *0*, 4803-4805.
[41] Miyazawa, K. Synthesis of fullerene nanowhiskers using the liquid–liquid interfacial precipitation method and their mechanical, electrical and superconducting properties. *Sci. Technol. Adv. Mater.* **2015**, *16*, 013502.
[42] Sathish, M., Miyazawa, K. Size-tunable hexagonal fullerene (C_{60}) nanosheets at the liquid− liquid interface. *J. Am. Chem. Soc.* **2007**, *129*, 13816-13817.
[43] Sathish, M., Miyazawa, K., Sasaki, T. Nanoporous fullerene nanowhiskers. *Chem. Mater.* **2007**, *19*, 2398-2400.
[44] Shrestha, R. G., et al. Demonstration of ultrarapid interfacial formation of 1D fullerene nanorods with photovoltaic properties. *ACS Appl. Mater. Interfaces* **2014**, *6*, 15597-15603.
[45] Schwartz, E., Koepf, M., Kitto, H. J., Nolte, R. J., Rowan, A. E. Helical poly (isocyanides): past, present and future. *Poly. Chem.* **2011**, *2*, 33-47.
[46] Okoshi, K., Nagai, K., Kajitani, T., Sakurai, S., Yashima, E. Anomalous stiff backbones of helical poly (phenyl isocyanide) derivatives. *Macromolecules* **2008**, *41*, 7752-7754.
[47] Onouchi, H., et al. Two-and three-dimensional smectic ordering of single-handed helical polymers. *J. Am. Chem. Soc.* **2008**, *130*, 229-236.
[48] Strzelecka, T. E., Davidson, M. W., Rill, R. L. Multiple liquid crystal phases of DNA at high concentrations. *Nature* **1998**, *331*, 457.
[49] Giraud-Guille, M. M., Besseau, L., Chopin, C., Durand, P., Herbage, D. Structural aspects of fish skin collagen which forms ordered arrays via liquid crystalline states. *Biomaterials* **2000**, *21*, 899-906.
[50] Lee, B. Y., et al. Virus-based piezoelectric energy generation. N*at. Nanotech.* **2012**, *7*, 351.
[51] Wu, Z. Q., Ono, R. J., Chen, Z., Bielawski, C. W. Synthesis of poly (3-alkylthiophene)-block-poly (arylisocyanide): Two sequential, mechanistically distinct polymerizations using a single catalyst. *J. Am. Chem. Soc.* **2010**, *132*, 14000-14001.
[52] Yin, J., et al. A facile synthetic route to stereoregular helical poly (phenyl isocyanide) s with defined pendants and controlled helicity. *Poly. Chem.* **2017**, *8*, 545-556.
[53] Xue, Y. X., et al. Living polymerization of arylisocyanide initiated by the phenylethynyl palladium (II) complex. *Poly. Chem*. **2014**, *5*, 6435-6438.
[54] Rotstein, B. H., Winternheimer, D. J., Yin, L. M., Deber, C. M., Yudin, A. K. Thioester-isocyanides: versatile reagents for the synthesis of cycle–tail peptides. *Chem. Commun*. **2012**, *48*, 3775-3777.
[55] Nakanishi, T. Supramolecular soft and hard materials based on self-assembly algorithms of alkyl-conjugated fullerenes. *Chem. Commun*. **2010**, *46*, 3425-3436.
[56] Bairi, P. et al. Hierarchically structured fullerene C_{70} cube for sensing volatile aromatic solvent vapors. *ACS nano* **2016**, *10*, 6631-6637.
[57] Tong, H., et al. Protein detection and quantitation by tetraphenylethene-based fluorescent probes with aggregation-induced emission characteristics. *J. Phys. Chem. B* **2007**, *111*, 11817-11823.
[58] Stingelin-Stutzmann, N., et al. Organic thin-film electronics from vitreous solution-processed rubrene hypereutectics. *Nat. Mater.* **2005**, *4*, 601-606.
[59] Minari, T., et al. Molecular-packing-enhanced charge transport in organic field-effect transistors based on semiconducting porphyrin crystals. *Appl. Phys. Lett*. **2007**, *91*, 123501.
[60] Premila, M. et al. Pressure induced dimerisation of C_{70}. *Solid State Commun.* **1997**, *104*, 237-242.
[61] Henn, D. E., Williams, W. G., Gibbons, D. J. Crystallographic data for an orthorhombic form of rubrene. *J. Appl. Crystallogra.* **1971**, *4*, 256-256.
[62] Hoekstra, A., Vos, A. The crystal and molecular structures of tetraphenylhydrazine and related compounds at –160° C. II. The crystal structures of tetraphenylethylene (TPE) and diphenylaminotriphenylmethane (DTM). *Act. Crystallogr. Sec. B* **1975**, *31*, 1716-1721.
[63] Silvers, S. J., Tulinsky, A. The crystal and molecular structure of triclinic tetraphenylporphyrin. *J. Am. Chem. Soc.* **1967**, *89*, 3331-3337.
[64] Adams, M., Dogic, Z., Keller, S. L., Fraden, S. Entropically driven microphase transitions in mixtures of colloidal rods and spheres. *Nature* **1998**, *393*, 349.
[65] van der Schoot, P. Depletion interactions in lyotropic nematics. *J. Chem. Phys*. **2000**, *112*, 9132-9138.
[66] Gu, X., Shaw, L., Gu, K., Toney, M. F., Bao, Z. The meniscus-guided deposition of semiconducting polymers. *Nat. Commun*. **2018**, *9*, 534.
[67] Sun, Y. P., Ma, B., Bunker, C. E., Liu, B. All-carbon polymers (polyfullerenes) from photochemical reactions of fullerene clusters in room-temperature solvent mixtures. *J. Am. Chem. Soc.* **1995**, *117*, 12705-12711.
[68] Dattani, R., et al. Conformation and interactions of polystyrene and fullerenes in dilute to semidilute solutions. *Macromolecules* **2014**, *47*, 6113-6120.
[69] Koda, T., Numajiri, M., Ikeda, S. Smectic-A phase of a bidisperse system of parallel hard rods and hard spheres. *J. Phys. Soc. Japan* **1996**, *65*, 3551-3556.
[70] Tanaka, T., Kato, I., Okoshi, K. Nano-Segregation of Squalane between Smectic Layers of Rigid-Rod Polysilane. *e-J. Surf. Sci.*

Nanotech. **2015**, *13*, 121-124.
[71] Laurent, S., et al. Magnetic iron oxide nanoparticles: synthesis, stabilization, vectorization, physicochemical characterizations, and biological applications. *Chem. Rev.*, **2008**, *108*, 2064-2110.
[72] Lin, Y. L. et al. Facile synthesis of optically active and magnetic nanoparticles carrying helical poly (phenyl isocyanide) arms and their application in enantioselective crystallization. *Macromol. Rapid Commun*., **2018**, *39*, 1700685.
[73] Minato, J. I., Miyazawa, K. I. Solvated structure of C_{60} nanowhiskers. *Carbon*, **2005**, *43*, 2837-2841.

Experimental

Procedure for formylation reaction

To the oven-dried three neck flask were added 4-aminobenzoic acid (15.00 g, 109 mmol) and formic acid (50 mL). The solution was heated up to 55 °C. Then, acetic anhydride (40 mL) was added dropwise via syringe, and the reaction mixture was stirred for 30 min at 55 °C and for another 3 h at room temperature. The solvent was evaporated under reduced pressure. The obtained solid was suspended in diethylether overnight to remove the residual acid. The suspension was filtered to afford white solid (17.75 g, 98%). This product was used in the subsequent reactions without further purification.

Procedure for condensation and dehydration reactions

Typical procedure as follows. To the flask were added 4-formamidobenzoic acid (5.01 g, 30.2 mmol) in DMF (50 mL), HOBt·H_2O (4.63 g, 30.2 mmol), EDC·HCl (5.80 g, 30.2 mmol), TEA (4.2 mL, 30.2 mmol), and 3,7-dimethyl-1-octanol (11.51 g, 72.7 mmol). The reaction mixture was stirred at room temperature 17 h. The mixture was extracted with ethyl acetate, and washed with Na_2CO_3aq, $NaHCO_3$aq, water, and brine. The combined organic phase was dried over $MgSO_4$. The crude product was purified by column chromatography (hexane/ethyl acetate = 4/1 - 3/2 (v/v)) and subsequent vacuum drying to afford very viscous colorless oil (7.11 g, 77%). To the oven-dried two neck flask were added (3,7-dimethyloctyl)-4-formamidobenzoate (2.95 g, 6.0 mmol), DCM (20 mL), and TEA (3.4 mL, 15 mmol) under Ar gas atmosphere. The mixture was cooled to 0 °C in the ice bath. Then $POCl_3$ (0.87 mL, 6.0 mmol) was added dropwise over 10 min. The reaction mixture was stirred at 0 °C for 2.5 h. The reaction was quenched by addition of Na_2CO_3aq at 0 °C and vigorously stirred for 1 h. The mixture was washed with Na_2CO_3aq, $NaHCO_3$aq, water, and brine three times, respectively. The organic phase was dried over Na_2SO_4. The crude product was purified by column chromatography (hexane/ethyl acetate = 4/1 (v/v)) to afford pale yellow-green oil (1.53 g, 55%).

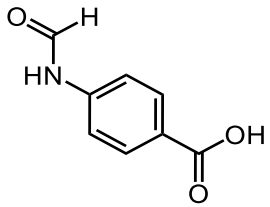

4-Formamidobenzoic acid; White solid (Yield: 98%). This product was synthesized according to the literature[2] with a little modification. The structure was confirmed by matching its spectroscopic data with corresponding reported data[2]. ^{1}H NMR (400 MHz, DMSO-d_6, δ from TMS): δ 10.52 (s, 0.9H) 10.44 (d, 0.4H, J = 10.4 Hz), 8.96 (d, 0.3H, J = 10.8 Hz), 8.34 (d, 0.9H, J = 2.0 Hz), 7.92 – 7.87 (2.6H), 7.69 (d, 2H), 7.30 (d, 0.7H, J = 8.0 Hz). ^{13}C NMR (100 MHz, DMSO-d_6, δ from TMS): δ 160.00, 142.02, 130.82, 130.41, 118.41, 116.26, 99.37.

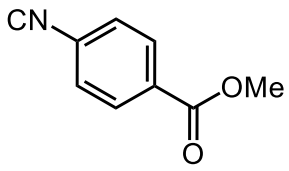

Methyl-4-isocyanobenzoate (1); Yellow solid. The structure was confirmed by matching its spectroscopic data with corresponding reported data[3]. ^{1}H NMR (400 MHz, $CDCl_3$, δ from TMS): δ 8.09 (d, 2H, J = 8.8 Hz), 7.45 (d, 2H, J = 8.8 Hz), 3.94 (s, 3H).

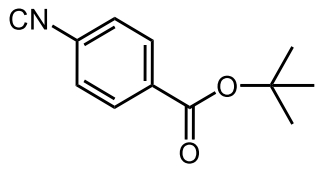

tert-Butyl-4-isocyanobenzoate (2); White crystal (Yield: 36% in 2 steps). This product was synthesized from tert-butyl-4-aminobenzoate. The structure was confirmed by matching its spectroscopic data with corresponding reported data[4]. ^{1}H NMR (400 MHz, $CDCl_3$, δ from TMS): δ 8.02 (dd, 2H, *J* = 6.8 Hz), 7.42 (dd, 2H, *J* = 6.8 Hz), 1.60 (s, 9H).

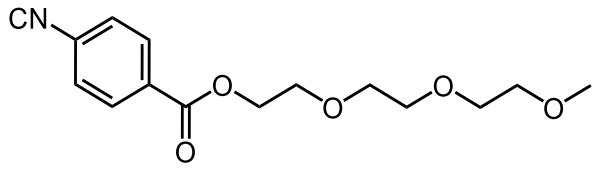

(Triethylene glycol monomethyl)-4-isocyanobenzoate (3); Yellow liquid (Yield: 9% in 2 steps). The structure was confirmed by matching its spectroscopic data with corresponding reported data[5]. ^{1}H NMR (400 MHz, $CDCl_3$, δ from TMS): δ 8.11 (dd, 2H, *J* = 6.8 Hz), 7.45 (d, 2H, *J* = 8.8 Hz), 4.49 (t, 2H, *J* = 4.8 Hz), 3.84 (t, 2H, *J* = 4.8 Hz), 3.73-3.64 (m, 6H), 3.55-3.53 (m, 2H), 3.37 (s, 3H).

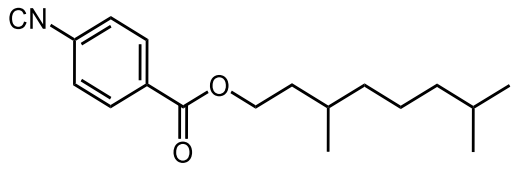

(3,7-Dimethyloctyl)-4-isocyanobenzoate (4); Yellow-green liquid (Yield: 42% in 2 steps). ^{1}H NMR (400 MHz, $CDCl_3$, δ from TMS): δ 8.08 (dd, 2H, *J* = 6.8 Hz), 7.44 (dd, 2H, *J* = 6.8 Hz), 4.40-4.36 (m, 2H), 1.82-1.80 (m, 1H), 1.62-1.51 (m, 3H), 1.35-1.31 (m, 3H), 1.19-1.14 (m, 3H), 0.96 (d, 3H, *J* = 6.4 Hz), 0.87 (d, 6H, *J* = 6.4 Hz). ^{13}C NMR (100 MHz, $CDCl_3$, δ from TMS): δ 166.96, 164.94, 131.22, 130.70, 126.32, 64.12, 39.08, 37.01, 35.38, 29.86, 27.85, 27.84, 24.52, 22.60, 22.50, 19.51. FT-IR (KBr, cm^{-1}): 2121 ($\nu_{C\equiv N}$), 1725 ($\nu_{C=O}$).

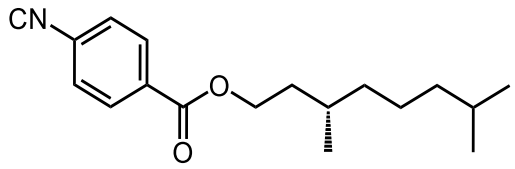

((3S)-3,7-Dimethyloctyl)-4-isocyanobenzoate (5); Yellow-green liquid (Yield: 42% in 2 steps). ^{1}H NMR (400 MHz, $CDCl_3$, δ from TMS): δ 8.08 (dt, 2H, *J* = 8.4 Hz), 7.44 (dd, 2H, *J* = 6.8 Hz), 4.40-4.35 (m, 2H), 1.80 (m, 1H), 1.61-1.49 (m, 3H), 1.35-1.25 (m, 3H), 1.19-1.12 (m, 3H), 0.96 (d, 3H, *J* = 6.8 Hz), 0.87 (d, 6H, *J* = 6.4 Hz). ^{13}C NMR (100 MHz, $CDCl_3$, δ from TMS): δ 168.96, 165.04, 131.31, 130.78, 126.41, 64.21, 39.16, 37.09, 35.46, 29.95, 27.93, 24.60, 22.65, 22.57, 19.57.

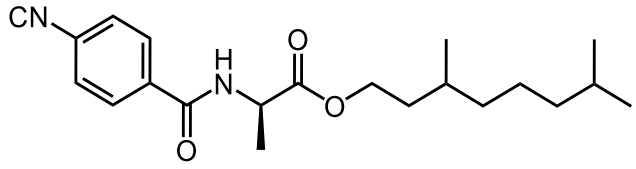

(L-alanine-based-3,7-dimethyloctylester)-4-isocyanobenzamine (6); Yellow solid (Yield: 25% in 2 steps). ^{1}H NMR (400 MHz, $CDCl_3$, δ from TMS): δ 7.85 (d, 2H, *J* = 8.8 Hz), 7.45 (d, 2H, *J* = 8.8 Hz), 6.87 (d (broad), 1H, *J* = 7.2 Hz), 7.85 (quint., 1H, *J* = 7.2 Hz), 4.26-4.21 (m, 2H), 1.76-1.70 (m, 2H), 1.56-1.46 (m, 6H), 1.32-1.22 (m, 3H), 1.18-1.11 (m, 3H), 0.91 (d, 3H, *J* = 6.0 Hz), 0.87 (d, 6H, *J* = 7.2 Hz). ^{13}C NMR (100 MHz, $CDCl_3$, δ from TMS): δ 204.97,

173.13, 134.69, 128.34, 126.58, 64.41, 54.63, 48.72, 48.70, 39.11, 37.06, 36.99, 35.35, 30.26, 29.75, 29.72, 27.90, 24.58, 22.64, 22.55, 19.40, 18.55.

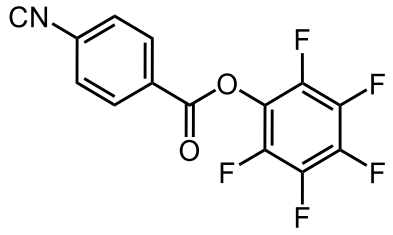

Pentafluorophenyl-4-isocyanobenzoate (7); Yellow solid (Yield: 41% in 2 steps). The structure was confirmed by matching its spectroscopic data with corresponding reported data[6]. ^{1}H NMR (400 MHz, $CDCl_3$, δ from TMS): δ 8.26 (d, 2H, *J* = 8.8 Hz), 7.57 (d, 2H, *J* = 8.8 Hz).

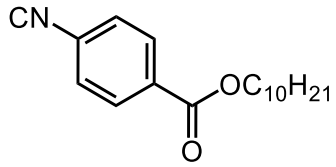

Decyl-4-isocyanobenzoate (8); Pale-yellow solid (Yield: 17% in 2 steps). The structure was confirmed by matching its spectroscopic data with corresponding reported data[7]. ^{1}H NMR (400 MHz, $CDCl_3$, δ from TMS): δ 8.08 (dt, 2H), 7.45 (dt, 2H), 4.33 (t, 2H, *J* = 6.4 Hz), 1.77 (quint., 2H, *J* = 7.2 Hz), 1.45-1.28 (m, 14H), 0.88 (t, 3H, *J* = 6.8 Hz).

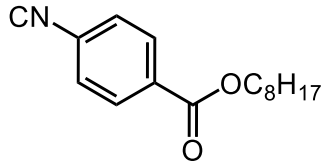

Octyl-4-isocyanobenzoate (9); This product was synthesized in our previous report[8], and the same sample was used in this study.

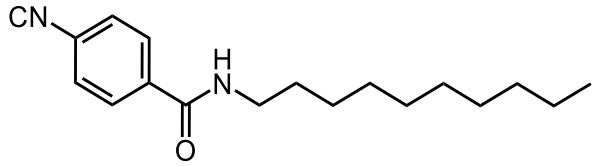

N-decyl-4-isocyanobenzamine (10); White crystal (Yield: 10% in 2 steps). ^{1}H NMR (400 MHz, $CDCl_3$, δ from TMS): δ 7.80 (d, 2H, *J* = 8.0 Hz), 7.44 (d, 2H, *J* = 8.0 Hz), 6.18 (broad, 1H), 3.44 (quart., 2H, *J* = 6.8 Hz), 1.61 (quint., 2H, *J* = 7.6 Hz), 1.35-1.26 (m, 14H), 0.88 (t, 3H, *J* = 6.8 Hz). ^{13}C NMR (100 MHz, $CDCl_3$, δ from TMS): δ 216.38, 172.74, 165.70, 135.64, 128.13, 126.57, 40.30, 31.84, 29.54, 29.50, 29.26, 26.95, 22.64, 14.09.

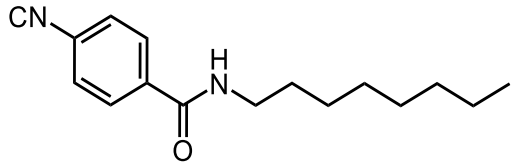

N-octyl-4-isocyanobenzamine (11); White crystal (Yield: 8% in 2 steps). ^{1}H NMR (400 MHz, $CDCl_3$, δ from TMS): δ 7.80 (d, 2H, *J* = 8.8 Hz), 7.45 (d, 2H, *J* = 8.8 Hz), 6.08 (broad, 1H), 3.46 (quint., 2H, *J* = 6.0 Hz), 1.62 (quint., 2H, *J* = 6.8 Hz), 1.38-1.27 (m, 10H), 0.88 (t, 3H, *J* = 6.8 Hz). ^{13}C NMR (100 MHz, $CDCl_3$, δ from TMS): δ 209.37, 186.68, 165.70, 135.66, 128.12, 126.62, 40.32, 31.77, 29.57, 29.24, 29.18, 26.96, 22.62, 14.08.

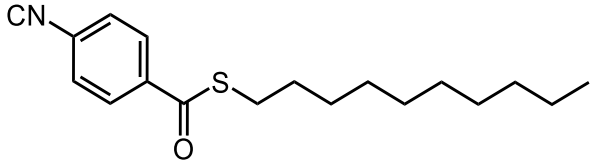

4-Isocyanobenzoic acid decyl thioester (12); Yellow solid (Yield: 18% in 2 steps). ^{1}H NMR (400 MHz, $CDCl_3$, δ from TMS): δ 8.00 (dt, 2H), 7.46 (dt, 2H), 3.09 (t, 2H, *J* = 7.2 Hz), 1.67 (quint., 2H, *J* = 7.6 Hz), 1.46 - 1.38 (m, 2H), 1.34 - 1.26 (m, 12H), 0.88 (t, 3H, *J* = 7.2 Hz). ^{13}C NMR (100 MHz, $CDCl_3$, δ from TMS): δ 190.58, 182.03, 162.88, 137.58, 128.38, 126.65, 93.07, 84.40, 31.86, 29.52, 29.46, 29.40, 29.36, 29.28, 29.11, 28.89, 22.66, 14.11, 8.13. FT-IR (KBr, cm^{-1}): 2138 and 2123 ($\nu_{C\equiv N}$), 1658 ($\nu_{C=O}$).

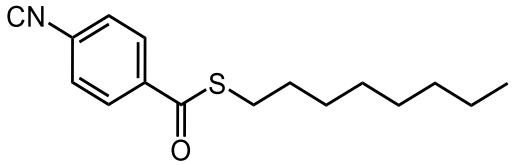

4-Isocyanobenzoic acid octyl thioester (13); Yellow solid (Yield: 18% in 2 steps). This compound was synthesized by the same procedure as compound 12. ^{1}H NMR (400 MHz, $CDCl_3$, δ from TMS): δ 8.00 (dt, 2H, *J* = 8.4 Hz), 7.45 (dt, 2H, *J* = 8.8 Hz), 3.09 (t, 2H, *J* = 7.6 Hz), 1.68 (quint., 2H, *J* = 7.2 Hz), 1.58-1.39 (m, 2H), 1.36-1.28 (m, 8H), 0.88 (t, 3H, *J* = 6.8 Hz),. ^{13}C NMR (100 MHz, $CDCl_3$, δ from TMS): δ 209.66, 190.53, 137.58, 135.11, 128.36, 126.63, 31.75, 29.38, 29.35, 29.11, 29.05, 28.87, 22.60, 14.05.

Polymerization

Pd complex initiated living polymerization for controlled molecular weight, narrowly dispersed ***poly8 (entry 15-27)***

Into an oven-dried three neck flask was added decyl-4-isocyanobenzoate (288 mg, 1.0 mmol) in THF (9.5 mL) under Ar gas atmosphere. The solution was heated up to 55 °C, and then 4-methoxy-phenylethynyl Pd complex (2.65 mg, 0.0052 mmol) in THF (0.5 mL) was added to the solution to initiate the living polymerization. The reaction mixture was stirred at 55 °C. During the polymerization, the aliquots (0.1-0.5 mL) were taken from the reaction mixture at different time periods (20 min, 40 min, 1h, 1.5 h, 2 h, 2.5 h, 4 h, 5.5 h, 6.5 h, 7.5 h, 8 h, 9 h, 9.5 h) to monitor the progress of the living polymerization (Figure S1). Each aliquot was quenched with methanol to yield yellow precipitates. The precipitated polymers were collected by centrifugation (15000 rpm, 20 min) and washed with methanol 3 times. The collected polymers were dried under vacuum to afford controlled molecular weight, narrowly dispersed **poly8**.

$NiCl_2{\cdot}6H_2O$ catalyzed polymerization of isocyanide for PPIs

Typical procedure is as follows: Into an oven-dried Schlenk flask was added isocyanide monomer solution in THF or in DCM 3 mL (0.1 M) under Ar gas atmosphere. Then, $NiCl_2{\cdot}6H_2O$ (0.02 equiv.) in ethanol (0.01 M) was added. The reaction mixture was stirred at room temperature for 1-3 days, where the solution turned into viscous orange from pale yellow. The reaction was quenched with methanol to yield yellow fiber-like precipitates. The precipitated PPIs were collected by centrifugation (3000 rpm, 10 min) and washed with methanol 3 times. The collected PPIs were dried under vacuum.

$NiCl_2$ catalyzed polymerization of isocyanide for PPIs

Typical procedure is as follows: Into an oven-dried Schlenk flask was added isocyanide monomer solution in DCM 3 mL (0.1 M) under Ar gas atmosphere. Then, $NiCl_2$ (0.02 equiv.) solid was added and dispersed. The reaction mixture was stirred at room temperature for 3 days, where the solution turned into viscous orange from pale yellow. The reaction was quenched with methanol to yield yellow fiber-like precipitates. The precipitated PPIs were collected by centrifugation (3000 rpm, 10 min) and washed with methanol 3 times. The collected PPIs were dried under vacuum.

References

[1] Xue, Y. X.; Chen, J. L.; Jiang, Z. Q.; Yu, Z.; Liu, N.; Yin, J.; Zhu, Y. Y.; Wu, Z. Q. *Poly. Chem.* **2014**, 5, 6435.
[2] Xu, A.; Hu, G.; Hu, Y.; Zhang, X.; Liu, K.; Kuang, G.; Zhang, A. *Chem.–An Asian J.* **2013**, 8, 2003.
[5] Kamijo, S.; Jin, T.; Yamamoto, Y. *J. Am. Chem. Soc.* **2001**, 123, 9453.
[4] Yamada, T., Suginome, M. *Macromolecules*, **2010**, 43, 3999-4002.
[5] Yu, Z. P., Liu, N., Yang, L., Jiang, Z. Q., Wu, Z. Q. *Macromolecules*, **2017**, 50, 3204-3214.
[6] Su, M.; Liu, N.; Wang, Q.; Wang, H.; Yin, J.; Wu, Z. Q. *Macromolecules* **2015**, 49, 110.
[7] Wu, Z. Q.; Ono, R. J.; Chen, Z.; Bielawski, C. W. *J. Am. Chem. Soc.* **2010**, 132, 14000.
[8] Hayashi, H.; Iseki, T.; Nimori, S.; Goto, H. *Sci. Rep.* **2017**, 7, 3948.

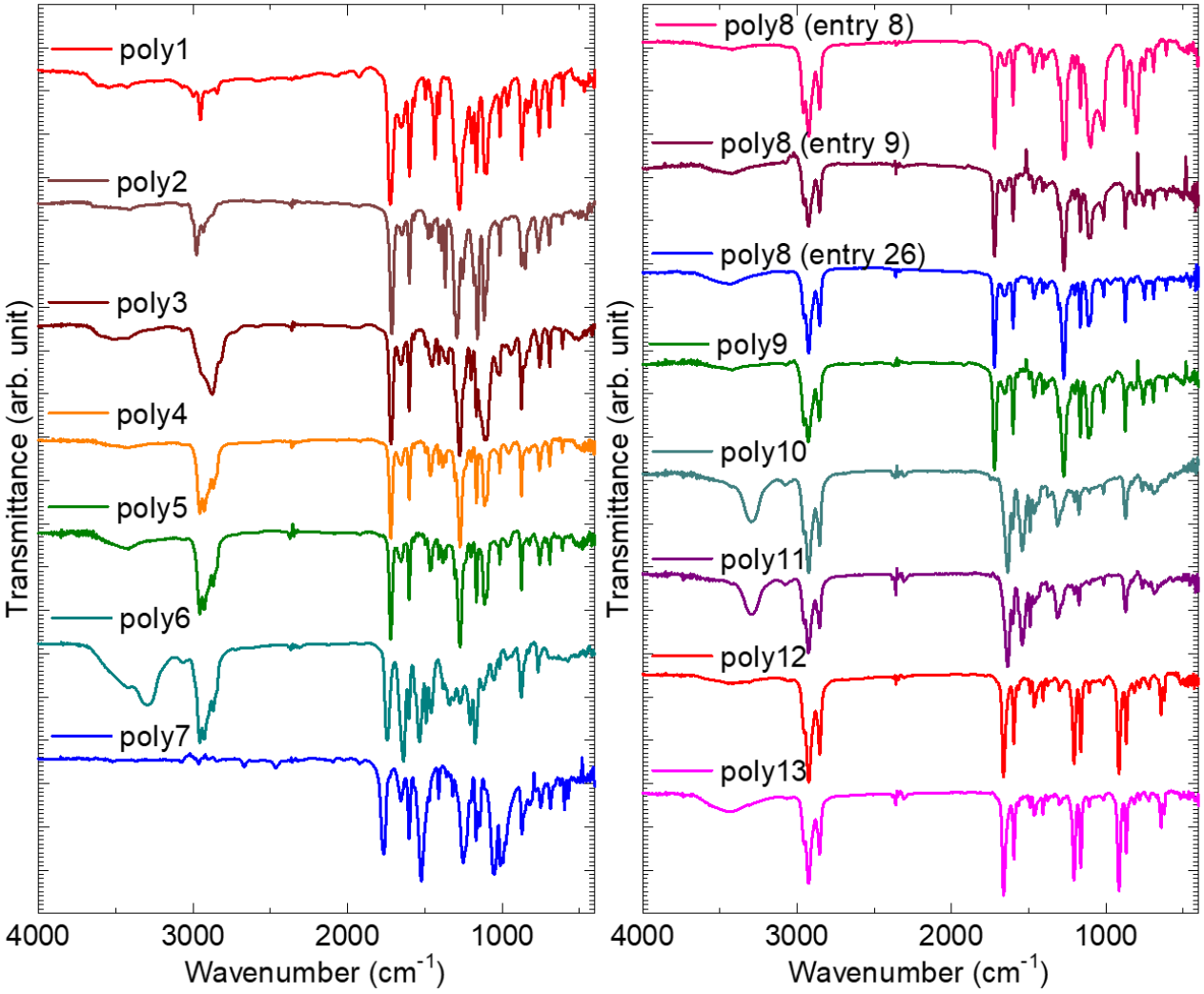

Figure 4-S1. FT-IR spectra of **poly1-7**, **poly8** (**entry 8** (prepared by $NiCl_2 \cdot 6H_2O$), **entry 9** (prepared by $NiCl_2$), **entry 26** (prepared by Pd complex, M_n = 29.9 (kDa), M_w/M_n = 1.10), and **poly9-13.**

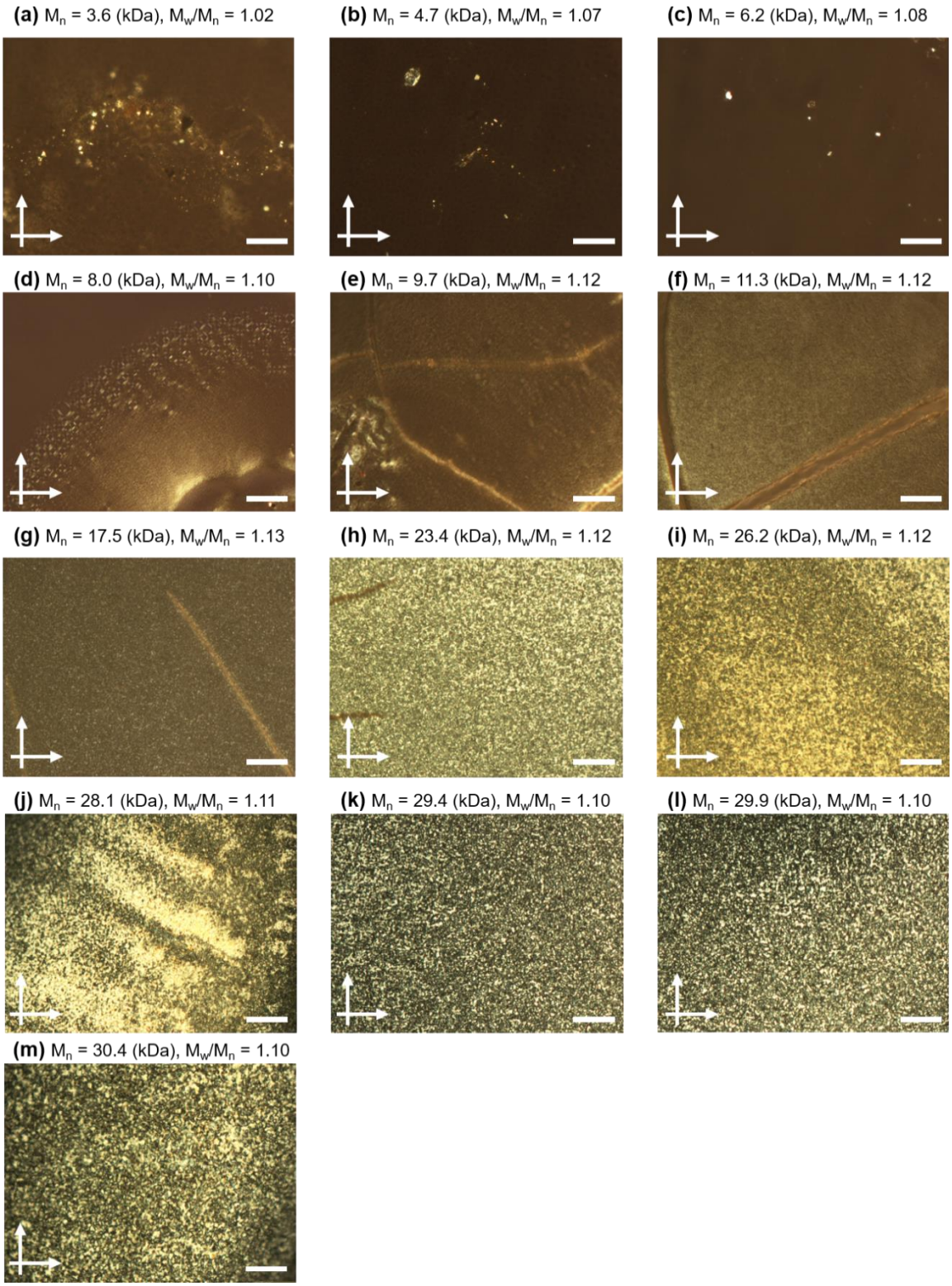

Figure 4-S2. POM images of well-defined, controlled molecular weight, narrowly dispersed **poly8 (entry 15-27)** with different molecular weight (M_n = 3.6 - 30.4 (kDa), M_w/M_n < 1.13) films without fullerene C_{60} prepared from the corresponding toluene solution. The films were observed without annealing treatment. Scale bars, 20 μm.

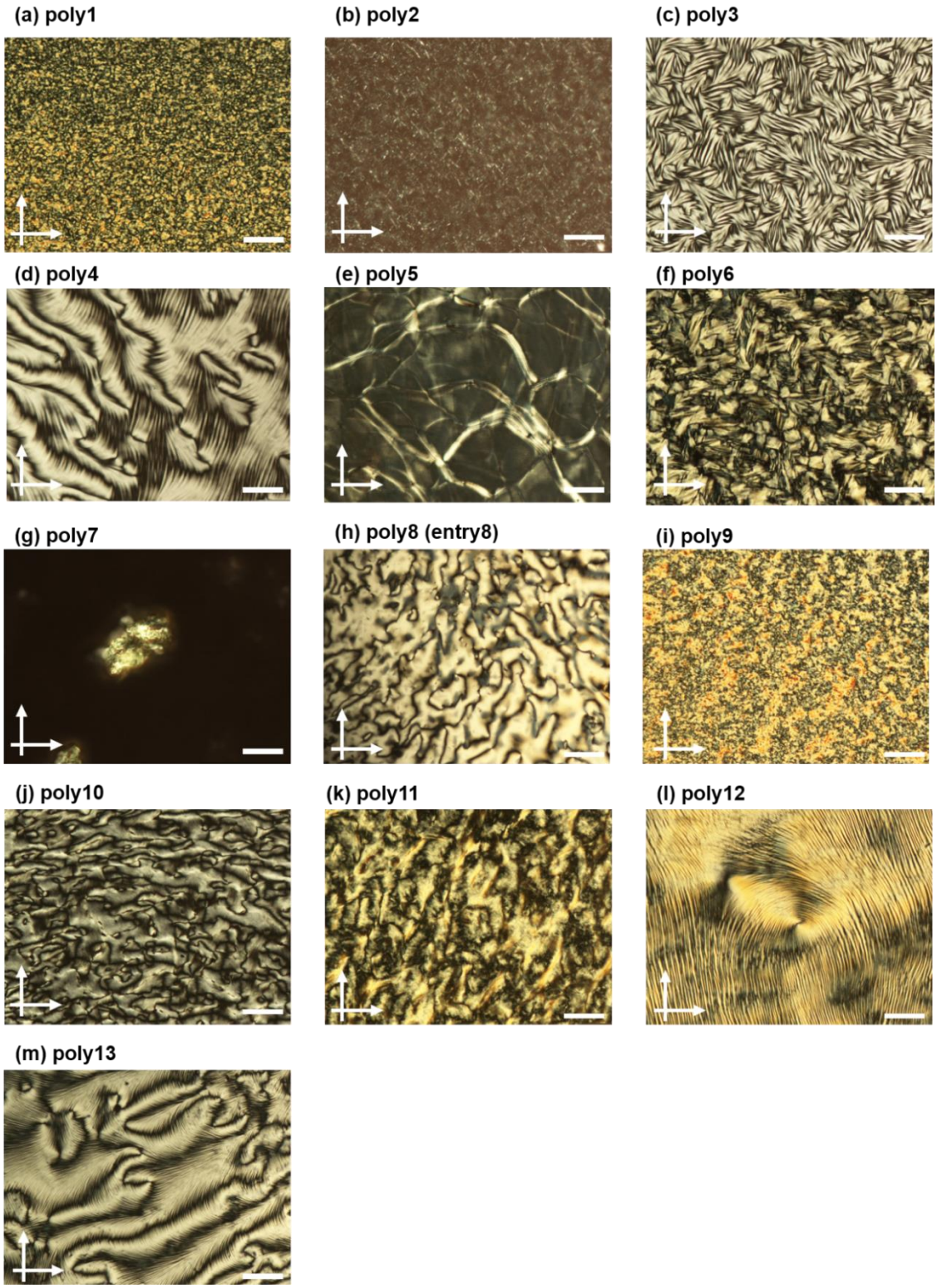

Figure 4-S3. POM images of **PPI** films without fullerene C_{60} prepared from the corresponding toluene solution (for **poly1,2,3,5,6**) or 1,1,2,2-tetrachloroethane (for **poly4**). The films were observed after THF vapor annealing treatment. **Poly7** did not form uniform film but particles that exhibits birefringence. Scale bars, 20 μm.

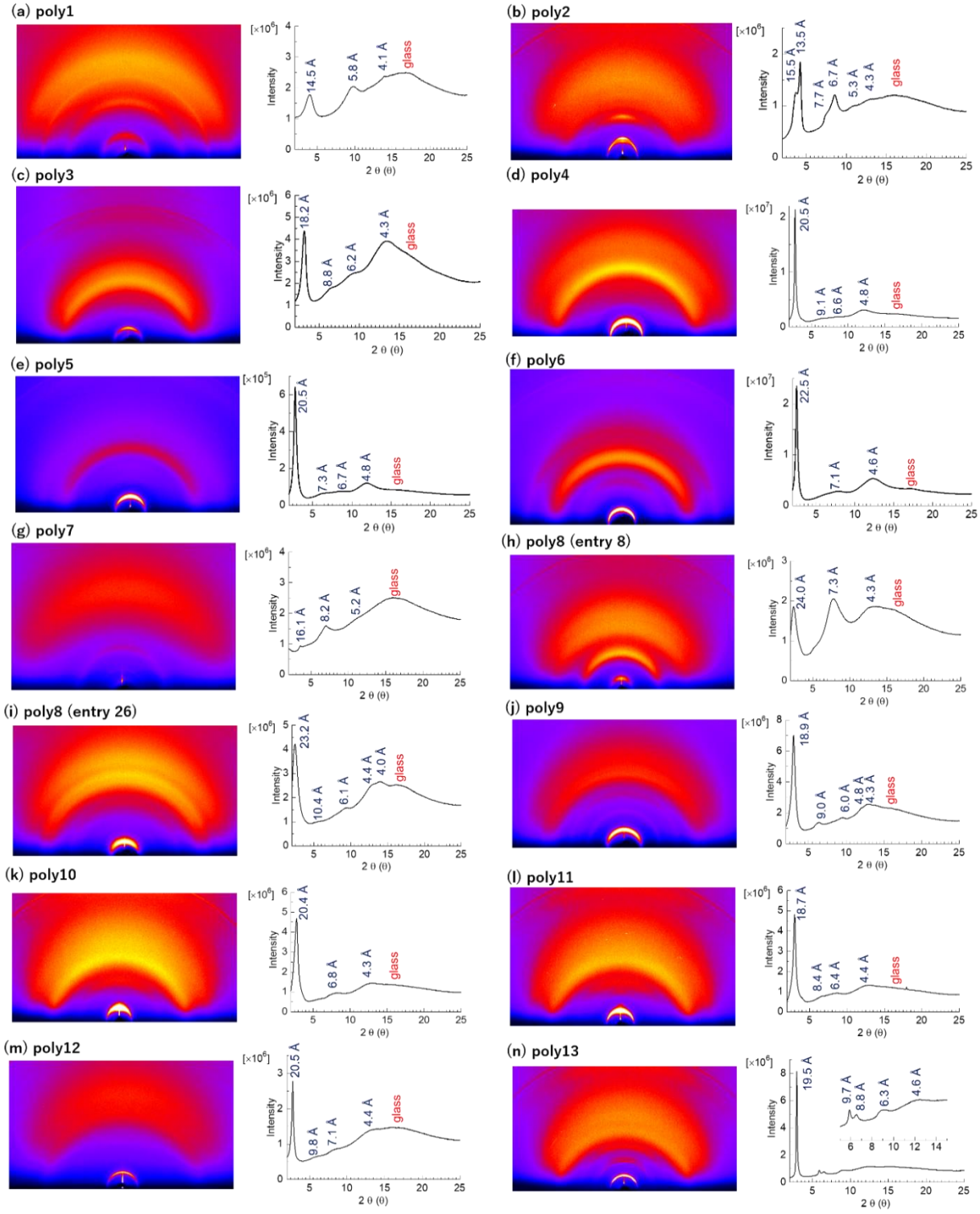

Figure 4-S4. GIXRD profiles for the drop-cast **PPI** films (**poly1,2,3,4,5,6**). **Poly1,2,3,5,6** films were prepared from the corresponding THF solutions, while **poly4** film was prepared from the corresponding chloroform solution. **poly1** was synthesized by Pd complex (M_n = 29.9 (kDa), M_w/M_n = 1.10). The broad halo at 2θ~16° is due to the amorphous diffraction of the glass substrate.

Chapter 5: Toward helix-sense-selective living polymerization in cholesteric liquid crystalline medium for highly stereoregular helical poly(phenyl isocyanide)s

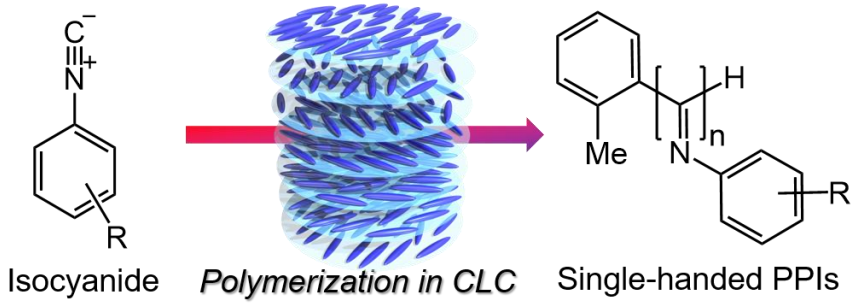

5.1 Abstract

Enzymes and ribosomes possess vital roles of production of chiral biopolymers with accurately-controlled molecular weight and helical senses utilizing an asymmetric environment within living cell in condensed state. Here we show living polymerization in living cell-inspired liquid crystal solvent for single-handed helical poly(phenyl isocyanide)s with high stereoregularity. We successfully synthesized controlled molecular weight, preferencially single-handed helical PPIs with narrow polydispersity (M_w/M_n ~ 1.1) in moderate yield in CLC medium at ambient condition. The as-prepared PPI exhibits positive signal around 365 nm in circular dichroism (CD) spectrum derived from helical arrangement of imino moiety (n-π* transition). The CD result indicates that PPI prepared in CLC form preferentially single-handed helical backbones. As far as we know, this is the first report on helix-sense-selective living polymerization in CLC medium.

5.2 Introduction

In living cells of our body, there exist various kinds of biomolecules, such as proteins, nucleic acids and complex sugars in very condensed state (up to 400 grams per litre). The efficiency of biochemical reactions and folding behavior of proteins confined in cells are much different from those in dilute solution conditions, which is called "macromolecular crowding" effect[1]. This condensed aqueous solution is confined by the cell wall composed of lipid bilayer with the liquid-crystalline like lamellae structure. In such condensed phase, enzymes and ribosome possess vital roles of production of chiral biopolymers with accurately-controlled molecular weight and helical senses utilizing an asymmetric environment. Here mesophase, in other word liquid crystal, has close relationship with biological functions. Very recently, it is revealed that nematic liquid crystal-like topological defects are seen epithelia, and they have crucial role in cell death and extrusion[2,3]. Other liquid crystalline assemblies are also seen in brain, muscle and other biological systems.

From organic chemistry viewpoint, there have been substantial interests in the development of chiral selective syntheses for enantiopure compounds. In general, organic polymer syntheses including asymmetric syntheses are usually implemented in dilute solution condition[4,5], where solute-solvent molecular interaction is low and usually

only the polarity of solvent is taken into consideration. Herein we envision that asymmetric polymerization in condensed environment like cholesteric liquid crystal as chiral reaction field allows for syntheses of chiral polymers from achiral monomers through the pronounced geometrical interaction in condensed state, which may provide new insight into the biochemical reactions in living cells.

Herein we focused on synthesis of poly(phenyl isocyanide) (PPI) by helix-sense-selective polymerization in cholesteric liquid crystal. Polyisocyanide is one of the synthetic helical polymers with main chain helicity[6,7]. If PPI possesses sufficiently bulky substituents, the backbone forms helical structure by the steric effects from the substituents. For the synthesis of chiral PPI, usually chiral monomers[8,9], chiral catalysts[10], or chiral additives[11] are required to construct preferentially single-handed PPI. On the other hand, cholesteric liquid crystal environment affords "chiral reaction field" for production of chiral materials[12]. Our group has reported on a series of asymmetric polymerization methods in cholesteric liquid crystal (CLC) to afford chiral polymers from achiral monomers using CLC as chiral reaction field: electrochemical polymerization[13,14], cross-coupling chemical polymerization (Migita-Kosugi-Stille coupling)[15,16], and Ni-catalyzed polymerization for one-handed helical poly(aryl isocyanide)s[17,18]. For synthesis of poly(aryl isocyanide)s in CLC, it is suggested that ortho-substitution has significant effects on preparation of one-handed helical PPIs[18]. During polymerization, we assume that CLC medium facilitates the one-side attack of the neighboring coordinated isocyanide on propagating process, which results in the formation of single-handed helical polyisocyanide through inter-lock manner. Very recently, Lee et al. also reported that ortho-methyl substituted poly(aryl isocyanide) form helical structures with much higher stereoregularity compared to those of poly(aryl isocyanide)s without ortho-substitutions, which are prepared in THF by o-tol(dppe)NiCl[19]. To date, however, living polymerization of aryl isocyanide or even other synthetic monomers in liquid crystal has never been accomplished so far. If one can obtain the controlled polymerization protocols to create well-defined polymers using liquid crystals as solvent, it would lead to the new insight into chiral polymer synthesis and the mechanism of chiral biomolecular synthesis in our body.

5.3 Preparation of polymerization system in CLC

Cholesteric liquid crystalline (CLC) medium was prepared by adding chiral dopant, (*R*)- 8BpB2 or cholesterol pelargonate (CP), to nematic liquid crystal host, 4-cyano-4'-pentylbiphenyl (5CB). *Ortho*-methyl substituted phenyl isocyanide monomers are designed and synthesized according to the reported scheme for phenyl isocyanides. Into a vial containing CLC media (0.9 mL) with a stirrer bar was added phenyl isocyanide monomer (0.1 mmol), and the mixture was heated to isotropic state to dissolve the monomer into CLC. Into another vial containing CLC media (0.1 mL) was added o-tol(dppe)NiCl at certain ratio, and the mixture was heated gently. After the both vials are cool down to room temperature, which is confirmed by selective reflection characteristic of CLC, the suspension of o-tol(dppe)NiCl in CLC was added to the monomer solution in CLC to initiate the polymerization. To maintain liquid crystalline order against the shear stress by stirring, the rate of stirring speed was controlled to be constant 72 rpm. After 30 min, the reaction was quenched by adding $NaBH_4$. The crude product was purified by reprecipitation in methanol and acetone and subsequent filtration or centrifugation. All the polymerization procedure was carried out in aerated condition at room temperature. The GPC results are summarized in **Table 5.1**.

Table 5.1. Poly(phenyl isocyanide) (poly15) prepared in CLC media.

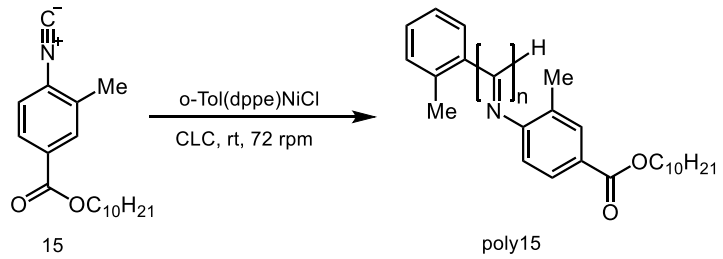

Host nematic LC

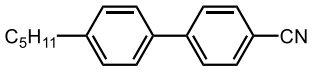

5CB

Chiral dopant

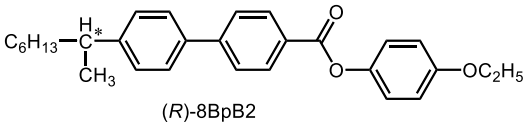

(*R*)-8BpB2

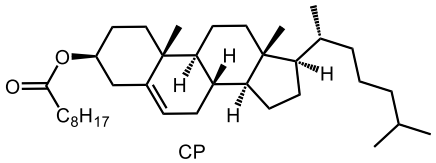

CP

Ni catalyst

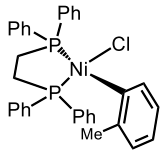

o-tol(dppe)NiCl

Entry	monomer	solvent	Temp.	Chiral dopant	[M]/[I]	M_n (kDa)[a]	M_w/M_n[a]	Yield[b]
1	15	CLC	rt	(*R*)-8BpB2	100	17.7	1.17	79%
2	15	CLC	rt	CP	100	18.8	1.12	63%

a. Molecular weight and molecular distribution were estimated by GPC analysis calibrated by PS standard (eluent: THF, rt.). b. isolated yield. M: monomer, I: initiator, CLC: cholesteric liquid crystal.

5.4 Asymmetric living polymerization nature in CLC

Ni-catalyzed polymerization of phenyl isocyanide monomer (15) proceeded very well in CLC media. Although the polymer precipitation was observed during the reaction in CLC, the obtained PPIs showed very narrow dispersity (M_w/M_n = 1.12-1.17) and the controlled molecular weight (**Table 5.1 and Figure 5.1a**) in moderate yield. This narrow dispersity is comparable to that is prepared in THF solution (M_w/M_n ~ 1.05). The as-prepared PPI exhibits positive signal around 365 nm in circular dichroism (CD) spectrum derived from helical arrangement of imino moiety (n-π* transition) (**Figure 5.1b**). The CD result indicates that PPIs prepared in CLC form preferentially one-handed helical backbones.

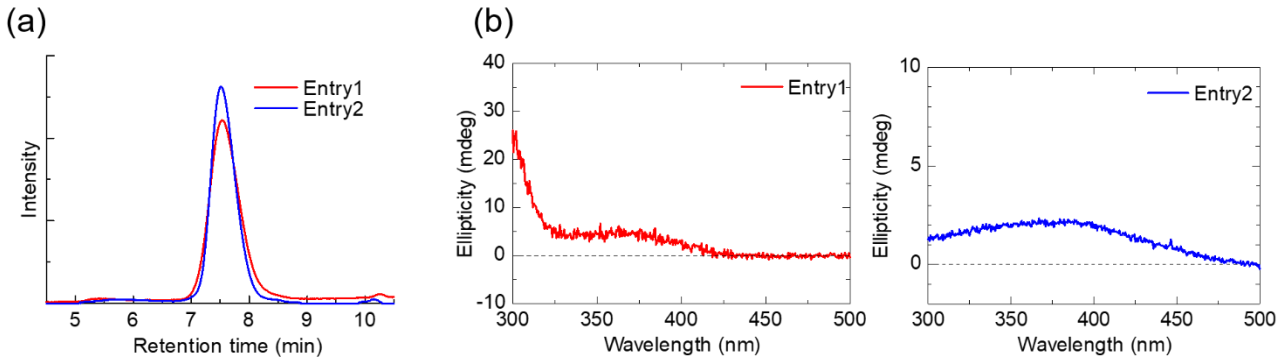

Figure 5.1. (a) GPC profile and (b) CD spectra of poly15 prepared in CLC media. For CD, the concentration is 0.2 mg/mL in THF.

As far as we know, this is the first report on possibility for helix-sense-selective living polymerization in CLC medium. The very narrow dispersity of PPI suggests that the propagating chain has "living" end. It should be noted that the helical pitch of PPIs is much smaller than that of CLC medium. We previously proposed the catalyst directional asymmetric polymerization mechanism in CLC, where the direction of polymerization propagation was regulated by the cooperative effects from steric effects of ortho-substitution of isocyanide monomer and 3D chiral environment of the CLC solvent to afford predominantly single-handed helical structure. PPIs prepared in this study also probably form preferentially single-handed helical backbone owing to chiral environment of CLC media.

5.5 Conclusion and perspective

We demonstrated that asymmetric polymerization of achiral ortho-methyl substituted phenyl isocyanide in cholesteric liquid crystalline media to afford single-handed helical PPIs with controlled molecular weight and narrow polydispersity. Although the present study is preliminary, the possibility for living polymerization nature in CLC media would provide new polymerization methodology in organic polymer chemistry. As future work, high temperature nematic LC molecules like 4-cyano-4'-pentyloxybiphenyl (5OCB) and 4-cyano-4'-octyloxybiphenyl (8OCB) provide the availability of the reaction temperature which is required for the reaction. The chiral environment, helical pitch, can be also tuned by the concentration and helical twisting power of chiral dopants. The binaphthyl-based chiral dopant possessing intrinsic high helical twisting power would provide more strong "chiral reaction field". We envision that asymmetric polymerization in condensed environment like cholesteric liquid crystal solvent allows for the new insight into the biochemical reactions in living cells.

References

[1] Ellis, R. J., & Minton, A. P. (2003). Cell biology: join the crowd. Nature, 425(6953), 27.
[2] Kawaguchi, K., Kageyama, R. & Sano, M. Topological defects control collective dynamics in neural progenitor cell cultures. Nature 545, 327–331 (2017).
[3] Saw, T. B. et al. Topological defects in epithelia govern cell death and extrusion. Nature 544, 212–216 (2017)
[4] Yashima, E., Maeda, K., & Furusho, Y. (2008). Single-and double-stranded helical polymers: synthesis, structures, and functions. Accounts of chemical research, 41(9), 1166-1180.
[5] Yashima, E., Ousaka, N., Taura, D., Shimomura, K., Ikai, T., & Maeda, K. (2016). Supramolecular Helical Systems: Helical Assemblies of Small Molecules, Foldamers, and Polymers with Chiral Amplification and Their Functions.
[6] Nolte, R. J. (1994). Helical poly (isocyanides). Chemical Society Reviews, 23(1), 11-19.
[7] Schwartz, E., Koepf, M., Kitto, H. J., Nolte, R. J., & Rowan, A. E. (2011). Helical poly (isocyanides): past, present and future. Polymer Chemistry, 2(1), 33-47.
[8] Wu, Z. Q., Nagai, K., Banno, M., Okoshi, K., Onitsuka, K., & Yashima, E. (2009). Enantiomer-selective and helix-sense-selective living block copolymerization of isocyanide enantiomers initiated by single-handed helical poly (phenyl isocyanide) s. Journal of the American Chemical Society, 131(19), 6708-6718.
[9] Kajitani, T., Okoshi, K., Sakurai, S. I., Kumaki, J., & Yashima, E. (2006). Helix-sense controlled polymerization of a single phenyl isocyanide enantiomer leading to diastereomeric helical polyisocyanides with opposite helix-sense and cholesteric liquid crystals with opposite twist-sense. Journal of the American Chemical Society, 128(3), 708-709.
[10] Kamer, P. C., Nolte, R. J., & Drenth, W. (1988). Screw sense selective polymerization of achiral isocyanides catalyzed by optically active nickel (II) complexes. Journal of the American Chemical Society, 110(20), 6818-6825.
[11] Ishikawa, M., Maeda, K., & Yashima, E. (2002). Macromolecular chirality induction on optically inactive poly (4-carboxyphenyl isocyanide) with chiral amines: a dynamic conformational transition of poly (phenyl isocyanide) derivatives. Journal of the American Chemical Society, 124(25), 7448-7458.
[12] Akagi, K., Piao, G., Kaneko, S., Sakamaki, K., Shirakawa, H., & Kyotani, M. (1998). Helical polyacetylene synthesized with a chiral nematic reaction field. Science, 282(5394), 1683-1686.
[13] Goto, H., & Akagi, K. (2005). Asymmetric electrochemical polymerization: Preparation of polybithiophene in a chiral nematic

liquid crystal field and optically active electrochromism. Macromolecules, 38(4), 1091-1098.
[14] Kawabata, K., Takeguchi, M., & Goto, H. (2013). Optical activity of heteroaromatic conjugated polymer films prepared by asymmetric electrochemical polymerization in cholesteric liquid crystals: structural function for chiral induction. Macromolecules, 46(6), 2078-2091.
[15] Goto, Hiromasa, and Kazuo Akagi. "Optically active conjugated polymers prepared from achiral monomers by polycondensation in a chiral nematic solvent." Angewandte Chemie 117.28 (2005): 4396-4402.
[16] Goto, H. (2007). Cholesteric liquid crystal inductive asymmetric polymerization: Synthesis of chiral polythiophene derivatives from achiral monomers in a cholesteric liquid crystal. Macromolecules, 40(5), 1377-1385.
[17] Goto, Hiromasa, Satoshi Ohkawa, and Reina Ohta. "Structural chirality of cholesteric liquid crystal produces atropisomerism: Chiroptical polyisocyanides from achiral monomer in cholesteric liquid crystal matrix." Polymer 52.9 (2011): 1932-1937.
[18] Iseki, Tomokazu, et al. "Catalysis direction selective asymmetric polymerization in chiral liquid crystal medium." polymer 55.1 (2014): 66-72.
[19] Lee, J., Shin, S., & Choi, T. L. (2018). Fast Living Polymerization of Challenging Aryl Isocyanides Using an Air-Stable Bisphosphine-Chelated Nickel (II) Initiator. Macromolecules, 51(19), 7800-7806.

Experimental

Syntheses

Synthesis of nematic LC solvent

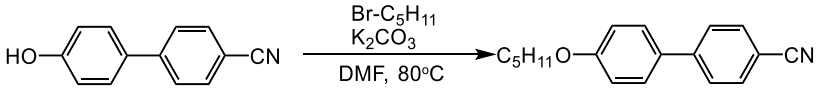

4-cyano-4'-pentyloxybiphenyl (5OCB): Into a three-neck flask, 4-cyano-hydroybiphenyl (3.58 g, 18.36 mmol), K_2CO_3 (5.58 g, 40.39 mmol), and DMF (50 mL) were added and warmed up to 80°C under nitrogen atmosphere. To the suspension was added 1-bromopentane (2.5 mL, 20.2 mmol) in DMF (20 mL) dropwise over 5 min. The reaction mixture was stirred at 80°C for another 21 h. The mixture was extracted with ethylacetate and washed by water, $NaHCO_3$ aq, and brine. The organic phase was dried over Na_2SO_4. The crude product was purified by column chromatography (eluent: hexane/ethylacetate = 4/1 (v/v)) to afford white powder (4.33 g, 89%). ^{1}H NMR (400 MHz, $CDCl_3$, δ from TMS): δ 7.69 (dt, 2H, J = 8.0 Hz), 7.63 (dd, 2H, J = 6.8 Hz), 7.52 (dd, 2H, J = 6.8 Hz), 6.99 (dd, 2H, J = 6.8 Hz), 4.00 (t, 3H, J = 6.8 Hz), 1.82 (quint., 2H, J = 7.2 Hz), 1.46-1.39 (m, 4H), 0.94 (t, 3H, J = 7.2 Hz). ^{13}C NMR (100 MHz, $CDCl_3$, δ from TMS): δ 159.77, 145.25, 132.53, 131.19, 128.28, 127.03, 119.11, 115.03, 109.97, 68.12, 28.88, 28.15, 22.43, 14.01.

Synthesis of Ni catalyst for living polymerization of phenylisocyanides

Scheme

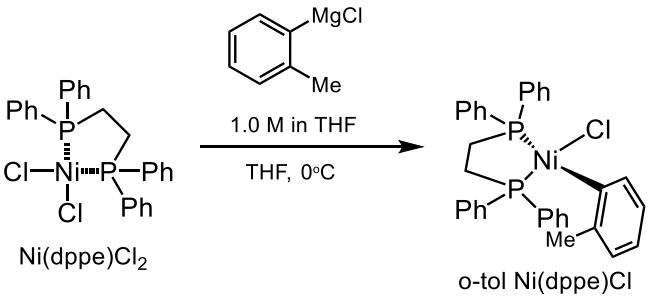

Ortho-tol(dppe)NiCl; Into an oven-dried 200 mL three-neck flask, $Ni(dppe)Cl_2$ (2.11 g, 4.0 mmol) and THF (150 mL) were added, and cooled down to 0°C. To the suspension was added o-tolylmagnesium chloride (1.0 M in THF, 4.0 mL, 4.0 mmol) dropwise, in which the color turned into black green. After stirring for 15 min at 0°C, the unreacted $Ni(dppe)Cl_2$ was filtered off, and the filtrate was evaporated. The crude product was purified by recrystallization in MeOH (20 mL) at -20°C to afford yellow-orange powder (390 mg, 17%).

Synthesis of chiral dopants

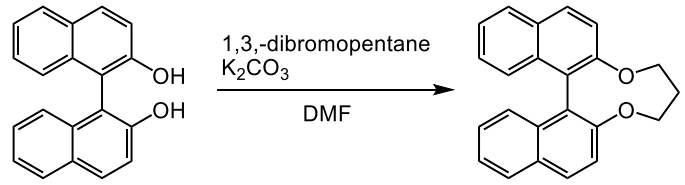

(*S*)-6: Into a three-neck flask, (*S*)-BINOL (4.30 g, 15 mmol), K_2CO_3 (4.56 g, 33 mmol), and DMF (70 mL) were added and warmed up to 80°C. To the suspension was added 1,3-dibromopropane (1.7 mL, 16.5 mmol) in DMF (50 mL) dropwise over 2h. The reaction mixture was stirred at 80°C for another 19h. The mixture was extracted with ethyl acetate and washed by water and brine. The organic phase was dried over Na_2SO_4. The crude product was purified by column chromatography (eluent: hexane/DCM = 7/3 (v/v)) to afford white powder (2.92 g, 60%). ^{1}H NMR (400 MHz, $CDCl_3$, δ from TMS): δ 7.95 (d, 2H, J = 9.2 Hz), 7.88 (d, 2H, J = 8.0 Hz), 7.46 (d, 2H, J = 8.8 Hz), 7.38-7.34 (m, 2H), 7.27-7.21 (m, 4H), 4.42-4.30 (m, 4H), 1.98-1.93 (m, 2H). ^{13}C NMR (100 MHz, $CDCl_3$, δ from TMS): δ 154.65, 133.42, 130.41, 129.61, 128.11, 126.33, 126.18, 124.23, 123.88, 119.21, 71.93, 30.66.

(*R*)-6: Synthesized by the same procedure as (*S*)-6, starting from (*R*)-BINOL. Whiter powder (2.68 g, 55%).

Synthetic procedure for newly phenyl isocyanide monomers

Scheme

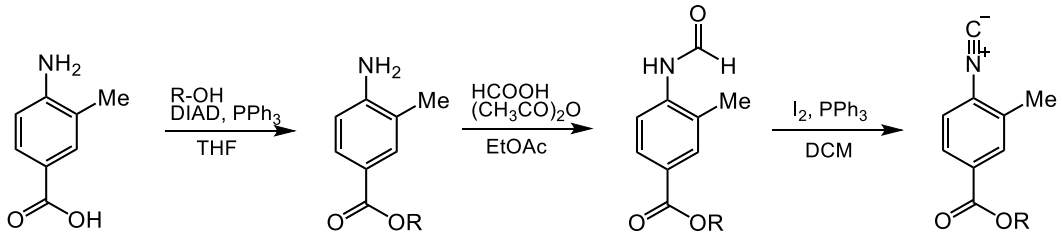

Procedure for esterification reaction

Typical procedure as follows: Into an oven dried two-neck flask were charged 4-amino-3-methylbenzoic acid (1.51 g, 10 mmol), triphenylphosphine (2.62 g, 11 mmol), alcohol (11 mmol) and THF (20 mL) under argon atmosphere. The solution was cooled to 0°C in ice bath. Then into the solution was added dropwise DIAD (40% in toluene, 5.8 mL, 11 mmol), and the solution was stirred at 0°C for another 15 min. After removing the ice bath, the reaction was continued at rt overnight. The yellow solution was evaporated under vacuum and suspended in hexane/ethyl acetate to precipitate crystalline triphenylphosphine oxide. After filtration, the crude mixture was purified by column chromatography (eluent: hexane/ethyl acetate = 4/1 (v/v)) and vacuum drying to afford desired product.

Procedure for formylation reaction

Typical procedure as follows: Into a two-neck flask were charged formic acid (0.95 mL, 25 mmol) and acetic anhydride (1.18 mL, 12.5 mmol), and the mixture was stirred at rt for 1 h under argon atmosphere. To that mixture was added dropwise alkyl-4-amino-3-methylbenzoate (5.0 mmol) in ethyl acetate (25 mL) at 0°C over 15 min. After removing the ice bath, the reaction was continued at rt overnight. The completion of reaction was monitored by thin-layer chromatography (TLC). After the reaction, the reaction solution was evaporated under vacuum. This alkyl-4-*N*-formyl-3-methylbenzoate was used in the next reaction without further purifications.

Procedure for dehydration reaction

Dehydration reaction was carried out according to the reported procedure. Into oven dried flask were charged alkyl-4-*N*-formyl-3-methylbenzoate, iodo (I_2) (1.90 g, 7.5 mmol), and DCM (15 mL). After dissolution triphenylphosphine (1.97 g, 7.5 mmol) was added to the solution. Then triethylamine (2.09 mL, 15 mmol) was added

dropwise to the reaction mixture at rt, and the reaction was continued for 2 h. After reaction, the solution was diluted by DCM and washed with $Na_2S_2O_3$ aq, then dried over Na_2SO_4. The crude product was purified by column chromatography (eluent: hexane/ethyl acetate = 4/1 (v/v)) and vacuum drying to afford desired aryl isocyanide monomers.

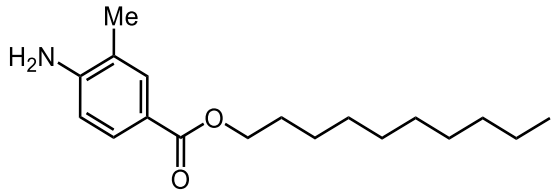

3-Methyl-4-decyl-isocyanobenzoate; white solid (Yield: 96%). ^{1}H NMR (400 MHz, $CDCl_3$, δ from TMS): δ 7.71 and 7.73 (s and d, 2H), 6.63 (d, 1H, J = 8.0 Hz), 4.25 (t, 2H, J = 7.2 Hz), 4.02 (br, 2H), 2.17 (s, 3H), 1.75 (quint., 2H, 6.8 Hz), 1.44-1.27 (m, 14H), 0.88 (t, 3H, 7.2 Hz). ^{13}C NMR (100 MHz, $CDCl_3$, δ from TMS): δ 166.95, 149.02, 132.12, 129.20, 120.93, 119.93, 113.58, 64.44, 31.84, 29.50, 29.27, 28.78, 26.03, 22.63, 17.11, 14.07.

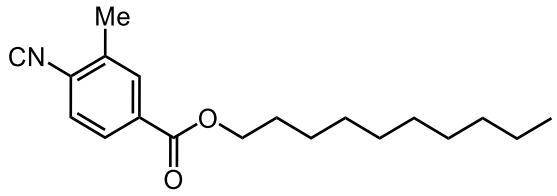

3-Methyl-4-decyl-isocyanobenzoate; Yellow solid (Yield: 58% in 2 steps). ^{1}H NMR (400 MHz, $CDCl_3$, δ from TMS): δ 7.96 (s, 1H), 7.88 (dd, 1H, J = 8.0 Hz), 7.40 (d, 1H, J = 8.0 Hz), 4.32 (t, 2H, J = 7.2 Hz), 2.49 (s 3H), 1,77 (quint., 2H, J = 7.2 Hz), 1.44-1.27 (m, 14H), 0.88 (t, 3H, 7.2 Hz). ^{13}C NMR (100 MHz, $CDCl_3$, δ from TMS): δ 168.37, 165.35, 135.18, 131.67, 131.04, 127.95, 126.64, 126.49, 65.68, 37.22, 31.86, 31.85, 29.51, 29.49, 29.27, 29.23, 28.60, 25.96, 22.65, 18.57, 14.09.

Chapter 6: Conclusion and prospects

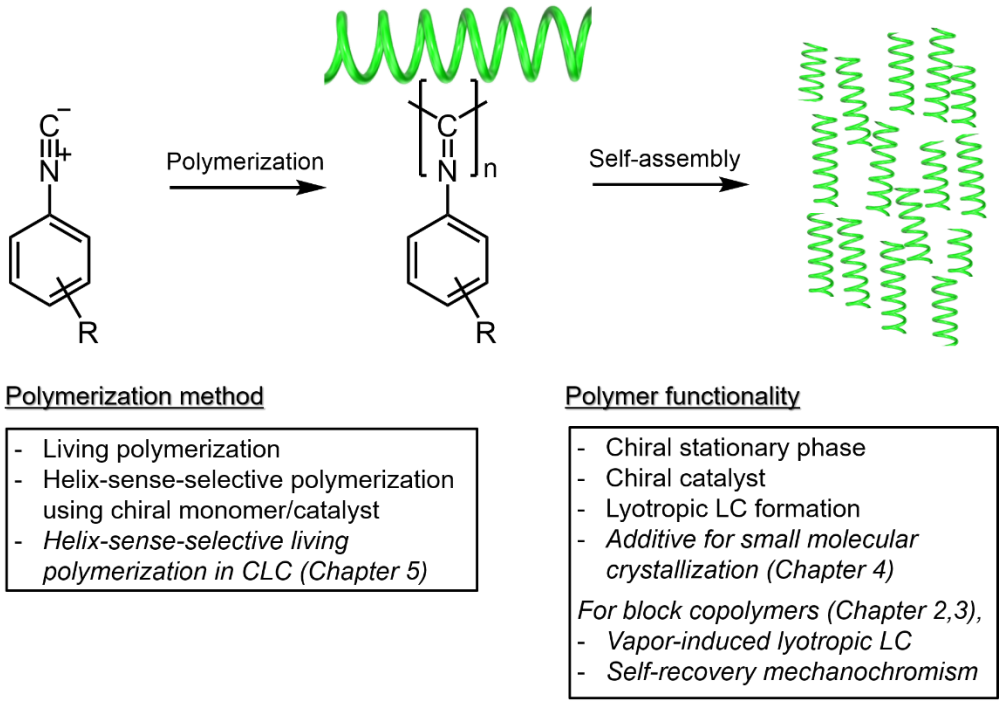

Figure 6.1. Conceptual illustration of this study compared to the previous studies.

Herein we demonstrated new asymmetric polymerization methodology using cholesteric liquid crystal solvent, and pioneered new functionalities originating from rod-shaped helical poly(phenyl isocyanide)s (PPIs) and the resulting lyotropic liquid crystalline assembly of PPIs.

In Chapter 2, a series of block copolymers comprising semiconducting polythiophene (PTh) derivatives and rod-shaped helical poly(phenyl isocyanide)s were synthesized. incorporation of PPI allows the corresponding semiconducting block copolymers to show vapor-induced liquid crystallinity, magnetic field-assisted orientation and self-recover mechanochromism.

In Chapter 3, based on the results in Chapter 2, functional block copolymers with mesogenic pendants were synthesized. Azobenzene containing light-responsive PTh-*b*-PPI copolymer and cyanobiphenyl containing, colloid-forming PTh-*b*-PPI copolymer were developed.

In Chapter 4, 1D C_{60} crystallization was systematically investigated using well-defined PPIs with various side chains and different length, demonstrating the significant impact of rod-shape of PPIs and the resulting lyotropic liquid crystalline assembly on the C_{60} crystallization. This methodology is widely applicable to other substances such as organic building blocks, and even inorganic Fe_3O_4 nanoparticles. This study gives new insight into the rod-shaped polymers with long persistence length as additives for small molecular crystallization.

In Chapter 5, asymmetric polymerization of achiral ortho-methyl substituted phenyl isocyanide in cholesteric liquid crystalline media to afford single-handed helical PPIs with controlled molecular weight and narrow polydispersity. Although the present study is preliminary, we envision that asymmetric polymerization in condensed environment like cholesteric liquid crystal solvent allows for the new insight into the biochemical reactions in living cells.

In conclusion, we have developed a series of PPIs with various molecular weight and different side chains with controlled manner to explore the novel functionalities mainly derived from rod-shaped structure of PPIs and the resulting lyotropic liquid crystalline assemblies. We believe these findings not only improve the understanding of the nature of PPIs but also pave the way for unconventional functionalities for next generation materials developments.

List of publications

1.Hiroki Hayashi, Kohsuke Kawabata, Hiromasa Goto*
"Synthesis of new chiral inducer and preparation of semi-conducting polymer films showing fingerprint structure" *International Letters of Chemistry, Physics and Astronomy* 8 (2014) 6-12

2.Hiroki Hayashi, Hiromasa Goto* (IWP2014 proceeding)
"Preparation of Polythiophene Films Showing Optical Activity by Electrochemical Polymerisation in Cholesteric Liquid Crystal Containing Coumarine" *International Letters of Chemistry, Physics and Astronomy* **7** (2015) 42-47

3.Hayashi, Hiroki; Kawabata, Kohsuke ; Nimori, Shigeki; Goto, Hiromasa
*"*A Poly(ter(3,4-ethylenedioxythiophene)) Showing Concentric-Circle Morphology Prepared by Electrochemical Synthesis in Smectic A Liquid Crystal under Vertical Strong Magnetic Field" *Chemistry Letters*, **45**, 170–172, 2016

4.Hayashi, Hiroki; Iseki Tomokazu ; Goto, Hiromasa
*"*Induction of Reaction Environment by Optically Active Menthyl-based Compound for Electrochemical Polymerization in Cholesteric and Smectic Liquid Crystal" *Chemistry Letters*, **45**, 511-513, 2016

5.H. Hayashi, T. Iseki, S. Nimori, H. Goto
*"*Vapour-Induced Liquid Crystallinity and Self-Recovery Mechanochromism of Helical Block Copolymer" *Scientific Reports*, **7**, Article number: 3948, (2017)

6.H. Hayashi, R. Kikuchi, R. Kumai, H. Sagayama, H. Goto
*"*Rod-Shaped 1D Polymer-Assisted Unidirectional Self-Assembly of 0D Nanoparticles by Solution-Drying Method" *Submitted (10 December 2018)*

List of awards

1. Hiroki Hayashi, Tomokazu Iseki, Hiromasa Goto
"**Synthesis of Cholesteric Liquid Crystals Having Menthol"**
Distinguished Presentation Prize
International Workshop on Science and Patents 2013, IWP 2013 (U. Tsukuba, 2013.9.6)

2. Hiroki Hayashi, Kohsuke Kawabata, Shigeki Nimori, Hiromasa Goto
"**Electrochemical Synthesis of High Anisotropic Polymer Films in Magnetically Aligned Smectic Liquid Crystal"**
Distinguished Presentation Prize
International Workshop on Science and Patents 2014, IWP 2014 (U. Tsukuba, 2014.9.5)

3. 林宏紀, 川畑公輔, 二森茂樹, 後藤博正
"**スメクチック液晶溶媒を用いた磁場配向下液晶中電解重合による高異方性ポリマーフィルムの作製"**
優秀ポスター発表賞
第 4 回 CSJ 化学フェスタ 2014 (タワーホール船堀, 2014.10.14)

4. 林宏紀, 二森茂樹, 後藤博正
"**液晶磁場電解重合による配向性導電性高分子の開発"**
研究奨励賞 (35 歳以下)

日本磁気科学会　第 9 回年会 (**岐阜** 高山市民会館, 2014.11.13)

5. 林宏紀, **林仁志**, **後藤博正**
"配向液晶中電解重合を用いた配向性共役系高分子薄膜の開発"
優秀ポスター賞
第 64 回高分子討論会 (**東北大学** 川内キャンパス, 2015.9.17)

6. 林宏紀, **林仁志**, **後藤博正**
"液晶を鋳型とする電解重合法により配向制御した共役系ポリマーの電気伝導度評価"
ポスター発表優秀賞
高分子学会関東支部茨城地区第 30 回若手交流会 (**つくばセミナーハウス**, 2015.10.29)

7 筑波大学学長表彰 (受賞日 2016.3.25)

8. Hiroki Hayashi, Nimori Shigeki, Hiromasa Goto
"Multi-responsive chromic block copolymers: solvent vapor- / mechanical stress-induced color changes"
Best poster award
Tsukuba Global Science Week 2017, Student Poster Presentation on Materials Research (NIMS Collaborative Doctoral Program & TIMS) (Tsukuba International Congress Center, September 25, 2017)

9. Hiroki Hayashi, Ryosuke Kikuchi, Reiji Kumai, Hiromasa Goto
"Polymer-Assisted Fullerene C_{60} Crystallization: Ultralong Nanofibers and their morphologies**"**
Poster prize
Tsukuba Global Science Week 2018, TGSW-Interdisciplinary Workshop on Science and Patents 2018 (Tsukuba International Congress Center, September 21, 2018)

10. 林 宏紀, 熊井玲児、二森茂樹、後藤博正
"棒状らせん高分子の添加によるフラーレン C_{60} 結晶の異方的集合体形成"
ポスター発表優秀賞
第 33 回茨城地区「若手の会」交流会 (**つくばセミナーハウス**, 2018.11.1)

List of grants

1. 戸部真紀財団　2016 年度奨学生　60 万円/年
2. つくば共鳴プログラム海外武者修行プログラム
   アメリカハーバード大学 Weitz 研究室に留学（2016 年 10 月から 2017 年 1 月まで）
3. 日本学術振興会特別研究員 DC2 (2017 年 4 月から 2019 年 3 月まで)
   Grant Number JP17J05652